Polynorbornenes for Advanced Applications and Processes

A Dissertation Presented for the
Doctor of Philosophy
Degree
The University of Tennessee, Knoxville

Xinyi Wang
August 2022

Copyright © 2022 by Xinyi Wang.
All rights reserved.

ACKNOWLEDGEMENTS

First and foremost, I would like to thank my family and my parents, Xiqing Wang and Chunhui Pan, who taught me the importance of perseverance, respect, and who support me for the critical decisions I have made in my life. Thank you to my grandparents, Jiong Pan and Meidi Yu, who directed my initial interest in science and always cared about my health even under difficult conditions. I wish good health to my grandfather. Thank you to my boyfriend, Tianyu Li, who always stands with me no matter what happens and gives me the courage to overcome difficulties.

I would also like to thank my committee members, Dr. Gila Stein, Dr. John Brantley, and Dr. Mark Dadmun, who provided many valuable suggestions and feedback during my graduate studies and led me to become a better scientist. Especially, I want to thank my advisor, Dr. Brian Long, who always provides important insight into my work, who presents opportunities for my future success, and who exposes me to different cultures. I would also like to thank all my collaborators for their help, hard effort, and excellent teamwork.

I am also extremely appreciative of my colleagues and friends. Chris, you are a good mentor that led me into the field of gas separation membranes. Alicia and Liz, you are both my friends who have always been supportive and have taught me to voice my opinion. Justin, you are the most friendly and helpful person I have ever known, and I learned how to maintain an inclusive mindset from you. Cameron, you are always creative and help to maintain a joyful working environment. Nick, you are an amazing desk mate and always keep the lab clean and orderly. Christy, though we only overlapped for a short time, your earnest attitude always encourages me. Especially, I want to thank the current members of “team membrane,” Maggie and Trevor. I enjoyed working with you and I am looking forward to the accomplishments you will achieve in our projects. Jinchao, you are the hardest-working person I have ever met, and you always remind

me how beautiful science and life can be. I am so grateful that we have developed this fantastic friendship.

Thanks to you all. Without any of you, I could not grow into who I am now. I wish you all the best in the future.

ABSTRACT

Polynorbornenes have dramatically different properties and various applications depending on their chemical structures. The modular nature of norbornene-based systems provides a facile route toward synthesizing diverse polymeric materials, thus making them ideal materials for systematic structure-property investigations. Herein, their application as gas separation membranes and the correlation between their gas-transport properties and polymer structures will be investigated. Though many valuable correlations between gas-permeability and polynorbornene structure have been studied previously, many of these efforts have focused heavily on designing materials with various chemical structures to achieve high permeabilities. In contrast, the influence of molecular structure on: a) polynorbornene chain packing and ultimate gas separation performance, and b) material processibility have been less studied.

In this work, we have designed a series of fundamental studies that leverage careful monomer and catalyst design to investigate: 1) The influence of incorporation of fluorine content into vinyl-addition polynorbornene on gas separation and transportation mechanism; 2) The influence of block copolymer phase separation on gas separation performance, and the influence of catalyst induced backbone tacticity and corresponding chain packing on gas separation performance; 3) The influence of substituents on the glass transition temperature and decomposition temperature of APNBs, and their potential melt-processibility.

TABLE OF CONTENTS

Chapter 1 Polynorbornenes for Advanced Applications and Processes 1

1.1 Polynorbornene Origins and Advanced Applications Thereof 2

1.2 General Synthesis and Characteristics of Norbornene-Based Monomers and Polymers 3

1.3 Gas Separation Performance and Gas Transport Theory in Dense Polymeric Membranes 8

1.4 Performance of Organosilicon Containing MPNBs and APNBs as Gas Separation Membranes 11

1.4.1 MPNBs Bearing Organosilicon Substituents 13

1.4.2 APNBs Bearing Organosilicon Substituents 20

1.4.3 Comparing MPNB and APNB Gas Separation Performance 23

1.5 Influence of Polymer Chain Packing on Gas Separation Membrane Performance 24

1.5.1 Block Copolymers with Microphase Separation as Gas Separation Membranes 25

1.5.2 Influence of Polymer Tacticity on Gas Separation Performance 28

1.6 Current limitations of APNB processibility 31

1.7 Research Objectives 32

References 36

Chapter 2 Fluoroalkoxysilyl-substituted, Vinyl-addition Polynorbornene Membranes for CO_2/CH_4 Separation 44

2.1 Abstract 45

2.2 Introduction 46

2.3 Experimental Section..... 49

2.4 Results and Discussion 60

2.5 Conclusions..... 80

References..... 81

Chapter 3 Metathesis Polynorbornene-based Block Copolymer Gas Separation Membranes 85

3.1 Abstract..... 86

3.2 An Introduction to Block Copolymers and Phase Diagrams..... 86

3.3 Preparation of Microphase Separated Membranes 89

3.4 Characterization of Microphase Separated Membranes..... 90

3.5 Design of MPNB Block Copolymer Membranes for Gas Separations 92

3.6 Preliminary Results and Discussion..... 92

3.7 Future Work..... 101

References..... 105

Chapter 4 Design, Synthesis, and Characterization of Vinyl-addition Polynorbornenes with Tunable Thermal Properties 107

4.1 Abstract..... 108

4.2 Introduction..... 109

4.3 Experimental Section..... 112

4.4 Discussion 118

4.5 Conclusions..... 136

References..... 138

Chapter 5 Conclusion and Future Work..... 142

Appendices..... 146

Appendix A Influence of Addition Polynorbornene Backbone Tacticity on Polymer Properties 147

Appendix B Supporting Information for Chapter 2 166

Appendix C Supporting Information for Chapter 4 193

Vita 235

LIST OF TABLES

Table 1.1 Gas transport properties of metathesis polynorbornenes (MPNBs) bearing organosilicon substituents..... 14

Table 1.2 Gas transport properties of epoxidated and *gem*-difluorocyclopropanated MPNBs. .. 19

Table 1.3 Gas transport properties of addition polynorbornenes (APNBs) bearing organosilicon substituents..... 21

Table 1.4 Gas transport properties of selected addition polynorbornenes (APNBs). 33

Table 2.1 Synthesis and Characterization of all Homopolymers and Copolymers[a] 63

Table 2.2 Density, Fractional Free Volume (FFV), and *d*-Spacing for Polymer Films..... 65

Table 2.3 Ideal Permeability and Selectivity of the **P1**/**P1F**, **P2**/**P2F** and **P3**/**P3F** Polymer Series. 67

Table 2.4 Diffusion and Solubility Coefficients of the **P1**/**P1F**, **P2**/**P2F**, and **P3**/**P3F** Copolymer Series, as well as Individual Henry's Law and Langmuir Sorption Parameters..... 73

Table 3.1 Peak positions (expressed as q/q^*) of Bragg reflections for various structures..... 91

Table 3.2 Synthesis of homopolymers and corresponding block and random copolymers.[a]..... 96

Table 3.3 Ideal Permeability and Selectivity of the **P1**-*b*-**P2** and **P1**-*r*-**P2** Polymer Series[a] 100

Table 3.4 SAXS scattering peaks of the **P1**-***b***-**P2** block copolymer series. 103

Table 4.1 Homo- and co-polymerization of substituted norbornene monomers.[a] 121

Table 4.2 T_g values of **PS**, **P2**, **P6**, and the **P2P6** copolymer series as measured by MDSC, DMA, and ellipsometry..... 124

Table A.1 Selected Polymerization Conditions and Observations[a] 155

Table B.1 Calculated *d*-spacing (d_B and d_{ic}) for **P1/P1F** copolymer series. 187

Table B.2 Calculated *d*-spacing (d_B and d_{ic}) for **P2/P2F** copolymer series. 188

Table B.3 Calculated *d*-spacing (d_B and d_{ic}) for the **P3/P3F** copolymer series. 189

Table C.1 T_g, T_d, and service window of substituted APNB derivatives and unsubstituted PNB. 193

Table C.2 T_g, T_d, and service window of substituted APNB derivatives and unsubstituted PNB. 194

LIST OF FIGURES

Figure 1.1 Representative catalyst examples used in polynorbornene synthesis. Reprinted with permission from Reference [33]. Copyright 2021 The Royal Society of Chemistry. 6

Figure 1.2 Schematic representation of a membrane driven gas separations. Reprinted with permission from Reference [33]. Copyright 2021 The Royal Society of Chemistry. 9

Figure 1.3 Robeson plot[47, 48] of CO_2/N_2 separation performance for a breadth of previously reported non-norbornene-based materials (open gray), and norbornene-based materials described herein (blue). Reprinted with permission from Reference [33]. Copyright 2021 The Royal Society of Chemistry..... 9

Figure 1.4 Robeson plot[47-49] showing CO_2/CH_4 separation performance for a breadth of previously reported non-norbornene-based materials (open gray), and norbornene-based materials described herein (blue). Reprinted with permission from Reference [33]. Copyright 2021 The Royal Society of Chemistry..... 10

Figure 1.5 Metathesis polynorbornenes (MPNBs) bearing organosilicon substituents. Reprinted with permission from Reference [33]. Copyright 2021 The Royal Society of Chemistry. 14

Figure 1.6 Addition polynorbornenes (APNBs) and bearing organosilicon substituents. Reprinted with permission from Reference [33]. Copyright 2021 The Royal Society of Chemistry. 21

Figure 1.7 Models for the permeation of inert gases through the S-B block copolymers: (a) Series model, (b) Parallel model. Adapted with permission from Reference [99]. Copyright 1977 John Wiley and Sons. 27

Figure 1.8 Different backbone connectivity of unsubstituted APNBs. Left: 2,3-threo disyndiotactic conformation, and right: 2,3-erythro diisotactic conformation. Adapted with permission from Reference [105]. Copyright 1998 John Wiley and Sons. 29

Figure 2.1 Differential solubility of fluorocarbon and hydrocarbon gasses within fluorocarbon and hydrocarbon polymer matrices,[150, 151] and proposed fluorination of APNBs to enhance CO_2/CH_4 selectivity. Reprinted with permission from Reference [153]. Copyright 2022 American Chemical Society..... 50

Figure 2.2 Robeson plot of polymers tested in this study. Grey, blue, and red symbols represent **P1**/**P1F**, **P2**/**P2F**, **P3**/**P3F** polymer series, respectively. Error bars are included for each data point, but in some cases, the error bars are smaller than the data marker. Reprinted with permission from Reference [153]. Copyright 2022 American Chemical Society. 68

Figure 2.3 (A) CO_2 sorption isotherms for the **P1**/**P1F** copolymer series. (B) CO_2 sorption isotherms for the **P2**/**P2F** and **P3**/**P3F** copolymer series. (C) CH_4 sorption isotherms for the **P1**/**P1F** copolymer series and (D) CH_4 sorption isotherms for the **P2**/**P2F** and **P3**/**P3F** copolymer series. All isotherms were generated at 35 °C. **P1**/**P1F** copolymer series isotherms were fit using the dual-mode sorption model, whereas **P2**/**P2F** and **P3**/**P3F** series (with no observable Langmuir contributions) were fit linearly to provide the highest possible R^2. Trend lines are included to guide the reader's eye. Reprinted with permission from Reference [153]. Copyright 2022 American Chemical Society. 71

Figure 2.4 Calculated ΔE of gas–monomer interactions. Calculations were performed on saturated analogs of polymer repeat units **1**–**3** and **1F**–**3F**. Reprinted with permission from Reference [153]. Copyright 2022 American Chemical Society. 77

Figure 2.5 Calculated $\Delta\Delta E$ values for CO_2 and CH_4 for all nonfluorinated and fluorinated polymer series. Calculations were performed on saturated analogs of polymer repeat units **1**–**3** and **M1F**–**M3F**. Reprinted with permission from Reference [153]. Copyright 2022 American Chemical Society..... 77

Figure 3.1 (a) Equilibrium morphologies of AB diblock copolymers in bulk: S and S' = body-centered-cubic spheres, C and C' = hexagonally packed cylinders, G and G' = bicontinuous gyroids, and L = lamellae. (b) Theoretical phase diagram of AB diblocks predicted by the self-consistent mean-field theory, depending on volume fraction (f_A) of the blocks and the segregation parameter, χN, where χ is the Flory–Huggins segment–segment interaction energy and N is the degree of polymerization; CPS and CPS' = closely packed spheres. (c) Experimental phase portrait of polyisoprene-block-polystyrene copolymers, in which f_A represents the volume fraction of polyisoprene, PL = perforated lamellae. Reprinted with permission from Reference [178]. Copyright 2012 The Royal Society of Chemistry..... 88

Figure 3.2 Schematic illustration of the possible polymer chain arrangements in different morphologies of AB diblocks changing from sphere (a) to cylinder (b) and to lamella (c), as the volume fraction (f_A) of the A block (black) increases to ~ 0.5. The dash curve in each morphology represents a part of the interface between A and B domains. Reprinted with permission from Reference [178]. Copyright 2012 The Royal Society of Chemistry..... 88

Figure 3.3 a) Plot of $\ln([M]/[M]_0)$ versus time for the ROMP of **M2** (toluene, 25 °C, [hexylNB] = 0.05M, [M]:[C] = 300:1, 100 eq pyridine). b) Plot of molecular weight (M_n) versus monomer conversion. 94

Figure 3.4 NMR of homopolymers and corresponding block copolymers..... 96

Figure 3.5 GPC trace of successful chain extension of **P1-*b*-P2** block copolymer series. 97

Figure 3.6 DOSY of block copolymer $\mathbf{P1^{48}}$-***b***-$\mathbf{P2^{52}}$. The major polymer peaks all have similar diffusion coefficient, suggested that the two blocks are connected. 98

Figure 3.7 Robeson plot of polymers tested in this study. Error bars are included for each data point, but in some cases, the error bars are smaller than the data marker. 99

Figure 3.8 Example of as-cast **P1^{48}-*b*-P2^{52}** film (left), **P1** film (middle), and **P1/P2** blend (right). 100

Figure 3.9 SAXS spectra of the **P1-*b*-P2** block copolymer series. 102

Figure 3.10 SAXS spectra of **P1^{48}-*b*-P2^{52}** annealed at 100 °C for different period. 102

Figure 4.1 Series of APNBs (**P1-P6**) chosen to probe the effects of substituent architecture on resultant thermal properties. Reprinted with permission from Reference [188]. Copyright 2021 The Royal Society of Chemistry. 119

Figure 4.2 T_g, T_d, and service window (T_d-T_g) of unsubstituted APNB[5, 198] and substituted homo-APNBs **P1-P6**. Reprinted with permission from Reference [188]. Copyright 2021 The Royal Society of Chemistry..... 126

Figure 4.3 T_g, T_d, and service window for the a) **P2P4**, b) **P2P5**, and c) **P2P6** copolymer series. Reprinted with permission from Reference [188]. Copyright 2021 The Royal Society of Chemistry. 128

Figure 4.4 Comparison of experimental T_g (as determined by DMA) and theoretical T_g as predicted by the Fox and Gordon-Taylor equations for the a) **P2P4** series, b) **P2P5** series, and c) **P2P6** series. W_{m2} is defined in each plot as the weight fraction of comonomer **M2** in each copolymer. Error bars encompass the minimum and maximum values of two independent measurements. *Note:* in some series, the error bars are smaller than the symbol size. Reprinted with permission from Reference [188]. Copyright 2021 The Royal Society of Chemistry. 130

Figure 4.5 Melt extruded bars of APNB P2. The dark color is presumed to be a consequence of residual catalyst decomposition/oxidation that occurs during melt processing. Reprinted with permission from Reference [188]. Copyright 2021 The Royal Society of Chemistry. 132

Figure 4.6 . Stress-strain curves for polymers **P2** and **PS**. Reprinted with permission from Reference [188]. Copyright 2021 The Royal Society of Chemistry. 134

Figure A.1 HSQC NMR study of polymer obtained by *trans*-Ni(C_6F_5)$_2$($SbPh_3$)$_2$ catalyst (top) and MePdP(*i*-Pr)$_3$Cl/LiBArF catalyst system (bottom). The polymer obtained by Pd catalyst have more dispersed CH_2 signal than that obtained by Ni catalyst, suggesting that the former polymer may have more irregular back bone structure. 157

Figure A.2 ^{1}H NMR spectrum of *cis*-5-norbornene-*exo*-2,3-dicarboxylic anhydride 158

Figure A.3 ^{13}C NMR spectrum of *cis*-5-norbornene-*exo*-2,3-dicarboxylic anhydride 158

Figure A.4 ^{1}H NMR spectrum of *exo*-5,6-bis(hydroxymethyl)-2-norbornene 159

Figure A.5 ^{13}C NMR spectrum of *exo*-5,6-bis(hydroxymethyl)-2-norbornene 159

Figure A.6 ^{1}H NMR spectrum of *exo*-5,6-bis(methoxymethyl)-2-norbornene (MeOMeNB) 160

Figure A.7 ^{1}H NMR spectrum of *exo*-5,6-bismesylate-2-norbornene 160

Figure A.8 ^{13}C NMR spectrum of *exo*-5,6-bismesylate-2-norbornene 161

Figure A.9 ^{1}H NMR spectrum of *exo*-5,6-bis(bromomethyl)-2-norbornene (BrMeNB) 161

Figure A.10 ^{13}C NMR spectrum of *exo*-5,6-bis(bromomethyl)-2-norbornene (BrMeNB) 162

Figure A.11 ^{1}H NMR spectrum of *exo*-5,6-dimethyl-2-norbornene (MeNB) 162

Figure A.12 ^{13}C NMR spectrum of *exo*-5,6-dimethyl-2-norbornene (MeNB) 163

Figure B.1 Computational methodology used for this study. 166

Figure B.2 ^{1}H NMR spectrum of **V1F.** 167

Figure B.3 ^{13}C {^{1}H} NMR spectrum of **V1F.** 167

Figure B.4 ^{1}H NMR spectrum of **M1F**. 168

Figure B.5 ^{13}C {^{1}H} NMR spectrum of **M1F.** 168

Figure B.6 ^{1}H NMR spectrum of **V2F.** 169

Figure B.7 ^{13}C {^{1}H} NMR spectrum of **V2F.** 169

Figure B.8 ^{1}H NMR spectrum of **M2F.** 170

Figure B.9 ^{13}C {^{1}H} NMR spectrum of **M2F.** 170

Figure B.10 ^{1}H NMR spectrum of **V3F.** 171

Figure B.11 ^{13}C {^{1}H} NMR spectrum of **V3F.** 171

Figure B.12 ^{1}H NMR spectrum of **M3F.** 172

Figure B.13 ^{13}C {^{1}H} NMR spectrum of **M3F.** 172

Figure B.14 ^{1}H NMR spectrum of **V3.** 173

Figure B.15 ^{13}C {^{1}H} NMR spectrum of **V3.** 173

Figure B.16 ^{1}H NMR spectrum of **M3**. 174

Figure B.17 ^{1}H NMR spectrum of **M3**. 174

Figure B.18 ^{1}H NMR spectrum of **P1.** 175

Figure B.19 ^{1}H NMR spectrum of **P1^{84}P1F^{16}.** 175

Figure B.20 ^{1}H NMR spectrum of **P1^{67}P1F^{33}.** 176

Figure B.21 ^{1}H NMR spectrum of **P1^{48}P1F^{52}.** 176

Figure B.22 Stacked ^{1}H NMR spectra of **P1** series copolymers**.** Homopolymer P1F was not shown due to limited solubility in $CDCl_3$ and thus unable to access ^{1}H NMR. 177

Figure B.23 ^{1}H NMR spectrum of **P2.** 177

Figure B.24 ^{1}H NMR spectrum of **P2^{87}P2F^{13}.** 178

Figure B.25 ^{1}H NMR spectrum of **P2^{72}P2F^{28}.** 178

Figure B.26 Stacked ^{1}H NMR spectra of **P2** series copolymers**.** 179

Figure B.27 ^{1}H NMR spectrum of **P3.** 179

Figure B.28 ^{1}H NMR spectrum of **P3^{87}P3F^{13}.** 180

Figure B.29 ^{1}H NMR spectrum of **P3** series copolymers. 180

Figure B.30 GPC analysis of **P1**. 181

Figure B.31 GPC analysis of **P1^{84}P1F^{16}**. 181

Figure B.32 GPC analysis of **P1^{67}P1F^{33}**. 182

Figure B.33 GPC analysis of **P1^{48}P1F^{52}**. *NOTE: the high molar mass portion of this sample exceed the calibration standards used for this GPC and hence the molecular weight and dispersity values are likely inaccurate.* 182

Figure B.34 GPC analysis of **P1F**. 183

Figure B.35 GPC analysis of **P2**. 183

Figure B.36 GPC analysis of **P2^{87}P2F^{13}**. 184

Figure B.37 GPC analysis of **P2^{72}P2F^{28}**. 184

Figure B.38 GPC analysis of **P3**. 185

Figure B.39 GPC analysis of **P3^{87}P3F^{13}**. 185

Figure B.40 Example surface area measurement of permeation sample using ImageJ. 186

Figure B.41 WAXS spectra of the **P1/P1F** copolymer series. 187

Figure B.42 WAXS spectra of the **P2/P2F** copolymer series. 188

Figure B.43 WAXS spectra of the **P3/P3F** copolymer series. 189

Figure B.44 SAXS spectra of the **P1/P1F** copolymer series. 190

Figure B.45 SAXS spectra of the **P2/P2F** copolymer series. 191

Figure B.46 SAXS spectra of the **P3/P3F** copolymer series. 192

Figure C.1 ^{1}H NMR spectrum of monomer **M3**. 195

Figure C.2 ^{13}C NMR spectrum of monomer **M3**. 195

Figure C.3 ^{1}H NMR spectrum of monomer **M4**. 196

Figure C.4 ^{13}C NMR spectrum of monomer **M4**. 196

Figure C.5 ^{1}H NMR spectrum of monomer **M5**. 197

Figure C.6 ^{13}C NMR spectrum of monomer **M5**. 197

Figure C.7 ^{1}H NMR spectrum of polymer **P1**. 198

Figure C.8 ^{1}H NMR spectrum of polymer **P2**. 198

Figure C.9 ^{1}H NMR spectrum of polymer **P3**. 199

Figure C.10 ^{1}H NMR spectrum of polymer **P4**. 199

Figure C.11 ^{1}H NMR spectrum of polymer **P5**. 200

Figure C.12 ^{1}H NMR spectrum of polymer **P6**. 200

Figure C.13 Stacked ^{1}H NMR spectra of copolymer **P2P4** series. Monomer incorporation was not determine due to significant overlap of all peaks in the alkyl region. Thus, the superscript represents the theoretical monomer incorporation based upon feed ratios. 201

Figure C.14 Stacked ^{1}H NMR spectra of copolymer **P2P5** series. Resonances at 1.27 and 0.88 ppm correspond to the aliphatic protons in the alkyl pendant group of monomer **M2**, while the resonances at 7.23, 7.15 and 2.59 ppm correspond to the phenyl and benzylic protons of the phenylpropyl pendant group of monomer **M5**. Incorporation ratios were determined based upon integration the benzylic proton resonances (2.59 ppm) to all remaining protons in the alkyl region. 202

Figure C.15 Stacked ^{1}H NMR spectra of copolymer **P2P6** series. Resonances at 1.27 and 0.88 ppm correspond to the aliphatic protons on the alkyl pendant group of monomer **M2**, while the resonances at 7.25, 4.49 and 3.42 ppm correspond to the phenyl, benzylic, and ethereal protons of the benzyloxymethyl pendant group of monomer **M6**. Incorporation ratios were determined based

upon the integration the benzylic proton resonance (4.49 ppm) to all remaining protons in the alkyl region. 203

Figure C.16 TGA analysis of polymer **P1**. 204

Figure C.17 TGA analysis of polymer **P2**. 204

Figure C.18 TGA analysis of polymer **P3**. 205

Figure C.19 TGA analysis of polymer **P4**. 205

Figure C.20 TGA analysis of polymer **P5**. 206

Figure C.21 TGA analysis of polymer **P6**. First derivative of weight loss versus temperature have two peaks, indicating the side group decompose before the decomposing of the polymer backbone, resulting in a depressed T_d. 206

Figure C.22 TGA analysis of polymer $\mathbf{P2^{75}P4^{25}}$. 207

Figure C.23 TGA analysis of polymer $\mathbf{P2^{50}P4^{50}}$. 207

Figure C.24 TGA analysis of polymer $\mathbf{P2^{25}P4^{75}}$. 208

Figure C.25 TGA analysis of polymer $\mathbf{P2^{68}P5^{32}}$. 208

Figure C.26 TGA analysis of polymer $\mathbf{P2^{44}P5^{56}}$. 209

Figure C.27 TGA analysis of polymer $\mathbf{P2^{15}P5^{85}}$. 209

Figure C.28 TGA analysis of polymer $\mathbf{P2^{86}P6^{14}}$. 210

Figure C.29 TGA analysis of polymer $\mathbf{P2^{65}P6^{35}}$. 210

Figure C.30 TGA analysis of polymer $\mathbf{P2^{28}P6^{72}}$. 211

Figure C.31a DSC of **PS** control. Grey curve was the first heating cycle to erase sample thermal history. 212

Figure C.31b T_g of **PS** control obtained by ellipsometry. 212

Figure C.31c T_g of **PS** control obtained by DMA..... 213

Figure C.32a T_g of polymer **P2** obtained by MDSC..... 213

Figure C.32b T_g of polymer **P2** obtained by ellipsometry..... 214

Figure C.32c T_g of polymer **P2** obtained by DMA..... 214

Figure C.33a T_g of polymer **P2^{86}P6^{14}** obtained by MDSC..... 215

Figure C.33b T_g of polymer **P2^{86}P6^{14}** obtained by ellipsometry..... 215

Figure C.33c T_g of polymer **P2^{86}P6^{14}** obtained by DMA..... 216

Figure C.34a T_g of polymer **P2^{65}P6^{35}** obtained by MDSC..... 216

Figure C.34b T_g of polymer **P2^{65}P6^{35}** obtained by ellipsometry..... 217

Figure C.34c T_g of polymer **P2^{65}P6^{35}** obtained by DMA..... 217

Figure C.35a T_g of polymer **P2^{28}P6^{72}** obtained by MDSC..... 218

Figure C.35b T_g of polymer **P2^{28}P6^{72}** obtained by ellipsometry..... 218

Figure C.35c T_g of polymer **P2^{28}P6^{72}** obtained by DMA..... 219

Figure C.36a T_g of polymer **P6** obtained by MDSC..... 219

Figure C.36b T_g of polymer **P6** obtained by ellipsometry..... 220

Figure C.36c T_g of polymer **P6** obtained by DMA..... 220

Figure C.37 DMA analysis of polymer **P1**..... 221

Figure C.38 DMA analysis of polymer **P3**..... 221

Figure C.39 DMA analysis of polymer **P4**..... 222

Figure C.40 DMA analysis of polymer **P5**..... 222

Figure C.41 DMA analysis of polymer **P2^{75}P4^{25}**..... 223

Figure C.42 DMA analysis of polymer **P2^{50}P4^{50}**..... 223

Figure C.43 DMA analysis of polymer **P2^{25}P4^{75}**..... 224

Figure C.44 DMA analysis of polymer **P2^{68}P5^{32}**..... 224

Figure C.45 DMA analysis of polymer **P2^{44}P5^{56}**. 225

Figure C.46 DMA analysis of polymer **P2^{15}P5^{85}**. 225

Figure C.47 DMA analysis of polymer **P2***, which has same repeat unit and similar M_n as **P2**, but synthesized using the Ni-based catalyst *trans*-[Ni(C_6F_5)$_2$($SbPh_3$)$_2$]. The T_g defined by tan δ is averaged as 241 °C by two individual tests, which is about 30 °C higher than that of **P2** (209 °C). 226

Figure C.48 DMA analysis of polymer **P3***, which has same repeat unit and similar M_n as **P3**, but synthesized using the Ni-based catalyst *trans*-[Ni(C_6F_5)$_2$($SbPh_3$)$_2$]. The T_g defined by tan δ is averaged as 194 °C by two individual tests, which is about 4 °C higher than that of **P3** (190 °C). Since **M3** contains tricyclopentadiene impurities, here the difference between T_g of **P3** and **P3*** was hypothesized to be diminished by some degree of crosslinking..... 227

Figure C.49 DMA analysis of polymer **P4***, which has same repeat unit and similar M_n as **P4**, but synthesized using the Ni-based catalyst *trans*-[Ni(C_6F_5)$_2$($SbPh_3$)$_2$]. The T_g defined by tan δ is averaged as 133 °C by two individual tests, which is about 14 °C higher than that of **P4** (119 °C). 228

Figure C.50 ^{1}H NMR spectrum of **P2** after melt extrusion. A small set of new peak appear around 5.3 ppm (enlarged in blue square). These NMR signal correlate well with those found by Boydston and coworkers who showed that mechanical activation of APNB may lead to vinyl species following norbornyl ring-opening..... 229

Figure C.51 GPC trace of **P2** before (blue curve) and after (red curve) melt extrusion..... 229

Figure C.52 DMA analysis of polymer **P2** before (blue curve) and after (red curve) melt extrusion. The averaged T_g over triplicate data points before and after are 209 °C and 205 °C, respectively. The deviation is ~2%. 230

Figure C.53 DMA analysis of polymer **P2** before (dark blue curve of storage modulus E' and light blue curve of loss modulus E'') and after (red curve of storage modulus E' and pink curve of loss modulus E'') melt extrusion. Before melt extrusion: E'(100 °C) = 0.49 GPa, E'' (100 °C) = 0.031 GPa; after melt extrusion: E'(100 °C) = 0.32 GPa, E'' (100 °C) = 0.027 GPa. 231

Figure C.54 Cyclic loading (three cycles) stress-strain curve of polymer **P2**. 232

Figure C.55 The influence of M_n on the T_g of polymer **P2**. Blue symbols represent experimental data obtained for polymers with a M_n of 64, 84, 170, 207 kDa, respectively. The black curve represents the T_g predicted by the Flory-Fox equation. Red symbols in the box represent the deviation of experimental data from the predicted $T_{g,\infty}$. 232

Figure C.56 The influence of M_n on the T_g of polymer **P4**. Blue symbols represent the experimental data obtained for polymers with a M_n of 92, 97, 129 kDa, respectively. The black curve represents the T_g predicted by the Flory-Fox equation. Red symbols in the box represent the deviation of experimental data from the predicted $T_{g,\infty}$. Both **Figures S73** and **S74** supported our hypothesis that in the molecular weight range studied, that the T_g of the polymer is asymptotic approaching to the $T_{g,\infty}$, and thus molecular weight effect is neglected in the rest comparison and analysis. 233

Figure C.57 WAXS data for polymer films of **P3** and **P4**, no crystalline peak was detected, indicating amorphous polymers. 234

Chapter 1 Polynorbornenes for Advanced Applications and Processes

A version of sections 1.2-1.4 was originally published by Xinyi Wang‡, Trevor J. Wilson‡, Dmitry Alentiev, Maria Gringolts, Eugene Finkelshtein, Maxim Bermeshev* and Brian K. Long*: "Substituted polynorbornene membranes: a modular template for targeted gas separations" Polymer Chemistry **2021**, *12* (20), 2947-2977.

Xinyi Wang was responsible for surveying the literature, drafting sections 2 and 8, editing, and formatting the manuscript. Trevor J. Wilson was responsible for drafting section 1, generating figures and schemes for sections 1-2, editing, and formatting the manuscript. Dmitry Alentiev, Maria Gringolts, and Eugene Finkelshtein were responsible for surveying the literature, drafting sections 3-7, and editing the manuscript. Dr. Maxim Bermeshev and Dr. Brian K. Long advised this work and aided in the preparation of the manuscript.

1.1 Polynorbornene Origins and Advanced Applications Thereof

Norbornene monomers are typically synthesized via reaction of cyclopentadiene with a corresponding dienophile, both of which are often readily available from petroleum-based resource. In a market analysis, the global 2-norbornene market was quoted at $440.9 million (USD) in 2020 and is estimated to reach USD $470.4 million by the end of 2026, with more than 97% of the products being used int the synthesis of cyclic olefin (co)polymer (COC or COP).[1] Depending on the polymer type, and by appending various side-chains and functional groups, these polymers can display myriad properties, such as high vibration absorption capability,[2] high grip performance,[2] high thermal, chemical, and oxidative stability,[3] low birefringence,[4] low dielectric constant,[5, 6] and low moisture absorbance.[7, 8] These properties make polynorbornenes suitable for a variety of advanced applications, including high-performance tires,[2, 9] oil spill recovery

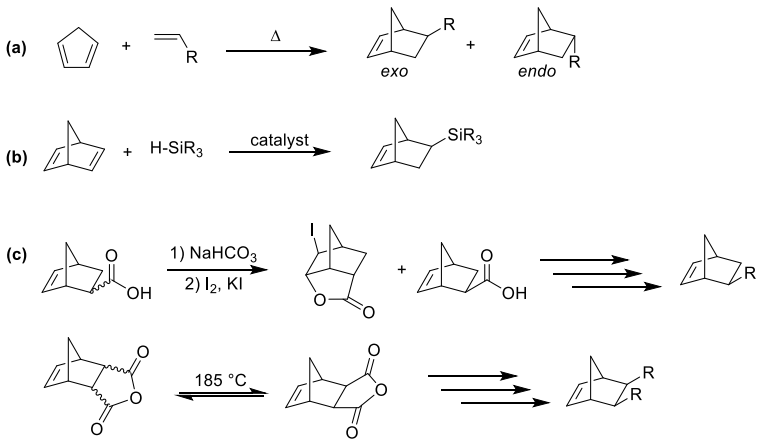
elastomer,[9] dental and orthopedic devices,[2] gas separations,[3, 10-12] pervaporation membranes,[13] ion-exchange membranes,[14, 15] high-frequency interconnects,[16] and nonlinear-optical devices.[4, 9]

1.2 General Synthesis and Characteristics of Norbornene-Based Monomers and Polymers

Norbornene is a bicyclic hydrocarbon-based monomer that consists of a cyclohexene ring bridged with a methylene group connecting the 1st and 4th carbons. As a monomer, the norbornyl moiety offers several key advantages: 1) the relative ease of monomer synthesis via cycloaddition facilitates the synthesis of norbornyl monomers with a wide range of appended side-chains and functionalities, 2) the strained bicyclic olefin can be polymerized through several mechanisms, and 3) a variety of thermomechanical properties may be obtained by employing various polymerization mechanisms, which is heavily dictated by the resultant polymer backbone structure accessed.

The most convenient and straight-forward synthetic route to substituted norbornyl monomers involves the prototypical [4π + 2π] cycloaddition between a diene and a dienophile, more commonly known as a Diels-Alder reaction (Scheme 1.1a). These reactions provide the unique [2.2.1]bicyclic structure of norbornene-derivatives in a single step, and can often be performed on a multi-gram-scale in moderate to excellent yields. However, the synthesis of substituted norbornenes via Diels-Alder reaction typically provides a mixture of *exo*- and *endo*-substituted isomers that have differential polymerization reactivity, with the former often showing higher reactivity, regardless of polymerization mechanism.[16-21] In addition to the formation of *endo*- and *exo*- diastereomers, a mixture of 5- and 6-substituted enantiomers are also spontaneously formed in the case of mono-substituted norbornene monomers. Thus, the monomer obtained via the Diels-Alder route is typically a mixture of 4 different isomers.

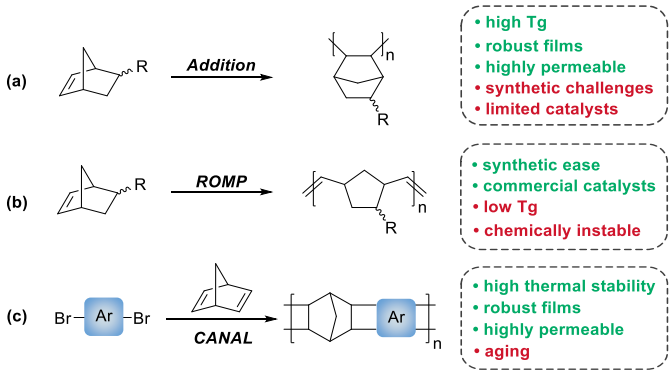
To obviate the reactivity differences of *exo*- and *endo*-substituted isomers (Scheme 1.1a), pure *exo*-substituted norbornenes have been synthesized via stereoselective catalytic transformation of norbornadiene (Scheme 1.1b).[22-24] In addition, pure *exo*-norbornene carboxylic acid and *exo*-norbornene dicarboxylic anhydride can be separated via iodolactionization or thermal isomerization, and with sequential reactions, both mono- and di-substituted *exo*-norbornene can be synthesized (Scheme 1.1c).



Scheme 1.1 Representative synthetic routes to various substituted norbornene monomers.

Norbornene-based monomers may be polymerized through a variety of mechanisms. These include radical, ionic, ring-opening metathesis polymerization (ROMP), addition polymerization (AP), and catalytic arene-norbornene annulation (CANAL). While radical and ionic polymerizations of norbornene derivatives have been reported, these mechanisms tend to produce ill-defined oligomers that are poorly suited for membrane fabrication.[25-29] As such, most PNB membrane literature is focused on materials synthesized through AP, and ROMP (Scheme 1.2a and 1.2b, respectively). An additional and more recently developed polymerization technique has

been the advent of CANAL, which yields ladder type structures that demonstrate high thermal stability, high BET surface areas, and promising gas transport properties (Scheme 1.2c).[30-32]



Scheme 1.2 Polymerization methods that are applicable to norbornene-based polymers.

While all PNB materials are derived from related norbornyl monomers, the final polymers display markedly different bulk properties. For example, PNBs synthesized through ROMP, which we will refer to as metathesis PNBs (MPNBs), tend to have significantly lower T_g's, lower T_d's, lower gas permeabilities, exhibit greater main chain flexibility, and are prone to oxidation along the residual backbone olefin making them less chemically stable. In many cases, the unsaturated backbone is hydrogenated to impart greater chemical stability. However, these main chain olefins have also been used as reactive handles for intentional post-polymerization modifications (PPM). While the material properties of MPNBs are less attractive than their AP counterparts, their synthesis is well-established with many commercial ROMP catalysts available. Most notable of which are the ruthenium centered Grubbs, and molybdenum-based Schrock catalysts that exhibit rapid polymerization kinetics (Figure 1.1a-c), and are less prone to substrate stereochemistry and substituent incompatibilities relative to most AP catalysts. In contrast to the material limitations

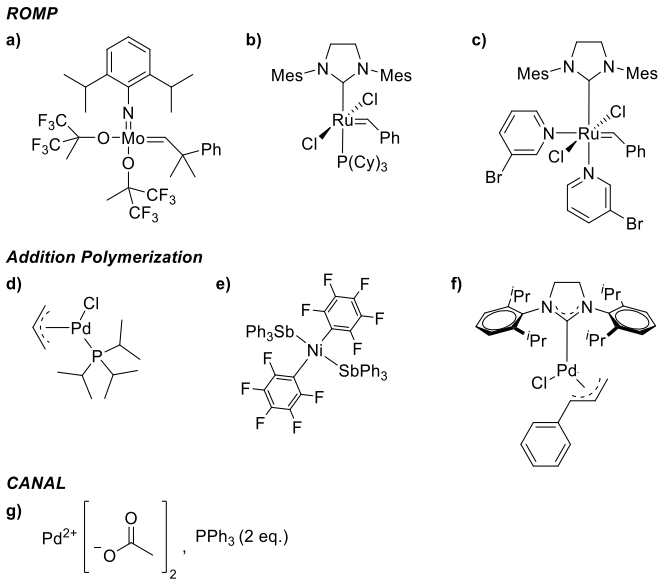


Figure 1.1 Representative catalyst examples used in polynorbornene synthesis. Reprinted with permission from Reference [33]. Copyright 2021 The Royal Society of Chemistry.

of MPNBs, addition polynorbornenes (APNBs) tend to display high thermal stability, higher gas permeabilities, better mechanical integrity, and are more chemically inert than their MPNB counterparts due to their rigid, saturated polymer backbone. Additionally, APNBs frequently display higher T_g's due to the retention of the rigid bicyclic norbornane motif along the polymer backbone. While APNBs have more attractive thermal and mechanical properties, they are synthetically more challenging to access. Many AP catalysts capable of polymerizing unsubstituted norbornene exhibit poor tolerance to polar and/or heteroatom-functionalized monomers. Recent successes in catalyst screening and development have enabled access to a wide range of polar and heteroatom functionalized APNBs.[11, 13, 34-39] A select few of these catalysts are shown in (Figure 1.1d-f).

Polymers synthesized through CANAL are among the newest norbornene derived materials to be applied to gaseous separations. Since the seminal report by Xia and coworkers in 2014,[31] a variety of CANAL derived materials have been synthesized.[30, 32, 34, 40] These materials exhibit robust mechanical properties and high thermal stabilities. These properties are likely due to the highly rigid backbone structure provided by the retention of the bicyclic norbornane motif and the planar arene fragments that constitute the backbone repeat unit. In the initial synthetic report of CANAL polymers, Xia and coworkers demonstrated that the highest conversions were achieved using $Pd(OAc)_2$ in the presence of two equivalents of triphenyl phosphine (Figure 1.1g). While other ligands were investigated, no other system was capable of granting comparable yields as those seen with the triphenyl phosphine system (>98%).[31]

As mentioned, the inherently modular nature of norbornyl-based monomers, presence of multiple chiral centers, and varieties of available polymerization methods make it a suitable candidate to study the structure-property relationship. In the following chapter, its performance

when applied as gas separation membranes will be chosen as an example to elucidate this relationship. Specifically, the ability to easily alter monomeric substituents enables researchers to design materials that take advantage of noncovalent polymer-gas interactions without changing the commonality of the polymer backbone. In addition to the tunability of substituent chemistry, careful catalyst selection can afford structurally distinct backbone architectures and/or tacticity by controlling the mechanism through which the polymerization propagates.[22, 41-44] The combination of both advantages also helps us to access block copolymers with microphase separation, which allows us to investigate the influence of that on gas transportation properties.

1.3 Gas Separation Performance and Gas Transport Theory in Dense Polymeric Membranes

As previously mentioned, one of the most promising applications of PNBs is their use as gas separation membranes.[3, 10-12] The development of membrane-mediated gas separation technology has been the focus of extensive academic and industrial research efforts for many decades. As shown in Figure 1.2, these systems utilize thin polymer films that preferentially permeate one gaseous species over another, enriching the downstream in the more permeable species. Membrane systems are an attractive alternative to conventional separations due to their low energy requirements, small footprint, and mechanical simplicity.[45] This technology has matured rapidly and has been successfully applied to several notable industrial separations such as: hydrogen recovery, nitrogen production, natural gas processing, and industrial vapor recovery.[46]

Permeability (P) and selectivity (α) are frequently used to benchmark membrane performance and can be plotted on a log-log plot of ideal selectivity versus permeability, as is shown in Figures 1.3 and 1.4. Generally, attempts to increase membrane permeability via chemical

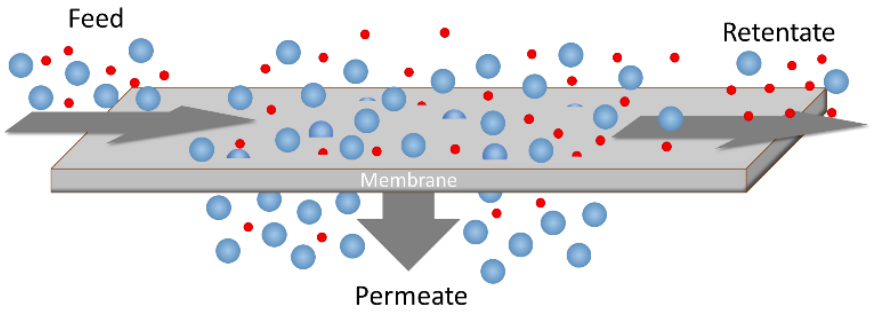


Figure 1.2 Schematic representation of a membrane driven gas separations. Reprinted with permission from Reference [33]. Copyright 2021 The Royal Society of Chemistry.

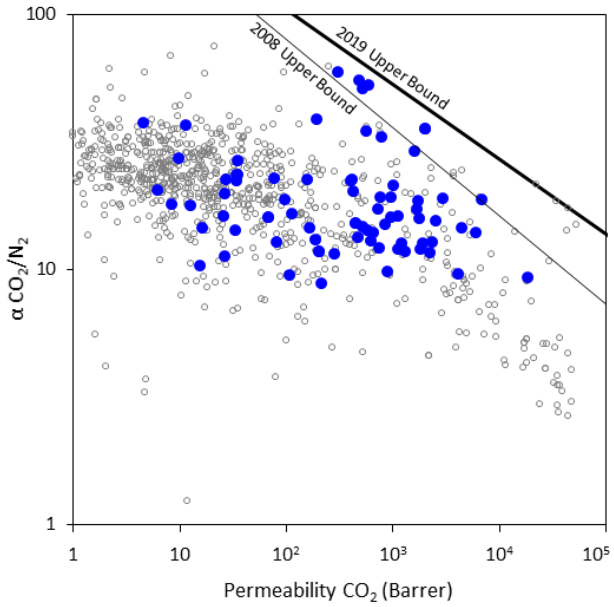


Figure 1.3 Robeson plot[47, 48] of CO_2/N_2 separation performance for a breadth of previously reported non-norbornene-based materials (open gray), and norbornene-based materials described herein (blue). Reprinted with permission from Reference [33]. Copyright 2021 The Royal Society of Chemistry.

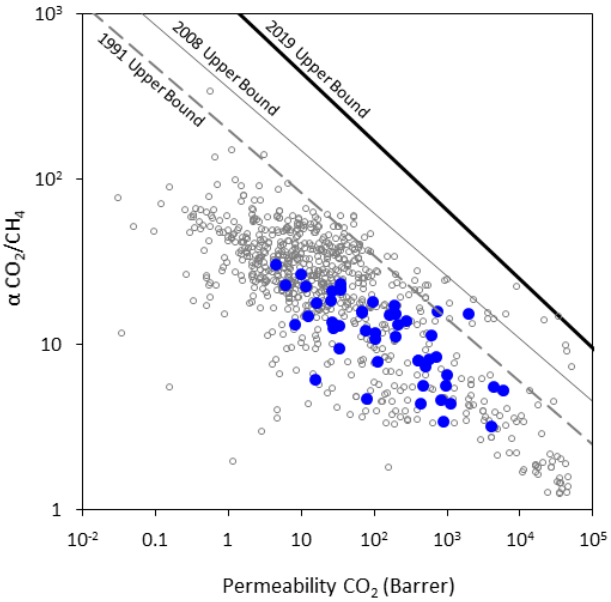


Figure 1.4 Robeson plot[47-49] showing CO_2/CH_4 separation performance for a breadth of previously reported non-norbornene-based materials (open gray), and norbornene-based materials described herein (blue). Reprinted with permission from Reference [33]. Copyright 2021 The Royal Society of Chemistry.

modification of the membrane material are met with a proportional decrease in selectivity, and *vice-versa.* This problematic behavior is referred to as the permeability-selectivity tradeoff and has made the realization of membranes that are both high permeability and high selectivity a challenging endeavor.

Within the membrane community, the solution-diffusion model is frequently used to describe mass transport in dense polymeric membranes.[46, 50-57] According to this model; as a pressure differential is applied across a membrane, penetrant molecules sorb into the upstream side of the membrane, diffuse through the polymer matrix down a chemical potential gradient, then desorb into the downstream side of the membrane. Thus, for a given penetrant molecule "A", the overall permeability (P_A) can be expressed as the product of its solubility coefficient (S_A) and its diffusivity coefficient (D_A) according to:

$$P_A = S_A \cdot D_A$$

The ratio of permeabilities of gas A over gas B is defined as the ideal selectivity ($\propto_{A/B}$), where by convention, gas A is the faster permeating gas, as shown below:

$$\alpha_{A/B} = \frac{P_A}{P_B}$$

1.4 Performance of Organosilicon Containing MPNBs and APNBs as Gas Separation Membranes

Various PNBs have been investigated for their gas separation properties, including PNBs bearing organosilicon, fluorine, hydrocarbon, aromatic biphenyl fragments, and rigid ladder type sidechains, as well as a new class of ladder type polymers synthesized through annulation reactions between norbornadiene and haloarenes. Post polymerization modification (PPM), and NB-based

composites have also been studied. However, in the Long Research Group, we focus heavily on the development of PNBs bearing organosilicon containing substituents for membrane-based gas separations.

The incorporation of pendant silicon containing substituents onto PNBs has become an increasingly common synthetic trope in recent literature.[11, 22, 23, 42, 44, 53, 58, 59] This is particularly true for membranes designed to target CO_2/N_2 separation and hydrocarbon separations where the gases of interest are the more condensable component. This strategy was initially inspired by silicone rubbers, such as polydimethylsiloxane (PDMS), whose gas transport properties obey solubility-controlled selectivity, or "reverse selectivity", for hydrocarbon gases. For these materials, the higher molecular weight hydrocarbons, such as propane and butane, are more permeable than lighter hydrocarbons (e.g. methane), and thus valuable heavy hydrocarbon petrochemical precursors can be separated in higher flux.

Despite their desirable transport properties, silicone rubbers are often crosslinked to achieve good film forming properties, which limits their processability for practical membrane applications. It was found that affixing organosilicon pendant chains to a glassy polymer backbone, such as APNB, not only imbues the material with drastically increased gas permeability, but in some cases retains the solubility-controlled selectivity that is observed when using rubbery PDMS, which is rarely for observed for other high T_g glassy polymers.[41, 42, 44, 53, 60-62] In the last five years, a host of materials bearing various silicon containing substituents have been synthesized and their gas transport properties studied in-depth. This section is not intended to exhaustively review these materials, but rather to provide a select perspective regarding recent developments in the field of silicon containing MPNB and APNB materials.

1.4.1 MPNBs Bearing Organosilicon Substituents

The synthetic ease of ROMP chemistry has facilitated the synthesis of a wide variety of organosilicon functionalized MPNBs. Among the earliest materials of this type to be applied to gas separation membranes were trimethylsilyl functionalized MPNBs. It was found that nearly an order of magnitude increase in gas permeability was achieved by introducing a single trimethylsilyl substituent per repeat unit relative to unsubstituted MPNB (**1.2** vs. **1.1**, Table 1.1).[63-67] Subsequent studies replacing these methyl groups with other aryl, alkyl or alkylsilyl groups, such as Ph (**1.3**), *i*-Pr (**1.4**), or CH_2SiMe_3 (**1.5**), typically resulted in reduced gas permeabilities.[67-69]

Introduction of additional trimethylsilyl groups, as well as varying the relative position of the trimethylsilyl substituents, has been studied for MPNBs (**1.11**, **1.12)**, with a marked 3-4-fold increase in gas permeability coefficients was observed.[63, 66, 67] The most pronounced effects were observed when these groups were *trans*-vicinal to one another (**1.11**) while geminal-substituted analogues experienced this to a lesser effect (**1.12**).[63, 66, 67, 69] Many of these studies, such as those describing polymers (**1.3**-**1.7)** and (**1.11**-**1.12**), were discussed in a previous review and will not be discussed in detail here.[69, 70]

The *exo*-/*endo*-orientation of the monomers used also strongly influences the gas permeability of MPNB bearing $SiMe_3$ groups (**1.2**). The permeability of ***exo*-1.2**, which was synthesized from the pure *exo*-monomer isomer, turned out 1.5–2 fold higher than that of **1.2** that contains a mixture of *exo*- and *endo*-isomers (Table 1.1).[22] This effect is explained by the difference in microstructure between the polymer chains forming from *exo*- and *endo*-isomers of the initial monomer. The chains formed from the *endo*-isomer are believed to pack with less free volume than the chains formed from *exo*-isomer.[22]

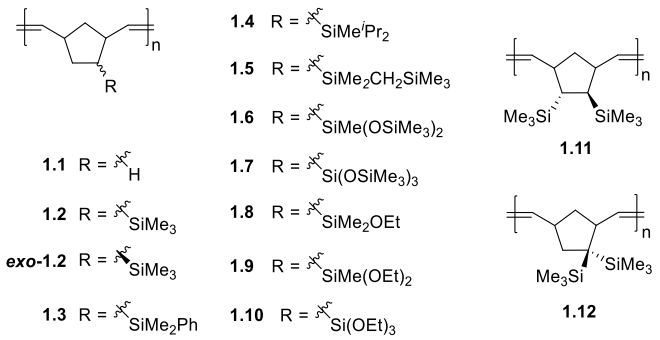


Figure 1.5 Metathesis polynorbornenes (MPNBs) bearing organosilicon substituents. Reprinted with permission from Reference [33]. Copyright 2021 The Royal Society of Chemistry.

Table 1.1 Gas transport properties of metathesis polynorbornenes (MPNBs) bearing organosilicon substituents.

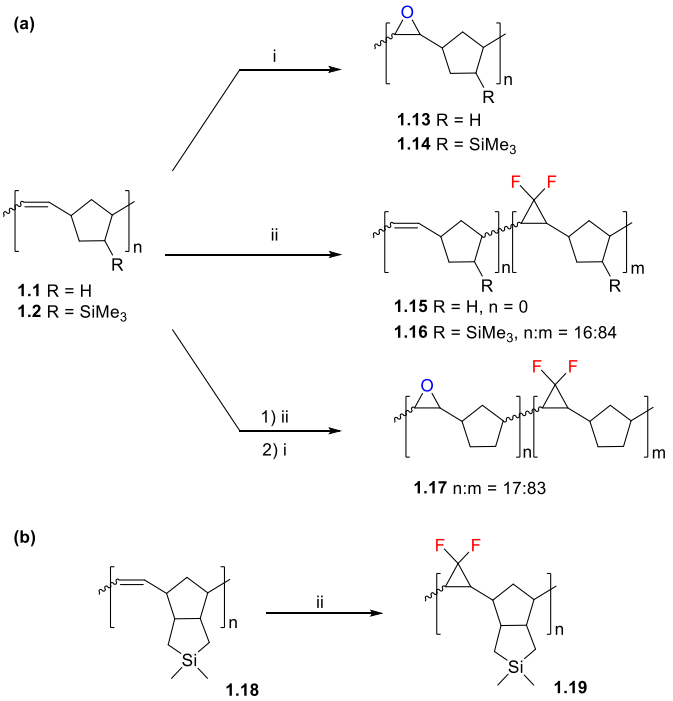
Polymer	*P* (Barrer)							$\alpha_{ij} = P_i/P_j$				Ref.
	N_2	O_2	CO_2	CH_4	C_2H_6	C_3H_8	C_4H_{10}	O_2/N_2	CO_2/CH_4	CO_2/N_2	C_4H_{10}/CH_4	
1.1	1.5	2.8	15.4	2.5	-	-	-	1.9	6.3	10.3	-	[64]
1.2	4.2	16.9	63.4	7.3	-	-	-	4.0	8.7		-	[63]
1.2	-	-	-	-	11.1	3.2	-	-	-	-	-	[44]
***exo*-1.2**	7.1	28	118	17	-	-	-	-	6.9	16.6	-	[22]
1.8	-	-	-	1.4	-	1.0	10.2	-	-	-	7.4	[44]
1.9	-	-	-	13.3	-	12.8	75.1	-	-	-	5.7	[44]
1.10	-	-	-	97.7	-	241.8	2099.8	-	-	-	21.5	[44]

The highly flexible siloxane (-Si-O-Si-) linkage is also hypothesized to be a key structural feature responsible for the high gas diffusion seen in PDMS, as it potentially contributes tolarger free volumes combined with rapid segmental chain dynamics.[71, 72] This segmental chain motion is of key importance in the formation of transient inter-chain gaps believed to govern gaseous diffusion through dense polymer matrices. Inspired by this structure-property relationship, a variety of siloxane functionalized MPNBs, such as **1.6** and **1.7**, have been developed and their gas transport properties studied in-depth and discussed in a recent review.[72] Generally, their gas permeability increased for all tested gases without significant decrease in ideal selectivity.

Inspired by the exceptional permeabilities and selectivities seen in polymers bearing siloxane moieties for a variety of gas pairs, it was hypothesized that incorporation of alkoxysilane (Si-O-C) fragments may also improve membrane performance relative to polymers bearing trimethylsilyl substituents. One report by Sundell, Lawrence and coworkers revealed such improvements in a series of MPNBs (**1.2**, **1.8**-**1.10**).[44] This systematic investigation incrementally replaced the methyl groups in the MPNB (**1.2**) with one, two, and three ethoxy groups (**1.8, 1.9,** and **1.10** respectively). This structural perturbation increased C_4H_{10}/CH_4 selectivity from $\alpha = 5.7$ to $\alpha = 21.5$ without significantly compromising permeability. In the case of **1.10**, CH_4 permeability increased by 5-fold compared to MPNB **1.2**.[44] This initial study revealed that MPNBs **1.8-1.10** exhibit solubility-controlled separation for light hydrocarbon gases,[44] which is believed to originate from their flexible alkoxysilyl substituents. These characteristics make them particularly well suited for the separation of gaseous hydrocarbons, while the presence of the ethoxysilyl moieties also enables them to be crosslinked through sol-gel chemistry under milder conditions via exposure to ambient conditions and adventitious humidity. [44, 73] The obtained crosslinked film

showed improve stability over time (Selectivity did not change up to 800 psi),[44] as well as potentially further enhanced diffusivity selectivity.

Lastly, it should be noted that the double bond embedded within the backbone of MPNBs may also be subjected to PPM, which may improve their stability over time or improve their performance in some cases. There are examples of MPNB backbone double bonds modified by hydrogenation,[71, 74, 75] sulfonation,[76, 77] bromination,[78-80] epoxidation,[79, 81, 82] catalytic dihydroxylation,[83] cycloaddition reaction,[84] thiol-ene chemistry,[85] etc. Nevertheless, only hydrogenation,[71, 74, 75] epoxidation, and *gem*-difluorocyclopropanation[86-88] have been used as a means of tuning gas-transport properties of MPNBs (Scheme 1.3).



Scheme 1.3 a) Epoxidation and gem-difluorocyclopropanation of double bonds along the backbone of MPNBs 1.1 and 1.2[87, 89] and b) poly(4,4-dimethyltricyclo[5.2.1.02,6]-4-siladec-8-ene).[88] Conditions: i) m-chloroperbenzoic acid; ii) sodium chlorodifluoroacetate, Δ.

Most often, MPNBs are hydrogenated to obviate oxidation reactions that compromise the chemical stability of unsaturated MPNBs. Exhaustive hydrogenation of MPNBs is generally performed via diimide reduction, which is generated in situ from *p*-toluenesulfonylhydrazide,[71, 74, 75, 90] or by using hydrogen over Ru- or Pd-catalysts.[90, 91] The effect of hydrogenation on the gas permeability of MPNBs has been described in previous reviews,[69, 70] and in most cases it has been found to lead to a slight decrease in permeability coefficients.

The main goal of epoxidation and *gem*-difluorocyclopropanation of MPNBs was to increase the rigidity of the polymer backbone, which would hypothetically result in higher gas permeability. Epoxidation of MPNBs was carried out using *m*-chloroperbenzoic acid though some degradation of the MPNBs was observed, which was more prevalent when using chloroform as a solvent than toluene.[89] However, careful selection of reaction conditions resulted in the exhaustive epoxidation of double bonds to yield polymers **1.13-1.14**. *Gem*-difluorocyclopropanation of MPNBs was performed by using difluorocarbene, which was generated in situ. The presence of bulky trimethylsilyl (-$SiMe_3$) substituents in MPNBs (e.g. **1.2**, Scheme 1.3) significantly reduced the rate of both epoxidation and difluorocyclopropanation of the double bonds. In the case of difluorocyclopropanation of **1.2**, it was impossible to modify all double bonds with polymer **1.16** reaching ~84% conversion to the difluorocyclopropanated form.[87] The authors attributed the lower activity of double bonds in MPNB **1.2** to steric shielding by the trimethylsilyl substituents.[87] Indeed, it was found that moving the silicon-containing fragment away from the double bond in silacyclopentane-containing MPNB **1.18** yielded complete difluorocyclopropanation of the double bonds to produce polymer **1.19** (Scheme 1.3b).[88] It should be noted that polymer **1.19** is the first reported PNB with both silicon- and fluorine-containing substituents.

Gas permeation testing revealed that epoxidized (**1.13**) and difluorocyclopropanated (**1.15**) MPNBs exhibited opposite behaviors in regard to gas permeability, as compared to the native unsaturated MPNB **1.1** (Table 1.2). For example, the permeability coefficients of epoxidized polymers **1.13** and **1.14** were much lower across all gases tested than **1.1** and **1.2**. This decrease in permeability was accompanied by a more significant decrease in diffusion coefficients than was observed for solubility coefficients. The only exception was the $S(CO_2)$, which increased after epoxidation. In contrast, *gem*-difluorocyclopropanation resulted in a significant increase in gas permeability for polymers **1.15**, **1.16** and **1.19**. This was attributed to the increase in solubility coefficients (especially, in the case of CO_2), while the diffusion coefficients did not change significantly.[87] Similar to epoxidized MPNBs, the effect of *gem*- difluorocyclopropanation on gas permeability was less pronounced in the case of the more permeable silicon-substituted MPNBs. Interestingly, this series (**1.1**, **1.15**, **1.16**) did not obey typical permeability-selectivity trade-off behavior (Table 1.2). Moreover, the ideal selectivity for gas pairs containing CH_4 increased after difluorocyclopropanation, which is consistent with previous observations that fluorine-containing polymers may have increased ideal selectivity for separations involving CH_4.[92]

An interesting result was observed for a polymer **1.17**, which contains both epoxidized and difluorocyclopropanated monomer units (Table 1.2).[87] Dual modification of MPNB led to a simultaneous increase in selectivity and permeability, and the resulting "copolymer" possessed the highest $S(CO_2)$ value among its analogues (**1.1**, **1.13**, **1.15**). This was hypothesized to result due to the combination of increased gas permeability arising from the presence of CF_2 units, as well as increased CO_2 solubility arising from the epoxy groups present. These modified polymers demonstrated reasonably high thermal stability, good mechanical properties, and better storage stability under ambient conditions, as compared to films of unmodified MPNB **1.1**.[87]

Table 1.2 Gas transport properties of epoxidated and *gem*-difluorocyclopropanated MPNBs.

	T_g	P (Barrer)				$\alpha_{ij} = P_i/P_j$				$D(O_2) \times 10^8$		S (cm^3 (STP) m^{-3} atm^{-1})		
Polymer	(°C)	O_2	N_2	CO_2	CH_4	O_2/N_2	CO_2/N_2	CO_2/CH_4	D_{CO2}/D_{N2}	(cm^2s^{-1})	S_{CO2}/S_{N2}	O_2	CO_2	Ref.
1.1	41	2.3	0.43	9.3	0.78	5.2	21	12	1.5	12.8	14	0.14	1.3	[86]
1.2	103	34	8.3	140	19	4.1	17	7.4	1.4	57	12	0.45	3.6	[86]
1.13	64	0.2	0.03	1.1	0.04	6.8	35	26	1.1	2.1	31	0.08	2.4	[86]
1.14	118	10	2.2	47	4.2	4.7	22	11	0.8	22	23	0.36	5.2	[86]
1.15	94	5.1	1.1	23.1	1.5	4.6	21	15	1.1	11.5	20	0.34	4.4	[87]
1.16	117	44	11	217	21	4.0	20	10	1.2	56.5	17	0.60	6.6	[87]
1.17	90	3.3	0.64	13.8	0.77	5.2	22	18	0.8	6.7	27	0.37	5.6	[87]
1.18	111	5.7	1.2	24	2.5	4.8	20	9.7	1.4	17.8	14	0.24	2.1	[88]
1.19	171	26	9.2	115	13.5	2.8	13	8.5	0.7	26.2	18	0.75	8.8	[88]

1.4.2 APNBs Bearing Organosilicon Substituents

The synthesis of homo-APNBs bearing organosilicon substituents has proven a greater synthetic challenge than those synthesized via ROMP. This is primarily due to the poor tolerance of many AP catalysts to polar and/or heteroatom functionalized monomers. In recent literature, considerable progress has been made addressing this synthetic limitation, and several catalysts are now known to polymerize polar and/or heteroatom functionalized monomers through AP. [11, 36, 41, 42, 44, 53, 59, 62, 93] Alternatively, copolymerization with unsubstituted NB has been used to achieve polymers of sufficient molecular weight for film formation when homopolymerization has proven challenging.[94] However, this approach is becoming less common as the availability of tolerant catalysts continues to increase. Though these synthetic challenges have limited studies of APNB in the past, the permeability of these polymers is typically several folds higher than their ROMP analogues without compromising selectivity, which makes them promising candidates for commercial membrane applications.

Initial studies on APNBs revealed that the permeability coefficients of trimethylsilyl-substituted APNB (**1.21**, Figure 1.6) increased several-fold as compared to unfunctionalized PNB (**1.20**). Interestingly, the difference in permeability between ***exo*-1.21** (Table 1.3) and **1.21**, which is produced from a mixture of *exo*-/*endo*-monomer isomers, is significantly less than the analogous difference in the case of metathesis polymers (**1.2** vs. ***exo*-1.2**, Table 1.1). This is hypothesized to arise as the APNB **1.21** is enriched in the *exo*-monomer isomer due to the low addition polymerization reactivity of the *endo*-isomer, whereas the metathesis polymerization of *exo*-/*endo*-monomers mixtures frequently contain *endo*-isomer contents that are more similar to that of the initial monomer feed.[22] Nonetheless, the resultant gas selectivities of trimethylsilyl-substituted APNBs **1.21** and ***exo*-1.21** were not high enough to draw near the upper bound for a variety gas

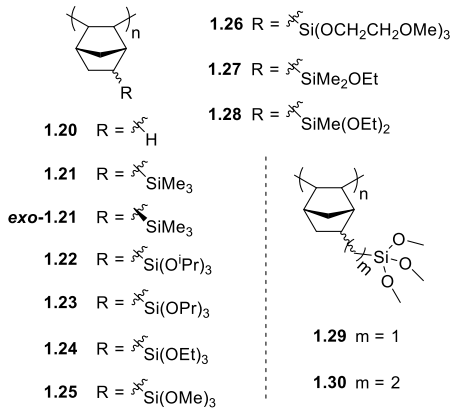


Figure 1.6 Addition polynorbornenes (APNBs) and bearing organosilicon substituents. Reprinted with permission from Reference [33]. Copyright 2021 The Royal Society of Chemistry.

Table 1.3 Gas transport properties of addition polynorbornenes (APNBs) bearing organosilicon substituents.

Polymer	*P* (Barrer)							$\alpha_{ij} = P_i/P_j$				Ref.
	N_2	O_2	CO_2	CH_4	C_2H_6	C_3H_8	C_4H_{10}	O_2/N_2	CO_2/CH_4	CO_2/N_2	C_4H_{10}/CH_4	
1.20	1.5	6.9	33.6	2.6	-	-	-	4.6	12.9	22.4	-	[61]
1.21	297	780	4350	790	1430	1740	17500	2.6	5.5	14.6	-	[61]
1.21	-	-	-	678.9	-	856.4	7040.7	-	-	-	8.22	[44]
***exo*-1.21**	430	1100	5500	1100	1600	1800	15200	2.5	5.0	12.7	14.2	[22]
1.22	90	-	1120	-	-	-	-	-	-	12	-	[53]
1.23	47	-	650	-	-	-	-	-	-	14	-	[53]
1.24	57	-	940	-	-	-	-	-	-	16	-	[53]
1.24	-	-	-	176.2	-	499.1	3837.6	-	-	-	21.8	[44]
1.25	56	-	1600	-	-	-	-	-	-	29	-	[53]
1.29	23	-	770	-	-	-	-	-	-	33	-	[53]
1.30	16	-	560	-	-	-	-	-	-	35	-	[53]
1.26	21	-	755	-	-	-	-	-	-	36	-	12
1.27	-	-	-	57.7	-	112.7	1620.9	-	-	-	28.1	[44]
1.28	-	-	-	49.0	-	100.1	1104.3	-	-	-	22.5	[44]

pairs, and improvements are required before reaching industrial relevance.[61, 67, 95]

It has been proposed that incorporation of siloxane fragments could also improve the APNB membranes selectivity, as was previously observed in MPNBs. Slight perturbations in the structure of alkoxysilyl substituents in various APNBs have been shown to have a strong influence on the CO_2/N_2 and C_4H_{10}/CH_4 transport properties of the resulting membranes (Table 1.3). For example, changes in alkoxysilane branching (**1.22** and **1.23**) and tether length (**1.25**, **1.29** and **1.30**) both led to traditional permeability-selectivity tradeoffs with CO_2/N_2 separation (i.e., from **1.22** to **1.23**, CO_2 permeability decreased by 40% while CO_2/N_2 selectivity increased by 16%; from **1.25** to **1.30**, CO_2 permeability decreased by 52% while CO_2/N_2 selectivity increased by 81%). In contrast, changes in alkoxysilane chain-length (**1.23-1.25**) led to a perpendicular approach towards the 2008 upper bound for CO_2/N_2 (for polymers **1.23-1.25**, CO_2 permeability increased by 146% and CO_2/N_2 selectivity increased by 107%).[53]

In another study of APNBs utilized for heavy gas separation, the methyl groups in **1.21** were replaced with one, two, or three ethoxy groups (**1.27, 1.28, and 1.24** respectively). This led to an initial increase in C_4H_{10}/CH_4 selectivity but decrease in permeability as compared to **1.21**. Triethoxysilyl-substituted polymer **1.24** showed that some degree of permeability was restored (C_4H_{10} permeability of 3837 Barrer), albeit with slightly decreased selectivity ($\alpha(C_4H_{10}/CH_4)$ = 21.8).[42, 44, 62] These materials can also be treated with non-solvents, such as lower alcohols, to swell the polymer matrix, increase free volume size, and thus improve membrane performance.[42]

To optimize the CO_2/N_2 separation performance of alkoxysilyl APNBs, previous work in our group proposed that the incorporation of CO_2-philic groups may enhance CO_2 solubility, and therefore overall CO_2 selectivity of these membrane materials. Toward this goal, tris(2-methoxyethoxy)silyl moieties were introduced onto the rigid APNB backbone (**1.26**), with the

hypothesis that this combination would achieve both the advantages of larger free volume induced by frustrated interchain packing, and thus high permeability, as well as favorable interactions between CO_2 and the Lewis basic ether functionalities.[12] Among a series of homo- and copolymers containing this tris(2-methoxyethoxy)silyl-substituent, homopolymer **1.26** displayed the highest performance with a CO_2/N_2 selectivity of 36.7 and CO_2 permeability of 755 Barrer, achieving a near vertical increase in performance on the CO_2/N_2 upper bound plot relatively to homopolymer **1.24** and their copolymers in between. Following mechanism studies revealed that, instead of increasing CO_2 solubility by introducing CO_2-philic moiety as expected, the superior solubility selectivity actually was attributed to large declines in N_2 solubility.[12, 96] Interestingly, a subsequent study using **1.26** revealed that its H_2S/CH_4 separation performance exceeds the 2008 Robeson upper bound for this gas pair, and also possesses moderate CO_2/CH_4 performance. This observation is noteworthy in that most membranes that have good H_2S/CH_4 separation performance often exhibit poor CO_2/CH_4 separation performance, and *vice-versa*. Thus, the high performance of **1.26** makes it a potential promising candidate for dual-purpose natural gas processing membranes.[62]

1.4.3 Comparing MPNB and APNB Gas Separation Performance

In general, APNBs typically have higher permeabilities than their metathesis analogues. This is due in part as most APNBs are glassy materials at room temperature, and therefore possess excess non-equilibrium free volume that often leads to higher permeabilities and may contribute to diffusivity-controlled selectivity (separating gases primarily based upon individual gas diffusivity and differences in kinetic diameters). In contrast, MPNBs are often in their rubbery state at room temperature (with some exceptions that include bulky substituents or relatively more

rigid backbones, such as **1.2**), and often possess smaller free volume, lower overall permeabilities, and solubility-controlled selectivity.

The disparate physical characteristics between MPNBs and APNBs lead to stark differences in gas separation performance, even when comparing APNB and MPNB products with identical substituents. For example, MPNBs **1.8-1.10** bearing alkylsilyl and alkoxysilyl substituents generally show enhanced diffusivity due to self-plasticization and enhancement of gas solubility (especially for hydrocarbons) for polymers containing greater alkoxysilyl content. In contrast, APNBs **1.27-1.28** and **1.24** have the same change in substituents, but display a slightly different trend in performance wherein the more flexible substituents are shown to decrease excess non-equilibrium free volume in the membranes, leading to decreased diffusivity. However, these substituents also enhance gas solubility (especially for hydrocarbons).[44] One of the notable highlights of these organosilicon containing APNBs is that many of them exhibit solubility-controlled selectivity.[41, 44, 97] This desirable separation mechanism, combined with their high gas permeability, makes these membranes promising candidates for commercial gas separation applications.

1.5 Influence of Polymer Chain Packing on Gas Separation Membrane Performance

In addition to what has been discussed in Section 1.4 in which the membrane gas separation performance can be tuned by careful design of polymer chemical structures, researchers noted that the performance is also related to how the polymer chains physically pack even if they have the same chemical compositions. In the following section, common factors that influence polymer

physical chain packing will be discussed including the microphase separation of block copolymers, and tacticity-induced polymer chain packing.

1.5.1 Block Copolymers with Microphase Separation as Gas Separation Membranes

One way to alter the physical chain packing of polymers within a dense matrix is to construct block copolymers that thermodynamically disposed to undergo microphase separation. It is well known that many block copolymers display differing properties, such as thermal and mechanical properties, as compared to their random copolymer analogues, which is often due to the difference in chain packing and arrangement achieved by block copolymers.[98] In fact, previous studies have suggested that microphase separated block copolymers may alter gas transport properties as well.[99-104] Because one of the critical steps in gas transport is the diffusion of gas molecules through the membrane, the different chain packing achieved by random and block copolymers, with or without varying microphase separation, may introduce different pathways for the molecules to permeate through the polymer matrix. Kurata and coworkers were among the first to report gas transport through block copolymers by investigating the *P*, *D*, *S* of polystyrene-*b*-polybutadiene(S-B) block copolymers.[99] Two morphologies were studied, including a sample of polystyrene rods dispersed in a polybutadiene continuous phase, and a sample of alternating lamellae of styrene and butadiene components. They found that the sample with dispersed PS rods is in higher performance than the sample with alternating PS lamellae, and they proposed that the overall *P* and *D* of inert gases in the S-B block copolymer are primarily governed by the rubbery polybutadiene matrix. Two simple models were proposed to demonstrate the gas transportation in the block copolymer – the series and parallel models – as are shown in Figure 1.7. More specifically, the parallel model corelated

well to the experimental data for both morphologies, while the series model only correlated well with the lamellae samples and developed discrepancies when the penetrate molecule size increased. To eliminate the influence of copolymer composition on the block copolymer performance, Cohen and coworkers studied a series of S-B copolymers with the same composition but forming lamellae parallel, perpendicular, and misoriented to the direction of gas permeation.[100, 101] They found that the membrane with lamellae parallel to the gas permeation direction (abbreviated as parallel film in the following discussion) had the highest permeability, and thus, the orientation of the nanodomains is of critical importance to the overall membrane performance. The permeation performance of the parallel film can also be explained by the parallel model, though they proposed that a third interface layer (considered as a S-B random copolymer whose composition varies spatially within the interfacial area) should be introduced between two different lamellae block, and a tortuosity factor τ (considering the imperfect, wavy or crooked pathway for the gases molecules to pass through the membrane) must be taken into consideration.[100] In another semicrystalline diblock copolymer study, it was proposed that the parallel film defined an upper bound and the series film defined a lower bound for the overall diblock lamellae film gas separation performance.[102] Recently, Buonomenna, Golemme and coworkers prepared a series of styrene-*b*-butadiene-*b*-styrene triblock copolymer membranes with constant composition but differing morphologies by manipulating their self-assembly in solution.[103] The highest performance membrane has a hexagonal PS cylinders normal to the membrane surface, with an unexpected ideal CH_4/N_2 selectivity of 7.2, a CH_4 permeability of 41 Barrer, an ideal CO_2/N_2 selectivity of 50, and CO_2 permeability of 289 Barrer. This made this material a good candidate for post-combustion CO_2 capture and suggested that the membrane morphology and chain packing is an important factor to be considered when designing gas separation membranes.

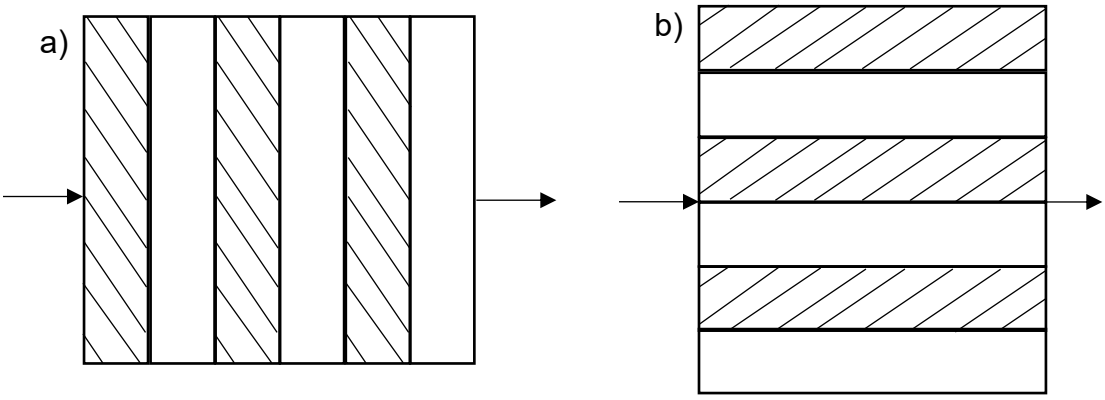


Figure 1.7 Models for the permeation of inert gases through the S-B block copolymers: (a) Series model, (b) Parallel model. Adapted with permission from Reference [99]. Copyright 1977 John Wiley and Sons.

1.5.2 Influence of Polymer Tacticity on Gas Separation Performance

In addition to the differences in gas separation performance that may arise from polymers exhibiting varying chain packing due to the presence of microphase separation, polymer chain packing may also be strongly influenced by the tacticity of the polymer, which can often be varied based upon the catalyst used for polymerization. In the case of unsubstituted APNB, the two-bridge head carbons are stereocenters, and based upon how the norbornyl unit is enchained, may yield tactic polymers. More specifically, when synthesizing a APNB chain, the neighboring repeat units could be enchained so as to form a 2,3-*threo* disyndiotactic configuration, wherein the bridge heads are pointing in the same direction; or a 2,3-erythrodiisotactic configuration, in which the bridge head carbons are pointing in opposite directions, as are shown in Figure 1.8.[105, 106] Similar to other vinyl monomer species, the configuration of APNBs are largely influenced by the catalyst used during the polymerization. Cationic nickel- and palladium-based catalysts are two common classes of late transition metal catalysts used for the synthesis of APNBs. Researchers have tried to investigate the influence of different metal center (Ni or Pd) on the configuration of unsubstituted APNB; however, due to the limited solubility of unsubstituted APNB obtained using many Pd catalysts in common organic solvents (i.e., unsubstituted APNB polymerized by a Ni-based catalyst is soluble in 1,2,4-trichlorobenzene, while that polymerized by a Pd-based catalyst is insoluble, presumably due to the difference in chain packing), the effect of metal catalyst choice on polymer tacticity is difficult to be quantified using traditional methods such as quantitative ^{13}C NMR spectroscopy.[107, 108] Instead, quantative ^{13}C NMR was conducted on two APNBs polymerized via two unique Ni-based catalysts ([(η^3-crotyl)Ni(1,4-COD)]PF_6 and $Ni(dpm)_2/AlEt_3/B(C_6F_5)_3$ system), and differences in the spectra obtained strongly suggest they exhibit different tacticities.[107] To improve polymer solubility, it is common to introduce

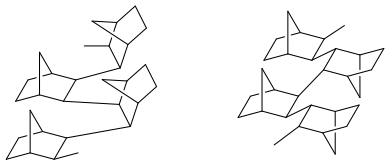


Figure 1.8 Different backbone connectivity of unsubstituted APNBs. Left: 2,3-threo disyndiotactic conformation, and right: 2,3-erythro diisotactic conformation. Adapted with permission from Reference [105]. Copyright 1998 John Wiley and Sons.

substituents onto the norbornyl monomer (e.g. a simple methyl group) to dramatically improve the solubility and the polymers obtained by both Ni- and Pd-based catalysts in common organic solvents such as chloroform.[109] Gas permeation tests have also been performed, and it was revealed that the polymers obtained using Pd-based catalysts are often about twice as permeable for a varieties of gases as analogous polymers obtained using Ni-based catalysts. It was proposed that the APNBs obtained using Pd-based catalysts likely have greater stereoregularity with ~100% 2,3-erythro diisotactic conformation, whereas the APNB obtained using Ni-based catalysts are often atactic with only ~75% 2,3-erythro diisotactic and ~25% 2,3-threo disyndiotactic configurations randomly distributed along the polymer backbone. Simulations suggested that the APNBs obtained by Pd-based catalysts have fewer kinks in the backbone, while those produced by Ni-based catalysts have many kinks in their backbone and are thus packed more tightly, potentially explaining why these polymer membranes are less permeable.[109] It should be noted that in this study, in addition to the backbone tacticity, the introduction of methyl substituents onto the norbornene monomer unit introduces a third chiral center in the monomer (*endo*-/*exo*-isomer), which may also impact the physical chain packing, but is an effect which is hard to differentiate from that which results from polymer backbone tacticity. Additionally, though methyl groups are relatively small and thus may not introduce any significant steric effects, one should still consider the head-to-head effect, which is when methyl groups in two continuous repeat units are next to each other, as compared to the head-to-tail effect, wherein two methyl groups are separated by an unsubstituted CH_2 group on the norbornene ring.

Thus, all of the studies noted above suggest that polymers with widely varying gas separation performance may be created, even with the same polymer composition, by precisely regulating the

PNB's physical chain packing through either a) accessing different phase separation morphologies or b) by synthesizing polymers with controlled tacticity simply by utilizing different catalysts.

1.6 Current limitations of APNB processibility

As previously mentioned, APNBs have been investigated for myriad advanced applications in the academic laboratory. However, fabrication of robust APNB films and other products are typically limited to solution casting due to the proximity of most APNB's decomposition temperature (T_d) to their glass transition temperatures (T_g), resulting in small service windows (T_d - T_g) that prohibit methods such as melt processing. Solution processing usually requires large quantities of organic solvents, which is environment unfriendly, and is largely limited to the production of films and bulk samples that lack complex architectures. In contrast, melt processing is a more commonly used industrial method. Therein, polymers are heated above their T_g for amorphous polymers and complex shapes and form factors may be produced; however, in the case of APNBs, this often results in polymer decomposition due to the proximity of their T_g and T_d. Table 1.4 lists some common APNBs and their T_d, T_g, and corresponding service windows (T_d - T_g).

To address this issue, several companies, such as BFGoodrich and Promerus, have commercialized several APNB derivatives with T_gs well below that of unsubstituted APNB and that may enable melt processing.[4, 5, 8, 110-114] Prior literature reports have also demonstrated that certain functionalized APNBs may also exhibit depressed T_g's while simultaneously maintaining high T_d's,[10, 11, 14-16, 115, 116] and one very recent example has even demonstrated the melt processability of APNBs.[115] However, the overall structure-property relationships between thermal characteristics, and therefore their melt processability, and molecular design are difficult

to infer from current literature due to broad variability in synthetic and thermal characterization methods used.[6, 12, 13, 39, 117-119]

1.7 Research Objectives

In this dissertation, I will present a series of fundamental studies aimed to improve the gas separation membrane performance of APNBs, understand the influence of polymer chain packing and arrangement of MPNBs and APNBs on gas transportation, and improve the processability of APNBs. More specifically, the following research objectives will be discussed:

I. Introduce fluorinated substituents onto alkoxysilane APNBs and evaluate their performance as CO_2/CH_4 gas separation membranes.

II. Construct MPNB block copolymers to study the influence of different microphase separated film morphologies on gas separation performance, as well as synthesize *exo*-dimethyl substituted APNBs to study the influence of different catalysts on polymer backbone tacticity and chain packing.

III. Construct a systematic series of substituted APNBs designed to lower polymer T_g while maintaining high T_d, thus enlarging their service windows to promote APNB melt processability.

As discussed in Section 1.4.2, prior studies revealed that some alkoxysilane APNBs developed by our group possess excellent H_2S/CH_4 separation performance, but with moderate CO_2/CH_4 performance.[62] Previous research also suggests that fluorine-containing polymers may exhibit increased ideal selectivity for separations involving CH_4.[92] Thus, we hypothesized that introducing fluorine content into alkoxysilane APNBs would improve their CO_2/CH_4 selectivity without compromising overall CO_2 permeability. This idea was validated, and the work is detailed

Table 1.4 Gas transport properties of selected addition polynorbornenes (APNBs).

APNB	T_g	T_d	T_d-T_g	Ref.
1.22	344	416	72	[53]
1.23	318	407	89	[53]
1.24	325	380	55	[53]
1.25	365	428	63	[53]
1.29	319	418	99	[53]
1.30	276	427	151	[53]
n-butyl	340	~410	~70	[120]
n-hexyl	265-280	-	-	[10, 120]
n-decyl	150	-	-	[10, 108]
4-phenyl butyl	148	353	205	16
Dicarboxylic acid dibenzyl ester	277	350	73	16

in **Chapter 2**, including a discussion of the synthesis and characterization of fluorinated APNBs via ^{1}H and ^{13}C NMR spectroscopy, high-resolution mass spectroscopy (HRMS), and gel permeation chromatography (GPC), as well as characterization of *P*, *D*, and *S* via permeation and sorption test and simulations of gas-polymer and polymer-polymer interactions via DFT computational methods. These studies add critical insight into our fundamental understanding of how CO_2/CH_4 gas transport is influenced as a function of polymer design.

As discussed in Section 1.5, block copolymer microphase separated morphology and polymer tacticity may strongly influence polymer chain packing, and thus potentially influence the gas separation performance. Both MPNBs and APNBs block copolymers have been synthesized, and current efforts are aimed at accessing different microphase separated morphologies, and their performance will be compared to corresponding random copolymers with similar overall monomer compositions. These efforts are discussed in **Chapter 3**. Prior reports of catalyst effects on APNB backbone tacticity are limited to a few examples, including unsubstituted APNB and mono-substituted methyl APNBs. Studies of unsubstituted APNB are largely restricted to those synthesized using Ni-based catalysts due to the limited solubility of analogous polymers obtained using Pd catalysts. Mono-substituted methyl APNBs have better solubility in organic solvents, however, the introduction of the new stereocenter introduces the potential for side chain tacticity effects (*exo*-, *endo*-isomer), as well as regiochemical head-head and head-tail effects (substituents from two neighboring monomers pointing toward/away from each other). Polymer chain packing is also affected by these substituent tacticity effects, and thus the catalyst-induced polymer backbone tacticity effects on the physical chain packing are obscured. Herein, we designed an *exo*-dimethyl substituted norbornene monomer, so that both tacticity effects from the substituents can

be eliminated, and the catalyst effect on the backbone tacticity will be isolated and examined. These efforts will be discussed in **Appendix I**.

As discussed in section 1.6, the processing of most APNBs is primarily limited to solvent casting, which is not industrially and environmentally favored. Our systematic studies to introduce different substituents onto APNBs and investigate how they impact T_g and T_d are discussed in **Chapter 4**. Monomer and polymer synthesis and characterization are performed via ^{1}H and ^{13}C NMR spectroscopy, as well as HRMS. Polymer T_ds were characterized by thermogravimetric analysis (TGA) and polymer T_g was characterized by modulated differential scanning calorimetry (MDSC), dynamic mechanical analysis (DMA), and ellipsometry. Finally, a selected polymer was melt extruded into bar samples to prove the feasibility of our approach and tensile tests were performed.

References

1. Norbornene Market research report 2022-2026 gather 121.4 Million and 8% CAGR by wide Application in Varied Industry, Types, Major Players with Top Contries Data. https://www.wicz.com/story/45395118/global-2-norbornene (accessed May 22 2022).
2. Li, J.; Stachowski, M.; Zhang, Z., Application of responsive polymers in implantable medical devices and biosensors. *Switchable and responsive surfaces and materials for biomedical applications* **2015**, 259-298.
3. Finkelshtein, E. S.; Bermeshev, M. V.; Gringolts, M. L.; Starannikova, L.; Yampolskii, Y. P., Substituted polynorbornenes as promising materials for gas separation membranes. *Russian Chemical Reviews* **2011,** *80* (4), 341.
4. Park, K. H.; Twieg, R. J.; Ravikiran, R.; Rhodes, L. F.; Shick, R. A.; Yankelevich, D.; Knoesen, A., Synthesis and nonlinear-optical properties of vinyl-addition poly (norbornene) s. *Macromolecules* **2004,** *37* (14), 5163-5178.
5. Grove, N. R.; Kohl, P. A.; Bidstrup Allen, S. A.; Jayaraman, S.; Shick, R., Functionalized polynorbornene dielectric polymers: adhesion and mechanical properties. *J. Polym. Sci. B Polym. Phys.* **1999,** *37* (21), 3003-3010.
6. Chen, M.; Zou, W.; Cai, Z.; Chen, C., Norbornene homopolymerization and copolymerization with ethylene by phosphine-sulfonate nickel catalysts. *Polymer Chemistry* **2015,** *6* (14), 2669-2676.
7. Bai, Y.; Chiniwalla, P.; Elce, E.; Shick, R. A.; Sperk, J.; Allen, S. A. B.; Kohl, P. A., Photosensitive polynorbornene based dielectric. I. Structure–property relationships. *Journal of Applied Polymer Science* **2004,** *91* (5), 3023-3030.
8. Goodall, B. Addition polymers derived from norbornene-functional monomers and process therfor. 95/14048, 1995.
9. Mol, J., Industrial applications of olefin metathesis. *Journal of Molecular Catalysis A: Chemical* **2004,** *213* (1), 39-45.
10. Dorkenoo, K. D.; Pfromm, P. H.; Rezac, M. E., Gas transport properties of a series of high Tg polynorbornenes with aliphatic pendant groups. *J. Polym. Sci. B Polym. Phys.* **1998,** *36* (5), 797-803.
11. Gmernicki, K. R.; Hong, E.; Maroon, C. R.; Mahurin, S. M.; Sokolov, A. P.; Saito, T.; Long, B. K., Accessing siloxane functionalized polynorbornenes via vinyl-addition polymerization for CO2 separation membranes. *ACS Macro Lett.* **2016,** *5* (7), 879-883.
12. Maroon, C. R.; Townsend, J.; Gmernicki, K. R.; Harrigan, D. J.; Sundell, B. J.; Lawrence III, J. A.; Mahurin, S. M.; Vogiatzis, K. D.; Long, B. K., Elimination of CO2/N2 Langmuir Sorption and Promotion of "N2-Phobicity" within High-T g Glassy Membranes. *Macromolecules* **2019,** *52* (4), 1589-1600.
13. Kim, D.-G.; Takigawa, T.; Kashino, T.; Burtovyy, O.; Bell, A.; Register, R. A., Hydroxyhexafluoroisopropylnorbornene block and random copolymers via vinyl addition polymerization and their application as biobutanol pervaporation membranes. *Chemistry of Materials* **2015,** *27* (19), 6791-6801.
14. Liu, S.; Chen, Y.; He, X.; Chen, L.; Zhou, W., Stable crosslinked vinyl-addition-type polynorbornene graft copolymer proton-exchange membranes. *Journal of Applied Polymer Science* **2011,** *121* (2), 1166-1175.

15. Mandal, M.; Huang, G.; Kohl, P. A., Anionic multiblock copolymer membrane based on vinyl addition polymerization of norbornenes: Applications in anion-exchange membrane fuel cells. *Journal of membrane science* **2019,** *570*, 394-402.
16. Mulpuri, S. V.; Shin, J.; Shin, B.-G.; Greiner, A.; Yoon, D. Y., Synthesis and characterization of substituted polynorbornene derivatives. *Polymer* **2011,** *52* (19), 4377-4386.
17. Blank, F.; Janiak, C., Metal catalysts for the vinyl/addition polymerization of norbornene. *Coordination Chemistry Reviews* **2009,** *253* (7-8), 827-861.
18. Hennis, A. D.; Polley, J. D.; Long, G. S.; Sen, A.; Yandulov, D.; Lipian, J.; Benedikt, G. M.; Rhodes, L. F.; Huffman, J., Novel, efficient, palladium-based system for the polymerization of norbornene derivatives: scope and mechanism. *Organometallics* **2001,** *20* (13), 2802-2812.
19. Mathew, J. P.; Reinmuth, A.; Melia, J.; Swords, N.; Risse, W., (η3-Allyl) palladium (II) and palladium (II) nitrile catalysts for the addition polymerization of norbornene derivatives with functional groups. *Macromolecules* **1996,** *29* (8), 2755-2763.
20. Byun, G. S.; Kim, S. Y.; Cho, I., Pd (II)-catalyzed polymerization of optically active norbornene carboxylic acid esters. *Journal of Polymer Science Part A: Polymer Chemistry* **2006,** *44* (3), 1263-1270.
21. Miyasako, N.; Matsuoka, S. i.; Suzuki, M., Ring-Opening Metathesis Polymerization of endo-and exo-Norbornene Lactones. *Macromolecular Rapid Communications* **2021,** *42* (8), 2000326.
22. Alentiev, D. A.; Bermeshev, M. V.; Starannikova, L. E.; Bermesheva, E. V.; Shantarovich, V. P.; Bekeshev, V. G.; Yampolskii, Y. P.; Finkelshtein, E. S., Stereoselective synthesis and polymerization of Exo-5-trimethylsilylnorbornene. *Journal of Polymer Science Part A: Polymer Chemistry* **2018,** *56* (12), 1234-1248.
23. Guseva, M. A.; Alentiev, D. A.; Bermesheva, E. V.; Zamilatskov, I. A.; Bermeshev, M. V., The selective hydrosilylation of norbornadiene-2,5 by monohydrosiloxanes. *RSC Advances* **2019,** *9* (57), 33029-33037.
24. Sundell, B. J.; Lawrence III, J. A.; Harrigan, D. J.; Lin, S.; Headrick, T. P.; O'Brien, J. T.; Penniman, W. F.; Sandler, N., Exo-selective, Reductive Heck Derived Polynorbornenes with Enhanced Molecular Weights, Yields, and Hydrocarbon Gas Transport Properties. *ACS Macro Letters* **2020,** *9* (9), 1363-1368.
25. Kennedy, J. P.; Hinlicky, J. A., Cationic transannular polymerization of norbornadiene. *Polymer* **1965,** *6* (3), 133-140.
26. Zutty, N. L., Copolymerization studies. IV. Transannular copolymerization of bicyclo[2.2.1] hepta-2,5-diene. *Journal of Polymer Science Part A: General Papers* **1963,** *1* (6), 2231-2236.
27. Gaylord, N. G.; Mandal, B. M.; Martan, M., Peroxide-induced polymerization of norbornene. *Journal of Polymer Science: Polymer Letters Edition* **1976,** *14* (9), 555-559.
28. Tunoglu, N.; Balcioglu, N., Anionic and cationic polymerization of norbornadiene in hydrocarbon. *Macromolecular Rapid Communications* **1999,** *20* (10), 546-548.
29. Balciog`lu, N.; Tunog`lu, N., MoCl5/EtAlCl2-catalysed nonmetathesis polymerization of norbornadiene. *Journal of Polymer Science Part A: Polymer Chemistry* **1996,** *34* (12), 2311-2317.
30. Abdulhamid, M. A.; Lai, H. W. H.; Wang, Y.; Jin, Z.; Teo, Y. C.; Ma, X.; Pinnau, I.; Xia, Y., Microporous Polyimides from Ladder Diamines Synthesized by Facile Catalytic Arene–Norbornene Annulation as High-Performance Membranes for Gas Separation. *Chemistry of Materials* **2019,** *31* (5), 1767-1774.

31. Liu, S.; Jin, Z.; Teo, Y. C.; Xia, Y., Efficient Synthesis of Rigid Ladder Polymers via Palladium Catalyzed Annulation. *Journal of the American Chemical Society* **2014,** *136* (50), 17434-17437.
32. Teo, Y. C.; Lai, H. W. H.; Xia, Y., Synthesis of Ladder Polymers: Developments, Challenges, and Opportunities. *Chemistry - A European Journal* **2017,** *23* (57), 14101-14112.
33. Wang, X.; Wilson, T. J.; Alentiev, D.; Gringolts, M.; Finkelshtein, E.; Bermeshev, M.; Long, B. K., Substituted polynorbornene membranes: a modular template for targeted gas separations. *Polymer Chemistry* **2021,** *12* (20), 2947-2977.
34. Bermesheva, E. V.; Wozniak, A. I.; Andreyanov, F. A.; Karpov, G. O.; Nechaev, M. S.; Asachenko, A. F.; Topchiy, M. A.; Melnikova, E. K.; Nelyubina, Y. V.; Gribanov, P. S.; Bermeshev, M. V., Polymerization of 5-Alkylidene-2-norbornenes with Highly Active Pd–N-Heterocyclic Carbene Complex Catalysts: Catalyst Structure–Activity Relationships. *ACS Catalysis* **2020,** *10* (3), 1663-1678.
35. Lipian, J.; Mimna, R. A.; Fondran, J. C.; Yandulov, D.; Shick, R. A.; Goodall, B. L.; Rhodes, L. F.; Huffman, J. C., Addition polymerization of norbornene-type monomers. High activity cationic allyl palladium catalysts. *Macromolecules* **2002,** *35* (24), 8969-8977.
36. Kim, D.-G.; Bell, A.; Register, R. A., Living Vinyl Addition Polymerization of Substituted Norbornenes by a t-Bu3P-Ligated Methylpalladium Complex. *ACS Macro Letters* **2015,** *4* (3), 327-330.
37. Yamashita, M.; Takamiya, I.; Jin, K.; Nozaki, K., Syntheses and structures of bulky monophosphine-ligated methylpalladium complexes: application to homo-and copolymerization of norbornene and/or methoxycarbonylnorbornene. *Organometallics* **2006,** *25* (19), 4588-4595.
38. Kang, B.-G.; Kim, D.-G.; Register, R. A., Vinyl Addition copolymers of norbornylnorbornene and hydroxyhexafluoroisopropylnorbornene for efficient recovery of n-butanol from dilute aqueous solution via pervaporation. *Macromolecules* **2018,** *51* (10), 3702-3710.
39. Tsai, S. D.; Register, R. A., Endo/Exo Reactivity Ratios in Living Vinyl Addition Polymerization of Substituted Norbornenes. *Macromolecular Chemistry and Physics* **2018,** *219* (11), 1800059.
40. Lai, H. W. H.; Benedetti, F. M.; Jin, Z.; Teo, Y. C.; Wu, A. X.; Angelis, M. G. D.; Smith, Z. P.; Xia, Y., Tuning the Molecular Weights, Chain Packing, and Gas-Transport Properties of CANAL Ladder Polymers by Short Alkyl Substitutions. *Macromolecules* **2019,** *52* (16), 6294-6302.
41. Alentiev, D. A.; Egorova, E. S.; Bermeshev, M. V.; Starannikova, L. E.; Topchiy, M. A.; Asachenko, A. F.; Gribanov, P. S.; Nechaev, M. S.; Yampolskii, Y. P.; Finkelshtein, E. S., Janus tricyclononene polymers bearing tri(n-alkoxy)silyl side groups for membrane gas separation. *Journal of Materials Chemistry A* **2018,** *6* (40), 19393-19408.
42. Belov, N.; Nikiforov, R.; Starannikova, L.; Gmernicki, K. R.; Maroon, C. R.; Long, B. K.; Shantarovich, V.; Yampolskii, Y., A detailed investigation into the gas permeation properties of addition-type poly(5-triethoxysilyl-2-norbornene). *European Polymer Journal* **2017,** *93*, 602-611.
43. Bermeshev, M. V.; Starannikova, L. E.; Sterlin, S. R.; Tyutyunov, A. A.; Tavtorkin, A. N.; Yampolskii, Y. P.; Finkelshtein, E. S., Synthesis and gas-separation properties of metathesis poly(3-fluoro-3-pentafluoroethyl-4,4-bis(trifluoromethyl)tricyclonene-7). *Pet. Chem.* **2015,** *55* (9), 753-758.

44. Sundell, B. J.; Lawrence III, J. A.; Harrigan, D. J.; Vaughn, J. T.; Pilyugina, T. S.; Smith, D. R., Alkoxysilyl functionalized polynorbornenes with enhanced selectivity for heavy hydrocarbon separations. *RSC Advances* **2016,** *6* (57), 51619-51628.
45. Park, H. B.; Kamcev, J.; Robeson, L. M.; Elimelech, M.; Freeman, B. D., Maximizing the right stuff: The trade-off between membrane permeability and selectivity. *Science* **2017,** *356* (6343), eaab0530.
46. Galizia, M.; Chi, W. S.; Smith, Z. P.; Merkel, T. C.; Baker, R. W.; Freeman, B. D., 50th Anniversary Perspective: Polymers and Mixed Matrix Membranes for Gas and Vapor Separation: A Review and Prospective Opportunities. *Macromolecules* **2017,** *50* (20), 7809-7843.
47. Robeson, L. M., The upper bound revisited. *Journal of membrane science* **2008,** *320* (1-2), 390-400.
48. Comesaña-Gándara, B.; Chen, J.; Bezzu, C. G.; Carta, M.; Rose, I.; Ferrari, M.-C.; Esposito, E.; Fuoco, A.; Jansen, J. C.; McKeown, N. B., Redefining the Robeson upper bounds for CO 2/CH 4 and CO 2/N 2 separations using a series of ultrapermeable benzotriptycene-based polymers of intrinsic microporosity. *Energy & Environmental Science* **2019,** *12* (9), 2733-2740.
49. Robeson, L. M., Correlation of separation factor versus permeability for polymeric membranes. *Journal of membrane science* **1991,** *62* (2), 165-185.
50. Bos, A.; Pünt, I. G. M.; Wessling, M.; Strathmann, H., CO2-induced plasticization phenomena in glassy polymers. *Journal of Membrane Science* **1999,** *155* (1), 67-78.
51. Freeman, B. D., Basis of Permeability/Selectivity Tradeoff Relations in Polymeric Gas Separation Membranes. *Macromolecules* **1999,** *32* (2), 375-380.
52. Kanehashi, S.; Nagai, K., Analysis of dual-mode model parameters for gas sorption in glassy polymers. *Journal of Membrane Science* **2005,** *253* (1), 117-138.
53. Maroon, C. R.; Townsend, J.; Higgins, M. A.; Harrigan, D. J.; Sundell, B. J.; Lawrence III, J. A.; O'Brien, J. T.; O'Neal, D.; Vogiatzis, K. D.; Long, B. K., Addition-type alkoxysilyl-substituted polynorbornenes for post-combustion carbon dioxide separations. *Journal of Membrane Science* **2020,** *595*, 117532.
54. Powell, C. E.; Qiao, G. G., Polymeric CO2/N2 gas separation membranes for the capture of carbon dioxide from power plant flue gases. *Journal of Membrane Science* **2006,** *279* (1), 1-49.
55. Swaidan, R.; Ghanem, B.; Litwiller, E.; Pinnau, I., Physical Aging, Plasticization and Their Effects on Gas Permeation in "Rigid" Polymers of Intrinsic Microporosity. *Macromolecules* **2015,** *48* (18), 6553-6561.
56. Wijmans, J. G.; Baker, R. W., The solution-diffusion model: a review. *Journal of Membrane Science* **1995,** *107* (1), 1-21.
57. Yampolskii, Y., Polymeric Gas Separation Membranes. *Macromolecules* **2012,** *45* (8), 3298-3311.
58. Chapala, P.; Bermeshev, M.; Starannikova, L.; Borisov, I.; Shantarovich, V.; Lakhtin, V.; Volkov, V.; Finkelshtein, E., Synthesis and Gas-Transport Properties of Metathesis Polytricyclononenes Bearing Three Me3Si Groups per Monomer Unit. *Macromolecular Chemistry and Physics* **2016,** *217* (17), 1966-1976.
59. Alentiev, D. A.; Korchagina, S. A.; Finkel'Shtein, E. S.; Nechaev, M. S.; Asachenko, A. F.; Topchiy, M. A.; Gribanov, P. S.; Bermeshev, M. V., Addition homo- and copolymerization of 3-triethoxysilyltricyclo[4.2.1.02,5]non-7-ene. *Russian Chemical Bulletin* **2018,** *67* (1), 121-126.
60. Alentiev, D. A.; Egorova, E. S.; Bermeshev, M. V.; Starannikova, L. E.; Yampolskii, Y. P.; Finkelshtein, E. S., Crosslinking of addition copolymers from tricyclononenes bearing (CH 3)

3 Si- and (C 2 H 5 O) 3 Si-groups as a modification of membran. *Polymer Engineering & Science* **2019,** *59* (12), 2502-2507.
61. Finkelshtein, E. S.; Makovetskii, K. L.; Gringolts, M. L.; Rogan, Y. V.; Golenko, T. G.; Starannikova, L. E.; Yampolskii, Y. P.; Shantarovich, V. P.; Suzuki, T., Addition-Type Polynorbornenes with Si(CH 3) 3 Side Groups: Synthesis, Gas Permeability, and Free Volume. *Macromolecules* **2006,** *39* (20), 7022-7029.
62. Lawrence III, J. A.; Harrigan, D. J.; Maroon, C. R.; Sharber, S. A.; Long, B. K.; Sundell, B. J., Promoting acid gas separations via strategic alkoxysilyl substitution of vinyl-added poly(norbornene)s. *Journal of Membrane Science* **2020,** *616*, 118569.
63. Gringolts, M.; Bermeshev, M.; Starannikova, L.; Rogan, Y. V.; Yampol'skii, Y. P.; Finkel'shtein, E. S., Synthesis and gas separation properties of metathesis polynorbornenes with different positions of one or two SiMe 3 groups in a monomer unit. *Polymer Science Series A* **2009,** *51* (11-12), 1233.
64. Steinhäusler, T.; Koros, W. J., Gas permeation and sorption studies on stereoregular polynorbornene. *Journal of Polymer Science Part B: Polymer Physics* **1997,** *35* (1), 91-99.
65. Yampolskii, Y. P.; Finkelshtein, E. S.; Makovetskii, K. L.; Bondar, V. I.; Shantarovich, V. P., Effects of cis-trans-configurations of the main chains of poly (trimethylsilyl norbornene) on its transport and sorption properties as well as free volume. *Journal of applied polymer science* **1996,** *62* (2), 349-357.
66. Finkelshtein, E. S.; Gringolts, M.; Ushakov, N.; Lakhtin, V.; Soloviev, S.; Yampol'skii, Y. P., Synthesis and gas permeation properties of new ROMP polymers from silyl substituted norbornadienes and norbornenes. *Polymer* **2003,** *44* (10), 2843-2851.
67. Gringol'ts, M. L.; Bermeshev, M. V.; Syromolotov, A. V.; Starannikova, L. E.; Filatova, M. F.; Makovetskii, K. L.; Finkel'shtein, E. S., Highly permeable polymer materials based on silicon-substituted norbornenes. *Pet. Chem.* **2010,** *50* (5), 352-361.
68. Finkelshtein, E. S.; Makovetskii, K.; Yampol'skii, Y. P.; Portnykh, E.; Ostrovskaya, I. Y.; Kaliuzhnyi, N.; Pritula, N.; Gol'berg, A.; Yatsenko, M.; Plate, N., Ring-opening metathesis polymerization of norbornenes with organosilicon substituents. Gas permeability of polymers obtained. *Die Makromolekulare Chemie* **1991,** *192* (1), 1-9.
69. Finkelshtein, E. S.; Bermeshev, M. V.; Gringolts, M. L.; Starannikova, L. E.; Yampolskii, Y. P., Substituted polynorbornenes as promising materials for gas separation membranes. *Russian Chemical Reviews* **2011,** *80* (4), 341-361.
70. Finkelshtein, E.; Gringolts, M.; Bermeshev, M.; Chapala, P.; Rogan, Y., Polynorbornenes. In *Membrane Materials for Gas and Vapor Separation*, John Wiley & Sons Inc. Chichester, West Sussex, UK: 2017; pp 143-221.
71. Katsumata, T.; Shiotsuki, M.; Sanda, F.; Masuda, T., Synthesis and properties of polynorbornenes bearing oligomeric siloxane pendant groups. *Polymer* **2009,** *50* (6), 1389-1394.
72. Bermeshev, M.; Finkelshteina, E. S., MACROMOLECULAR DESIGN AND SYNTHESIS OF POLYMERS FROM SILICON-CONTAINING NORBORNENES FOR MEMBRANE GAS SEPARATION. *INEOS OPEN* **2018,** *1* (1), 39-54.
73. Vaughn, J. T.; Harrigan, D. J.; Sundell, B. J.; Lawrence III, J. A.; Yang, J., Reverse selective glassy polymers for C3+ hydrocarbon recovery from natural gas. *Journal of Membrane Science* **2017,** *522*, 68-76.
74. Bermeshev, M. V.; Syromolotov, A. V.; Starannikova, L. E.; Gringolts, M. L.; Lakhtin, V. G.; Yampolskii, Y. P.; Finkelshtein, E. S., Glassy Polynorbornenes with Si–O–Si Containing

Side Groups. Novel Materials for Hydrocarbon Membrane Separation. *Macromolecules* **2013,** *46* (22), 8973-8979.
75. Vargas, J.; Santiago, A. A.; Cruz-Morales, J. A.; Tlenkopatchev, M. A.; de Lys, T.; López-González, M.; Riande, E., Gas Transport Properties of Hydrogenated and Fluorinated Polynorbornene Dicarboximides. *Macromolecular Chemistry and Physics* **2013,** *214* (22), 2607-2615.
76. Berron, B. J.; Payne, P. A.; Jennings, G. K., Sulfonation of Surface-Initiated Polynorbornene Films. *Industrial & Engineering Chemistry Research* **2008,** *47* (20), 7707-7714.
77. Planche, J. P.; Revillon, A.; Guyot, A., Chemical modification of polynorbornene. II. Extended sulfonation processes. *Journal of Polymer Science Part A: Polymer Chemistry* **1990,** *28* (6), 1377-1386.
78. Hyvl, J.; Autenrieth, B.; Schrock, R. R., Proof of Tacticity of Stereoregular ROMP Polymers through Post Polymerization Modification. *Macromolecules* **2015,** *48* (9), 3148-3152.
79. Kovačič, S.; Preishuber-Pflügl, F.; Slugovc, C., Macroporous Polyolefin Membranes from Dicyclopentadiene High Internal Phase Emulsions: Preparation and Morphology Tuning. *Macromolecular Materials and Engineering* **2014,** *299* (7), 843-850.
80. Perring, M.; Bowden, N. B., Assembly of Organic Monolayers on Polydicyclopentadiene. *Langmuir* **2008,** *24* (18), 10480-10487.
81. Boyd, T. J.; Schrock, R. R., Sulfonation and Epoxidation of Substituted Polynorbornenes and Construction of Light-Emitting Devices. *Macromolecules* **1999,** *32* (20), 6608-6618.
82. Perring, M.; Long, T. R.; Bowden, N. B., Epoxidation of the surface of polydicyclopentadiene for the self-assembly of organic monolayers. *Journal of Materials Chemistry* **2010,** *20* (39), 8679-8685.
83. Meier, S.; Stelzer, F.; Reisinger, H.; Haag, R.; Mecking, S.; Mülhaupt, R., Carbohydrate analogue polymers by ring opening metathesis polymerisation (ROMP) and subsequent catalytic dihydroxylation. *Chemical Communications* **2001,** (9), 855-856.
84. Zhao, Y.; Chen, J.; Zhu, W.; Zhang, K., Unique post-functionalization method for ROMP polymers based on Triazolinedione Alder-ene chemistry. *Polymer* **2015,** *74*, 16-20.
85. Lowe, A. B.; Liu, M.; Van Hensbergen, J. A.; Burford, R. P., Combining Ring-Opening Metathesis Polymerization and Thiol-Ene Coupling Chemistries: Facile Access to Novel Functional Linear and Nonlinear Macromolecules. *Macromolecular Rapid Communications* **2014,** *35* (4), 391-404.
86. Belov, N. A.; Gringolts, M. L.; Morontsev, A. A.; Starannikova, L. E.; Yampolskii, Y. P.; Finkelstein, E. S., Gas-transport properties of epoxidated metathesis polynorbornenes. *Polymer Science, Series B* **2017,** *59* (5), 560-569.
87. Morontsev, A. A.; Zhigarev, V. A.; Nikiforov, R. Y.; Belov, N. A.; Gringolts, M. L.; Finkelshtein, E. S.; Yampolskii, Y. P., A new approach to improvement of gas permeation properties of olefin metathesis derived poly(norbornenes): gem-difluorocyclopropanation of backbone double bonds. *European Polymer Journal* **2018,** *99*, 340-349.
88. Zhigarev, V. A.; Morontsev, A. A.; Nikiforov, R. Y.; Gringolts, M. L.; Belov, N. A.; Komalenkova, N. G.; Lakhtin, V. G.; Finkelshtein, E. S., Synthesis and Gas-Separation Properties of New Silacyclopentane-Containing Polynorbornenes. *Polymer Science, Series C* **2019,** *61* (1), 107-119.
89. Morontsev, A. A.; Gringolts, M. L.; Filatova, M. P.; Finkelshtein, E. S., Modification of silicon-substituted polynorbornenes by epoxidation of main chain double bonds. *Polymer Science Series B* **2016,** *58* (6), 695-702.

90. Klein, J. P.; Register, R. A., Tuning the phase behavior of semicrystalline hydrogenated polynorbornene via epimerization. *Journal of Polymer Science Part B: Polymer Physics* **2019,** *57* (18), 1188-1195.
91. Drouin, S. D.; Zamanian, F.; Fogg, D. E., Multiple Tandem Catalysis: Facile Cycling between Hydrogenation and Metathesis Chemistry. *Organometallics* **2001,** *20* (26), 5495-5497.
92. Yampolskii, Y.; Belov, N.; Alentiev, A., Perfluorinated polymers as materials of membranes for gas and vapor separation. *Journal of Membrane Science* **2020,** *598*, 117779.
93. Higgins, M. A.; Maroon, C. R.; Townsend, J.; Wang, X.; Vogiatzis, K. D.; Long, B. K., Evaluating the impact of functional groups on membrane-mediated CO 2 / N 2 gas separations using a common polymer backbone. *Journal of Polymer Science* **2020,** *58*, 2644–2653.
94. Tetsuka, H.; Isobe, K.; Hagiwara, M., Synthesis and Properties of Addition-Type Poly(norbornene)s with Siloxane Substituents. *Polymer Journal* **2009,** *41* (8), 643-649.
95. Gringolts, M.; Bermeshev, M.; Yampolskii, Y.; Starannikova, L.; Shantarovich, V.; Finkelshtein, E., New High Permeable Addition Poly(tricyclononenes) with Si(CH3)3 Side Groups. Synthesis, Gas Permeation Parameters, and Free Volume. *Macromolecules* **2010,** *43* (17), 7165-7172.
96. Corrado, T.; Guo, R., Macromolecular design strategies toward tailoring free volume in glassy polymers for high performance gas separation membranes. *Molecular Systems Design & Engineering* **2020,** *5* (1), 22-48.
97. Bermeshev, M. V.; Syromolotov, A. V.; Gringolts, M. L.; Starannikova, L. E.; Yampolskii, Y. P.; Finkelshtein, E. S., Synthesis of High Molecular Weight Poly[3-{tris(trimethylsiloxy)silyl}tricyclononenes-7] and Their Gas Permeation Properties. *Macromolecules* **2011,** *44* (17), 6637-6640.
98. Kenney, J., Properties of block versus random copolymers. *Polymer Engineering & Science* **1968,** *8* (3), 216-226.
99. Odani, H.; Taira, K.; Nemoto, N.; Kurata, M., Diffusion and solution of gases and vapors in styrene-butadiene block copolymers. *Polymer Engineering & Science* **1977,** *17* (8), 527-534.
100. Csernica, J.; Baddour, R.; Cohen, R., Gas permeability of a polystyrene-polybutadiene block copolymer with oriented lamellar domains. *Macromolecules* **1987,** *20* (10), 2468-2471.
101. Csernica, J.; Baddour, R.; Cohen, R., Gas permeability of a polystyrene/polybutadiene block copolymer possessing a misoriented lamellar morphology. *Macromolecules* **1989,** *22* (3), 1493-1496.
102. Kofinas, P.; Cohen, R. E.; Halasa, A. F., Gas permeability of polyethylene/poly (ethylene-propylene) semicrystalline diblock copolymers. *Polymer* **1994,** *35* (6), 1229-1235.
103. Buonomenna, M. G.; Golemme, G.; Tone, C. M.; De Santo, M. P.; Ciuchi, F.; Perrotta, E., Nanostructured poly (styrene-b-butadiene-b-styrene)(SBS) membranes for the separation of nitrogen from natural gas. *Advanced Functional Materials* **2012,** *22* (8), 1759-1767.
104. Buonomenna, M.; Yave, W.; Golemme, G., Some approaches for high performance polymer based membranes for gas separation: block copolymers, carbon molecular sieves and mixed matrix membranes. *RSC advances* **2012,** *2* (29), 10745-10773.
105. Ahmed, S.; Bidstrup, S. A.; Kohl, P.; Ludovice, P. In *Stereochemical structure-property relationships in polynorbornene from simulation*, Macromolecular Symposia, Wiley Online Library: 1998; pp 1-10.
106. Janiak, C.; Lassahn, P. G., The vinyl homopolymerization of norbornene. *Macromolecular rapid communications* **2001,** *22* (7), 479-493.

107. Barnes, D. A.; Benedikt, G. M.; Goodall, B. L.; Huang, S. S.; Kalamarides, H. A.; Lenhard, S.; McIntosh, L. H.; Selvy, K.; Shick, R. A.; Rhodes, L. F., Addition polymerization of norbornene-type monomers using neutral nickel complexes containing fluorinated aryl ligands. *Macromolecules* **2003,** *36* (8), 2623-2632.
108. Rieger, B.; Baugh, L. S.; Kacker, S.; Striegler, S., *Late transition metal polymerization catalysis*. Wiley Online Library: 2003.
109. Wilks, B. R.; Chung, W. J.; Ludovice, P. J.; Rezac, M. R.; Meakin, P.; Hill, A. J., Impact of average free-volume element size on transport in stereoisomers of polynorbornene. I. Properties at 35 C. *Journal of Polymer Science Part B: Polymer Physics* **2003,** *41* (18), 2185-2199.
110. McDougall, W.; Farling, S.; Shick, R.; Glukh, S.; Jayaraman, S.; Rhodes, L.; Vicari, R.; Kohl, P.; Bidstrup-Allen, S.; Chiniwalla, P., Avatrel™ dielectric polymers for HDP applications. Proc. International Conference and Exhibition on High-Density Interconnect and Systems Packaging: Denver, CO, USA, 1999; pp 1-4.
111. Goodall, B.; Barnes, D., Novel heat resistant cyclic olefin polymers made using single component nickel and palladium catalysts: Synthesis and applications. *Polymer Preprints(USA)* **1998,** *39* (1), 216-217.
112. Goodall, B.; Benedikt, G.; McIntosh III, L.; Barnes, D.; Rhodes, L. Process for making polymers containing a norbornene repeating unit by addition polymerization using an organo (nickel or palladium) complex. 5468819, 1995.
113. Goodall, B.; Risse, W.; Mathew, J. Addition polymers of polycycloolefins containing functional substituents. 5705503, 1998.
114. Promerus_MaterialsBrochure.pdf. https://cdn2.hubspot.net/hubfs/4540595/Promerus_MaterialsBrochure.pdf?__hstc=57055029.3e7d37bcde90d2b746a195957cad6ac3.1653276167607.1653276167607.1653276167607.1&__hssc=57055029.3.1653276167607&__hsfp=341068549 (accessed May 22, 2022).
115. Kim, E. C.; Kim, M.-J.; Thi Ho, L. N.; Lee, W.; Ka, J.-W.; Kim, D.-G.; Shin, T. J.; Huh, K. M.; Park, S.; Kim, Y. S., Synthesis of Vinyl-Addition Polynorbornene Copolymers Bearing Pendant n-Alkyl Chains and Systematic Investigation of Their Properties. *Macromolecules* **2021**.
116. Goodall, B. L., Cycloaliphatic polymers via late transition metal catalysis. In *Late transition metal polymerization catalysis*, Bernhard Rieger, L. S. B., Smita Kacker, Susanne Striegler, Ed. WILEY-VCH Verlag GmbH & Co. KGaA: Weinheim, 2003; pp 101-154.
117. Shin, B.-G.; Cho, T.-Y.; Yoon, D. Y.; Liu, B., Structure and Properties of Polynorbornene Derivatives: Poly (norbornene dicarboxylic acid dialkyl ester) s and Poly (norbornene dimethyl dicarboxylate) s. *Macromolecular research* **2007,** *15* (2), 185-190.
118. Breunig, S.; Risse, W., Transition-metal-catalyzed vinyl addition polymerizations of norbornene derivatives with ester groups. *Die Makromolekulare Chemie: Macromolecular Chemistry and Physics* **1992,** *193* (11), 2915-2927.
119. Kim, D.-G.; Bell, A.; Register, R. A., Living Vinyl Addition Polymerization of Substituted Norbornenes by at-Bu3P-Ligated Methylpalladium Complex. *ACS Macro Lett.* **2015,** *4* (3), 327-330.
120. Grove, N. R.; Kohl, P. A.; Bidstrup Allen, S. A.; Jayaraman, S.; Shick, R., Functionalized polynorbornene dielectric polymers: adhesion and mechanical properties. *Journal of Polymer Science Part B: Polymer Physics* **1999,** *37* (21), 3003-3010.

Chapter 2 Fluoroalkoxysilyl-substituted, Vinyl-addition Polynorbornene Membranes for CO_2/CH_4 Separation

A version of this chapter was originally published by Xinyi Wang,‡ Trevor J. Wilson,‡ Christopher R. Maroon, Jeffrey A. Laub, Savannah E. Rheingold, Konstantinos D. Vogiatzis, Brian K. Long*

"Vinyl-Addition Fluoroalkoxysilyl-Substituted Polynorbornene Membranes for CO_2/CH_4 Separation." *ACS Applied Polymer Materials* **2022**, ASAP.

DOI: https://doi.org/10.1021/acsapm.1c01833.

Xinyi Wang and Trevor J. Wilson were responsible for the synthesis and characterization of all monomers, polymers, film preparation, permeation and sorption tests, and corresponding data analyses. Xinyi Wang was also responsible for drafting the manuscript introduction and discussion, corelating experimental and simulation data. Trevor J. Wilson was responsible for drafting the experimental section and support information. Christopher R. Maroon initiated this project and obtained the preliminary results, Jeffrey A. Laub was in charge of the computational work and drafting corresponding discussion section. Savannah E. Rheingold was the REU students helped with monomer synthesis. Dr. Konstantinos D. Vogiatzis and Dr. Brian K. Long advised this work and aided in the preparation of the manuscript.

2.1 Abstract

Natural gas production and utilization has grown tremendously in recent decades, which highlights the need for improved, high-throughput purification methods. In the field of polymeric membrane-based gas separations, a detailed understanding of molecular structure–property relationships are critical to overcoming the permeability–selectivity trade–off. Prior work has highlighted that alkoxysilyl–substituted vinyl–addition polynorbornenes (APNBs) are promising

candidates for natural gas purification, having exceptional H_2S/CH_4 and modest CO_2/CH_4 permselectivity. To improve their CO_2/CH_4 separation performance, we herein describe a series of fluoroalkoxysilyl-substituted APNBs. We demonstrate that the incorporation of fluoroalkoxysilyl substituents yields a series of polymeric materials whose CO_2/CH_4 permselectivity increases as a function of fluorine incorporation. Interestingly, these enhanced selectivity characteristics are realized with minimal decreases to overall CO_2 permeability. While it was initially hypothesized that introduction of fluorinated units would decrease CH_4 solubility, detailed sorption analysis revealed that the observed increases in CO_2/CH_4 permselectivity were due almost exclusively to enhanced CO_2 sorption in fluorine containing APNBs. Computational studies provided insights into the electronic interaction energies between gas molecules and polymer repeat units across the non-fluorinated and fluorinated series, respectively.

2.2 Introduction

The world has experienced a surge in natural gas production and utilization in recent decades. This is particularly true in the United States, where the leap in production is largely due to advances in horizontal drilling and hydraulic fracturing techniques that were applied to hydrocarbon-rich shale formations starting in the mid-2000s.[121, 122] In the decade between 2005 and 2015, U.S. domestic natural gas production increased by 66% and is an increasingly attractive energy source due to the lower costs associated with the shale gas, as well as its high molar enthalpy of combustion. Natural gas combustion emits 117 lb CO_2/MBtu of energy released compared to 228.6 lb CO_2/MBtu for coal. Unsurprisingly, many electrical utilities have begun retrofitting coal fired power plants to run on natural gas. A change that not only lowers CO_2 emissions by roughly 50%, but drastically reduces SO_2 and NO_x emissions while virtually

eliminating fly ash generation. These economic and environmental advantages suggest strong growth in the natural gas sector for the foreseeable future.

Recent estimates place global natural gas reserves at 270 trillion cubic meters with virtually all of it requiring some degree of purification to meet pipeline specifications. Raw natural gas is composed primarily of methane with varying amounts of higher hydrocarbons, as well as undesirable impurities such as H_2O, CO_2, N_2, and H_2S. While the relative ratios of these impurities can vary widely in raw gas, the composition of gas permitted into commercial pipeline grids is tightly controlled. H_2S and CO_2 are especially regulated, as the corrosive nature of these gasses can compromise pipeline integrity, as well as decrease the calorific value of natural gas.[123, 124] Typical pipeline specifications mandate H_2S concentrations lower than 4 ppm, and CO_2 concentrations lower than 2 mole%.[121, 125] The technique most widely used to remove these impurities is amine scrubbing, which is energy intensive, high maintenance, generates sizeable waste streams, and scales poorly with contaminant concentration.[126-128] Alternately, membrane-based separations are more environmentally friendly, energy saving, cost-efficient, and requires a smaller operational footprint.[46, 121, 129-134] For this purpose, membrane separations have been limited to processing small gas flows with relatively high contaminant concentrations.[135] This is partly due to the low permeability of incumbent dense polymeric membrane materials (e.g., polyimide, cellulose acetate).[136] DuPont commercialized Kapton polyimide films for CO_2/CH_4 separation, with a very low CO_2 permeability of 0.22 Barrer, but with a high CO_2/CH_4 selectivity of 68.8.[137] Similarly, cellulose acetate has a moderate selectivity of ~20 but extremely low permeability of CO_2 (~10 Barrer) under a mixed gas feed.[46, 138, 139] These characteristics have limited membranes to applications with low flowrate feed streams that contain relatively high contaminant concentrations.[135] Development of membranes with enhanced CO_2 permeability and

comparable CO_2/CH_4 selectivity could broaden the scope of feed streams to which membrane separation could be practically employed.

In order to be more competitive with other separation technologies, interest in improving membrane-based separation performance by studying detailed structure-property relationships has recently grown. Among them, fluorinated polyimides containing 2,2'-bis(3,4'dicarboxyphenyl) hexafluoropropane dianhydride (6FDA) units showed promising performance, mainly manifesting as increased CO_2 permeability accompanied by moderately depressed CO_2/CH_4 selectivity, as compared to non-fluorinated polyimides.[140-143] It was hypothesized that the reason for the increased permeability was a reduction in segmental chain mobility and frustrated chain packing due to the presence of bulky -$C(CF_3)_2$- groups.[144, 145] On the other hand, polymer of intrinsic microporosity (PIMs) are a class of high permeable polymers with good CO_2/CH_4 separation performance, having a CO_2 permeability of 2300 Barrer and a CO_2/CH_4 selectivity of 18.4. Additionally, thermal rearrangement or crosslinking of these types of polymers has also been studied to further improve their performance.[143, 146]

Recently, we found that certain alkoxysilane substituted vinyl-addition polynorbornenes (APNBs) have exceptional H_2S/CH_4 separation performance under mixed feed gas conditions, demonstrating both high permeability (~2000 Barrer for H_2S) and selectivity (~50) that surpassed the 2015 upper-bound for H_2S/CH_4 separation. However, these membranes displayed only modest CO_2/CH_4 separation performance with high permeability (~1000 Barrer for CO_2) but moderate selectivity (~10).[147] These preliminary results motivated our subsequent efforts to improve the CO_2/CH_4 separation performance of alkoxysilane substituted APNB membranes for natural gas purification.

Inspired by previous literature, where the mutual solubility of hydrocarbons and fluorocarbons is very low,[148, 149] and reports in which the introduction of fluorine content into polymers tends to inhibit hydrocarbon solubility,[146, 150-152] we hypothesized that fluorinated alkoxysilane APNBs would demonstrate improved CO_2/CH_4 selectivity while potentially maintaining high CO_2 permeability due to the inherent rigid, bicyclic ring structure of their polymeric backbone (Figure 2.1). Herein, we describe the synthesis of fluorinated and nonfluorinated APNB membranes and evaluation of their gas separation performance. Indeed, the incorporation of fluorinated moieties into alkoxysilane substituted APNB did show improved CO_2/CH_4 selectivity while maintaining high CO_2 permeability. This behavior overcomes the traditional permeability–selectivity trade–off relationship. Furthermore, quantum chemical calculations were performed for the understanding of the atomistic interactions between gas molecules and the repeat units of the polymeric materials that affect the separation processes.

2.3 Experimental Section

Materials and Methods. All air-sensitive reactions were conducted under an inert atmosphere using an MBraun glovebox filled with nitrogen gas. All monomers were synthesized using standard laboratory techniques and worked up in air. Synthesized monomers were dried using CaH_2, purified by vacuum distillation, degassed via iterative freeze-pump-thaw cycles (3×), and stored over 3 Å molecular sieves in the glovebox prior to use. Triethoxyvinylsilane and vinyltrichlorosilane were purchased from Gelest. Vinyltrichlorosilane was cannula transferred to Schlenk glassware for storage and air-free handling to minimize exposure to adventitious water. 2,2,2-Trifluoro-1-ethanol, 2,2,3,3,3-pentafluoro-1-propanol, 2,2,3,3,4,4,4-heptafluoro-1-butanol, and CaH_2 were purchased from Oakwood Chemical and used as received. Dicyclopentadiene was

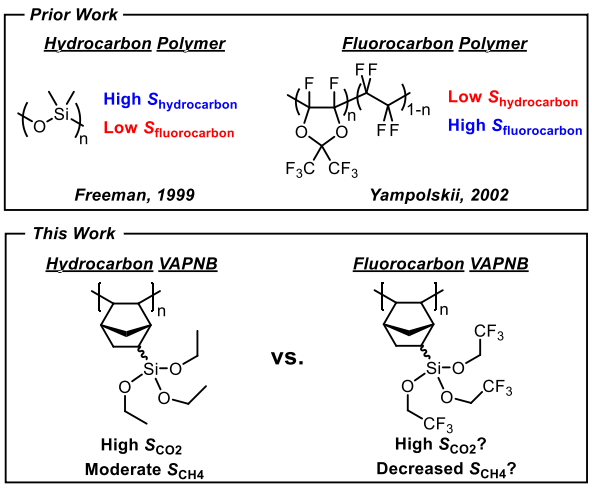


Figure 2.1 Differential solubility of fluorocarbon and hydrocarbon gasses within fluorocarbon and hydrocarbon polymer matrices,[150, 151] and proposed fluorination of APNBs to enhance CO_2/CH_4 selectivity. Reprinted with permission from Reference [153]. Copyright 2022 American Chemical Society.

purchased from Acros Organics and used as received. Imidazole was purchased from Beantown Chemical and used as received. Dichloromethane was purchased from Fisher Scientific, dried via passage through an Innovative Technologies PureSolv solvent purification system, and degassed via iterative freeze-pump-thaw cycles (3×) prior to use. n-Hexanes and methanol for polymer precipitation, as well as tetrahydrofuran for film casting were purchased from Fisher Scientific and used as received. Triphenylantimony, and nickel (II) bromide dimethoxyethane adduct were purchased from Strem and stored in the glovebox prior to use. n-Butyllithium (1.6 M in hexanes) was purchased from Fisher Scientific and cannula transferred to Schlenk glassware for storage and air-free handling. The catalyst, *trans*-[$Ni(C_6F_5)_2(SbPh_3)_2$] was synthesized following literature procedures.[154] The monomers 5-triethoxysilyl-2-norbornene (**M1**)[155] and 5-tripropoxysilyl-2-norbornene (**M2**) [156, 157] were synthesized via Diels-Alder reaction following established literature procedures, respectively.

Monomer and Polymer Characterization. ^1H and ^{13}C NMR spectra of all monomers and their respective vinyl precursors were obtained in $CDCl_3$ using a Varian 600 MHz or 300 MHz spectrometer. ^1H NMR spectra of polymers were obtained using a Varian 500 MHz spectrometer. All NMR spectra were referenced to the residual $CHCl_3$ peaks at $\delta = 7.26$ ppm for ^1H spectra, and $\delta = 77.00$ ppm for ^{13}C spectra. High-resolution mass spectrometry (HRMS) was performed using a JEOL AccuTOF equipped with a DART source. Polymer molecular weights were measured relative to polystyrene standards using a Tosoh EcoSEC GPC system with tetrahydrofuran eluent at 40 °C. Polymer densities were determined via Archimedes principle using a Mettler Toledo MS-DNY-43 density kit interfaced with a Mettler Toledo MS204S analytical balance.

Permeation Analysis. Pure gas flux was measured using a custom-built, constant-volume, variable-pressure permeation instrument. Flux measurements were used to calculate permeability coefficients according to eq 1.

$$P = \frac{V_d l}{P_u ART}\left[\left(\frac{dp}{dt}\right)_{ss} - \left(\frac{pd}{dt}\right)_{leak}\right] \qquad (1)$$

Downstream volumes (V_d) were determined through sequential Burnett expansions using He gas, as reported in the literature.[158] Membrane thicknesses (l) were directly measured using a Mitutoyo 293-832-30 digital micrometer, and typically ranged between 80 μm and 150 μm. Upstream pressure (P_u) was recorded as a time weighted average for the duration of steady state flux measurement. Effective membrane surface area (A) was measured using the open-source image analysis software platform ImageJ, using images generated with an Epson Perfection V19 flatbed scanner. An example of membrane surface area measurement using ImageJ can be found in the Supplemental Information. $R = 0.278\frac{[cm{\cdot}Hg{\cdot}cm^3]}{[cm^3(STP){\cdot}K]}$. Temperature ($T$) was recorded using an analog alcohol thermometer mounted directly outside the permeation cell.

Determination of Diffusivity and Solubility Coefficients. According to the solution-diffusion model of gas transport in dense polymeric membranes, membrane permeability is the product of its solubility and diffusivity coefficients, as described by eq 2. To determine individual solubility and diffusivity coefficients, sorption isotherms were generated for each membrane material using a custom-built dual-volume dual-transducer pressure decay instrument. Concentration of absorbed gas was calculated as described by Koros and Paul.[159] Sorption isotherms were fit to eq 3 using a custom python script utilizing a truncated Newton curve fitting method. Solubility coefficients were then calculated as $p \rightarrow 0$ using the k_d, C'_H, and b parameters determined through curve fitting. With both P and S measured directly, diffusivity coefficients D were determined algebraically using eq 2.

$$P = S \cdot D \qquad (2)$$

$$S = \frac{c}{p} = k_d + \frac{c'_H b}{1+bp} \qquad (3)$$

Synthesis of tris(2,2,2-trifluoroethoxy)vinylsilane (V1F). To a 1000 mL round bottom flask equipped with a magnetic stir bar was added 2,2,2-trifluoro-1-ethanol (60 g, 0.600 mol), imidazole (40.83 g, 0.600 mol), and DCM (500 mL). The resulting solution was cooled to 0 °C before adding vinyltrichlorosilane (24.20 g, 0.150 mol) dropwise over 30 min. After complete addition, the reaction mixture was stirred for an additional 16 h at room temperature. The reaction flask was then equipped with a reflux condenser and refluxed at 60 °C for 2 h. The crude reaction mixture was filtered, passed through a silica gel plug to remove residual imidazolium chloride salt, and concentrated *in-vacuo* to afford 46.08 g of clear colorless liquid (88% isolated yield). ^{1}H NMR ($CDCl_3$, 600 MHz) δ (ppm) = 6.34 (1H, dd, *J* = 15.11, 3.23 Hz), 6.18 (1H, dd, *J* = 20.54, 3.23 Hz), 5.86 (1H, dd, *J* = 20.66, 15.18 Hz), 4.12 (6H, q, J = 8.33). ^{13}C{^{1}H} NMR ($CDCl_3$, 151 MHz) δ (ppm) = 141.3 (s), 124.0 (s), 123.5 (q, *J* = 279.4 Hz), 61.3 (q, *J* = 36.9 Hz).

Synthesis of tris(2,2,3,3,3-pentafluoropropoxy)vinylsilane (V2F). V2F was synthesized using the general procedure outlined for the synthesis of **V1F.** Isolated yield = 73%. ^{1}H NMR ($CDCl_3$, 600 MHz) δ (ppm) = 6.35 (1H, dd, *J* = 15.19, 3.15 Hz), 6.17 (1H, dd, *J* = 20.61, 3.15 Hz), 5.83 (1H, dd, *J* = 20.62, 15.18 Hz), 4.20 (6H, t, *J* = 12.67 Hz). ^{13}C{^{1}H} NMR ($CDCl_3$, 151 MHz) δ (ppm) = 141.6 (s), 123.9 (s), 118.9 (qt, *J* = 285.5, 35.1 Hz), 112.7 (tq, *J* = 254.4, 37.3Hz), 60.6 (t, *J* = 28.6 Hz).

Synthesis of tris(2,2,3,3,4,4,4-heptafluorobutoxy)vinylsilane (V3F). V3F was synthesized using the general procedure outlined for the synthesis of **V1F**. Isolated yield = 60%. ^{1}H NMR ($CDCl_3$, 600 MHz) δ (ppm) = 6.35 (1H, dd, *J* = 15.11, 3.23 Hz), 6.18 (1H, dd, *J* = 20.61, 3.15 Hz), 5.84 (1H, dd, *J* = 20.63, 15.17 Hz), 4.24 (6H, tt, *J* = 13.35, 1.42 Hz). ^{13}C{^{1}H} NMR

($CDCl_3$, 151 MHz) δ (ppm) = 141.2 (s), 123.7 (s), 117.6 (qt, *J* = 286.7, 33.61 Hz), 114.2 (tt, *J* = 256.0, 30.2 Hz), 108.8 (tqt, *J* = 265.8, 38.6, 34.0 Hz), 60.4 (t, *J* = 27.7 Hz).

Synthesis of tributoxyvinylsilane (V3). V3 was synthesized using the general procedure outlined for the synthesis of **V1F**. Isolated yield = 63%. ^{1}H NMR ($CDCl_3$, 300 MHz) δ (ppm) = 6.11 (1H, dd, *J* = 13.84, 5.05 Hz), 6.00 (1H, dd, *J* = 20.58, 5.05 Hz), 5.87 (1H, dd, *J* = 20.61, 13.84 Hz), 4.75 (6H, t, *J* = 6.60 Hz), 1.54 (6H, m), 1.37 (6H, m), 0.91 (3H, t, *J* = 7.31 Hz). ^{13}C{^{1}H} NMR ($CDCl_3$, 75 MHz) δ (ppm) = 136.9 (s), 129.3 (s), 62.6 (s), 34.5 (s), 18.9 (s), 13.8 (s).

Synthesis of 5-tris(2,2,2-trifluoroethoxy)silyl-2-norbornene (M1F). To a 150 mL pressure-rated round bottom flask equipped with a magnetic stir bar was added tris(2,2,2-trifluoroethoxy)vinylsilane (17.38 g, 0.049 mol), dicyclopentadiene (3.26 g, 0.025 mol), and hydroquinone (15 mg, 0.136 mmol). The flask was sealed and heated to 180 °C for 12 h. The crude reaction mixture was then purified and dried by vacuum distillation from CaH_2 to afford 11.38 g of clear colorless liquid (55% yield) as a mixture of *exo*- and *endo*-isomers (*exo*:*endo* = 54:46), b.p. 48 °C (0.5 mmHg). ^{1}H NMR ($CDCl_3$, 600 MHz, *endo* isomer) δ (ppm) = 6.07 (1H, dd, *J* = 5.74, 3.06 Hz), 6.00 (1H dd, *J* = 5.71, 2.90 Hz), 4.05 (6H, q, *J* = 8.36 Hz), 3.07 (1H, br s), 2.96 (1H, br s), 1.93 (1H, ddd, *J* = 11.41, 9.82, 3.69 Hz), 1.44 (1H, dq, *J* = 8.09, 1.81 Hz), 1.35 (1H, ddd, *J* = 9.80, 5.39, 3.05 Hz), 1.27-1.10 (2H, m, overlapped with *exo*-isomer resonance). ^{13}C{^{1}H} NMR ($CDCl_3$, 151 MHz, *exo*/*endo* mixture) δ (ppm). 137.2 (s), 136.3 (s), 134.2 (s), 134.0 (s), 123.60 (q, *J* = 278.0 Hz), 123.57 (q, *J* =278.0 Hz), 61.3 (q, *J* = 37.0 Hz), 61.1 (q, *J* = 37.0 Hz), 50.6 (s), 46.9 (s), 43.9 (s), 42.44 (s), 42.37 (s), 42.1 (s), 26.2 (s), 25.6 (s), 20.2 (s), 19.5 (s). HRMS^{calc} $C_{13}H_{15}F_9O_3Si$ (H^+ adduct) = 419.0725 m/z. HRMS^{expt} $C_{13}H_{15}F_9O_3Si$ (H^+ adduct) = 419.0834 m/z.

Synthesis of 5-tris(2,2,3,3,3-pentafluoropropoxy)silyl-2-norbornene (M2F). Monomer **M2F** was synthesized using the general procedure outlined for the synthesis of **M1F**. Isolated yield = 47%. *exo*:*endo* = 52:48. Boiling point = 55 °C (0.3 mmHg). ^{1}H NMR ($CDCl_3$, 600 MHz, *endo* isomer) δ (ppm) = 6.08 (1H, dd, *J* = 5.73, 3.07 Hz) 5.99 (1H, dd, overlapped with *exo*-isomer resonance), 4.13 (6H, t, *J* = 12.68 Hz), 3.06 (1H, br s), 2.98 (1H, br s), 1.93 (1H, ddd, *J* = 11.43 Hz), 1.45 (1H, dq, *J* = 8.20, 1.88 Hz), 1.35 (1H, ddd, *J* = 9.94, 5.40, 3.06 Hz), 1.28-1.08 (2H, m, overlapped with *exo*-isomer resonance). ^{13}C{^{1}H} NMR ($CDCl_3$, 151 MHz, *exo*/*endo* mixture) δ (ppm). 137.2 (s), 136.3 (s), 134.2 (s), 134.0 (s), 118.63 (qt, *J* = 285.4, 34.8 Hz), 118.62 (qt, *J* = 285.4, 34.8 Hz), 112.5 (tq, *J* = 254.5, 37.1 Hz), 60.3 (q, *J* = 28.3 Hz), 50.6 (s), 46.9 (s), 43.8 (s), 42.4 (s), 42.3 (s), 42.0 (s), 26.0 (s), 25.5 (s), 20.1 (s), 19.4 (s). HRMS^{calc} $C_{16}H_{15}F_{15}O_3Si$ (H^+ adduct) = 569.0629 m/z. HRMS^{expt} $C_{16}H_{15}F_{15}O_3Si$ (H^+ adduct) = 569.0824 m/z.

Synthesis of 5-tris(2,2,3,3,4,4,4-heptafluorobutoxy)silyl-2-norbornene (M3F). Monomer **M3F** was synthesized using the general procedure outlined for the synthesis of **M1F**. Isolated yield = 68%. *exo*:*endo* = 50:50. Boiling point = 65 °C (0.35 mmHg). ^{1}H NMR ($CDCl_3$, 600 MHz, *endo* isomer) δ (ppm) = 6.08 (1H, dd, *J* = 5.73, 3.04 Hz) 5.99 (1H, dd, overlapped with *exo*-isomer resonance), 4.18 (6H, t, *J* = 13.34 Hz), 3.07 (1H, br s), 2.98 (1H, br s), 1.94 (1H, ddd, *J* =11.38, 9.76, 3.67 Hz), 1.45 (1H, dq, *J* = 8.15, 1.95 Hz), 1.36 (1H, ddd, *J* = 9.91, 5.43, 3.03 Hz), 1.28-1.08 (2H, m, overlapped with *exo*-isomer resonance). ^{13}C{^{1}H} NMR ($CDCl_3$, 151 MHz, *exo*/*endo* mixture) δ (ppm). 137.3 (s), 136.6 (s), 134.4 (s), 134.2 (s), 117.8 (qt, *J* = 278.1, 33.8 Hz), 114.4 (tt, *J* = 256.0, 30.0 Hz), 109.0 (tqt, *J* = 264.3, 38.7, 34.3 Hz), 60.6 (q), 50.7 (s), 47.0 (s), 44.0 (s), 42.6 (s), 42.5 (s), 42.2 (s), 26.2 (s), 25.7 (s), 20.3 (s), 19.6 (s). HRMS^{calc} $C_{19}H_{15}F_{21}O_3Si$ (H^+ adduct) = 719.0533 m/z. HRMS^{expt} $C_{19}H_{15}F_{21}O_3Si$ (H^+ adduct) = 719.0714 m/z.

Synthesis of 5-tributoxysilyl-2-norbornene (M3). Monomer **M3** was synthesized using the general procedure outlined for the synthesis of **M1F**. Isolated yield = 62%. *exo*:*endo* = 64:36. Boiling point = 85 °C (0.2 mmHg). ^{1}H NMR ($CDCl_3$, 600 MHz, *endo* isomer) δ (ppm) = 6.00 (1H, dd, *J* = 5.55, 2.89 Hz), 5.97 (1H, dd, *J* = 5.65, 2.93 Hz) 3.69 (6H, t, *J* = 6.61 Hz), 3.01 (1H, br s), 2.87 (1H, br s), 1.85 (1H, ddd, *J* = 10.75, 9.54, 3.72 Hz), 1.58-1.47 (6H, m, overlapped with *exo*-isomer resonance), 1.42-1.30 (6H, m, overlapped with *exo*-isomer resonance), 1.19 (1H, ddd, *J* = 13.84, 6.50, 3.76 Hz), 1.17-1.04 (3H, m, overlapped with *exo*-isomer resonance) 0.88-0.94 (9H, m, overlapped with *exo*-isomer resonance). ^{13}C{^{1}H} NMR ($CDCl_3$, 151 MHz, *exo*/*endo* mixture) δ (ppm). 137.7 (s), 135.1 (s), 134.7 (s), 133.7 (s), 62.6 (s), 62.3 (s), 50.7 (s), 47.0 (s), 44.2 (s), 42.8 (s), 42.4 (s), 42.2 (s), 34.69 (s), 34.66 (s), 26.9 (s), 26.3 (s), 20.7 (s), 20.2 (s), 18.9 (s), 13.8 (s). HRMS^{calc} $C_{19}H_{36}O_3Si$ (H^+ adduct) = 341.2512 m/z. HRMS^{expt} $C_{19}H_{36}O_3Si$ (H^+ adduct) = 341.2611 m/z.

General Homopolymer Synthesis. All homopolymerizations were conducted in an MBraun glovebox using *trans*-[$Ni(C_6F_5)_2(SbPh_3)_2$] as the vinyl-addition catalyst in dry and degassed DCM. For example, homopolymer **P1** was synthesized by adding 800 μL of catalyst solution in DCM (4.9 mM) to a stirred solution of 5-triethoxysilyl-2-norbornene (**M1**) (1.0 g, 3.9 mmol) in DCM (3.1 mL). The polymerization was stirred for 16 h before being removed from the glovebox, diluted with 3 mL of additional DCM, and precipitated into methanol. The resultant polymer was isolated via vacuum filtration and dried *in-vacuo* to constant weight (isolated yield = 62%, M_n = 217.0 kg/mol, $Đ$ = 1.2). Homopolymers **P2** and **P3** were synthesized using this general procedure. Homopolymer **P1F** was synthesized via a similar procedure but using a higher monomer concentration (5 M), as 1 M polymerizations only afforded low molecular weight polymers with insufficient mechanical integrity for membrane fabrication. Polymer **P1F** was

precipitated into hexane. Each polymer's isolated yield, molecular weight, and dispersity can be found in the discussion section.

General Copolymer Synthesis. All copolymerizations were conducted in an MBraun glovebox using *trans*-[Ni(C_6F_5)$_2$($SbPh_3$)$_2$] in dry and degassed DCM. For example, copolymer **P1^{84}P1F^{16}** was synthesized by adding 800 μL of a DCM catalyst solution (4.9 mM) to a stirred solution of 5-triethoxysilyl-2-norbornene (**M1**) (0.75 g, 2.93 mmol), 5-tris(2,2,2-trifluoroethoxy)silyl-2-norbornene (**M1F**) (0.41 g, 0.97 mmol), and DCM (3.1 mL). The polymerization was stirred for 16 h before being removed from the glovebox, and precipitated into methanol. The resultant polymer was isolated via vacuum filtration and dried *in-vacuo* to constant weight (isolated yield = 49%, M_n = 114.6 kg/mol, $Đ$ = 2.1). All copolymers discussed herein were synthesized using this general procedure. However, copolymers targeting higher fluorinated monomer contents (i.e. **P1^{48}P1F^{52},** and **P3^{87}P3F^{13}**) used higher initial monomer concentrations (5 M), as 1 M polymerizations only afforded low molecular weight polymers with insufficient mechanical integrity for membrane fabrication. Lastly, we found that polymers containing higher fluorinated monomer incorporation (e.g. **P1^{48}P1F^{52}**) ratios precipitated poorly into methanol, and were therefore precipitated into hexanes prior to filtration and drying. Their isolated yield, molecular weight, and dispersity can be found in discussion section.

Membrane Preparation. Membranes of all polymers discussed herein were prepared through solution casting 5.3 wt% polymer solutions in THF. As an example, 10 mL of THF was added to a vial containing 0.501 g of polymer and a PTFE coated magnetic stir bar. This mixture was stirred until the polymer was fully dissolved. The resulting polymer solution was filtered through a 0.45 μm PTFE syringe filter into a freshly cleaned, 6.5 cm diameter, flat-form PTFE dish. The PTFE dishes containing polymer solutions were covered with aluminum foil to slow the

evaporation of solvent. Fabricated membranes were removed from the casting dishes after slowly evaporating for 48–72 h. Polymers with higher fluorine content exhibited strong adhesion to glass substrates, and as-such could not be cast using glass dishes. Therefore, PTFE dishes were used in all membrane preparation to maintain consistent membrane fabrication conditions across all materials studied herein.

Wide angle X-ray scattering. Polymers were illuminated at normal incidence (transmission through the film thickness) using A Xenocs GeniX 3D microfocus source with a copper target (wavelength λ = 0.154 nm) under ambient conditions. The sample–detector distance was 0.045 m. A Pilatus3 R_300 K detector (Dectris) was used with pixel size of 172 μm × 172 μm. The data acquisition time was 5 min. The two-dimensional images from each measurement were azimuthally-integrated to yield a one-dimensional scattering profile of intensity I (a.u.) versus scattering vector q ($Å^{-1}$). Interchain distances were calculated via Braggs law (eq 4) to give d_B or a modified form of the Bragg law (eq 5) in which a correction factor of 1.22 is applied to give d_{ic}. This correction factor has been proposed to reflect interchain spacing more accurately for polymeric materials.[160, 161]

$$d_B = \frac{\lambda}{2 \sin \theta} \quad (4)$$

$$d_{ic} = \frac{1.22\lambda}{2 \sin \theta} \quad (5)$$

Computational Details. Quantum chemical calculations were performed for the elucidation of the noncovalent interaction strength between individual repeat units of these functionalized APNBs **P1**–**P3** and **P1F**–**P3F**, and the respective gas molecules CO_2, and CH_4 (monomer–gas interactions), as well as interactions between individual repeat units (monomer–monomer interactions). Due to the large number of degrees of freedom and the different interaction motifs between the gas molecules and the functionalized APNB repeat units, a hybrid molecular

dynamics/quantum chemical scheme was applied to screen a large number of near-isoenergetic conformers. The computational protocol implemented is shown schematically in Figure B.1, and allowed us to perform density functional theory (DFT) calculations with unbiased initial structures. All molecular geometries were first optimized with DFT using the PBE0[162] functional, a small basis set (def2-SVP)[163], and Grimme's D3 dispersion correction[164] with the Becke-Johnson damping function[165] as implemented within the TURBOMOLE 7.2 program package.[166] Force-field input structures were generated from the preoptimized structures using LigParGen[167] for simulations using the LAMMPS[168] software package. The OPLS-AA force field[169] was used with a periodic box at 200 K in a NVT ensemble with a Nosé-Hoover thermostat using a 1.0 ps time constant and a 1.0 fs time step. For each system, 50,000 time steps were used to reduce the bias produced by the MD dependence on the initial structure and still provide a structure that is not trapped on a local minimum on the potential energy surface (PES).[155] The thirty lowest energy structures were acquired and then optimized with DFT at the PBE0-D3(BJ)/def2-TZVPP level of theory. Tight convergence and the resolution identity for the two-electron integrals were also implemented for all DFT calculations.

The interaction energies (ΔE_{AB}) between two structures, *A* and *B*, were computed as demonstrated by Eq. 6:

$$\Delta E_{AB} = E_{AB} - E_A - E_B \qquad (6)$$

where E_{AB} represents the energy of the interacting supersystem, and E_A and E_B represent the energies of the isolated systems. For calculations on monomer–gas interactions, *A* corresponds to a saturated monomer analog of the repeat unit of **P1**, **P2**, **P3**, **P1F**, **P2F** or **P3F**, and *B* to either CO_2 or CH_4. For the monomer–monomer examination $A = B$ and correspond to a saturated monomer analog of the repeat unit of **P1**, **P2**, **P3**, **P1F**, **P2F** or **P3F**.

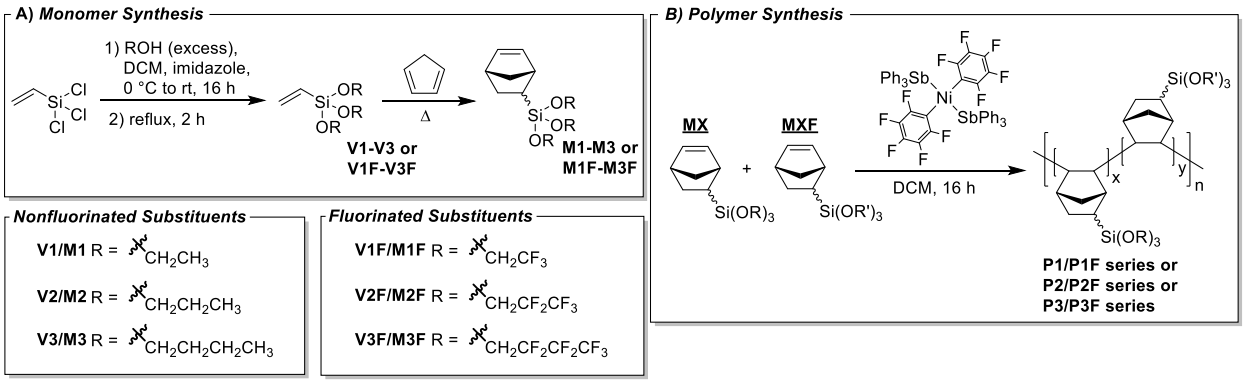
Due to the large number of degrees of freedom of the monomer-monomer superstructures, an additional set of geometry optimizations was performed for the further validation of the computational results. Initial geometries of the monomers with short chains were generated from the most stable structures by manually removing atoms from the monomeric units that incorporate lengthier chains, which were further optimized by the same level of theory (PBE0-D3(BJ)/def2-TZVPP).

2.4 Results and Discussion

The proposed fluorinated monomer structures **M1F**–**M3F** and their hydrocarbon counterpart **M1**–**M3** are shown in Scheme 2.1. This systematic series of monomers was chosen so that the influence of polymer fluorination on pure gas separation performance could be investigated. For example, employing monomers **M1F**–**M3F** enables tailoring of weight percent fluorine in each monomer from 40.9% to 55.5%, respectively. Furthermore, polymer fluorine content could be manipulated via copolymerization of fluorinated and hydrocarbon-based monomers **M1**/**M1F**, **M2**/**M2F**, and **M3**/**M3F** to yield the corresponding copolymer series. Lastly, as the pendant alkoxysilyl groups increase in bulkiness from **M1** to **M3**, and from **M1F** to **M3F**, the influence of polymer fluorination on chain packing could be examined in regards to membrane performance.

All vinylalkoxysilane derivatives, except triethoxyvinylsilane which is commercially available, were synthesized via nucleophilic substitution of vinyltrichlorosilane with the appropriate alcohol in the presence of imidazole in dry DCM to yield nonfluorinated reagents **V1**–**V3** and fluorinated reagents **V1F**–**V3F** (Scheme 2.1). These vinyl species were isolated as clear colorless liquids in good yield (60%-88%). Norbornene-based monomers **M1**–**M3** and **M1F**–**M3F** were then synthesized via Diels-Alder reaction between dicyclopentadiene (as a molecular

surrogate for cyclopentadiene) and the corresponding vinylalkoxysilane following an established literature procedure.[154] Monomers **M1**–**M3** and **M1F**–**M3F** were purified by iterative vacuum distillation until reaching >99% purity (by NMR), yielding clear colorless oils that were isolated in moderate yield (47%–68%) as a mixture of *endo*- and *exo-isomers*. Each of the synthesized vinylalkoxysilanes and their corresponding monomers were characterized via ^{1}H and ^{13}C NMR spectroscopy, as well as HRMS (see the Supporting Information).



Scheme 2.1. (A) Synthesis of nonfluorinated and fluorinated monomers **M1**–**M3** and **M1F**–**M3F**, respectively and (B) general synthesis of nonfluorinated and fluorinated polymers **P1**-**P3** and **P1F**-**P3F** respectively, and copolymers thereof.

Monomers **M1**–**M3** were homopolymerized in dry DCM using the catalyst *trans*-$[Ni(C_6F_5)_2(SbPh_3)_2]$ to yield non-fluorinated homopolymers **P1–P3** following previously reported procedures (Scheme 2.1).[154] These polymers exhibit excellent solubility in common organic solvents such as DCM, THF, and toluene. In contrast to polymers **P1–P3**, which were synthesized using initial monomer concentrations of $M_0 = 1.0$ M in DCM, attempts to homopolymerize **M1F** at this concentration were unsuccessful and resulted in low molecular weight polymers with insufficient mechanical integrity for membrane fabrication. Instead, **M1F** was successfully

polymerized at higher concentration (M_0 = 5.0 M) in DCM. Fluorinated polymer **P1F** is soluble in THF, but insoluble in $CHCl_3$; however, fluorinated homopolymers **P2F** and **P3F** were virtually insoluble in these solvents, which resulted in the premature precipitation of polymer from solution during homopolymerization. Attempts to redissolve the resultant **P2F** and **P3F** polymers were unsuccessful, which precluded further characterization of these materials.

While solubility issues precluded access to high molecular weight **P2F** and **P3F** homopolymers, soluble copolymers of **P2**/**P2F** and **P3**/**P3F** were readily synthesized and characterized. Overall, three series of statistical copolymers with different molar incorporation ratios of nonfluorinated:fluorinated monomers were produced. The statistical copolymers described herein are denoted **PX^{a}PXF^{b}**, where **PX** and **PXF** signify the non-fluorinated repeat unit and its fluorinated analogue, respectively; and the superscripts **a** and **b** represent the mole percent of **MX** and **MXF** incorporated into the polymer (as determined via ^{1}H NMR spectroscopy). Monomer incorporation ratios were determined by the relative integration of the resonances at 3.79 and 4.08 ppm, which correspond to the methylene protons directly adjacent to the oxygen atoms of the alkoxysilyl-substituents in the **PX** and **PXF** repeat units, respectively (see Supplemental Information). Specifically, the **P1**/**P1F** series covered a broad range of 0%–100% incorporation of **M1F** monomer, while **P2**/**P2F** and **P3**/**P3F** series were limited to lower fluorinated monomer incorporation of 0–30% due to solubility constraints. All polymers were recovered by precipitation into methanol or hexanes and dried *in-vacuo* to a constant weight.

As shown in Table 2.1, polymer yield decreased as a function of increasing incorporation of fluorinated monomer for all three polymer series (62% to 26% for **P1**/**P1F** series, Table 2.1, entry 1–5), (57% to 38% for **P2**/**P2F** series, entry 6–8), and (65% to 63% for **P3**/**P3F** series, entry 11-12). Additionally, this decreasing trend in yield was accompanied by a corresponding decrease in

Table 2.1 Synthesis and Characterization of all Homopolymers and Copolymers[a]

entry	polymer	Feed ratio (MX:MXF)	Actual ratio (MX:MXF)	Yield (%)	Mn (kg/mol)	*Đ*
1	**P1**	100:0	100:0	62	217.0	1.2
2	**P1^{84}P1F^{16}**	75:25	84:16	49	114.6	2.1
3	**P1^{67}P1F^{33}**	50:50	67:33	37	115.2	3.0
4[b]	**P1^{48}P1F^{52}**	30:70	48:52	26	-[e]	-[e]
5[b]	**P1F**	0:100	0:100	26	49.4	3.7
6	**P2**	100:0	100:0	57	88.1	1.9
7	**P2^{87}P2F^{13}**	75:25	87:13	43	77.5	1.9
8	**P2^{72}P2F^{28}**	50:50	72:28	38	42.3	3.2
9[c]	**P2^{50}P2F^{50}**	30:70	-	25[f]	-	-
10[c]	**P2F**	0:100	-	36[f]	-	-
11	**P3**	100:0	100:0	65	188.2	1.8
12[d]	**P3^{87}P3F^{13}**	75:25	87:13	63	184.6	1.8
13[c]	**P3^{73}P3F^{27}**	50:50	-	87[f]	-	-
14[c]	**P3^{50}P3F^{50}**	30:70	-	86[f]	-	-
15[c]	**P3F**	0:100	-	83[f]	-	-

[a]General polymerzation conditions: total monomer = 3.9 mmol, catalyst = 3.9 μmol, 3.9 mL of DCM, T_{rxn} = 20 °C, and t = 16 h. Polymers were purified by precipitation into MeOH. [b]Polymerizations were run with initial monomer concentration of 5 M and were purified by precipitation into hexane. [c]Polymer precipitated out of solution during polymerization and could not be redissolved for further analysis. [d]Polymerizations were run with initial monomer concentration of 5 M and were purified by precipitation into MeOH. [e]This polymer exceeds the GPC calibration standards available; therefore, the molecular weight and dispersity values obtained are likely inaccurate. [f]As the polymer prematurely precipitates out of solution, forming an insoluble gel, the isolated material likely contains some residual monomer.

molecular weight and overall broadening of dispersity. In all cases, the copolymers favored incorporation nonfluorinated monomers **M1**–**M3** over incorporation of the analogous fluorinated monomers **M1F**–**M3F**, as was demonstrated by the discrepancies between feed ratios and actual incorporation ratios determined via ^{1}H-NMR. In general, the incorporation of fluorinated monomer was approximately half of the feed ratio. We hypothesize that the increased steric bulk of the pendant fluorinated alkoxysilyl moieties either hinders monomer coordination to the active, propagating Ni-site, or that the increased monomer steric bulk slows subsequent migratory insertion during vinyl addition polymerization.

Polymer films for gas transport measurements were cast from 5.3 wt% solutions in THF. These polymer-THF solutions were syringe filtered into shallow PTFE dishes, which were then covered and solvent allowed to evaporate over several days. This procedure produced homogeneous, free-standing films between 80 to 150 μm thick. Wide-angle X-ray scattering (WAXS) revealed broad amorphous halos for all homo- and copolymers, and no sharp diffraction peaks, suggesting that these materials are amorphous. The calculated interchain *d*-spacing values only vary by a few angstroms, suggesting that the chain packing of these polymers are relatively consistent regardless of monomer type (Table 2.2).

As shown in Table 2.2, the density of these polymers was measured using Archimedes' principle, and those values were used to estimate fractional free volumes (FFV) using the Bondi method.[170-172] For all three polymer series studied, the density (ρ) generally increases as the mole fraction of incorporated fluorinated monomer increases (**P1**/**P1F** series, ρ = 1.077−1.432 g/cm^3, Table 2.2, entry 1–5), (**P2**/**P2F** series, ρ = 1.047–1.206 g/cm^3, entry 6–8), (**P3**/**P3F** series, ρ = 1.014–1.114 g/cm^3, entry 9–10). Despite these trends in bulk density, no clear trend between fluorine content and FFV was observed, as the FFV for all polymer films being tested generally

Table 2.2 Density, Fractional Free Volume (FFV), and *d*-Spacing for Polymer Films.

				d-spacing (Å)[c]		
entry	Polymer	Density (g/cm^3)[a]	FFV[b]	$(d_B/d_{ic})_1$	$(d_B/d_{ic})_2$	$(d_B/d_{ic})_3$
1	**P1**	1.077 (±0.009)	0.159	14.4/17.6	6.4/7.8	4.2/5.1
2	**P1^{84}P1F^{16}**	1.117 (±0.007)	0.181	14.6/17.8	6.4/7.8	4.2/5.1
3	**P1^{67}P1F^{33}**	1.199 (±0.043)	0.158	15.1/18.4	6.4/7.8	4.3/5.2
4	**P1^{48}P1F^{52}**	1.262 (±0.017)	0.172	15.3/18.7	-	4.3/5.3
5	**P1F**	1.432 (±0.031)	0.171	16.7/20.4	-	4.4/5.4
6	**P2**	1.047 (±0.021)	0.157	13.5/16.5	5.9/7.2	3.8/4.7
7	**P2^{87}P2F^{13}**	1.085 (±0.029)	0.194	13.7/16.8	-	3.9/4.8
8	**P2^{72}P2F^{28}**	1.206 (±0.036)	0.181	13.8/16.9	-	4.1/4.9
9	**P3**	1.014 (±0.006)	0.165	14.1/17.1	-	3.9/4.7
10	**P3^{87}P3F^{13}**	1.114 (±0.028)	0.170	14.4/17.6	-	4.1/5.0

[a]Determined using Archimedes' principle. [b]Estimated using the Bondi method.[170-172] [c]Measured using wide-angle X-ray scattering and *d*-spacing is calculated using Bragg's Law.

ranged from 0.157–0.194.

To test our hypothesis that the incorporation of fluorinated motifs improves the CO_2/CH_4 selectivity of APNBs, albeit while maintaining relatively consistent CO_2 permeability, we measured the ideal gas selectivity of our materials using the constant-volume variable-pressure gas flux method (Table 2.3). We observed that the CO_2/CH_4 selectivity of each copolymer series increased as a function of increasing fluorinated monomer incorporation, as is shown numerically in Table 2.3 as well as graphically in Figure 2.2. More specifically, the CO_2/CH_4 selectivity of the **P1**/**P1F** copolymer series increased from 5.7 to 9.5 (an increase of ~67%) as a function of increasing fluorinated comonomer incorporation, and displaying only marginal decreases in CO_2 permeability (i.e., 1026 → 920 Barrer, a decrease of ~10%) (Table 2.3, entries 1–5). For the copolymer series **P2**/**P2F** and **P3/P3F**, not only did CO_2/CH_4 selectivity increase, but these increases were accompanied by a corresponding increase in CO_2 permeability. For example, the CO_2/CH_4 selectivity of the **P2**/**P2F** copolymer series increased from 4.7 to 5.7 (an increase of ~21%) and CO_2 permeability increased from 510 to 763 Barrer (an increase of ~50%) (Table 2.3, entries 6–8). Comparatively, the increases in selectivity and permeability for the **P3/P3F** copolymer series were relatively small, which we attribute to lower incorporation ratios of fluorinated comonomer that were synthetically accessible, with CO_2/CH_4 selectivity increasing from 4.0 to 4.3 (an increase of ~7%) and CO_2 permeability increasing from 550 to 665 Barrer (an increase of ~21%) (Table 2.3, entries 9–10).

As can be seen in Figure 2.2, the increase in CO_2/CH_4 selectivity observed for the **P1**/**P1F** copolymer series, along with a negligible change in CO_2 permeability, manifests as a near vertical approach towards the 2008 upper bound. For the **P2**/**P2F** and **P3/P3F** copolymer series, simultaneous increases in CO_2/CH_4 selectivity and CO_2 permeability leads to trends moving

Table 2.3 Ideal Permeability and Selectivity of the **P1**/**P1F**, **P2**/**P2F** and **P3**/**P3F** Polymer Series.

		P (Barrer)[a]		
entry	Polymer	CO_2	CH_4	α (CO_2/CH_4)[b]
1	**P1**	1026 (±51)	180 (±8)	5.7 (±0.0)
2	**P1^{84}P1F^{16}**	1217 (±65)	199 (±16)	6.1 (±0.2)
3	**P1^{67}P1F^{33}**	1156 (±104)	177 (±19)	6.6 (±0.1)
4	**P1^{48}P1F^{52}**	910 (±55)	119 (±11)	7.7 (±0.3)
5	**P1F**	920 (±101)	97 (±13)	9.5 (±0.2)
6	**P2**	510 (±27)	109 (±5)	4.7 (±0.0)
7	**P2^{87}P2F^{13}**	660 (±13)	131 (±4)	5.0 (±0.1)
8	**P2^{72}P2F^{28}**	763 (±67)	133 (±12)	5.7 (±0.0)
9	**P3**	550 (±51)	139 (±13)	4.0 (±0.0)
10	**P3^{87}P3F^{13}**	665 (±28)	154 (±8)	4.3 (±0.0)

[a]Permeability values of free-standing polymer films were obtained using the constant-volume variable-pressure gas flux method at 20 psi upstream pressure. [b]Ideal selectivity was calculated as a ratio of pure gas $P(CO_2)/P(CH_4)$.

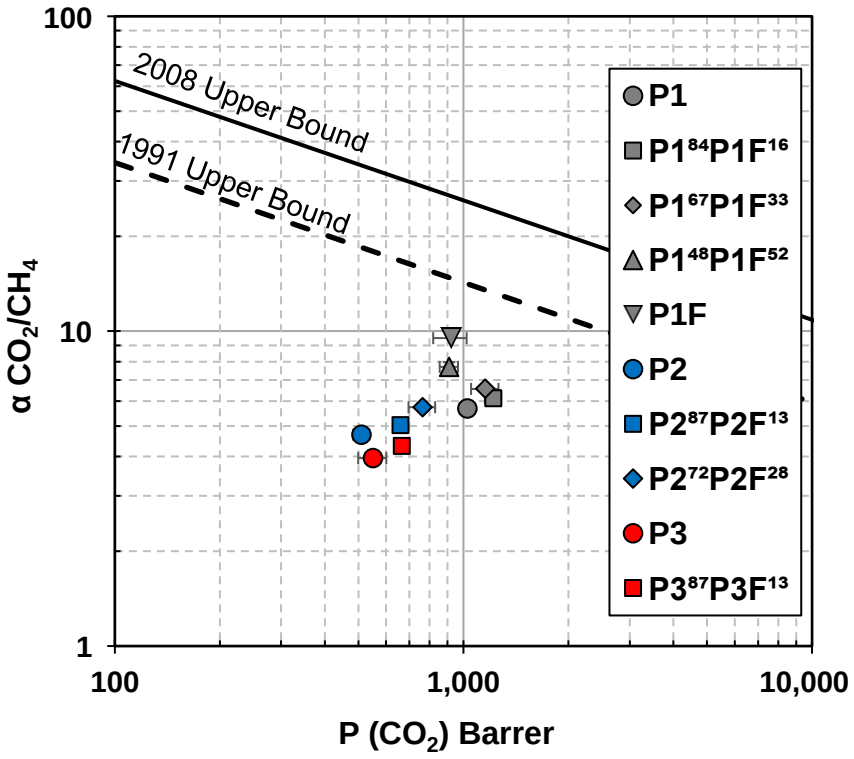


Figure 2.2 Robeson plot of polymers tested in this study. Grey, blue, and red symbols represent **P1**/**P1F**, **P2**/**P2F**, **P3**/**P3F** polymer series, respectively. Error bars are included for each data point, but in some cases, the error bars are smaller than the data marker. Reprinted with permission from Reference [153]. Copyright 2022 American Chemical Society.

almost perpendicular to the bound. Each of these observations defy traditional permeability-selectivity trade-off behavior. Because CO_2/CH_4 gas separation performance generally improves as a function of increasing fluorinated comonomer incorporation ratio, this suggests that increasing weight percent (wt%) of fluorine may be critical to optimal membrane performance. However, when comparing copolymers with similar molar ratios of nonfluorinated:fluorinated comonomers across multiple copolymer series (e.g. **P1^{84}P1F^{16}**, **P2^{87}P2F^{13}**, and **P3^{87}P3F^{13}**), CO_2/CH_4 selectivity and CO_2 permeability both generally decrease as the wt% of fluorine content becomes greater, with **P1^{84}P1F^{16}**, **P2^{87}P2F^{13}**, and **P3^{87}P3F^{13}** having 9.7, 11.1, and 13.3 wt% fluorine content, respectively. These results suggest that while simply increasing the wt% fluorinated content within a structurally analogous series of polymers (e.g. **P1** versus **P1F**) may prove a useful strategy to improve membrane performance, similar conclusions may not be drawn across polymer series that differ in their molecular size of design, even when structurally related (e.g. **P1F** versus **P3F**), likely due to differences in polymer chain packing and intermolecular interactions.

These data are consistent with prior observations regarding gas transport in addition type alkoxysilyl polynorbornenes. For example, Bermeshev and coworkers observed a proportional decrease in gas permeation for a series of vinyl addition tricyclononene polymers as the bulk of the alkoxysilyl substituent increased from methoxy to butoxy groups.[173] While a similar trend can be seen in the present work (i.e. for **P1, P2,** and **P3**, PCO_2 = 1026, 510, and 550 Barrer respectively), the incorporation of fluorinated substituents in the **P2/P2F** series and **P3/P3F** series not only increase CO_2 permeability (PCO_2 = 510 → 763 Barrer, and 550 → 665 Barrer for **P2/P2F** and **P3/P3F** series, respectively) but also enhances CO_2/CH_4 separation performance (PCO_2/PCH_4 = 4.7 → 5.7, and 4.0 → 4.3 for **P2/P2F** and **P3/P3F** series, respectively). This demonstrates a

promising avenue to enhance the CO_2/CH_4 separation capacity for alkoxysilyl containing polynorbornenes with longer alkoxy substituents.

In addition, the observed increase in CO_2/CH_4 selectivity with the increase in fluorinated content is similar to previous literature where similar structural analogs were compared. For example, both a slightly increase in CO_2 permeability and CO_2/CH_4 selectivity was observed in direct fluorination of the double bond along the backbone of metathesis polynorbornene.[174] In another example, according to Jansen, McKeown and coworkers, the incorporation of trifluoromethyl groups in PIMs had two different observations: in one case, the addition of trifluoromethyl group resulted in a slightly increase in both CO_2 permeability and CO_2/CH_4 selectivity, which is similar to what we observed; while in another case, the polymers with trifluoromethyl groups had higher CO_2 permeability but lower CO_2/CH_4 selectivity compared to their methyl polymer analogs,[175] which is similar to that observed in polyimide with 6FDA units as discussed in the introduction.[144, 145]

Encouraged by the promising permselectivity results described above, we sought to interrogate the origins of these fluorinated APNB's gas separation behavior through a detailed analysis of pure gas sorption parameters. As described by the solution-diffusion model of gas transport in dense polymeric membranes, gas permeability (*P*) is the product of the concentration-averaged effective diffusion coefficient (*D*) and solubility coefficient (*S*). To obtain *S*, pure gas sorption isotherms were generated by measuring the concentration of sorbed gas as a function of pressure using the dual-volume pressure-decay method.[159] As shown in Figure 2.3, the resulting sorption isotherms were then fit using a custom Python script to either the dual-mode sorption model or linearly, achieving good correlation factors ($R^2 \geq 0.999$ for CO_2 and ≥ 0.998 for CH_4). Pure gas solubility coefficients (*S*) were then extracted from these isotherms by solving eq 3 as

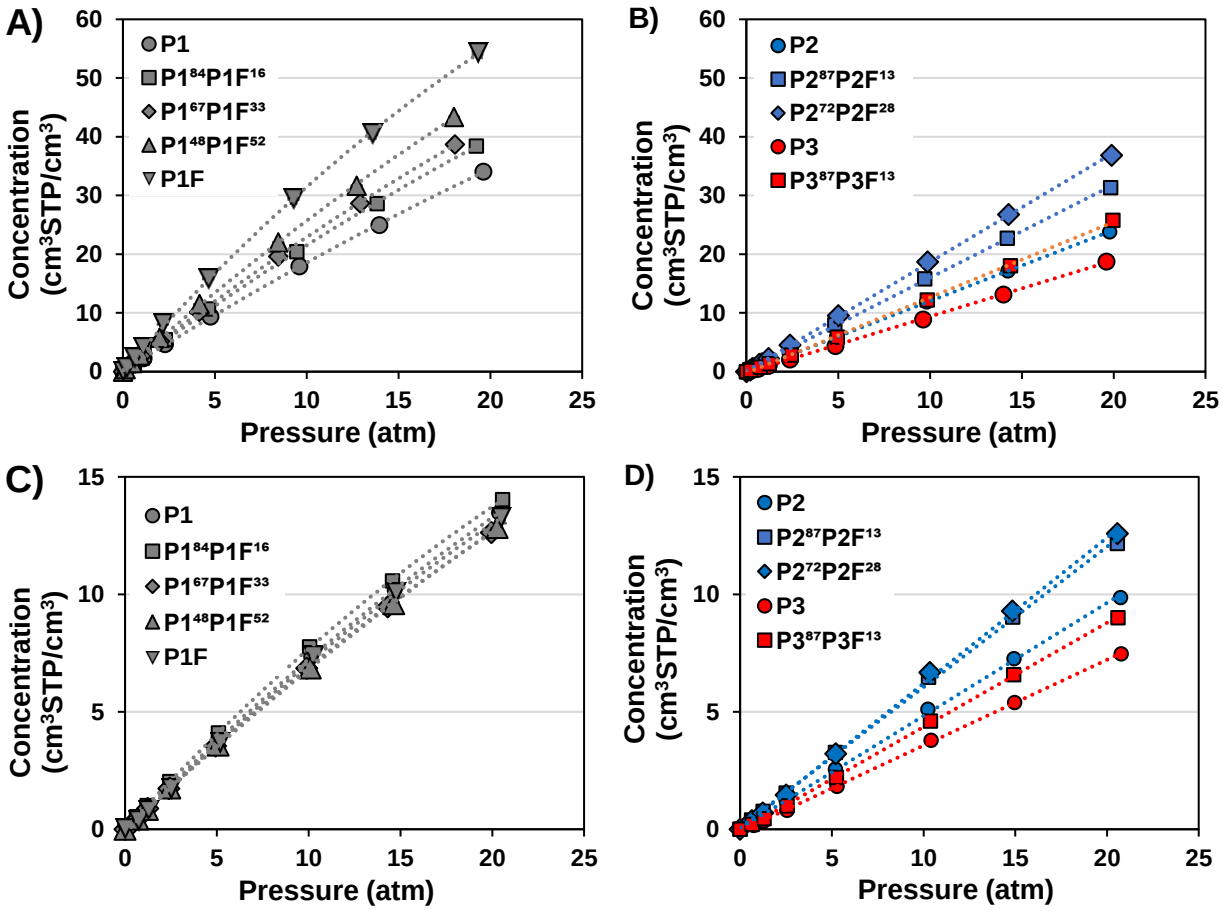


Figure 2.3 (A) CO_2 sorption isotherms for the **P1**/**P1F** copolymer series. (B) CO_2 sorption isotherms for the **P2**/**P2F** and **P3**/**P3F** copolymer series. (C) CH_4 sorption isotherms for the **P1**/**P1F** copolymer series and (D) CH_4 sorption isotherms for the **P2**/**P2F** and **P3**/**P3F** copolymer series. All isotherms were generated at 35 °C. **P1**/**P1F** copolymer series isotherms were fit using the dual-mode sorption model, whereas **P2**/**P2F** and **P3**/**P3F** series (with no observable Langmuir contributions) were fit linearly to provide the highest possible R^2. Trend lines are included to guide the reader's eye. Reprinted with permission from Reference [153]. Copyright 2022 American Chemical Society.

pressure approaches 0 atm. The diffusion coefficients (D) were then determined algebraically using the experimentally determined P and S coefficients using the equation $D = P/S$ (Table 2.4).

Through detailed analysis of sorption isotherms and the calculated D and S parameters, several notable trends were observed. First, the diffusion coefficients of CO_2 and CH_4 (D_{CO2} and D_{CH4}) decrease consistently with increased incorporation of fluorinated repeat units for each copolymer series. This is particularly notable for the **P1**/**P1F** copolymer series in which D_{CO2} (D_{CO2} = 3.62 to 1.80) and D_{CH4} (D_{CH4} = 1.70 to 0.96) each decrease by ~50% (Table 2.4, entries 1–5). Although both diffusion coefficients for CO_2 and CH_4 decrease as a function of fluorine content, the diffusivity selectivity (D_{CO2}/D_{CH4}) of each copolymer series is relatively constant (D_{CO2}/D_{CH4} = 2.13–1.87 for the **P1**/**P1F** series, 1.88–1.91 for the **P2**/**P2F** series, and 1.51–1.49 for the **P3**/**P3F** series) (Table 2.4). Thus, the observed overall increase of permselectivity (P_{CO2}/P_{CH4}) with increasing fluorinated comonomer incorporation for each copolymer series is a direct consequence of changes in solubility selectivity.

Indeed, analysis of individual solubility selectivity (S_{CO2}/S_{CH4}) values across each copolymer series demonstrate this relationship, wherein S_{CO2}/S_{CH4} increases by 90% for the **P1**/**P1F** copolymer series (S_{CO2}/S_{CH4} = 2.67–5.06) (Table 2.4, entries 1–5), 20% for the **P2**/**P2F** copolymer series (S_{CO2}/S_{CH4} = 2.50–3.01) (Table 2.4, entries 6–8), and 10% for the **P3**/**P3F** copolymer series (S_{CO2}/S_{CH4} = 2.63–2.90) (Table 2.4, entries 9–10), respectively. In contrast, analysis of copolymers across two or more copolymers with similar molar incorporation ratios of fluorinated monomers (e.g. **P1^{84}P1F^{16}** versus **P2^{87}P2F^{13}**) reveals that the observed decrease in CO_2/CH_4 selectivity as a function of increasing fluorine wt% may result from a combination of factors. Therein, both diffusivity and solubility selectivity decrease as fluorine wt% is increased. For example, the diffusivity selectivity of **P1^{84}P1F^{16}** and **P2^{87}P2F^{13}** are D_{CO2}/D_{CH4} = 2.12 and 1.90, respectively,

Table 2.4 Diffusion and Solubility Coefficients of the **P1**/**P1F**, **P2**/**P2F**, and **P3**/**P3F** Copolymer Series, as well as Individual Henry's Law and Langmuir Sorption Parameters.

		D^a ((cm^2 /s) ×10^{-6})			S^b (cm^3 [STP]/ (cm^3 atm))			CO_2		CH_4	
entry	polymer	CO_2	CH_4	D_{CO2}/D_{CH4}	CO_2	CH_4	S_{CO2}/S_{CH4}	k_d	$C'_H \cdot b$	k_d	$C'_H \cdot b$
1	**P1**	3.62	1.70	2.13	2.16	0.81	2.67	1.43	0.72	0.44	0.36
2	**P1^{84}P1F^{16}**	3.61	1.70	2.12	2.57	0.89	2.88	1.65	0.92	0.37	0.52
3	**P1^{67}P1F^{33}**	3.28	1.74	1.89	2.68	0.77	3.47	1.77	0.91	0.45	0.32
4	**P1^{48}P1F^{52}**	2.28	1.21	1.89	3.03	0.75	4.06	2.01	1.02	0.46	0.28
5	**P1F**	1.80	0.96	1.87	3.88	0.77	5.06	2.01	1.87	0.43	0.34
6	**P2**	3.22	1.71	1.88	1.20	0.48	2.50	1.20	-[c]	0.48	-[c]
7	**P2^{87}P2F^{13}**	3.14	1.65	1.90	1.59	0.60	2.65	1.59	-[c]	0.60	-[c]
8	**P2^{72}P2F^{28}**	3.11	1.63	1.91	1.87	0.62	3.01	1.87	-[c]	0.62	-[c]
9	**P3**	4.43	2.94	1.51	0.94	0.36	2.63	0.94	-[c]	0.36	-[c]
10	**P3^{87}P3F^{13}**	3.98	2.67	1.49	1.27	0.44	2.90	1.27	-[c]	0.44	-[c]

[a]Diffusion coefficients (D) were determined algebraically using the equation $D = P/S$. [b]Solubility coefficient (S) were measured using the dual-volume pressure decay method and reported as pressure approaches to 0. [c]Not applicable as these isotherms were fit linearly.

whereas their solubility selectivities are S_{CO2}/S_{CH4} = 2.88 and 2.65 for **P1^{84}P1F^{16}** and **P2^{87}P2F^{13}**, respectively.

Analysis of individual solubility coefficients reveals that S_{CO2} increases consistently with increasing in fluorinated monomer content for each copolymer series while S_{CH4} is relatively consistent (Table 2.4, entries 1–5, 6–8, and 9–10). This observation suggests that the observed enhancements in CO_2/CH_4 separation performance by incorporation of fluorinated monomer units arises via increased CO_2 solubility in the polymer matrix rather than inhibition of CH_4 solubility, which contrasts our initial hypothesis. In addition, though D_{CO2} decreases within each series, the observed increase in S_{CO2} appears to dominate overall permselectivity, potentially explaining why P_{CO2} only slightly decreases for the **P1**/**P1F** copolymer series, or increased in the case of the **P2**/**P2F** and **P3**/**P3F** copolymer series.

Though analysis of individual *D* and *S* coefficients offer insight into why P_{CO2} is maintained across each copolymer series, and reveal the source of each CO_2/CH_4 selectivity enhancement, the fundamental rationale governing why increasing fluorine content increases S_{CO2}, while S_{CH4} is relatively constant, was unclear. To better understand this, sorption isotherm fits were used to extract individual sorption components, including Henry's Law dependent dissolution (k_d) and Langmuir contributions (where C'_H and b are the Langmuir capacity parameter and Langmuir affinity parameter, respectively). Therein, we observed that both Henry's Law (k_d) and Langmuir ($C'_H \cdot b$) sorption of CO_2 increased continuously as a function of increasing fluorine content within the **P1**/**P1F** copolymer series (k_d = 1.43 – 2.01, $C'_H \cdot b$ = 0.72 – 1.87) (Table 2.4, entries 1–5). This suggests that the observed increase in CO_2 sorption as a function of increasing fluorine content are a consequence of both increased dissolution of CO_2 into the densified polymer matrix (k_d, Henry's law dissolution) and dissolution into nonequilibrium excess free volume elements ($C'_H \cdot b$,

Langmuir contributions). In contrast to our initial hypothesis that CH_4 sorption would decrease as a function of increasing fluorine content, the Henry's Law and Langmuir contributions to CH_4 sorption for the **P1**/**P1F** copolymer series is relatively constant (k_d = 0.37–0.46, $C'_H \cdot b$ = 0.36 – 0.34) (Table 2.4, entry 1–5).

In contrast to the **P1**/**P1F** copolymer series that exhibits nonlinear sorption isotherms (dual–mode sorption behavior), the **P2**/**P2F** and **P3**/**P3F** copolymer series showed no observable Langmuir contributions to either CO_2 or CH_4 sorption, and thus the sorption isotherms were fit linearly to elucidate the parameter k_d. Though **P2**/**P2F** and **P3**/**P3F** copolymers containing higher molar incorporation ratios of fluorinated repeat units were not synthetically accessible, two general trends were observed. First, Henry's law sorption of CO_2 increased as a function of increasing fluorine content for both the **P2**/**P2F** copolymer series (k_d = 1.20 – 1.87) and the **P3**/**P3F** copolymer series (k_d = 0.94 – 1.27) (Table 2.4, entries 6–10). Second, the Henry's Law contributions to CH_4 sorption for the **P2**/**P2F** and **P3**/**P3F** copolymer series also increased, albeit only slightly, as a function of increasing fluorine content (k_d = 0.48–0.62 for **P2**/**P2F** series, and k_d = 0.36–0.44 for **P3**/**P3F** series). Ultimately, this minor increase in Henry's Law contributions to CH_4 sorption is relatively small compared to their significantly increased Henry's law contribution to CO_2 sorption, thus resulting in the observed increases in S_{CO2}/S_{CH4} solubility selectivity for the **P2**/**P2F** and **P3**/**P3F** copolymer series.

Because these results suggest that the observed CO_2/CH_4 pure gas selectivities measured within these fluorinated APNBs are largely dominated by Henry's law contributions to gas dissolution, despite minimal Langmuir contributions present in some copolymers, deeper insight into specific polymer–polymer and polymer–gas interactions are critical to understanding overall membrane performance.[155] This importance is amplified as our experimental evidence suggests

that our observed increases in CO_2/CH_4 selectivity as a function of increasing fluorine content are a result of enhanced S_{CO2}, which suggests more favorable interactions of fluorinated polymers with CO_2, as opposed to unfavorable interactions of fluorinated polymers with CH_4 as originally hypothesized.

In addition to the general immiscibility of hydrocarbons and fluorocarbons that initially motivated this work, other explanations may contribute to our observed trends in membrane performance. For example, it was proposed through simulation that CO_2–fluorocarbon interactions may be improved compared to CO_2–hydrocarbon, due to potentially enhanced quadrupole^{CO2}-dipole$^{C–F}$ and induced dipole^{CO2}-dipole$^{C–F}$ interactions.[176] In this case, fluorinated polymers may be expected to have strengthened CO_2 interaction energies as compared to non-fluorinated analogs. To test this hypothesis for the fluorinated APNBs described herein, we performed electronic structure theory computations. Here, saturated analogues of monomers **1**–**3** and **1F**–**3F** were used as small molecule surrogates for polymers **P1**–**P3**, and **P1F**–**P3F**, respectively, and monomer−gas and monomer−monomer interactions were computed.

The DFT analysis reveal that the strength of interactions for the nonfluorinated APNBs **P1**–**P3** series agrees with the experimental findings. In detail, all polymers **P1**–**P3** are expected to have similar interactions with both CO_2 and CH_4, as their substituents are alkoxy analogs to each other which does not introduce additional interactions with either CO_2 or CH_4 gas molecules. As shown in Figure 2.4, the monomer–gas interaction ΔE is relatively consistent for both monomer–CO_2 interactions (-4.75 to -4.79 kcal/mol) and monomer–CH_4 interactions (-2.48 to -3.11 kcal/mol). In addition, as shown in Figure 2.5, the $\Delta\Delta E$ corresponds to a metric of the energy that is required to have one gas molecule perturb the monomer–monomer interaction and then form gas–monomer interaction defined as:

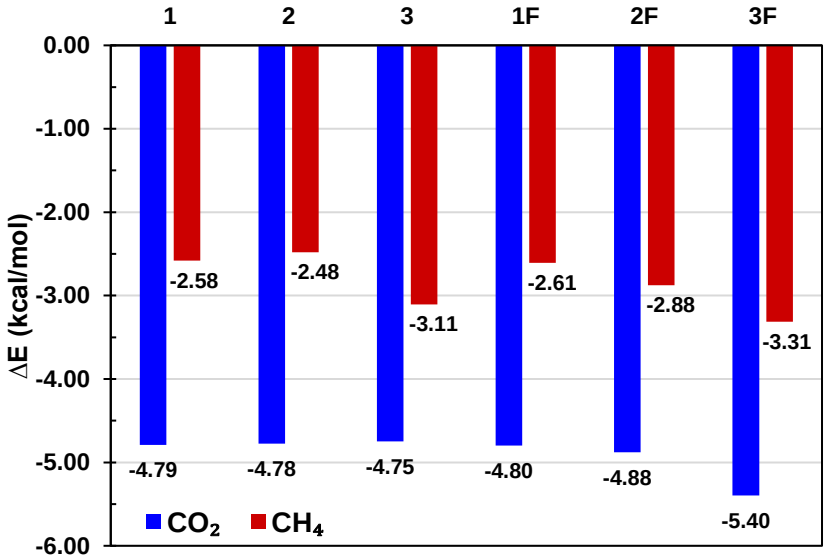


Figure 2.4 Calculated Δ*E* of gas–monomer interactions. Calculations were performed on saturated analogs of polymer repeat units **1**–**3** and **1F**–**3F**. Reprinted with permission from Reference [153]. Copyright 2022 American Chemical Society.

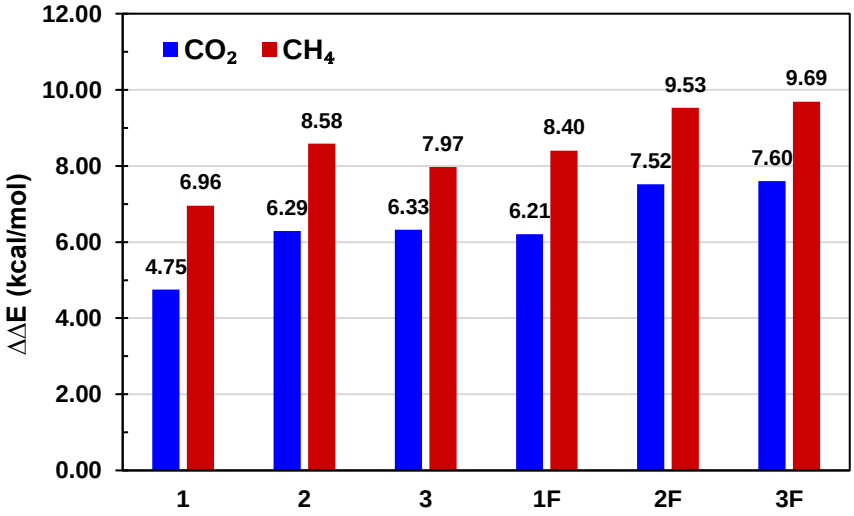


Figure 2.5 Calculated ΔΔ*E* values for CO_2 and CH_4 for all nonfluorinated and fluorinated polymer series. Calculations were performed on saturated analogs of polymer repeat units **1**–**3** and **M1F**–**M3F**. Reprinted with permission from Reference [153]. Copyright 2022 American Chemical Society.

$$\Delta\Delta E = \Delta E_{ii} - \Delta E_{i-\mathrm{gas}}, \qquad i = \mathbf{1}, \mathbf{2}, \mathbf{3}, \mathbf{1F}, \mathbf{2F}, \mathbf{3F} \quad (7)$$

where ΔE_{ii} represents the interaction energy between two monomer units and $\Delta E_{i-\mathrm{gas}}$ the interaction energy between a simulated polymer repeat unit *i* and a gas molecule (CO_2 or CH_4). It is expected that a lower energy difference $\Delta\Delta E$ between gas–monomer interactions and monomer–monomer interactions correlate to relatively easier Henry's law dissolution (k_d) of gas molecules into the polymer matrix. In regards to CO_2–monomer and monomer–monomer interactions, $\Delta\Delta E$ increased from 4.75 to 6.33 kcal/mol from **1** to **3**, which is in good agreement with the experimentally determined k_d that decreased from 1.43 to 0.94. For CH_4–monomer and monomer–monomer interactions, $\Delta\Delta E$ remains virtually similar for **2** to **3** (8.58 and 7.97 kcal/mol, respectively), which is in fair agreement with the experimentally measured values of k_d = 0.48 and 0.36, respectively. This correlation is also in fair agreement for **P1**, if it is taken into consideration that **P1** has a significant Langmuir component that does not allow a direct comparison between **P1** and **P2**/**P3**.

Though the homopolymers **P2F** and **P3F** are not experimentally accessible, the computational analysis shows a decreasing ΔE for both CO_2 and CH_4 as fluorine content is increased from **1F** to **3F** (Figure 2.4), suggesting that favorable gas–monomer interactions are expected as the wt% of fluorinated content in the homopolymer is increased. $\Delta\Delta E$ (Figure 2.5), for both CO_2–monomer as well as CH_4–monomer interactions, and monomer–monomer interactions also increase from **1F** to **3F**, suggesting that the energy penalty required for both CO_2 and CH_4 molecules to disturb monomer–monomer interaction is increased. Therefore, a decreased k_d would be expected.

Though a comparison between DFT data and experimental results for **P1** and **P1F** can still be analyzed, these data do not align as well as that obtained for the nonfluorinated APNBs **P1**–**P3**.

For CO_2–monomer interactions, it was previously reported that improved interactions may be observed due to the increase quadrupole-dipole/induced dipole-dipole interaction of CO_2 with fluorinated species; however, the ΔE observed in this case is similar (-4.79 and -4.80 kcal/mol for CO_2–**1** and CO_2–**1F**, respectively, Figure 2.4). For CH_4–monomer interactions, our initial hypothesis based on mutual immiscibility of fluorocarbon and hydrocarbon small molecules suggested that a decrease in ΔE may be expected; however, the observed ΔE is also similar (-2.58 and -2.61 kcal/mol for CH_4–**1** and CH_4–**1F**, respectively, Figure 2.4). Looking at $\Delta\Delta E$ (Figure 2.5), CO_2–monomer and monomer–monomer interactions increased from 4.75 kcal/mol for **1** to 6.21 kcal/mol for **1F**, suggesting that the energy penalty is higher for CO_2 to be inserted between two **1F** monomers and thus less likely to occur. However, the experimentally determined k_d values increase from 1.43 for **P1** to 2.01 for **P1F**, which show the opposite behavior predicted at the computational level. Similarly, looking at $\Delta\Delta E$ for CH_4–monomer and monomer–monomer interactions, these values increase from 6.96 kcal/mol for **M1** to 8.40 kcal/mol for **M1F**, which suggest that the energy penalty is higher for CH_4 to insert between two **M1F** monomers (k_d values are 0.44 for **P1** to 0.43 for **P1F**). Though the presence of Langmuir component in both **P1** and **P1F** may influence a direct comparison of k_d and $\Delta\Delta E$ values, these results indicate that this simple simulation model may not be ideal when comparing across nonfluorinated and fluorinated polymeric materials and modeling at the mesoscale can further elucidate these phenomena. We have already identified limitations in traditional force fields for atomistic simulations for the reliable modeling of polynorbornenes. For that reason, we are currently developing a new force field based on accurate quantum chemical data that will allow us to perform large scale simulations for this class of materials.

2.5 Conclusions

A series of nonfluorinated and fluorinated APNB homo- and copolymers (**P1**/**P1F**–**P3**/**P3F** series) were designed and synthesized. These fluorinated motifs were introduced into the membranes with the goal of improving CO_2/CH_4 selectivity utilizing the "hydrocarbon-phobicity" exhibited by many fluorinated materials. Pure gas permeation results revealed that as the molar ratio of fluorinated monomer increased, the CO_2/CH_4 selectivity increased for each (co)polymer series. The highest performing membrane, **P1F**, achieves a CO_2 permeability of 920 Barrer with a CO_2/CH_4 selectivity of 9.5. This represents a 67% increase in CO_2/CH_4 selectivity with only a 10% decrease in CO_2 permeability as compared to its non-fluorinated APNB analog, **P1**. Though we initially hypothesized that selectivity would be enhanced via depressed CH_4 sorption, sorption experiments reveal that the enhanced selectivity of **P1F** arose from increased CO_2 solubility. Individual analysis of diffusion and sorption coefficients reveal that each polymer's diffusivity selectivity remained relatively unchanged within each series, whereas sorption selectivity was increased as a function of increasing molar incorporation of fluorinated comonomers (**MXF**). To better understand the cause of this behavior, computational DFT analyses were employed. These calculations corelate well with our experimental observations for the nonfluorinated APNB series and suggest that CO_2 and CH_4 transport through the membrane are likely controlled via a delicate balance between polymer-polymer and polymer-gas interaction energies. However, some deviations computational and experimental results are observed when comparing across nonfluorinated and fluorinated polymeric materials, suggesting that this simple computational model may not fully capture all essential features of this complex process.

References

46. Galizia, M.; Chi, W. S.; Smith, Z. P.; Merkel, T. C.; Baker, R. W.; Freeman, B. D., 50th Anniversary Perspective: Polymers and Mixed Matrix Membranes for Gas and Vapor Separation: A Review and Prospective Opportunities. *Macromolecules* **2017,** *50* (20), 7809-7843.
121. Faramawy, S.; Zaki, T.; Sakr, A. A. E., Natural gas origin, composition, and processing: A review. *J. Nat. Gas Sci. Eng.* **2016,** *34*, 34-54.
122. U.S. Energy Information Administration. Natural gas explained: Where our natural gas comes from. https://www.eia.gov/energyexplained/natural-gas/where-our-natural-gas-comes-from.php (accessed Nov 14, 2019).
123. Adewole, J. K.; Ahmad, A. L.; Ismail, S.; Leo, C. P., Current challenges in membrane separation of CO_2 from natural gas: A review. *Int. J. Greenh. Gas Control.* **2013,** *17*, 46-65.
124. Xiao, Y.; Low, B. T.; Hosseini, S. S.; Chung, T. S.; Paul, D. R., The strategies of molecular architecture and modification of polyimide-based membranes for CO_2 removal from natural gas—A review. *Prog. Polym. Sci.* **2009,** *34* (6), 561-580.
125. Bhide, B. D.; Voskericyan, A.; Stern, S. A., Hybrid processes for the removal of acid gases from natural gas. *J. Membr. Sci.* **1998,** *140* (1), 27-49.
126. Olajire, A. A., CO_2 capture and separation technologies for end-of-pipe applications – A review. *Energy.* **2010,** *35* (6), 2610-2628.
127. Scholes, C. A.; Stevens, G. W.; Kentish, S. E., Membrane gas separation applications in natural gas processing. *Fuel.* **2012,** *96*, 15-28.
128. Yu, C.-H.; Huang, C.-H.; Tan, C.-S., A Review of CO_2 Capture by Absorption and Adsorption. *Aerosol and Air Qual. Res.* **2012,** *12* (5), 745-769.
129. Chawla, M.; Saulat, H.; Masood Khan, M.; Mahmood Khan, M.; Rafiq, S.; Cheng, L.; Iqbal, T.; Rasheed, M. I.; Farooq, M. Z.; Saeed, M., Membranes for CO_2/CH_4 and CO_2/N_2 gas separation. *Chem. Eng. Technol.* **2020,** *43* (2), 184-199.
130. Lozano, L.; Godínez, C.; De Los Rios, A.; Hernández-Fernández, F.; Sánchez-Segado, S.; Alguacil, F. J., Recent advances in supported ionic liquid membrane technology. *J. Membr. Sci.* **2011,** *376* (1-2), 1-14.
131. Mubashir, M.; Fong, Y. Y.; Leng, C. T.; Keong, L. K., Issues and Current Trends of Hollow-Fiber Mixed-Matrix Membranes for CO_2 Separation from N_2 and CH_4. *Chem. Eng. Technol.* **2018,** *41* (2), 235-252.
132. Norahim, N.; Yaisanga, P.; Faungnawakij, K.; Charinpanitkul, T.; Klaysom, C., Recent membrane developments for CO_2 separation and capture. *Chem. Eng. Technol.* **2018,** *41* (2), 211-223.
133. Pera-Titus, M., Porous inorganic membranes for CO_2 capture: present and prospects. *Chem. Rev.* **2014,** *114* (2), 1413-1492.
134. Wind, J. D.; Paul, D. R.; Koros, W. J., Natural gas permeation in polyimide membranes. *J. Membr. Sci.* **2004,** *228* (2), 227-236.
135. Baker, R. W.; Lokhandwala, K., Natural Gas Processing with Membranes: An Overview. *Ind. Eng. Chem.* **2008,** *47* (7), 2109-2121.
136. Han, S.; Lee, Y., Chapter 4 Recent High Performance Polymer Membranes for CO_2 Separation, Membrane Engineering for the Treatment of Gases: Volume 1: Gas-separation Problems with Membranes. The Royal Society of Chemistry: 2011.
137. Koros, W.; Fleming, G.; Jordan, S.; Kim, T.; Hoehn, H., Polymeric membrane materials for solution-diffusion based permeation separations. *Prog. Polym. Sci.* **1988,** *13* (4), 339-401.

138. Achoundong, C. S.; Bhuwania, N.; Burgess, S. K.; Karvan, O.; Johnson, J. R.; Koros, W. J., Silane modification of cellulose acetate dense films as materials for acid gas removal. *Macromolecules* **2013,** *46* (14), 5584-5594.
139. Houde, A.; Krishnakumar, B.; Charati, S.; Stern, S., Permeability of dense (homogeneous) cellulose acetate membranes to methane, carbon dioxide, and their mixtures at elevated pressures. *J . Appl. Polym. Sci.* **1996,** *62* (13), 2181-2192.
140. Cao, C.; Wang, R.; Chung, T. S.; Liu, Y., Formation of high-performance 6FDA-2, 6-DAT asymmetric composite hollow fiber membranes for CO_2/CH_4 separation. *J. Membr. Sci.* **2002,** *209* (1), 309-319.
141. Coleman, M.; Koros, W., The transport properties of polyimide isomers containing hexafluoroisopropylidene in the diamine residue. *J. Polym. Sci. B Polym. Phys.* **1994,** *32* (11), 1915-1926.
142. Koros, W. J.; Fleming, G., Membrane-based gas separation. *J. Membr. Sci.* **1993,** *83* (1), 1-80.
143. Zhang, Y.; Sunarso, J.; Liu, S.; Wang, R., Current status and development of membranes for CO_2/CH_4 separation: A review. *Int. J. Greenh. Gas Control.* **2013,** *12*, 84-107.
144. Kim, T.; Koros, W.; Husk, G.; O'brien, K., Relationship between gas separation properties and chemical structure in a series of aromatic polyimides. *J. Membr. Sci.* **1988,** *37* (1), 45-62.
145. Matsumoto, K.; Xu, P., Gas permeation properties of hexafluoro aromatic polyimides. *J . Appl. Polym. Sci.* **1993,** *47* (11), 1961-1972.
146. Robeson, L. M., The upper bound revisited. *J. Membr. Sci.* **2008,** *320* (1), 390-400.
147. Lawrence, J. A.; Harrigan, D. J.; Maroon, C. R.; Sharber, S. A.; Long, B. K.; Sundell, B. J., Promoting acid gas separations via strategic alkoxysilyl substitution of vinyl-added poly(norbornene)s. *J. Membr. Sci.* **2020,** *616*, 118569.
148. Dunitz, J. D., Organic fluorine: odd man out. *ChemBioChem* **2004,** *5* (5), 614-621.
149. Lemal, D. M., Perspective on fluorocarbon chemistry. *J. Org. Chem.* **2004,** *69* (1), 1-11.
150. Alentiev, A. Y.; Shantarovich, V. P.; Merkel, T. C.; Bondar, V. I.; Freeman, B. D.; Yampolskii, Y. P., Gas and Vapor Sorption, Permeation, and Diffusion in Glassy Amorphous Teflon AF1600. *Macromolecules* **2002,** *35* (25), 9513-9522.
151. Merkel, T.; Bondar, V.; Nagai, K.; Freeman, B., Hydrocarbon and perfluorocarbon gas sorption in poly (dimethylsiloxane), poly (1-trimethylsilyl-1-propyne), and copolymers of tetrafluoroethylene and 2, 2-bis (trifluoromethyl)-4, 5-difluoro-1, 3-dioxole. *Macromolecules* **1999,** *32* (2), 370-374.
152. Prabhakar, R. S.; Freeman, B. D.; Roman, I., Gas and Vapor Sorption and Permeation in Poly(2,2,4-trifluoro-5-trifluoromethoxy-1,3-dioxole-co-tetrafluoroethylene). *Macromolecules* **2004,** *37* (20), 7688-7697.
153. Wang, X.; Wilson, T. J.; Maroon, C. R.; Laub, J. A.; Rheingold, S. E.; Vogiatzis, K. D.; Long, B. K., Vinyl-Addition Fluoroalkoxysilyl-Substituted Polynorbornene Membranes for CO2/CH4 Separation. *ACS Applied Polymer Materials* **2022**.
154. Gmernicki, K. R.; Hong, E.; Maroon, C. R.; Mahurin, S. M.; Sokolov, A. P.; Saito, T.; Long, B. K., Accessing Siloxane Functionalized Polynorbornenes via Vinyl-Addition Polymerization for CO_2 Separation Membranes. *ACS Macro Lett.* **2016,** *5* (7), 879-883.
155. Maroon, C. R.; Townsend, J.; Gmernicki, K. R.; Harrigan, D. J.; Sundell, B. J.; Lawrence, J. A.; Mahurin, S. M.; Vogiatzis, K. D.; Long, B. K., Elimination of CO_2/N_2 Langmuir Sorption and Promotion of "N_2-Phobicity" within High-Tg Glassy Membranes. *Macromolecules* **2019,** *52* (4), 1589-1600.

156. Nagel, R.; Tamborski, C.; Post, H. W., Studies in Silico-Organic Compounds. XVIII. The Preparation and Properties of Vinyltrialkoxysilanes. *J. Org. Chem.* **1951,** *16* (11), 1768-1771.
157. Maroon, C. R.; Townsend, J.; Higgins, M. A.; Harrigan, D. J.; Sundell, B. J.; Lawrence, J. A.; O'Brien, J. T.; O'Neal, D.; Vogiatzis, K. D.; Long, B. K., Addition-type alkoxysilyl-substituted polynorbornenes for post-combustion carbon dioxide separations. *J. Membr. Sci.* **2019**, 117532.
158. Horst Czichos, T. S., Leslie Smith, Springer Handbook of Materials Measurement Methods. Springer: Berlin, 2006.
159. Koros, W. J.; Paul, D. R., Design considerations for measurement of gas sorption in polymers by pressure decay. *J. Polym. Sci. Polym. Phys. Ed.* **1976,** *14* (10), 1903-1907.
160. Klug, H. P.; Alexander, L. E., *X-Ray Diffraction Procedures: For Polycrystalline and Amorphous Materials, 2nd Edition*. Wiley: 1974.
161. Sundell, B. J.; Lawrence Iii, J. A.; Harrigan, D. J.; Vaughn, J. T.; Pilyugina, T. S.; Smith, D. R., Alkoxysilyl functionalized polynorbornenes with enhanced selectivity for heavy hydrocarbon separations. *RSC Adv.* **2016,** *6* (57), 51619-51628.
162. Adamo, C.; Barone, V., Toward reliable density functional methods without adjustable parameters: The PBE0 model. *J. Chem. Phys.* **1999,** *110* (13), 6158-6170.
163. Weigend, F., Hartree–Fock exchange fitting basis sets for H to Rn. *J. Comput. Chem.* **2008,** *29* (2), 167-175.
164. Grimme, S.; Antony, J.; Ehrlich, S.; Krieg, H., A consistent and accurate ab initio parametrization of density functional dispersion correction (DFT-D) for the 94 elements H-Pu. *J. Chem. Phys.* **2010,** *132* (15), 154104.
165. Grimme, S.; Ehrlich, S.; Goerigk, L., Effect of the damping function in dispersion corrected density functional theory. *J. Comput. Chem.* **2011,** *32* (7), 1456-1465.
166. Ahlrichs, R.; Bär, M.; Häser, M.; Horn, H.; Kölmel, C., Electronic structure calculations on workstation computers: The program system turbomole. *Chem. Phys. Lett.* **1989,** *162* (3), 165-169.
167. Dodda, L. S.; Cabeza de Vaca, I.; Tirado-Rives, J.; Jorgensen, W. L., LigParGen web server: an automatic OPLS-AA parameter generator for organic ligands. *Nucleic Acids Res.* **2017,** *45* (W1), W331-W336.
168. Plimpton, S., Fast parallel algorithms for short-range molecular dynamics. *J. Comput. Phys.* **1995,** *117* (1), 1-19.
169. Jorgensen, W. L.; Maxwell, D. S.; Tirado-Rives, J., Development and testing of the OPLS all-atom force field on conformational energetics and properties of organic liquids. *J. Am. Chem. Soc.* **1996,** *118* (45), 11225-11236.
170. Bondi, A., van der Waals Volumes and Radii. *J. Phys. Chem.* **1964,** *68* (3), 441-451.
171. Wu, A. X.; Lin, S.; Rodriguez, K. M.; Benedetti, F. M.; Joo, T.; Grosz, A. F.; Storme, K. R.; Roy, N.; Syar, D.; Smith, Z. P., Revisiting group contribution theory for estimating fractional free volume of microporous polymer membranes. *J. Membr. Sci.* **2021**, 119526.
172. Kelly, C. M.; Mathias, P. M.; Schweighardt, F. K., Correlating vapor pressures of perfluorinated saturated hydrocarbons by a group contribution method. *Ind. Eng. Chem.* **1988,** *27* (9), 1732-1736.
173. Alentiev, D. A.; Egorova, E. S.; Bermeshev, M. V.; Starannikova, L. E.; Topchiy, M. A.; Asachenko, A. F.; Gribanov, P. S.; Nechaev, M. S.; Yampolskii, Y. P.; Finkelshtein, E. S., Janus tricyclononene polymers bearing tri(n-alkoxy)silyl side groups for membrane gas separation. *J. Mater. Chem.* **2018,** *6* (40), 19393-19408.

174. Morontsev, A. A.; Zhigarev, V. A.; Nikiforov, R. Y.; Belov, N. A.; Gringolts, M. L.; Finkelshtein, E. S.; Yampolskii, Y. P., A new approach to improvement of gas permeation properties of olefin metathesis derived poly(norbornenes): gem-difluorocyclopropanation of backbone double bonds. *Eur. Polym. J.* **2018,** *99*, 340-349.
175. Comesaña-Gándara, B.; Chen, J.; Bezzu, C. G.; Carta, M.; Rose, I.; Ferrari, M.-C.; Esposito, E.; Fuoco, A.; Jansen, J. C.; McKeown, N. B., Redefining the Robeson upper bounds for CO_2/CH_4 and CO_2/N_2 separations using a series of ultrapermeable benzotriptycene-based polymers of intrinsic microporosity. *Energy Environ. Sci* **2019,** *12* (9), 2733-2740.
176. Cece, A.; Jureller, S. H.; Kerschner, J. L.; Moschner, K. F., Molecular modeling approach for contrasting the interaction of ethane and hexafluoroethane with carbon dioxide. *J. Phys. Chem.* **1996,** *100* (18), 7435-7439.

Chapter 3 Metathesis Polynorbornene-based Block Copolymer Gas Separation Membranes

3.1 Abstract

As discussed in Section 1.5.2, physical polymer chain packing within a dense polymer matrix is an important parameter that has been shown to strongly influence gas separation membrane performance.[99-101, 103] One method that can be employed to perturb chain packing, without changing polymer chemical composition, is to construct block copolymers that exhibit microphase separation and compare them with their random or statistical copolymer analogs. In this chapter, a brief introduction to block copolymers will be provided, as well as common methods to prepare microphase-separated membranes, general characterization methods, and our design criteria for MPNB block copolymers. Finally, preliminary results toward the synthesis of MPNB block copolymers and planned future work will be discussed.

3.2 An Introduction to Block Copolymers and Phase Diagrams

Block copolymers are a class of copolymers that are composed of two or more chemically distinct repeat units. In contrast to random or alternating copolymers, block copolymers differ in that the chemically distinct monomers are grouped together forming discrete homogeneous sections, or "blocks".[177] Among block copolymers, linear diblock copolymers are the simplest and most intensively studied copolymer systems, and can be conceptually visualized as two distinct homopolymers linked together via a covalent bond. If the two blocks are chemically distinct enough, they will tend to phase separate due to the unfavorable enthalpy of mixing.[178] However, due to the presence of a covalent bond linking the two blocks, and their small entropy of mixing, the phase separation behavior observed is frequently limited to microscale phase separation instead of macroscopic phase separation, which is usually observed when blending two corresponding homopolymers.[177]

The propensity for a block copolymer to achieve microphase separation at a given temperature is determined by three parameters: 1) the volume fraction of different blocks; 2) the total degree of polymerization (N); and 3) the Flory–Huggins interaction parameter (χ). Specifically, χ represents the incompatibility between the distinct blocks, and the product χN is defined as the segregation parameter.[179] To achieve microphase separation under a certain temperature, a block copolymer system should have a high enough χN; otherwise, the propensity of microphase separation is too low for observation, and thus lead to an order-to-disorder transition (ODT).[177, 178]

Various theories have been developed to describe the phase separation behavior of diblock copolymers, one of which is predicted through the self-consistent mean-field (SCMF) theory.[180, 181] As shown in Figure 3.1(b), at a fixed χN above the ODT (e.g., $\chi N > \sim 10.5$), the predicted phase diagram indicates that the order-to-order transition will start changing in order from closely packed spheres (CPS) to body-centered cubic spheres (S), hexagonally packed cylinders (C), bicontinuous gyroids (G), and lamellae (L) as a function of increasing volume fraction of one block (f_A),. After f_A exceeds half of the total volume, the composition can be considered inverted (f_A as the major component and forming the continuous phase), and the morphology order is also inverted (changing in the order of L, G', C', S', CPS', and finally disordered).[182] In addition to predicting phase diagrams, Bates and co-workers also constructed an experimentally determined phase diagram using a polyisoprene-*b*-polystyrene copolymer systems, which is shown in Figure 3.1(c). Though there are a few discrepancies, the overall trend is very similar to that of the theoretical diagram.[182]

The reason that the volume fraction, f_A, is a critical determinant in the microphase separation process can be visualized in Figure 3.2.[178, 183] Therein, a polymer system may minimize its

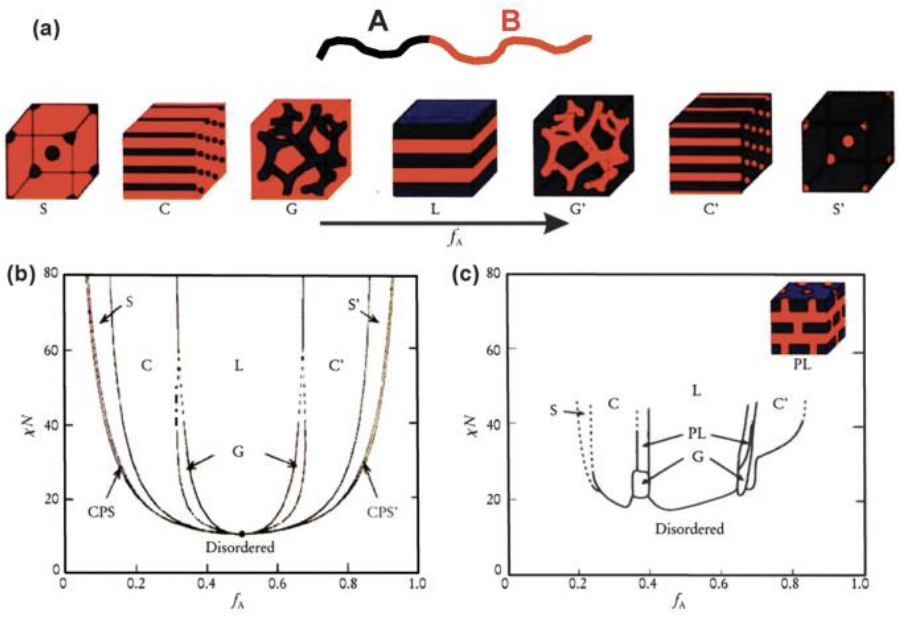


Figure 3.1 (a) Equilibrium morphologies of AB diblock copolymers in bulk: S and S' = body-centered-cubic spheres, C and C' = hexagonally packed cylinders, G and G' = bicontinuous gyroids, and L = lamellae. (b) Theoretical phase diagram of AB diblocks predicted by the self-consistent mean-field theory, depending on volume fraction (f_A) of the blocks and the segregation parameter, χN, where χ is the Flory–Huggins segment–segment interaction energy and N is the degree of polymerization; CPS and CPS' = closely packed spheres. (c) Experimental phase portrait of polyisoprene-block-polystyrene copolymers, in which f_A represents the volume fraction of polyisoprene, PL = perforated lamellae. Reprinted with permission from Reference [178]. Copyright 2012 The Royal Society of Chemistry.

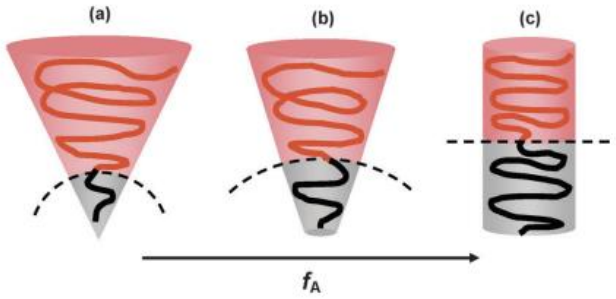


Figure 3.2 Schematic illustration of the possible polymer chain arrangements in different morphologies of AB diblocks changing from sphere (a) to cylinder (b) and to lamella (c), as the volume fraction (f_A) of the A block (black) increases to ~ 0.5. The dash curve in each morphology represents a part of the interface between A and B domains. Reprinted with permission from Reference [178]. Copyright 2012 The Royal Society of Chemistry.

interfacial area between two incompatible components by adopting a microphase separated morphology, thus lowering the total interfacial energy of the system. As the volume fraction f_A increases from 0, the polymer chain conformation will change from a random-coil to a cone-corona conformation with the small fraction of component A as the core. Furthermore, as f_A continues to increase, less curved interfaces are formed and the morphology changes into cylinders. Finally, when f_A reaches 0.5, the lamellae phase is formed.

3.3 Preparation of Microphase Separated Membranes

The formation of microphase-separated films often requires an annealing process to accelerate the phase separation and/or to minimize defects.[177] Two commonly used methods are thermal annealing and solvent annealing, both of which aim to increase chain mobility within a densified matrix. In thermal annealing, a copolymer film is typically heated at a temperature higher than its glass transition temperature (T_g), but lower than its decomposition temperature (T_d), under a vacuum or in an inert environment to minimize any deleterious oxidation or decomposition.[177] Once the polymer chains reach equilibrium at elevated temperature, the films are quenched to a temperature well below the polymer's T_g (i.e. liquid nitrogen temperature) and then gradually warmed to room temperature. In this case, the chain conformation is instantly frozen before returning to room temperature.[178]

In solvent annealing, a sample is held for a given period of time in a controlled solvent atmosphere so that the solvent vapors can swell and plasticize the polymer matrix, granting the polymer chains greater mobility. The efficiency of solvent annealing depends on the relative interaction of solvent on each block, and in certain situations a variety of solvents or solvent

mixtures can be used to achieve optimal results.[177] After solvent annealing, the solvent vapors are removed under vacuum before characterization.

3.4 Characterization of Microphase Separated Membranes

Scattering and imaging methods are both routinely employed to characterize microphase separation within polymer samples. Among scattering methods, small-angle X-ray scattering (SAXS) is one of the most widely used techniques, and can provide average information of large statistical samples by probing millions of unit cells.[184] In SAXS, the angle between the scattered and incident X-rays is defined as 2θ, and the information around 0.1 to 5° is typically collected. The scattering is a result of the interaction between the incident radiation and the inhomogeneous electron distribution of the measured materials, and generally, the structural features in the range of 1 to 100 nm can be elucidated.[185] For samples with ordered structures, a series of narrow peaks is expected and these peak positions can be used to identify different microphase separated morphologies. Table 3.1 summarizes the peak positions for some common morphologies.[186]

In contrast, scanning electron microscopy (SEM), transmission electron microscopy (TEM), and atomic force microscopy (AFM) are commonly used methods for direct imaging of microphase-separated morphologies.[184] In contrast to SAXS, which focuses on the average features of the samples, microscopy methods usually focus on local details over a small and selected area. Thus, both imaging and scattering methods are generally used in combination to fully characterize the microphase-separated features of polymer samples.

Table 3.1 Peak positions (expressed as q/q^*) of Bragg reflections for various structures.

Structure	Ratio q/q^*
Lam	1, 2, 3, 4, 5, 6, …
Hex	1, √3, √4, √7, √9, √12, …
BCC	1, √2, √3, √4, √5, √6, …
FCC	1, √(4/3), √(8/3), √(11/3), √(12/3) √(16/3), …
Gyr	1, √(4/3), √(7/3), √(8/3), √(10/3), √(11/3), …

3.5 Design of MPNB Block Copolymer Membranes for Gas Separations

Previous studies on the influence of block copolymer morphologies on gas separation performance are mostly limited to polystyrene (PS)-containing copolymers, wherein PS is a very low permeability membrane material that generally has no specific strong interactions with most gas molecules of interest to the gas separations community.[104] With the development of advanced olefin metathesis catalysts, such as Grubbs catalyst,[187] the living ring-opening polymerization of norbornene-based monomers can be readily employed to access MPNB block copolymers that are attractive targets to investigate fundamental morphology–gas separation performance relationships. For our studies, hexyl- and trimethoxysilyl-substituted norbornene (hexylNB and trimethoxysilylNB, respectively) are chosen as the initial monomer pair to construct block copolymer, and as they are expected to have high enough χ to introduce microphase separation. Additionally, the gas separation performance of the two homopolymers is expected to have a large difference, allowing us to analyze the potential influence of morphology and composition on gas separation performance.

3.6 Preliminary Results and Discussion

The monomers trimethoxysilylNB (**M1**) and hexylNB (**M2**), as well as Grubbs 3rd generation catalyst (**G3**) were synthesized following previous reports.[53, 188, 189] To achieve living polymerization conditions while minimizing deleterious secondary metathesis, homopolymerizations with each monomer were conducted to identify the kinetics and time needed to reach quantitative monomer consumption. Using the selected conditions ([M]:[C] = 300:1, room

temperature and [M] = 0.05 M in toluene), 120 s and 20 s is needed for full polymerization conversion of monomers **M1** and **M2**, respectively, to reach ~100% conversion (characterized via ^{1}H NMR). Attempts to slow down the polymerization and provide better control over the polymerization behavior were performed by addition of pyridine as a coordinating solvent and following a literature procedure (Figure 3.3).[189]

After identifying living polymerization conditions, larger scale homopolymers and block copolymers were synthesized. All polymerizations were conducted in a glove box at room temperature, and below is an example polymerization procedure. To a 250 mL round-bottom flask was added **M1** (2.5 mmol, 0.05 M) dissolved in 49 mL toluene and **G3** catalyst solution (1 mL, 5.56×10^{-3} M, 5.56×10^{-3} mmol). The mixture was stirred for 3 min before taking an aliquot for block 1. Next, **M2** monomer solution (2.5 mmol, 0.05 M, dissolved in 50 mL toluene) was added and mixture was stirred for an additional 30 s before taking an aliquot for block 2. The reaction and the aliquots were quenched with ethyl vinyl ether, and the catalyst was removed via passage through a neutral alumina column. Excess solvent was removed under reduced pressure and the reaction mixture was precipitated into MeOH, then dried under vacuum to obtain the purified copolymer. It is worth noting that the polymerization times for each block was chosen based upon our initial polymerization results, and when starting with **M2** as block 1, the resultant copolymers tended to have a larger dispersity and slight GPC shoulders, the origins of which is not fully understood at this time.

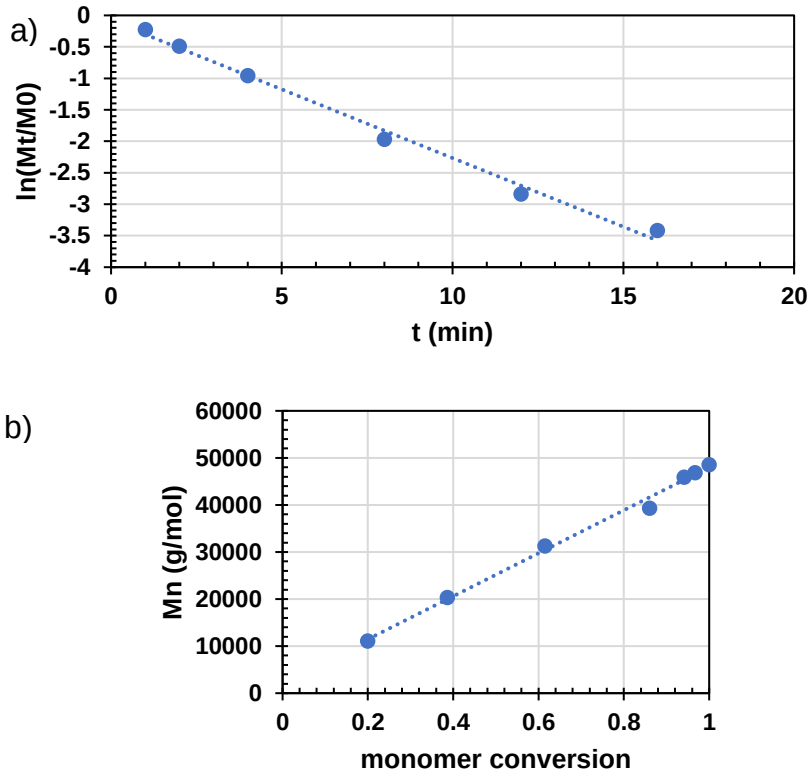


Figure 3.3 a) Plot of ln([M]/[M]$_0$) versus time for the ROMP of **M2** (toluene, 25 °C, [hexylNB] = 0.05M, [M]:[C] = 300:1, 100 eq pyridine). b) Plot of molecular weight (M_n) versus monomer conversion.

A series of homopolymer and block copolymer with different monomer incorporation were synthesized and are summarized in Table 3.2 and Figure 3.4. All polymerizations achieved high yields, with the actual measured monomer incorporation ratios being close to the feed ratios (actual monomer incorporation ratio determined via ^{1}H NMR spectroscopy by integrating the relative signal ratio of the methyl group of **M2** to the vinyl region). The GPC traces for the copolymers suggest successful chain extension (Figure 3.5), and DOSY NMR spectroscopy was conducted to further confirm the covalent linkage between the two blocks (Figure 3.6). The polymers were dissolved in THF as 5 wt% solutions, filtered through a 0.45 μm PTFE filter, and cast on a leveled PTFE petri dish. The solvent was evaporated slowly, and the films were collected once fully dried. The gas separation data are shown in Figure 3.7 and Table 3.3. As expected, homopolymer **P1** and **P2** had distinct gas separation performance, with **P1** having higher gas permeability and selectivity (for both CO_2/CH_4 and CO_2/N_2) compared to **P2**. This initial result suggested that similar to APNBs, in MPNBs, the trimethoxysilyl substituents of **P1** also facilitated non-covalent polymer-CO_2 interaction,[53] while as the hexyl substituents of **P2** were not expected to have specific interaction with penetrating gases. The large gap in the separation performance of **P1** and **P2** enabled the structure-property relationship study of a series of statistical and block copolymers. For the random copolymer series, the performance of **P1^{71}-*r*-P2^{29}** and **P1^{52}-*r*-P2^{48}** fell linearly in between the two homopolymers as expected. It is worth noting that the collected as-casted block copolymer films all have an uneven, "bubble-form" pattern across the membrane surface (Figure 3.8). These patterns remained even after overnight thermal annealing at 100 °C; thus, gas permeation measurements were not conducted at this point. Further studies are needed to understand this phenomenon.

Table 3.2 Synthesis of homopolymers and corresponding block and random copolymers.[a]

			M_n (kg/mol)[c]		$Đ$[c]	
entry	polymer[b]	yield (%)	block1	Polymer	block1	Polymer
1	**P1**	quan.	-	224	-	1.51
2	**P1^{65}-*b*-P2^{35}**	96	137	212	1.09	1.17
3	**P1^{48}-*b*-P2^{52}**	91	108	191	1.10	1.23
4	**P1^{35}-*b*-P2^{65}**	71[d]	59	183	1.09	1.24
5	**P2**	91	-	183	-	1.15
6	**P1^{71}-*r*-P2^{29}**		-	204	-	1.28
7	**P1^{52}-*r*-P2^{48}**		-	227	-	1.28

[a]General polymerization conditions: total monomer concentration = 5 mmol, [catalyst] = 5.6 μmol, 100 mL of toluene, room temperature. [b]Monomer incorporation ratios were calculated via ^{1}H NMR spectroscopy. [c]Molecular weights and dispersities were measured using gel permeation chromatography at 40 °C in THF and are reported relative to polystyrene standards. [d]The relative low yield could be result from the spill of some block2 monomer before block addition.

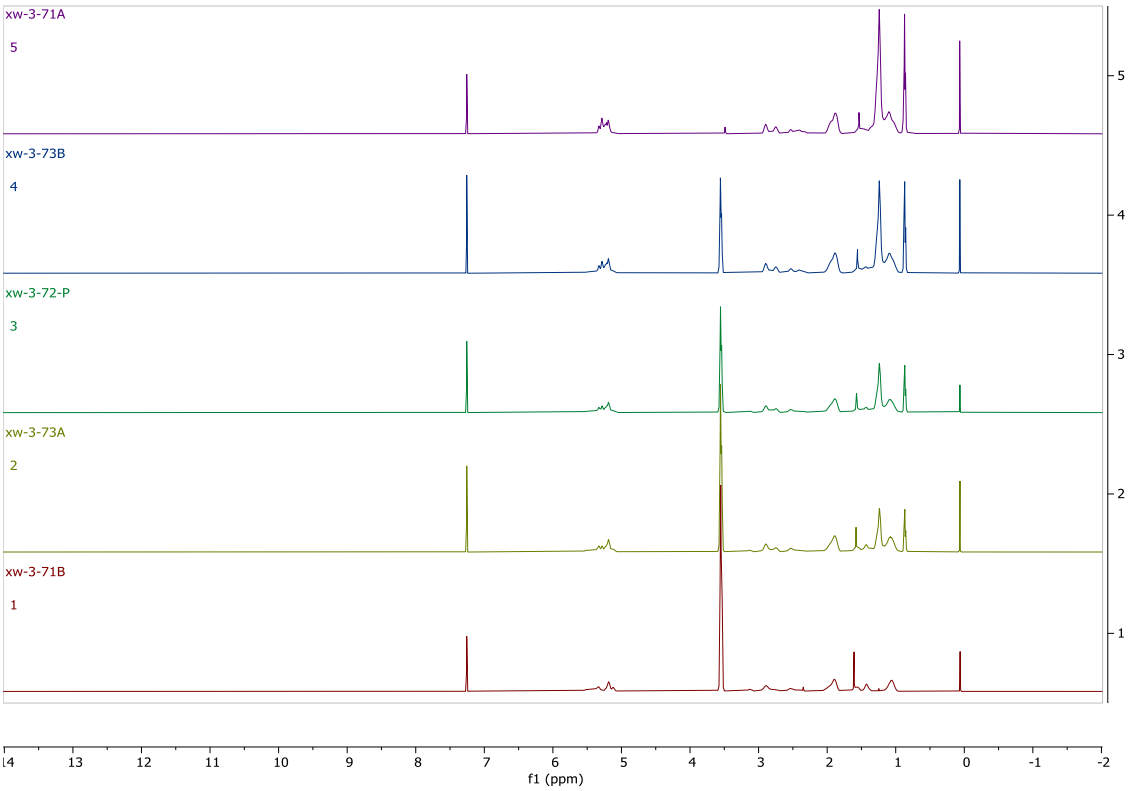


Figure 3.4 NMR of homopolymers and corresponding block copolymers.

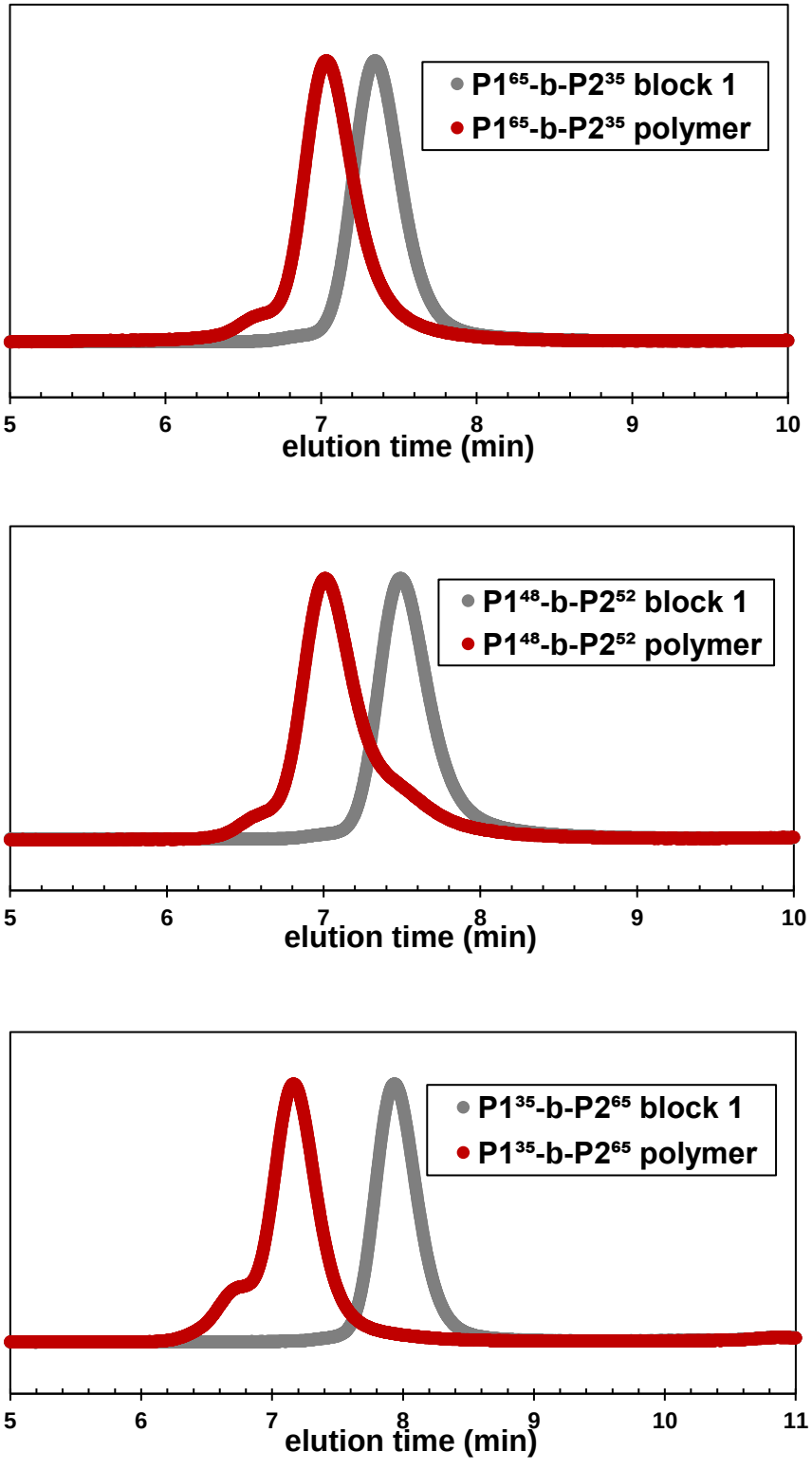


Figure 3.5 GPC trace of successful chain extension of **P1-*b*-P2** block copolymer series.

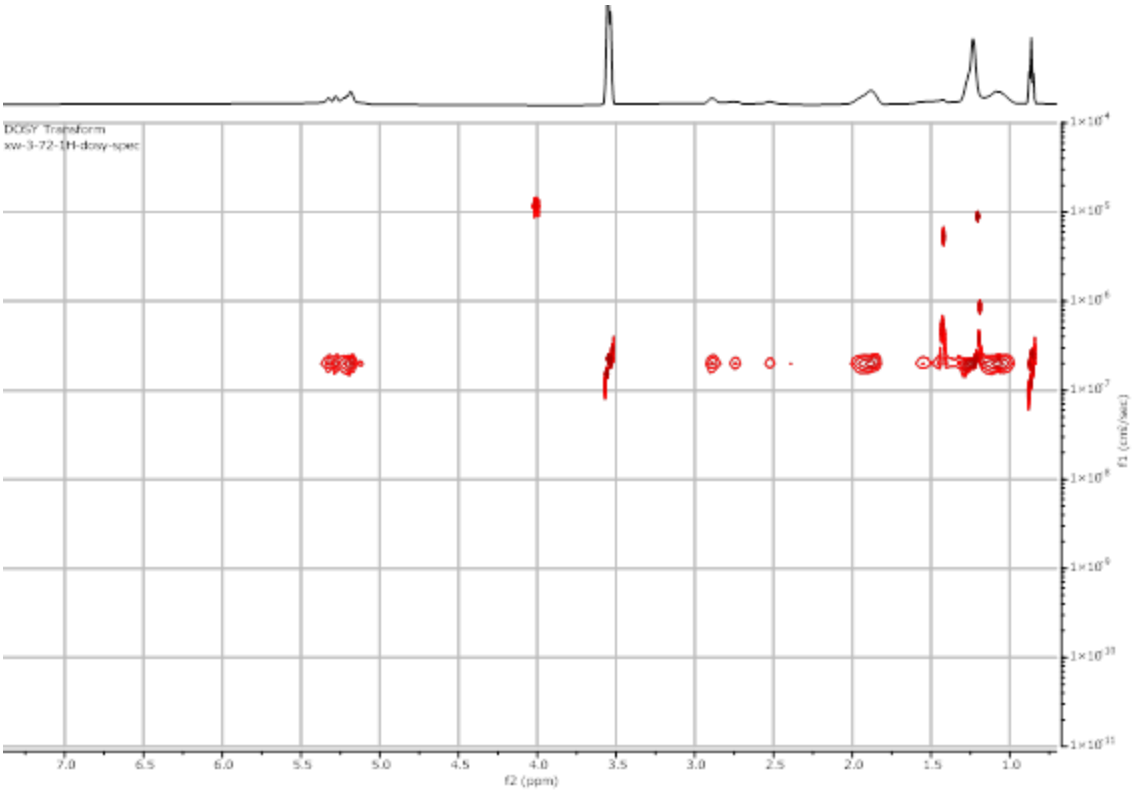


Figure 3.6 DOSY of block copolymer **P1^{48}-*b*-P2^{52}**. The major polymer peaks all have similar diffusion coefficient, suggested that the two blocks are connected.

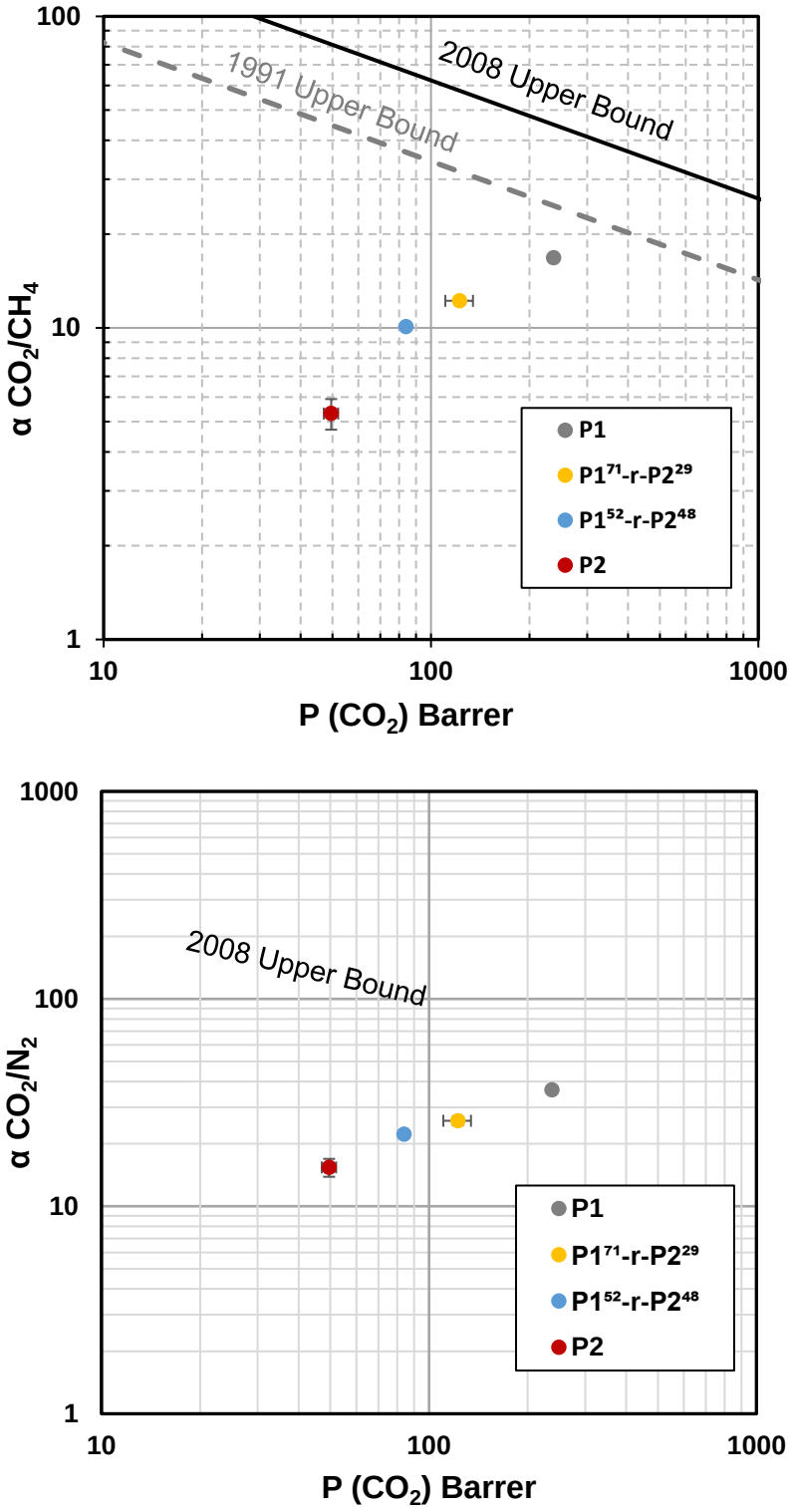


Figure 3.7 Robeson plot of polymers tested in this study. Error bars are included for each data point, but in some cases, the error bars are smaller than the data marker.



Figure 3.8 Example of as-cast **P1**^{48}-***b***-**P2**^{52} film (left), **P1** film (middle), and **P1/P2** blend (right).

Table 3.3 Ideal Permeability and Selectivity of the **P1**-*b*-**P2** and **P1**-*r*-**P2** Polymer Series[a]

		P (Barrer)[a]			*α* (CO_2/CH_4)[b]	
entry	Polymer	CO_2	CH_4	N_2	CO_2/CH_4	CO_2/N_2
1	**P1**	237.1(±3.3)	14.1(±0.3)	6.6(±0.1)	16.8(±0.1)	36.4
2	**P1**^{65}-***b***-**P2**^{35}					
3	**P1**^{48}-***b***-**P2**^{52}					
4	**P1**^{35}-***b***-**P2**^{65}					
5	**P2**	29.6(±2.5)	9.5(±1.4)	3.3(±0.4)	5.3(±0.6)	15.4
6	**P1**^{71}-***r***-**P2**^{29}	112.5(±11.9)	10.0(±1.0)	4.7(±0.2)	12.2(±0.0)	25.9
7	**P1**^{52}-***r***-**P2**^{48}	83.9(±0.5)	8.3(±0.1)	3.8(±0.1)	10.1(±0.1)	22.3

[a]Permeability values of free-standing polymer films were obtained using the constant-volume variable-pressure gas flux method at 20 psi upstream pressure. [b]Ideal selectivity was calculated as a ratio of pure gas $P(CO_2)/P(CH_4)$.

To investigate if any microphase separation was present in these block copolymer membranes, SAXS experiments were also conducted. Figure 3.9 showed the SAXS spectra of the **P1-*b*-P2** block copolymer series, and Figure 3.10 showed the SAXS spectra of **P1^{48}-*b*-P2^{52}** annealed at 100 °C for a different period. All spectra showed some scattering peaks, which indicated the presence of microdomains in the block copolymer membranes. The scattering peaks in Figure 3.9 were extracted and summarized in Table 3.4. Upon preliminary analysis, for all compositions, the ratio of higher-order peaks to the primary peak is roughly close to the characteristic of lamellae structure: for **P1^{65}-*b*-P2^{35}**, the ratio is 1, 1.93, 3.00; for **P1^{48}-*b*-P2^{52}**, the ratio is 1, 3.00, 5.14, 7.20, 9.28 (assuming even order scattering peaks were not observed); and for **P1^{35}-*b*-P2^{65}**, the ratio is 1, 2.08, 4.19, 5.16 (assuming 3rd scattering peak was not observed). The observation of the absence of some scattering peaks was also reported before, which was hypothesized as a result of minima in the respective form factor.[186] However, as some deviation from the ideal lamellae scattering pattern and the uneven surface morphology are still present, further optimization in the casting and annealing processes is necessary before drawing any conclusion.

3.7 Future Work

To facilitate better microphase separation in the MPNB block copolymer systems, fine-tuning in polymer composition and processing conditions will be needed. For example, different solvent or solvent mixtures can be used to dissolve the polymer during solvent casting, as the distinct interaction of solvent with two blocks may assist in different chain packing. Similarly, different substrates, such as glass and PTFE can be utilized as well. Once the films are obtained, different annealing processes can also be tested to find the optimal condition. Since the T_gs of

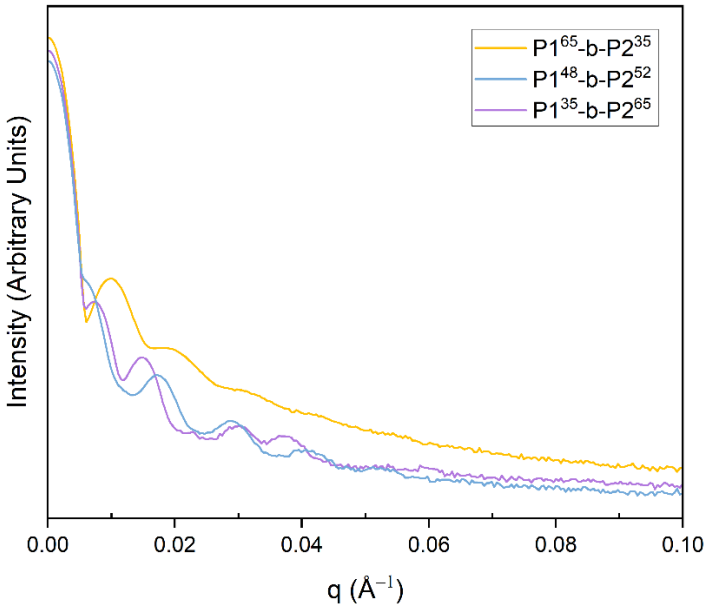


Figure 3.9 SAXS spectra of the **P1-*b*-P2** block copolymer series.

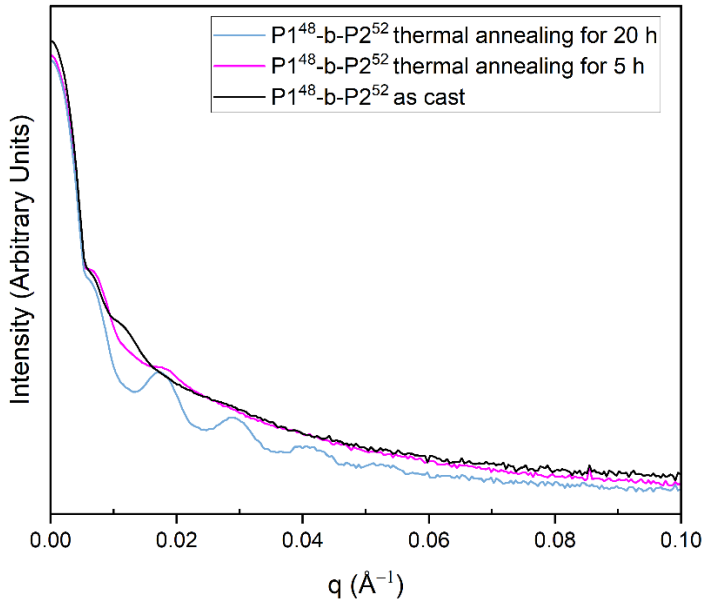


Figure 3.10 SAXS spectra of **P1^{48}-*b*-P2^{52}** annealed at 100 °C for different period.

Table 3.4 SAXS scattering peaks of the **P1-*b*-P2** block copolymer series.

	q					
Polymer	q_1	q_2	q_3	q_4	q_5	$q_1/q_2/q_3/q_4/q_5$
P1^{65}-*b*-P2^{35}	0.00993	0.01920	0.02979	/	/	1, 1.93, 3.00
P1^{48}-*b*-P2^{52}	0.00565	0.01694	0.02901	0.04069	0.05237	1, 3.00, 5.14, 7.20, 9.28
P1^{35}-*b*-P2^{65}	0.00720	0.01499	0.03018	0.03719	/	1, 2.08, 4.19, 5.16

MPNBs are relatively low, thermal annealing for different time periods is a feasible method to facilitate the formation of microphase separation, whereas solvent annealing is always another possible route.

Once optimizing the annealing condition, block copolymers with different compositions and morphologies will be designed and synthesized. All block copolymer films will then be tested for gas separation performance, and SAXS data will be collected to analyze their morphologies. The corresponding random copolymers will also be synthesized and tested to compare with their block copolymer analogs. Sorption and potential simulation experiments will also be performed to study the gas transportation mechanism.

References

53. Maroon, C. R.; Townsend, J.; Higgins, M. A.; Harrigan, D. J.; Sundell, B. J.; Lawrence III, J. A.; O'Brien, J. T.; O'Neal, D.; Vogiatzis, K. D.; Long, B. K., Addition-type alkoxysilyl-substituted polynorbornenes for post-combustion carbon dioxide separations. *Journal of Membrane Science* **2020,** *595*, 117532.

99. Odani, H.; Taira, K.; Nemoto, N.; Kurata, M., Diffusion and solution of gases and vapors in styrene-butadiene block copolymers. *Polymer Engineering & Science* **1977,** *17* (8), 527-534.

100. Csernica, J.; Baddour, R.; Cohen, R., Gas permeability of a polystyrene-polybutadiene block copolymer with oriented lamellar domains. *Macromolecules* **1987,** *20* (10), 2468-2471.

101. Csernica, J.; Baddour, R.; Cohen, R., Gas permeability of a polystyrene/polybutadiene block copolymer possessing a misoriented lamellar morphology. *Macromolecules* **1989,** *22* (3), 1493-1496.

103. Buonomenna, M. G.; Golemme, G.; Tone, C. M.; De Santo, M. P.; Ciuchi, F.; Perrotta, E., Nanostructured poly (styrene-b-butadiene-b-styrene)(SBS) membranes for the separation of nitrogen from natural gas. *Advanced Functional Materials* **2012,** *22* (8), 1759-1767.

104. Buonomenna, M.; Yave, W.; Golemme, G., Some approaches for high performance polymer based membranes for gas separation: block copolymers, carbon molecular sieves and mixed matrix membranes. *RSC advances* **2012,** *2* (29), 10745-10773.

177. Kim, H.-C.; Park, S.-M.; Hinsberg, W. D., Block copolymer based nanostructures: materials, processes, and applications to electronics. *Chemical reviews* **2010,** *110* (1), 146-177.

178. Mai, Y.; Eisenberg, A., Self-assembly of block copolymers. *Chemical Society Reviews* **2012,** *41* (18), 5969-5985.

179. Flory, P. J., *Principles of polymer chemistry*. Cornell university press: 1953.

180. Matsen, M. W.; Schick, M., Stable and unstable phases of a diblock copolymer melt. *Physical Review Letters* **1994,** *72* (16), 2660.

181. Matsen, M. W.; Bates, F. S., Unifying weak-and strong-segregation block copolymer theories. *Macromolecules* **1996,** *29* (4), 1091-1098.

182. Bates, F. S.; Fredrickson, G. H., Block copolymers-designer soft materials. *Physics today* **2000,** *52*.

183. Discher, D. E.; Ahmed, F., Polymersomes. *Annu. Rev. Biomed. Eng.* **2006,** *8*, 323-341.

184. Thomas, E.; Lescanec, R., Phase morphology in block copolymer systems. *Philosophical Transactions of the Royal Society of London. Series A: Physical and Engineering Sciences* **1994,** *348* (1686), 149-166.

185. Seidlitz, A.; Thurn-Albrecht, T., Small angle X-ray scattering for morphological analysis of semicrystalline polymers. *Polymer Morphology: Principles, Characterization, and Processing* **2016**, 153-164.

186. Hamley, I. W.; Castelletto, V., Small-angle scattering of block copolymers: in the melt, solution and crystal states. *Progress in polymer science* **2004,** *29* (9), 909-948.

187. Trnka, T. M.; Grubbs, R. H., The development of L2X2Ru CHR olefin metathesis catalysts: an organometallic success story. *Accounts of Chemical Research* **2001,** *34* (1), 18-29.

188. Wang, X.; Jeong, Y. L.; Love, C.; Stretz, H. A.; Stein, G. E.; Long, B. K., Design, synthesis, and characterization of vinyl-addition polynorbornenes with tunable thermal properties. *Polymer Chemistry* **2021,** *12* (40), 5831-5841.

189. Walsh, D. J.; Lau, S. H.; Hyatt, M. G.; Guironnet, D., Kinetic study of living ring-opening metathesis polymerization with third-generation Grubbs catalysts. *Journal of the American Chemical Society* **2017,** *139* (39), 13644-13647.

Chapter 4 Design, Synthesis, and Characterization of Vinyl-addition Polynorbornenes with Tunable Thermal Properties

A version of this chapter was originally published by Xinyi Wang, Yewon L. Jeong, Christopher Love, Holly Stretz, Gila E. Stein,* Brian K. Long*

"Design, Synthesis, and Characterization of Vinyl-addition Polynorbornenes with Tunable Thermal Properties" *Polymer Chemistry* **2021**, *12* (40), 5831-5841.

Xinyi Wang and was responsible for the synthesis and characterization of all monomers, polymers, thermal tests, corresponding data analyses, and drafting the manuscript. Yewon Jeong was an undergraduate student who helped with ellipsometry measurements and data analysis. Christopher Love was an REU who helped with synthesis. Dr. Holly Stretz helped with the polymer sample melt extrusion and data analysis. Dr. Gila Stein and Dr. Brian Long advised this work and aided in the preparation of the manuscript.

4.1 Abstract

Unfunctionalized vinyl-addition polynorbornene (APNB) possesses many outstanding properties such as high thermal, chemical, and oxidative stability. These features make APNB a promising candidate for many engineering applications. However, APNB has a small service window between its glass transition temperature (T_g) and decomposition temperature (T_d), and it cannot be readily processed in a melt state. In this work, we demonstrate that the service window of APNBs can be tailored through the use of norbornene monomers bearing alkyl, aryl, and aryl ether substituents. The vinyl addition homopolymerization and copolymerization of these functionalized norbornyl-based monomers yielded APNBs with high T_g's (> 150 °C) and large service windows (T_d - T_g > 100 °C), which is comparable to other commercial engineering thermoplastics. To further establish the feasibility of melt processing, a functionalized APNB

material with T_g = 209 °C and a service window of 170 °C was successfully extruded and molded into bars. Subsequent characterization of the bars by dynamic mechanical analysis (DMA), nuclear magnetic resonance spectroscopy (NMR), and gel permeation chromatography (GPC) revealed only minor signs of polymer degradation. These studies suggest that substituted APNBs could be developed into a new class of engineering thermoplastics that is compatible with workhorse melt processing techniques such as extrusion and injection molding, as well as emerging techniques such as extrusion-based 3D printing.

4.2 Introduction

Unfunctionalized vinyl-addition polynorbornene (APNB) possesses many outstanding properties, such as high thermal, chemical, and oxidative stability,[3] as well as low birefringence,[4] a low dielectric constant,[5, 6] and low moisture absorbance.[7, 8] These properties make APNB a promising candidate for many engineering and high-performance applications. However, unfunctionalized APNB has limited solubility in organic solvents,[117, 118] mechanical brittleness,[190] and a small service window between its glass transition (T_g) and decomposition temperatures (T_d),[117] all of which limit its processability.[190] Several studies have shown that the homopolymerization and/or copolymerization of norbornyl monomers bearing polar or nonpolar substituents can improve both polymer solubility and mechanical properties.[5, 10, 11, 13, 16, 115] Such functionalized APNBs can often be solution processed into mechanically robust, freestanding films that are suitable for a variety of potential applications, including gas separations,[3, 10-12] pervaporation membranes,[13] ion-exchange membranes,[14, 15] high-frequency interconnects,[16] and nonlinear-optical devices.[4] In contrast, in the fields of extrusion, injection molding, film blowing, or 3D printing, where commercial thermoplastics[191-196] are widely used, few comprehensive

studies of improving APNB melt processability by employing substituted norbornene monomers exist in the peer-reviewed literature.[115, 197]

To facilitate the melt processing of APNBs, their glass transition temperature (T_g) must be lowered while maintaining a high decomposition temperature (T_d) to establish a broad service window and enable melt flow without decomposition. Indeed, prior reports have demonstrated that certain functionalized APNBs may exhibit depressed T_g's while simultaneously maintaining high T_d's,[10, 11, 14-16, 115, 116] and companies such as BFGoodrich and Promerus have commercialized several APNB derivatives with T_gs well below that of unsubstituted APNB.[4, 5, 8, 110-113] As an example, Goodall and coworkers showed that copolymerization of alkyl-substituted norbornenes and unsubstituted norbornene could be used to fine-tune APNB T_g,[116] suggesting that melt processable APNBs may be accessed through careful substituent choice. This was also demonstrated by another recent report by Kim, Park, Huh and coworkers.[115] However, the overall relationships between thermal properties and molecular design are difficult to infer from current literature due to broad variability in the synthetic and thermal characterization methods used.[6, 12, 13, 39, 117-119] For example, polymer microstructure (i.e. stereoregularity, tacticity) may be strongly influenced by the type of catalyst used, and these attributes may impact resultant thermal properties.[3, 4, 198] Additional complications arise in that commonly employed techniques for characterization of T_g, such as differential scanning calorimetry (DSC),[118] spectroscopic ellipsometry,[199] and dynamic mechanical analysis (DMA),[10, 12, 16] often produce values that do not agree well with one another, particularly as each method probes a different property.

To provide fundamental insight into how monomer substituent structure may be used to tailor APNB T_g and service window (T_d - T_g), we examined a systematic series of substituted APNB homopolymers and copolymers bearing polar and/or nonpolar functional groups. To ensure

consistency and comparability of results, all polymers were synthesized using a single catalyst/activator system[35] under identical reaction conditions. The T_d of each polymer was measured by thermogravimetric analysis (TGA), and T_g was measured using DMA. For a few selected polymers, these T_g values were then compared to those measured using DSC and spectroscopic ellipsometry. Copolymer T_g values were compared to predictions based on homopolymer values using either the Fox or Gordon-Taylor equations, providing insight into the predictive capability of these simple correlations when substituents differing in structure and intermolecular interactions (e.g., London dispersion forces, π-π stacking, and dipole-dipole interactions) are introduced.

Though melt processing of VA-PNBs remains virtually unexplored in the peer-reviewed literature, recent work by Kim, Park, Huh and coworkers used melt pressing to prepare thin samples of unsubstituted-co-alkyl-substituted APNBs for tensile testing.[115] However, to the best of our knowledge, there are no literature examples in which melt extrudability is demonstrated. While a broad service window is required for thermal processing, this condition is not sufficient to establish processability by techniques such as melt extrusion. Therefore, to conclude our study, we selected a substituted APNB with a broad service window (T_d - $T_g \approx 200$ °C) for extrusion tests. We found that this substituted APNB exhibited melt processability similar to that of polystyrene (**PS**), and characterization of the extruded material by GPC, NMR spectroscopy, and DMA showed negligible signs of polymer degradation. These studies demonstrate that substituted APNBs may be engineered to enable their processing by workhorse techniques such as extrusion, thereby potentially broadening the application scope of this class of high-performing polyolefin-based materials.

4.3 Experimental Section

General Materials and Methods. All reactions were conducted under an inert atmosphere using an MBraun glovebox and a dry nitrogen atmosphere, unless noted otherwise. Synthesized monomers were purified via sequential distillations (≥ 98% purity, via GC) unless otherwise noted, degassed via freeze−pump−thaw (×3), and stored over 3 Å molecular sieves in a glovebox prior to use. Dicyclopentadiene, hydroquinone, 1-hexene, 1-octene, and sodium borohydride were purchased from Acros Organics and used as received. 1-Decene and 1-dodecene were purchased from TCI America and used as received. 5-Norbornene-2-carboxaldehyde and benzyl bromide were purchased from Alfa Aesar and used as received. Sodium hydride, allylmagnesium chloride solution (2.0 M in THF), and (2-bromoethyl)benzene were purchased from Sigma-Aldrich and used as received. Hexane, ethyl acetate, methanol, and chloroform were purchased from Fisher Scientific and used as received. Dichloromethane for polymerizations was purchased from Fisher Scientific and purified using an Innovative Technologies PureSolv Solvent Purification System and degassed via freeze-pump-thaw (×3) prior to use. The catalyst (η^3-allyl)Pd(i-Pr_3P)Cl was synthesized according to literature procedure and stored in a glovebox prior to use.[35] This catalyst is commonly used for vinyl-addition polymerization of norbornene-based monomers.[12, 13, 15, 39] Lithium tetrakis(pentafluorophenyl)borate ethyl etherate ($LiBAr^F_4$) was obtained as a gift from Boulder Scientific and used as received. Monomers **M1**-**M4** were synthesized according to prior literature reports with only minor modifications.[200, 201] The intermediate 5-phenyl-1-pentene,[202] 5-norbornene-2-methanol[203] and 5-benzyloxymethyl-2-norbornene (**M6**)[203-205] were synthesized according to prior literature reports and all characterization matched those previously reported. **PS** (M_w ~ 350 kg/mol, M_n ~ 170 kg/mol) was purchased from Sigma Aldrich and used as a comparison sample for thermal characterization, melt processing, and mechanical characterization.

Synthesis of 5-butyl-2-norbornene (M1). Monomer **M1** was synthesized following a modified literature procedure.[200, 201] 1-Hexene (4.0 g, 47.5 mmol), dicyclopentadiene (2.5 g, 18.9 mmol), and hydroquinone were added to a 50 mL glass pressure tube with a stir bar. The pressure tube was sealed and heated to 240 °C for 3 h with stirring. After cooling, the mixture was purified by two sequential distillations at reduced pressure (10 torr, 88-90 °C) to yield 0.58 g of monomer **M1** (10.3% yield) as a mixture of *endo*:*exo* isomers (*endo*:*exo* = 75:25). All characterizations matched prior literature reports.[200]

Synthesis of 5-hexyl-2-norbornene (M2). Monomer **M2** was synthesized following the procedure described for **M1.** The crude mixture of **M2** was purified by two sequential distillations at reduced pressure (4 torr, 113-115 °C) to yield 1.11 g of monomer **M2** (16.5% yield) as a mixture of *endo*:*exo* isomers (*endo*:*exo* = 79:21). All characterizations matched prior literature reports.[206]

Synthesis of 5-octyl-2-norbornene (M3). Monomer **M3** was synthesized following the procedure described for **M1.** The crude mixture of **M3** was purified by two sequential distillations at reduced pressure (4 torr, 132-134 °C) to yield 1.11 g of monomer **M3** (17.0% yield) as a mixture of *endo*:*exo* isomers (*endo*:*exo* = 79:21). ^{1}H NMR ($CDCl_3$, 293 K, *endo* isomer): δ (ppm) = 6.10 (1H, dd), 5.91 (1H, dd), 2.75 (2H, m), 1.96 (1H, m), 1.83 (1H, m), 1.39 (1H, m), 1.35-1.22 (12H, m), 1.19 (1H, m), 1.07 (2H, m), 0.88 (3H, t), 0.48 (1H, ddd). ^{13}C NMR ($CDCl_3$, 293 K, endo/exo mixture): δ (ppm) = 137.16, 137.03, 136.36, 132.67, 49.78, 46.59, 45.64, 45.44, 42.75, 42.09, 39.00, 36.87, 35.06, 33.33, 32.68, 32.17, 30.19, 30.17, 29.92, 29.90, 29.59, 29.13, 28.91, 22.93, 14.35. $HRMS^{calc}$ $C_{15}H_{26}$ (H^+ adduct) = 207.2113 m/z. $HRMS^{expt}$ $C_{15}H_{26}$ (H^+ adduct) = 207.1858 m/z.

Synthesis of 5-decyl-2-norbornene (M4). Monomer **M4** was synthesized following the procedure described for **M1.** The crude mixture of **M4** was purified by two sequential distillations

at reduced pressure (0.5 torr, 110-112 °C) to yield 1.11 g of monomer **M4** (12.1% yield) as a mixture of *endo*:*exo* isomers (*endo*:*exo* = 78:22). ^{1}H NMR ($CDCl_3$, 293 K, *endo* isomer): δ (ppm) = 6.10 (1H, dd), 5.91 (1H, dd), 2.75 (2H, m), 1.96 (1H, m), 1.83 (1H, m), 1.39 (1H, m), 1.35-1.22 (16H, m), 1.19 (1H, m), 1.07 (2H, m), 0.88 (3H, t), 0.48 (1H, ddd). ^{13}C NMR ($CDCl_3$, 293 K, endo/exo mixture): δ (ppm) = 137.16, 137.03, 136.36, 132.67, 49.78, 46.59, 45.64, 45.44, 42.75, 42.09, 39.00, 36.87, 35.07, 33.33, 32.68, 32.17, 30.19, 30.17, 29.96, 29.94, 29.90, 29.60, 29.14, 28.91, 22.93, 14.35. $HRMS^{calc}$ $C_{17}H_{30}$ (H^+ adduct) = 235.2426 m/z. $HRMS^{expt}$ $C_{17}H_{30}$ (H^+ adduct) = 235.2161 m/z.

Synthesis of 5-phenylpropyl-2-norbornene (M5). The reagent 5-phenyl-1-pentene was synthesized following a known literature procedure.[202] 5-phenyl-1-pentene (5.84 g, 39.9 mmol), dicyclopentadiene (2.14 g, 16.2 mmol), and hydroquinone were added to a 50 mL glass pressure tube with a stir bar. The pressure tube was then sealed and heated to 240 °C for 12 h with stirring. The mixture was cooled to room temperature and purified by two sequential distillations at reduced pressure (0.5 torr, 130-132 °C) to yield 1.75 g of monomer **M5** (25.4% yield) as a mixture of *endo*:*exo* isomers (*endo*:*exo* = 76:24). ^{1}H NMR ($CDCl_3$, 293 K, *endo* isomer): δ (ppm) = 7.31-7.17 (5H, m), 6.11 (1H, dd), 5.90 (1H, dd), 2.77 (2H, m), 2.58 (2H, m), 2.01 (1H, m), 1.84 (1H, m), 1.74-1.08 (6H, m), 0.50 (1H, ddd). ^{13}C NMR ($CDCl_3$, 293 K, endo/exo mixture): δ (ppm) = 143.12, 143.03, 137.16, 137.08, 136.40, 132.55,128.55, 128.45, 128.42,125.79, 125.76, 49.77, 46.56, 45.58, 45.45, 42.73, 42.09, 38.91, 38.86, 36.47, 36.43, 34.72, 33.26, 32.61, 30.98, 30.79. $HRMS^{calc}$ $C_{16}H_{20}$ (H^+ adduct) = 213.1643 m/z. $HRMS^{expt}$ $C_{16}H_{20}$ (H^+ adduct) = 213.1407 m/z.

General polymerization procedure. Under air-free conditions (glovebox), (η^3-allyl)Pd(i-Pr_3P)Cl (10 μmol), $LiBAr^F{}_4$ (10 μmol), and dry/degassed DCM (1 mL) were combined in a 20 mL scintillation vial and stirred for 20 min to activate the catalyst. In a separate vial, the monomer (or

monomers) (5 mmol, total) was dissolved in dry/degassed DCM (4 mL) and added to the stirred catalyst solution. All polymerizations were ran overnight, unless otherwise noted, before quenching via exposure to air, dilution with additional DCM (10 mL), and precipitation into 250 mL of methanol. All polymers were isolated by vacuum filtration and dried in *vacuo* until reaching constant weight.

Monomer and Polymer Characterization. ^{1}H and ^{13}C NMR spectra of monomers and polymers were obtained in $CDCl_3$ using a Varian 300 MHz or Varian 500 MHz NMR instrument, and spectra were referenced to the residual solvent peak at $\delta = 7.26$ ppm (^{1}H) and 77.23 ppm (^{13}C), respectively. High-resolution mass spectrometry (HRMS) was performed using a JEOL AccuTOF equipped with a DART source. Molecular weight and dispersity ($Đ$) of all polymers were determined using a Tosoh EcoSEC GPC with a refractive index detector and THF as the eluent at 40 °C. All MW's and dispersity values are reported relative to polystyrene standards.

Thermal Characterization of Polymers. Thermogravimetric analysis (TGA) was performed using a TA Instruments Q550 with a heating rate of 10 °C/min under a N_2 purge. All T_d values are reported as the temperature corresponding to 5% weight loss. To measure T_g, three methods were employed: modulated DSC (MDSC), spectroscopic ellipsometry, and DMA. MDSC measurements were performed using compressed polymer powders in T-zero pans with a TA Instruments Q2000 at a heating rate of 3 °C/minute (modulated at ± 1.00 °C per 60 s) from 80 to 300 °C under a nitrogen atmosphere. T_g was determined based upon the transition of reversing heat capacity. DMA was performed using a TA Instruments RSA-G2 solids analyzer equipped with a tension fixture. Thick APNB film samples (40-120 μm) were prepared by solution casting from $CHCl_3$ solutions (3 wt%) into a PTFE dish. For example, a desired polymer (0.5 g) was added to $CHCl_3$ (10 mL) and stirred until fully dissolved. The solution was filtered through a 0.45 μm PTFE

syringe filter into a clean and leveled PTFE dish that is approximately 6 cm in diameter. In contrast, polystyrene films were prepared by dissolving the commercial polystyrene sample (0.5 g) in toluene (3 mL), which was then filtered through a 0.45 μm PTFE syringe filter, degassed, and poured onto a levelled glass plate and drawn using a blade coater under a controlled shear rate. The solution cast APNB and drawn polystyrene films were covered to reduce the rate of evaporation while drying, and the polymer films were collected after complete solvent evaporation. Resultant films were determined to be 40-120 μm in thickness and were cut into strips (3-5 mm wide by 10-15 mm long) for DMA testing. The strips were mounted in the tension fixture, equilibrated at the starting temperature for 5 min, and the experiment was run at a heating rate of 5 °C/min from either 100 °C or 40 °C up to 300 °C under a nitrogen atmosphere with an axial force oscillated at 0.1% strain rate and 1 Hz. The T_g was taken as the maximum of the tan δ curve, and the reported value is the average of two measurements. Spectroscopic ellipsometry was used to measure thin film T_g's. Films were prepared by spin casting from a toluene solution (~5 wt%) onto a silicon wafer and heated to 240 °C for 20 min under a nitrogen atmosphere to drive-off residual solvent. All films were 500 ± 50 nm in thickness. A J.A. Woollam M-2000 spectroscopic ellipsometer (wavelengths λ = 300 – 1690 nm) was used to record the ellipsometry parameters Δ and ψ as a function of temperature. The incidence/detection angles were fixed at 70˚, and samples were heated/cooled at a rate of 1 °C/min from 80 to 240 °C under a nitrogen atmosphere. The ellipsometry parameters were modeled using a three-layer system of polymer, native oxide, and silicon (in air). The refractive index of the polymer layer was described by the Cauchy dispersion relation, $n(\lambda) = A + B/\lambda^2$, and the refractive index of both native oxide and silicon were fixed to known literature values. The Cauchy constants (A and B) and polymer film thickness h were adjustable parameters for regression analysis. Typical values for A and B parameters were around

1.5 and 0.005-0.008, respectively. The T_g was determined as the point of change in slope on a plot of polymer film thickness versus temperature[207] using data from the second cooling cycle. The T_g is taken as the intersection of the two lines that capture the rubber and glass regimes, as shown in the Supporting Information.

Melt Extrusion and Characterization of Mechanical Properties. All polymer samples were dried *in vacuo* at 85 °C overnight prior to use. Tensile bars were prepared using a DSM Micro-5 twin screw compounder and benchtop injection molding machine, which was operated at a barrel temperature of 210 °C for commercial polystyrene samples and 250 °C for APNBs, a mold temperature of 100 °C under N_2 purge, 90 rpm, a melt index of 10-12 g/10 min, and a back force of ~1000-1500 N on the screws. As limited quantities of the synthesized APNB materials were available, relative to what was needed for melt processing, these process conditions were deemed best, but were not optimized. A portion of the synthesized APNB material was used for purging the extruder to ensure clean extrusion conditions, and bars were checked for clarity by visual inspection using a light box, indicating completeness of purge throughout the process. Mechanical testing was performed using an Instron load frame model 5948 (horizontal testing, 1 kN load cell) at a strain rate of 0.1 mm/min according to ASTM D638. The modulus was obtained by plotting engineering/true stress verses corresponding strain. Cyclic loading moduli were obtained by testing two specimens, each with three cycles of load and unload between 110-360 N.

Wide Angle X-Ray Scattering. Select films (**P3**, **P4**) were illuminated at normal incidence (transmission through the film thickness) under ambient conditions using A Xenocs GeniX 3D microfocus source with a copper target (wavelength $\lambda = 0.154$ nm). The sample to detector distance was 0.045 m. A Pilatus3 R_300K detector (Dectris) was used with pixel size of 172 μm × 172 μm. The data acquisition time was 5 min. The two-dimensional images from each measurement were

azimuthally-integrated to yield a one-dimensional scattering profile of intensity I (a.u.) versus scattering vector q ($Å^{-1}$).

4.4 Discussion

As a basis for the design of melt processable APNBs, we surveyed the thermal characteristics of commercially available engineering thermoplastics, such as polysulfone, polyetherimide, and polycarbonate. This analysis revealed that each material displayed a T_g > 150 °C and a T_d - T_g > 100°C.[191-195] In an effort to design APNBs that provide a similarly large service window, albeit while maintaining a high T_d, a variety of homopolymers and copolymers were synthesized using substituted norbornene monomers. Monomers **M1-M4** (Figure 4.1) bear linear alkyl substituents of varying length, whereas monomers **M5** and **M6** incorporate bulky aromatic groups that are tethered by an alkyl or ether linkage, respectively. In addition to differences in flexibility and size, these substituents introduce the possibility of different types of intermolecular forces being present. For example, monomers **M1-M4** are believed to interact primarily via weak London-Dispersion forces, whereas monomers **M5** and **M6** introduce a bulky benzyl substituent that may participate in π-π stacking interactions that have been reported to improve film formation.[16] Furthermore, monomer **M6** also adds the potential to introduce dipole-dipole interactions as a result of its ethereal moieties.

Monomers **M1**-**M5** were synthesized via Diels-Alder reaction of *in-situ* cracked dicyclopentadiene and a corresponding dieneophile that was either commercially available or was synthesized following established literature procedures.[202] Each monomer was isolated as a clear liquid following successive vacuum distillations at reduced pressure (10-25% yield) until reaching >98% purity, as determined via gas chromatography. As a note, monomer **M3** could only be

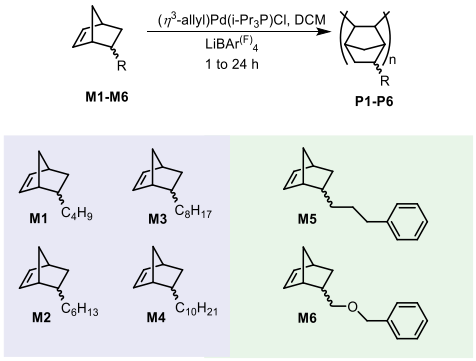


Figure 4.1 Series of APNBs (**P1-P6**) chosen to probe the effects of substituent architecture on resultant thermal properties. Reprinted with permission from Reference [188]. Copyright 2021 The Royal Society of Chemistry.

obtained in 85% purity due to the presence of impurities having similar boiling points that could not be readily removed via distillation or flash column chromatography. Monomer **M6** was synthesized via Williamson ether synthesis in which 5-norbornene-2-methanol was reacted with benzyl bromide, followed by column chromatography to obtain a clear liquid (61% yield). Each monomer was characterized using ^{1}H NMR spectroscopy to confirm functionalization and determine the *endo*:*exo* ratio of the norbornene substituent.

It is well known that the catalyst employed to access APNBs may influence the thermomechanical properties of the resultant materials, an effect that has been attributed to differences in polymer tacticity and stereoregularity.[116, 208, 209] We also observed this in our preliminary studies, wherein both Ni- and Pd-based catalysts were used (see Supporting Information). However, to avoid complications arising from tacticity and stereoregularity differences based upon catalyst choice, we chose to use the catalyst system (η^3-allyl)Pd(i-Pr_3P)Cl/LiBAr$^F_4$ (BAr$^F_4$ = tetrakis(pentafluorophenyl)-borate) for all polymer syntheses described herein. As shown in Scheme 1, monomers **M1**-**M6** were each homopolymerized to yield polymers **P1**-**P6**. In order to further investigate the influence of various substituents on the thermal properties of APNBs, a series of statistical copolymers denoted using the notation **PXPY** were synthesized, wherein X and Y signify the two monomer components copolymerized. Specifically, X was fixed as **M2** and Y was either **M4**, **M5**, or **M6** to yield copolymers **P2P4**, **P2P5**, and **P2P6**, respectively.

Each polymer was obtained in modest to excellent yield (62-98%) and was characterized via ^{1}H NMR spectroscopy and gel permeation chromatography (GPC). All polymer molecular weights (M_n) exceeded 60 kg/mol and dispersities ($Đ$) ranged from 1.3-2.8 (Table 4.1). It was noted that the homopolymerization of **M3** resulted in higher molecular weight, higher dispersity and poorer solubility as compared to other APNB analogues. We hypothesize that this is due to the presence

Table 4.1 Homo- and co-polymerization of substituted norbornene monomers.[a]

entry	polymer	feed ratio (**MX**:**MY**)	actual ratio[d] (**MX**:**MY**)	yield (%)	M_n[f] (kg/mol)	$Đ$[f]
1	**P1**	100:0	100:0	83	63	1.30
2	**P2**	100:0	100:0	85	84	1.35
3[b]	**P3**	100:0	100:0	64	163	2.81
4	**P4**	100:0	100:0	92	129	2.00
5	**P5**	100:0	100:0	76	89	1.41
6[c]	**P6**	100:0	100:0	62	66	1.32
7	$\mathbf{P2^{75}P4^{25}}$	75:25	-[e]	76	166	2.32
8	$\mathbf{P2^{50}P4^{50}}$	50:50	-[e]	97	159	2.20
9	$\mathbf{P2^{25}P4^{75}}$	25:75	-[e]	94	165	1.91
10	$\mathbf{P2^{68}P5^{32}}$	75:25	68:32	96	92	1.47
11	$\mathbf{P2^{44}P5^{56}}$	50:50	44:56	98	94	1.42
12	$\mathbf{P2^{15}P5^{85}}$	25:75	15:85	97	94	1.46
13[c]	$\mathbf{P2^{86}P6^{14}}$	75:25	86:14	83	126	1.28
14[c]	$\mathbf{P2^{65}P6^{35}}$	50:50	65:35	75	102	1.29
15[c]	$\mathbf{P2^{28}P6^{72}}$	25:75	28:72	78	96	1.32

[a]General polymerization conditions: total monomer concentration = 5 mmol, [catalyst] = 10 μmol, 5 mL of DCM, room temperature, and t_{rxn} = 16 h. [b]Reaction time (t_{rxn}) = 1 h. [c][mon]:[cat] = 1000:1 and t_{rxn} = 24 h. [d]Monomer incorporation ratios (**MX:MY**) were calculated via ^{1}H NMR spectroscopy. [e]The monomer incorporation ratio (**MX:MY**) could not be determined via ^{1}H NMR spectroscopy due to overlapping ^{1}H resonances. [f]Molecular weights and dispersities were measured using gel permeation chromatography at 40 °C in THF and are reported relative to polystyrene standards.

of impurities, such as tricyclopentadiene, that may have been incorporated into the polymer chain and could potentially lead to undesired crosslinking. Thus, a shorter reaction time (1 h) was applied to minimize the potential for crosslinking (Table 4.1, entry 3). In contrast, the homopolymerization of **M6** (Table 4.1, entry 6) led to decreased polymer yield and molecular weight, even when polymerized at a higher monomer:catalyst ratio ([mon]:[cat] = 1000:1) and extended reaction time (24 h). Similar observations have been reported in the literature, in which slower polymerization rates and lower yields are often hypothesized to result from deleterious interactions between the polar substituent and the electrophilic, active catalyst species.[13, 190, 208, 210] Similar trends were also found for all copolymerizations (Table 4.1, entries 13-15).

Copolymer compositions are denoted as **PX^{n}PY^{m}**, where the superscripts "n" and "m" represent the actual monomer incorporation ratios of each monomer (**MX**:**MY**). Monomer incorporation ratios for the **P2P4** copolymer series (entries 7-9) could not be determined by ^{1}H NMR spectroscopy due to the significant overlap of all peaks in the alkyl region; however, the incorporation ratios for the copolymer series **P2P5** and **P2P6** (Table 4.1, entries 10-15) were readily determined based upon integration of their benzylic proton resonances corresponding to monomers **M5** (2.59 ppm) and **M6** (4.49 ppm), respectively, to all remaining protons in alkyl region. Therein, we found that copolymerizations of **M2** and **M5** favored higher incorporations of **M5** than included in the feed, whereas copolymerizations of **M2** and **M6** favored higher incorporation of **M2** than predicted based upon the monomer feed ratio. The lower observed incorporations of monomer **M6** is consistent with the reduced polymerization rate often observed for monomers bearing polar substituents.[18]

As previously mentioned, APNB T_g values can be probed via several techniques, such as DSC, DMA, and ellipsometry.[10, 12, 16, 118, 199] Unfortunately, each of these methods determines T_g

by probing a different polymer property, resulting in data that may not be directly comparable to results obtained via another method. For example, DSC detects T_g through changes in heat capacity above and below the glass transition, whereas DMA probes changes in viscoelastic properties (and depends on whether T_g was determined based upon storage modulus (E'), loss modulus (E''), or tan δ peak), and ellipsometry detects T_g through changes in the linear coefficient of thermal expansion.[211] We chose to evaluate all three techniques using a subset of the polymers described in Table 2.1 so as to compare each method of T_g determination. The polymers selected for this comparison were homopolymers **P2**, **P6**, the **P2P6** copolymer series, and a **PS** control. Lastly, because the T_g of each substituted APNB could not be detected using conventional DSC, MDSC was used for all studies described herein.[212]

As shown in Table 4.2, the T_g values obtained from MDSC, DMA, and spectroscopic ellipsometry for the **PS** control are similar, falling within 10 °C of each other. However, for APNB **P2** and **P6**, a larger discrepancy (>30 °C) was observed. Similar results were found for the **P2P6** copolymer series (range of 30-50 °C). Each method showed a similar trend in that increasing the molar ratio of **M6** comonomer depressed the T_g, which was expected due to the increased flexibility of the ether linkage in monomer **M6** as compared to alkyl-substituted **M2**. With the exception of entry 3, T_g measurements obtained by MDSC and ellipsometry agree within 15 °C. This is consistent with a prior report that describes thermal characterization of APNB homopolymers,[199] and that can be attributed to the fact that heat capacity and thermal expansion coefficient are both thermodynamic properties. The discrepancy between these methods and DMA is likely explained by the fact that DMA does not probe a thermodynamic property, but rather employs both mechanical and thermal stimulation to measure a viscoelastic response. Ultimately, DMA was selected as the most useful method for characterizing the T_g of the functionalized

Table 4.2 T_g values of **PS**, **P2**, **P6**, and the **P2P6** copolymer series as measured by MDSC, DMA, and ellipsometry.

entry	polymer	T_g by MDSC (°C)	T_g by DMA (tan δ, °C)	T_g by ellipsometry (°C)[a]
1	**PS**	95[b]	104	100
2	**P2**	189	209	173
3	**P2^{86}P6^{14}**	186	202	154
4	**P2^{65}P6^{35}**	162	191	160
5	**P2^{28}P6^{72}**	163	191	160
6	**P6**	162	184	152

[a]Initial film thickness (h) was ~500 nm. [b]The T_g of PS was measured using conventional DSC.

APNBs for a variety of reasons. First, the transitions obtained using MDSC and ellipsometry are extremely weak, and therefore difficult to detect and quantify with great accuracy (see Supporting Information). In contrast, the tan δ peak obtained via DMA is strong and readily identifiable. Second, viscoelastic response is arguably more relevant to the design and tailoring of melt-processable polymers. Finally, the T_g values obtained by DMA provide the most conservative estimate of the service window between T_g and T_d.

The T_g (via DMA), T_d, and service window of all the substituted APNB homopolymers are summarized in Figure 4.2 and Table C.1. The T_g and T_d of unfunctionalized APNB are reported as approximately 390 °C and 415 °C, respectively.[5, 198] The T_gs of APNB homopolymers are significantly depressed by functionalization, which was expected due to the incorporation of flexible substituents.[213] Within the linear alkyl substituent series (**P1**-**P4**), the longer and more flexible substituents resulted in lower T_g's than their shorter analogues, with T_g decreasing from 280 °C for the butyl-substituted APNB (**P1**) to 119 °C for the decyl-substituted APNB (**P4**) (Figure 4.2). As shown in support information, WAXS measurements of **P3** and **P4** do not detect any crystallization of the long alkyl substituents. The addition of rigid and bulky phenyl substituents into polymer **P5** introduces potential π-π stacking interactions (**P5**) and was expected to increase the T_g relative to an alkyl substituent with the same number of carbons. Indeed, the T_g of **P5** which contains nine carbon atoms in its sidechain is similar to that of **P3**, which contains only 8 carbon atoms (Figure 4.2). Furthermore, when ether linkages are introduced (**P6**), substituent flexibility is increased due to the lower rotational barrier of ethereal linkages as compared to analogous hydrocarbon linkers. This added flexibility results in T_g being depressed from 193 °C for phenylpropyl-substituted **P5** to 184 °C for benzyloxymethyl-substituted **P6**, despite having substituents of similar size and composition.

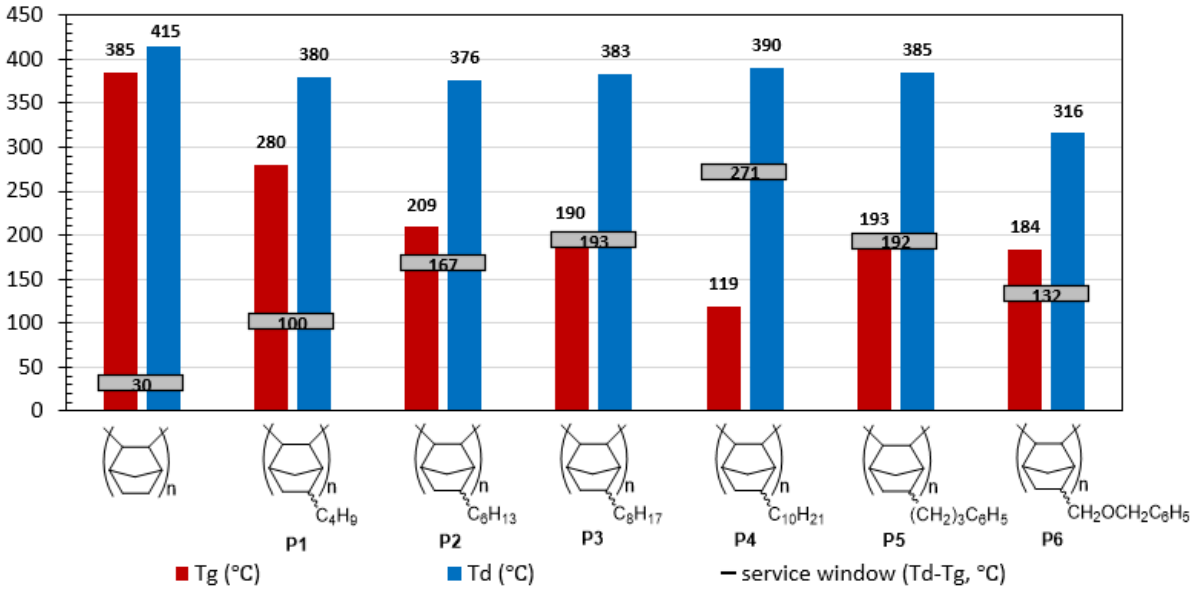


Figure 4.2 T_g, T_d, and service window (T_d-T_g) of unsubstituted APNB[5, 198] and substituted homo-APNBs **P1-P6**. Reprinted with permission from Reference [188]. Copyright 2021 The Royal Society of Chemistry.

It should be noted that the T_gs of the APNBs synthesized herein are generally lower than previously reported in the literature. Examples include **P1** (280 °C) which has been previously reported to be 330 °C;[110] **P2** (209 °C) which has been previously reported to be 265 °C,[5] 280 °C,[10] or 225 °C;[110] and lastly, **P4** (119 °C) which has been previously reported to be 150 °C,[10] or 180 °C.[110] As discussed previously, we hypothesize that this difference in measured T_g values may be attributed to the different catalysts and/or the characterization method being employed.

The T_d's of APNB homopolymers are moderately depressed by functionalization, but aside from **P6**, all T_d's exceeded ~380 °C. By inspecting the TGA data, the degradation behavior of **P6** is different from **P1**-**P5**. Specifically, the derivative of the TGA curve of **P6** suggests there are two stages of degradation, the first of which we hypothesize is degradation of the ether linkage prior to the second stage of backbone degradation (see Supporting Information). The key conclusion from the data in Figure 4.2 and Table C.1 is that functionalization more strongly depresses T_g than T_d, leading to a large service window for melt processing, while T_g remains high enough to expect good thermomechanical stability. Furthermore, the T_g's and service windows of these APNB materials are comparable to those of commercial amorphous engineering thermoplastics, such as polycarbonate, and polyetherimide.[191, 195, 214]

We also envisioned that the thermal properties of these APNB materials may be tuned via copolymerization, rather than relying solely on a single substituent chemistry. As an example, the T_d's of **P2** and **P4** are both approximately 380 °C, yet the T_g's of **P2** and **P4** are 209 °C and 120 °C, respectively. This suggests that copolymerization of **M2** and **M4** may enable tailoring of APNB T_g across a broad 90 °C window with little impact on T_d. As shown in Figure 4.3 and Table C.1, the T_g's of the **P2P4** copolymer series fall within the anticipated range and provide potential melt processing temperature ranging from 150-350 °C. Similarly, the **P2P5** and **P2P6**

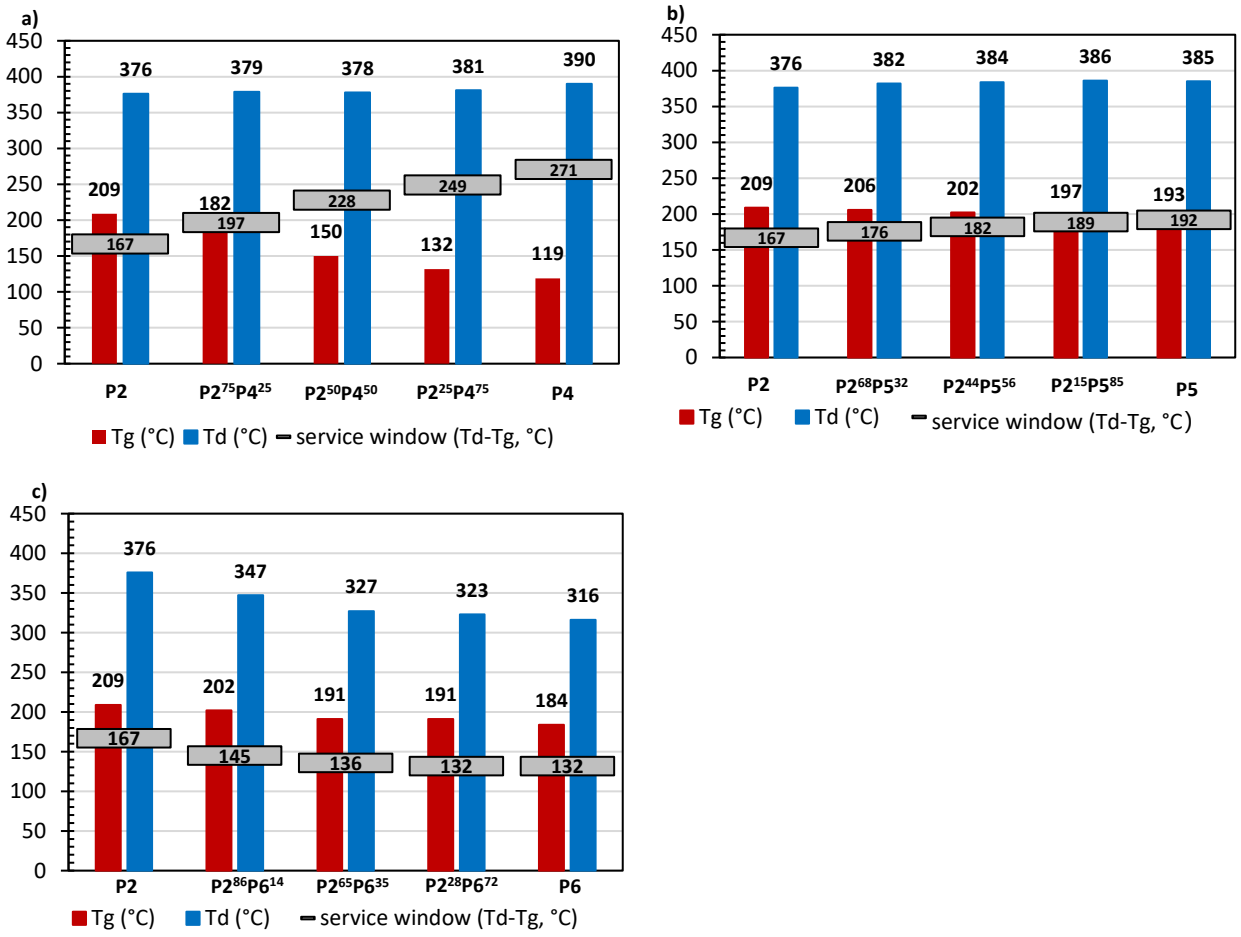


Figure 4.3 T_g, T_d, and service window for the a) **P2P4**, b) **P2P5**, and c) **P2P6** copolymer series. Reprinted with permission from Reference [188]. Copyright 2021 The Royal Society of Chemistry.

copolymer series also demonstrates that T_g's can be designed to fall in between their homopolymer analogues, though admittedly this range is small due to the small difference in T_g values for homopolymers **P2**, **P5**, and **P6**. Aside from the **P2P4** copolymer series that has high **M4** comonomer content, the T_g's of these statistical copolymers fall within the range of 180-280 °C. Furthermore, the measured T_d values for all copolymers exceeded ~380 °C, except the **P2P6** copolymer series which bears the **M6** ether-containing monomer units (see support information). The service windows of these copolymers are comparable to those of commercial amorphous engineering thermoplastics as well.

To better understand the relationship between copolymer T_g, comonomer composition, and potential intermolecular interactions present, we sought to compare our experimentally determined values to simple mathematical correlations. Starting with the alkyl substituted APNB copolymer series **P2P4**, theoretical copolymer T_g's were calculated using the Fox equation and compared to experimental T_g data obtained via DMA (Figure 4.4a). The Fox equation is as follows:

$$\frac{1}{T_g} = \frac{w_1}{T_{g1}} + \frac{1 - w_1}{T_{g2}}$$

where the parameters T_g, w_1, T_{g1}, and T_{g2} are the predicted glass transition temperature for the copolymer, the weight fraction of monomer type 1, and the measured glass transition temperatures of homopolymer types 1 and 2, respectively. The Fox equation provides excellent agreement with experimental data, confirming the validity of this simple model for alkyl substituted APNBs. Furthermore, there are no free parameters in this model, as T_{g1} and T_{g2} are measured from DMA. As a result, the T_g and service window can be predicted as a function of w_1 based solely on knowledge of the homopolymer T_g's.

In contrast to the simple alkyl substituted copolymer series **P2P4**, the **P2P5** series mixes hexyl and phenylpropyl substituents, where the latter substituent has bulkier side chains that have

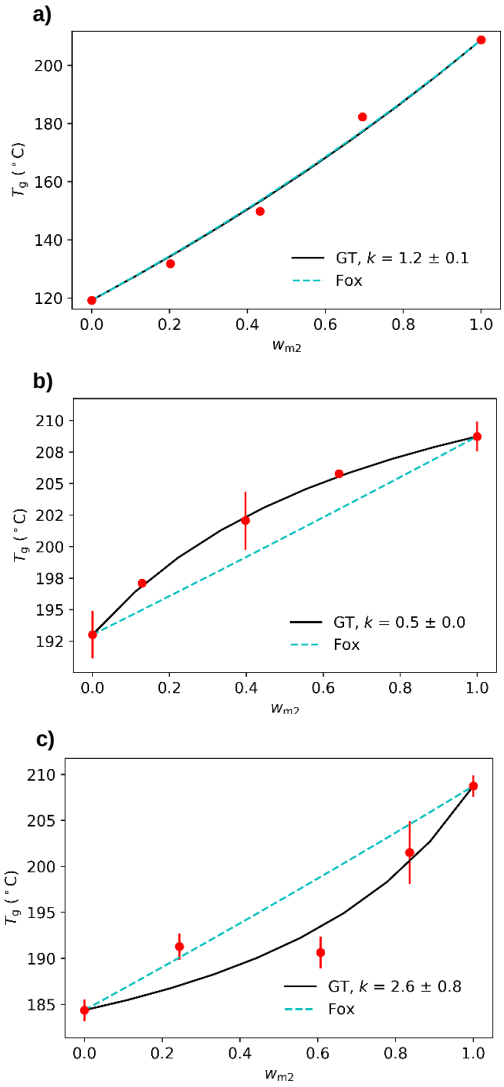


Figure 4.4 Comparison of experimental T_g (as determined by DMA) and theoretical T_g as predicted by the Fox and Gordon-Taylor equations for the a) **P2P4** series, b) **P2P5** series, and c) **P2P6** series. W_{m2} is defined in each plot as the weight fraction of comonomer **M2** in each copolymer. Error bars encompass the minimum and maximum values of two independent measurements. *Note:* in some series, the error bars are smaller than the symbol size. Reprinted with permission from Reference [188]. Copyright 2021 The Royal Society of Chemistry.

the potential to introduce π-π stacking interactions. As a result, chain packing in the solid state may be perturbed and experimental T_g values may be observed that deviate from those predicted using the simple Fox equation. As shown in Figure 4.4b, the **P2P5** copolymer series exhibits experimental T_g values that are larger than predicted using the simple Fox equation.

The **P2P6** series combines hexyl and benzyloxymethyl substituents, where the latter introduces a rigid and bulky pendant group, increased linkage flexibility, the potential for π-π stacking, and dipole-dipole interactions. As shown in Figure 4.4c, this series displays negative deviations from the Fox equation. To better estimate the copolymer thermal properties, the Gordon-Taylor equation is used to capture deviations from ideal behavior:[215, 216]

$$T_g = \frac{w_1 T_{g1} + k(1 - w_1) T_{g2}}{w_1 + k(1 - w_1)}$$

The variable *k* is an adjustable fitting parameter. For **P2P5** copolymer series, the trend is well-described with k = 0.5 (Figure 4.4b). Similarly, for **P2P6** copolymer series, an optimized value of k = 2.6 provides qualitative agreement with the experimental trends (Figure 4.4c).

While a broad service window is a requirement for melt processing, this criterion alone does not establish the suitability of a material for melt extrusion or injection molding. To demonstrate that substituted APNBs are indeed melt processable, homopolymer **P2** was selected as a model and compared to commercially available **PS**. As a note, the entanglement molecular weight (M_e) of **P2** is estimated to be 33.1 kg/mol,[217] and thus the samples synthesized herein (M_n = 163 kg/mol) are presumably entangled. As shown in Figure 4.5, polymer **P2** (T_g = 209 °C, T_d = 377 °C) was readily melt processed into bars at 250 °C under a nitrogen atmosphere. The microcompounder in which the melt was formed (for subsequent injection molding) had a force plateau after 10 min of processing, which was used to compare relative melt viscosity of PS and **P2** at low shear rate (90 rpm). In earlier work by Stretz and coworkers,[218] a **PS** (Styron 678 CW) sample reached 689 N

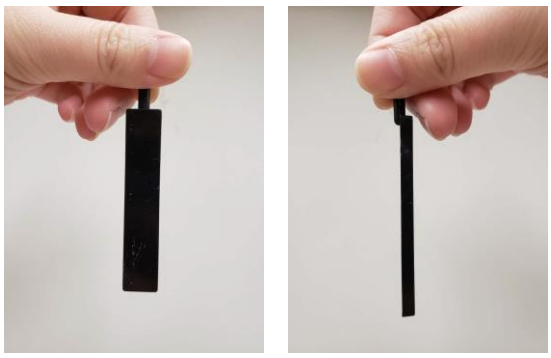


Figure 4.5 Melt extruded bars of APNB P2. The dark color is presumed to be a consequence of residual catalyst decomposition/oxidation that occurs during melt processing. Reprinted with permission from Reference [188]. Copyright 2021 The Royal Society of Chemistry.

of force when processed at 220 °C and 100 rpm; however, the commercial **PS** used in this study reached a force plateau of 1395 (± 12) N (5 replicates) at 210 °C and 90 rpm. This is remarkably similar to APNB **P2**, which reached a force plateau of 1483 (± 32) N (3 replicates) at 250 °C and 90 rpm. This comparison shows that **P2** may be readily processed in similarity to some **PS** samples, needing only slightly elevated melt temperatures (250 °C) that are close to the commercial processing temperatures of many other engineering polymers (e.g., nylon and polycarbonate).

Three additional qualitative processing observations were noted during melt extrusion. First, the extrudate was quite elastic, retracting a bit when cut. Second, the volume of the compounder (controlled by overflow at manufacturer specification of 5 cm^3) was constant, and the average masses of **PS** and **P2** melts were 2.43 g and 1.01 g, respectively. While these masses were recorded at different temperatures, the difference is larger than could be accounted for by temperature alone, suggesting that the **P2** melt is a low-density material. This may be one possible reason for **P2**'s surprisingly high degree of processibility compared to what might be expected for a rigid backbone polymer. Lastly, it was noted that the extruded specimens were dark in color, despite **P2** being colorless prior to processing. We hypothesize that this color results due to residual catalyst decomposition and/or oxidation during processing.[219] As a note, prior studies have shown that residual catalyst can be removed via a variety of methods, though this was not performed in this study.[115, 119, 219]

The mechanical properties of the melt processed, **P2** bar specimens were then evaluated via tensile testing. As shown in Figure 4.6, **P2** is softer (Young's modulus of 1291 MPa vs. 5765 MPa) and less brittle (0.01 mm/mm vs. 0.0025 mm/mm strain at yield) than **PS**. A cyclic loading test was also performed with **P2**, where the cyclic loading modulus is calculated to be 1349 MPa (see support information). While a complete study of substituted APNB mechanical properties is

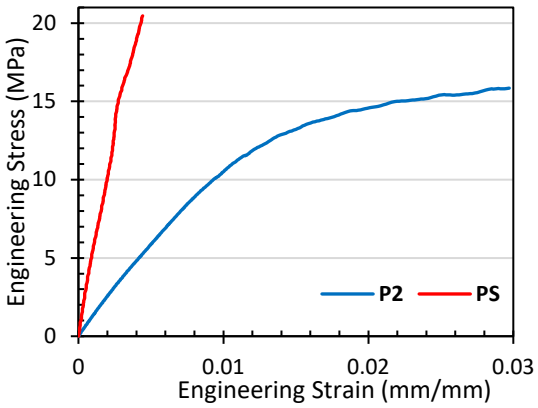


Figure 4.6 . Stress-strain curves for polymers **P2** and **PS**. Reprinted with permission from Reference [188]. Copyright 2021 The Royal Society of Chemistry.

beyond the scope of this paper, these data demonstrate that melt processed APNBs have potential for real-world applications.

To determine the intactness of the processed polymer **P2** after melt extrusion, thorough characterization of **P2** was performed before and after extrusion, including NMR, GPC, and DMA (see Supporting Information). ^{1}H NMR spectroscopy revealed that a minor set of new peaks (~5.3 ppm) were present in the processed material that were not present prior to melting. We hypothesize that these resonances may result due to ring-opening of the bicyclic ring of APNB (around 3% of total, calculated by relative integration) to produce alkene containing polymers analogous to those of polynorbornene synthesized via ring-opening metathesis polymerization. This is supported by a recent report by Boydston and coworkers that demonstrates that many APNBs have intrinsic mechanochemical reactivity, producing partially ring-opened sequences along the main chain of APNBs when they are placed under mechanical activation (e.g. sonication).[220] We suspect that melt extrusion may act as a source of mechanical activation and lead to this conversion.

GPC characterization of melt processed **P2** revealed that molecular weight decreased from M_n = 163 to 117 kg/mol following melt extrusion and exhibited a slightly increased dispersity ($Đ$ = 1.83 vs. 1.60 for the original unprocessed sample). This is consistent with previous reports in which polyolefins, such as polypropylene and polyethylene, undergo thermo-oxidative and/or thermo-mechanical induced chain scission.[221] Additionally, **P2**'s average T_g (from DMA) before and after melt extrusion was 209 °C and 205 °C, respectively. Though this observation is within one standard deviation of experimental results, the decreased T_g value is consistent with ^{1}H NMR spectroscopic analysis showing potential generation of ring-opened sequences along the main chain. Overall, it is concluded that the majority of the APNB **P2** is intact after melt extrusion, but a small portion of the polymer may undergo chain scission due to oxidation and/or mechanical

activation. DMA analysis also revealed that the extruded material's storage modulus (E') (at 100 °C) decreased slightly from E' = 0.49 GPa before melt extrusion to E' = 0.32 GPa after melt extrusion. In contrast, loss modulus (E'') before and after melt extrusion were similar at 0.031 GPa and 0.027 GPa, respectively.

4.5 Conclusions

High molecular weight APNB homopolymers and copolymers bearing alkyl, aryl, and aryl ether functional groups were synthesized using a (η^3 - allyl)Pd(i-Pr$_3$P)Cl/ LiBAr$^F{}_4$ catalyst system. Each polymer's thermal characteristics (T_g, T_d, and service window T_d - T_g) were evaluated using DMA and TGA. The T_g of all synthesized homopolymers and copolymers were depressed relative to that of unfunctionalized APNB (ca. 385 °C). The extent of T_g depression was tuned by the chemical structure of the substituent and was found to follow anticipated trends with substituent size, flexibility, and types of molecular interactions. Notably, the T_g remained at or above 150 °C for most samples, an important attribute for engineering thermoplastics. The T_d of APNBs with alkyl and aryl substituents was approximately 380 °C, which is slightly depressed relative to unfunctionalized APNB (ca. 415 °C), In contrast, the T_d of APNBs with ethereal substituents ranged from approximately 320-340 °C.

A key outcome of these studies is that APNB substituents have a much larger effect on T_g than T_d, so it is possible to broaden the service window from approximately 30 °C for unsubstituted APNB to 200 °C, all while maintaining a sufficiently high T_g to maintain mechanical integrity. To further establish the viability of melt processing, a functionalized APNB with T_g of 209 °C and T_d of 377 °C was melt extruded and molded into bars at 250 °C. The bars were subjected to tensile and DMA tests and then dissolved for characterization by GPC and NMR. These post-extrusion

analyses demonstrate that melt processed APNBs show only minor signs of degradation from processing at high temperatures under flow.

References

3. Finkelshtein, E. S.; Bermeshev, M. V.; Gringolts, M. L.; Starannikova, L.; Yampolskii, Y. P., Substituted polynorbornenes as promising materials for gas separation membranes. *Russian Chemical Reviews* **2011,** *80* (4), 341.
4. Park, K. H.; Twieg, R. J.; Ravikiran, R.; Rhodes, L. F.; Shick, R. A.; Yankelevich, D.; Knoesen, A., Synthesis and nonlinear-optical properties of vinyl-addition poly (norbornene) s. *Macromolecules* **2004,** *37* (14), 5163-5178.
5. Grove, N. R.; Kohl, P. A.; Bidstrup Allen, S. A.; Jayaraman, S.; Shick, R., Functionalized polynorbornene dielectric polymers: adhesion and mechanical properties. *J. Polym. Sci. B Polym. Phys.* **1999,** *37* (21), 3003-3010.
6. Chen, M.; Zou, W.; Cai, Z.; Chen, C., Norbornene homopolymerization and copolymerization with ethylene by phosphine-sulfonate nickel catalysts. *Polymer Chemistry* **2015,** *6* (14), 2669-2676.
7. Bai, Y.; Chiniwalla, P.; Elce, E.; Shick, R. A.; Sperk, J.; Allen, S. A. B.; Kohl, P. A., Photosensitive polynorbornene based dielectric. I. Structure–property relationships. *Journal of Applied Polymer Science* **2004,** *91* (5), 3023-3030.
8. Goodall, B. Addition polymers derived from norbornene-functional monomers and process therfor. 95/14048, 1995.
10. Dorkenoo, K. D.; Pfromm, P. H.; Rezac, M. E., Gas transport properties of a series of high Tg polynorbornenes with aliphatic pendant groups. *J. Polym. Sci. B Polym. Phys.* **1998,** *36* (5), 797-803.
11. Gmernicki, K. R.; Hong, E.; Maroon, C. R.; Mahurin, S. M.; Sokolov, A. P.; Saito, T.; Long, B. K., Accessing siloxane functionalized polynorbornenes via vinyl-addition polymerization for CO2 separation membranes. *ACS Macro Lett.* **2016,** *5* (7), 879-883.
12. Maroon, C. R.; Townsend, J.; Gmernicki, K. R.; Harrigan, D. J.; Sundell, B. J.; Lawrence III, J. A.; Mahurin, S. M.; Vogiatzis, K. D.; Long, B. K., Elimination of CO2/N2 Langmuir Sorption and Promotion of "N2-Phobicity" within High-T g Glassy Membranes. *Macromolecules* **2019,** *52* (4), 1589-1600.
13. Kim, D.-G.; Takigawa, T.; Kashino, T.; Burtovyy, O.; Bell, A.; Register, R. A., Hydroxyhexafluoroisopropylnorbornene block and random copolymers via vinyl addition polymerization and their application as biobutanol pervaporation membranes. *Chemistry of Materials* **2015,** *27* (19), 6791-6801.
14. Liu, S.; Chen, Y.; He, X.; Chen, L.; Zhou, W., Stable crosslinked vinyl-addition-type polynorbornene graft copolymer proton-exchange membranes. *Journal of Applied Polymer Science* **2011,** *121* (2), 1166-1175.
15. Mandal, M.; Huang, G.; Kohl, P. A., Anionic multiblock copolymer membrane based on vinyl addition polymerization of norbornenes: Applications in anion-exchange membrane fuel cells. *Journal of membrane science* **2019,** *570*, 394-402.
16. Mulpuri, S. V.; Shin, J.; Shin, B.-G.; Greiner, A.; Yoon, D. Y., Synthesis and characterization of substituted polynorbornene derivatives. *Polymer* **2011,** *52* (19), 4377-4386.
18. Hennis, A. D.; Polley, J. D.; Long, G. S.; Sen, A.; Yandulov, D.; Lipian, J.; Benedikt, G. M.; Rhodes, L. F.; Huffman, J., Novel, efficient, palladium-based system for the polymerization of norbornene derivatives: scope and mechanism. *Organometallics* **2001,** *20* (13), 2802-2812.

35. Lipian, J.; Mimna, R. A.; Fondran, J. C.; Yandulov, D.; Shick, R. A.; Goodall, B. L.; Rhodes, L. F.; Huffman, J. C., Addition polymerization of norbornene-type monomers. High activity cationic allyl palladium catalysts. *Macromolecules* **2002,** *35* (24), 8969-8977.
39. Tsai, S. D.; Register, R. A., Endo/Exo Reactivity Ratios in Living Vinyl Addition Polymerization of Substituted Norbornenes. *Macromolecular Chemistry and Physics* **2018,** *219* (11), 1800059.
110. McDougall, W.; Farling, S.; Shick, R.; Glukh, S.; Jayaraman, S.; Rhodes, L.; Vicari, R.; Kohl, P.; Bidstrup-Allen, S.; Chiniwalla, P., Avatrel™ dielectric polymers for HDP applications. Proc. International Conference and Exhibition on High-Density Interconnect and Systems Packaging: Denver, CO, USA, 1999; pp 1-4.
111. Goodall, B.; Barnes, D., Novel heat resistant cyclic olefin polymers made using single component nickel and palladium catalysts: Synthesis and applications. *Polymer Preprints(USA)* **1998,** *39* (1), 216-217.
112. Goodall, B.; Benedikt, G.; McIntosh III, L.; Barnes, D.; Rhodes, L. Process for making polymers containing a norbornene repeating unit by addition polymerization using an organo (nickel or palladium) complex. 5468819, 1995.
113. Goodall, B.; Risse, W.; Mathew, J. Addition polymers of polycycloolefins containing functional substituents. 5705503, 1998.
115. Kim, E. C.; Kim, M.-J.; Thi Ho, L. N.; Lee, W.; Ka, J.-W.; Kim, D.-G.; Shin, T. J.; Huh, K. M.; Park, S.; Kim, Y. S., Synthesis of Vinyl-Addition Polynorbornene Copolymers Bearing Pendant n-Alkyl Chains and Systematic Investigation of Their Properties. *Macromolecules* **2021**.
116. Goodall, B. L., Cycloaliphatic polymers via late transition metal catalysis. In *Late transition metal polymerization catalysis*, Bernhard Rieger, L. S. B., Smita Kacker, Susanne Striegler, Ed. WILEY-VCH Verlag GmbH & Co. KGaA: Weinheim, 2003; pp 101-154.
117. Shin, B.-G.; Cho, T.-Y.; Yoon, D. Y.; Liu, B., Structure and Properties of Polynorbornene Derivatives: Poly (norbornene dicarboxylic acid dialkyl ester) s and Poly (norbornene dimethyl dicarboxylate) s. *Macromolecular research* **2007,** *15* (2), 185-190.
118. Breunig, S.; Risse, W., Transition-metal-catalyzed vinyl addition polymerizations of norbornene derivatives with ester groups. *Die Makromolekulare Chemie: Macromolecular Chemistry and Physics* **1992,** *193* (11), 2915-2927.
119. Kim, D.-G.; Bell, A.; Register, R. A., Living Vinyl Addition Polymerization of Substituted Norbornenes by at-Bu3P-Ligated Methylpalladium Complex. *ACS Macro Lett.* **2015,** *4* (3), 327-330.
188. Wang, X.; Jeong, Y. L.; Love, C.; Stretz, H. A.; Stein, G. E.; Long, B. K., Design, synthesis, and characterization of vinyl-addition polynorbornenes with tunable thermal properties. *Polymer Chemistry* **2021,** *12* (40), 5831-5841.
190. Zhou, W.; He, X.; Chen, Y.; Chen, M.; Shi, L.; Wu, Q., Vinyl-addition copolymerization of norbornene and polar norbornene derivatives using novel bis (β-ketoamino) Ni (II)/B (C6F5) 3/AlEt3 catalytic systems. *Journal of applied polymer science* **2011,** *120* (4), 2008-2016.
191. Kuo, A. C., *Polymer data handbook*. Oxford University Press, Inc: 1999.
192. Stober, E. J.; Seferis, J. C., Fluid sorption characterization of PEEK matrices and composites. *Polymer Engineering & Science* **1988,** *28* (9), 634-639.
193. Molnár, G.; Botvay, A.; Pöppl, L.; Torkos, K.; Borossay, J.; Máthé, Á.; Török, T., Thermal degradation of chemically modified polysulfones. *Polymer degradation and stability* **2005,** *89* (3), 410-417.

194. Lisa, G.; Avram, E.; Paduraru, G.; Irimia, M.; Hurduc, N.; Aelenei, N., Thermal behaviour of polystyrene, polysulfone and their substituted derivatives. *Polymer degradation and stability* **2003,** *82* (1), 73-79.
195. Perng, L., Thermal degradation mechanism of poly (ether imide) by stepwise Py–GC/MS. *Journal of applied polymer science* **2001,** *79* (7), 1151-1161.
196. Alaboodi, A. S.; Sivasankaran, S., Experimental design and investigation on the mechanical behavior of novel 3D printed biocompatibility polycarbonate scaffolds for medical applications. *Journal of Manufacturing Processes* **2018,** *35*, 479-491.
197. Deng, G.; Hayakawa, S.; Rhodes, L. F. UV ACTIVE DERIVATIVES OF Pd (AcAc) 2 CATALYZED POLYCYCLOOLEFIN COMPOSITIONS AS OPTICAL MATERIALS. 20210198392, 2021.
198. Abu-Surrah, A. S.; Thewalt, U.; Rieger, B., Chiral palladium (II) complexes bearing tetradentate nitrogen ligands: synthesis, crystal structure and reactivity towards the polymerization of norbornene. *Journal of organometallic chemistry* **1999,** *587* (1), 58-66.
199. Lewis, E. A.; Vogt, B. D., Thickness dependence of structural relaxation in spin-cast polynorbornene films with high glass transition temperatures (> 613 K). *Journal of Polymer Science Part B: Polymer Physics* **2018,** *56* (1), 53-61.
200. Leber, P.; Kidder, K.; Viray, D.; Dietrich-Peterson, E.; Fang, Y.; Davis, A., Stereoselectivity in a series of 7-alkylbicyclo [3.2. 0] hept-2-enes: Experimental and computational perspectives. *Journal of Physical Organic Chemistry* **2018,** *31* (12), e3888.
201. Koch, H.; Haaf, W., Carbonsäuresynthese in der Bicycloheptan-und Tricyclodecan-Reihe. *Justus Liebigs Annalen der Chemie* **1960,** *638* (1), 111-121.
202. Jean, M.; Van de Weghe, P., Gold-catalyzed intramolecular hydroarylation of olefins. Scope evaluation and preliminary mechanistic studies. *Tetrahedron letters* **2011,** *52* (27), 3509-3513.
203. Blanco, J. M.; Fernández, F.; García-Mera, X.; Rodríguez-Borges, J. E., Divergent synthesis of two precursors of 3′-homo-2′-deoxy-and 2′-homo-3′-deoxy-carbocyclic nucleosides. *Tetrahedron* **2002,** *58* (43), 8843-8849.
204. Kim, S. H.; Worsley, M. A.; Valdez, C. A.; Shin, S. J.; Dawedeit, C.; Braun, T.; Baumann, T. F.; Letts, S. A.; Kucheyev, S. O.; Wu, K. J. J., Exploration of the versatility of ring opening metathesis polymerization: an approach for gaining access to low density polymeric aerogels. *Rsc Advances* **2012,** *2* (23), 8672-8680.
205. Driver, T. G.; Franz, A. K.; Woerpel, K., Diastereoselective silacyclopropanations of functionalized chiral alkenes. *Journal of the American Chemical Society* **2002,** *124* (23), 6524-6525.
206. Müller, K.; Chun, S.-H.; Greiner, A.; Agarwal, S., 2D NMR characterisation of 5-norbornene-2-nonaneacidethylester and 5-norbornene-2-hexane. *Designed monomers and polymers* **2005,** *8* (3), 237-248.
207. Richard, A., Interface and surface effects on the glass-transition temperature in thin polymer films. *Faraday Discussions* **1994,** *98*, 219-230.
208. Barnes, D. A.; Benedikt, G. M.; Goodall, B. L.; Huang, S. S.; Kalamarides, H. A.; Lenhard, S.; McIntosh, L. H.; Selvy, K. T.; Shick, R. A.; Rhodes, L. F., Addition Polymerization of Norbornene-Type Monomers Using Neutral Nickel Complexes Containing Fluorinated Aryl Ligands. *Macromolecules* **2003,** *36* (8), 2623-2632.
209. Alentiev, D. A.; Bermeshev, M. V.; Starannikova, L. E.; Bermesheva, E. V.; Shantarovich, V. P.; Bekeshev, V. G.; Yampolskii, Y. P.; Finkelshtein, E. S., Stereoselective

synthesis and polymerization of Exo-5-trimethylsilylnorbornene. *Journal of Polymer Science Part A: Polymer Chemistry* **2018,** *56* (12), 1234-1248.
210. García-Loma, R.; Albéniz, A. C., Vinylic Addition Polynorbornene in Catalysis. *Asian Journal of Organic Chemistry* **2019,** *8* (3), 304-315.
211. Kim, S.; Hewlett, S.; Roth, C.; Torkelson, J. M., Confinement effects on glass transition temperature, transition breadth, and expansivity: Comparison of ellipsometry and fluorescence measurements on polystyrene films. *The European Physical Journal E* **2009,** *30* (1), 83.
212. Gill, P.; Sauerbrunn, S.; Reading, M., Modulated differential scanning calorimetry. *Journal of Thermal Analysis* **1993,** *40* (3), 931-939.
213. Odian, G., *Principles of polymerization*. John Wiley & Sons: 2004.
214. Patel, P.; Hull, T. R.; McCabe, R. W.; Flath, D.; Grasmeder, J.; Percy, M., Mechanism of thermal decomposition of poly (ether ether ketone)(PEEK) from a review of decomposition studies. *Polymer Degradation and Stability* **2010,** *95* (5), 709-718.
215. Penzel, E.; Rieger, J.; Schneider, H., The glass transition temperature of random copolymers: 1. Experimental data and the Gordon-Taylor equation. *Polymer* **1997,** *38* (2), 325-337.
216. Gordon, M.; Taylor, J. S., Ideal copolymers and the second-order transitions of synthetic rubbers. I. Non-crystalline copolymers. *Journal of Applied Chemistry* **1952,** *2* (9), 493-500.
217. Müller, K.; Kreiling, S.; Dehnicke, K.; Allgaier, J.; Richter, D.; Fetters, L. J.; Jung, Y.; Yoon, D. Y.; Greiner, A., Synthesis and Rheological Properties of Poly (5-n-hexylnorbornene). *Macromolecular chemistry and physics* **2006,** *207* (2), 193-200.
218. Stretz, H.; Paul, D., Properties and morphology of nanocomposites based on styrenic polymers, Part II: Effects of maleic anhydride units. *Polymer* **2006,** *47* (26), 8527-8535.
219. Rhodes, L. F.; Vicari, R.; Langsdorf, L. J.; Sobek, A. A.; Boyd, E. P.; Bennett, B. Polymeric compositions and uses therefor. 2003050158A1, 2003.
220. Lee, D. C.; Kensy, V. K.; Maroon, C. R.; Long, B. K.; Boydston, A. J., The Intrinsic Mechanochemical Reactivity of Vinyl-Addition Polynorbornene. *Angewandte Chemie* **2019,** *131* (17), 5695-5698.
221. Hinsken, H.; Moss, S.; Pauquet, J.-R.; Zweifel, H., Degradation of polyolefins during melt processing. *Polymer degradation and stability* **1991,** *34* (1-3), 279-293.

Chapter 5 Conclusion and Future Work

In summary, this work provided the membrane and chemistry communities with a deep insight into the structure-property relationship of polynorbornenes utilized as gas separation membranes, as well as expanding their potential processing methods.

Previous studies revealed that some of our APNBs designed for CO_2/N_2 separation also showed promising performance for H_2S/CH_4 separations whilst maintaining fair CO_2/CH_4 performance. To improve their CO_2/CH_4 separation performance and expand their application towards natural gas sweetening, fluorinated motifs were incorporated into the polymers inspired by the fact that many fluorinated materials exhibited "hydrocarbon-phobicity". In Chapter 2, it was validated that the CO_2/CH_4 separation performance was improved without much sacrifice in CO_2 permeability by incorporating fluorinated motifs; however, detailed mechanism studies, including sorption and simulation experiments, revealed that this enhanced selectivity arose from increased CO_2 solubility rather than depressed CH_4 solubility. This observation provided the membrane communities with an alternative way to explain the CO_2/CH_4 separation performance of fluorinated polymers.

In addition to polymer chemical structures, the membrane separation performance is also related to how the polymer chains physically pack. In Chapter 3, initial efforts to construct microphase-separated MPNB block copolymer were discussed. Though some microphase separations were observed by SAXS in currently obtained block copolymer membranes, it was limited to presumably lamellae structures, and the surface of the membranes had an uneven, bubble-like pattern. Further studies will be focused on optimizing the process conditions and constructing different microphase separation patterns by tuning the block copolymer compositions, as well as comparing their performance with corresponding random copolymers. Polymer tacticity may also influence how the polymer chains physically pack. In Appendix A, the

catalyst effects on the backbone tacticity of APNBs were investigated. Several *exo*-disubstituted norbornene monomers were synthesized, while only *exo*-dimethyl norbornene exhibited reasonable polymerization activities with both *trans*-Ni(C_6F_5)$_2$($SbPh_3$)$_2$ catalyst and MePdP(*i*-Pr)$_3$Cl/LiBArF catalyst system. The polymer obtained by *trans*-Ni(C_6F_5)$_2$($SbPh_3$)$_2$ catalyst had limited solubility in common organic solvents. In contrast, the polymer obtained by MePdP(*i*-Pr)$_3$Cl/LiBArF catalyst system was easily soluble in solvents such as chloroform and toluene. The solubility difference and following HSQC experiment all suggested that the polymer obtained by *trans*-Ni(C_6F_5)$_2$($SbPh_3$)$_2$ catalyst had a more regular backbone tacticity than that obtained by MePdP(*i*-Pr)$_3$Cl/LiBArF catalyst system.

During these studies, we realized that one drawback that limits APNBs from achieving more industrial-related attention is their finite processing method (only solvent casting/coating). These polymers usually have small service windows (high glass transition temperatures that are close to their decomposition temperatures), which limits their melt-processibility. In Chapter 4, by introducing various substituents, the APNB glass transition temperatures were depressed while their decomposition temperatures were mostly maintained. These enlarged service windows made them more amenable to melt processing conditions, and APNB with hexyl substituent was melt-extruded into bars as an example. Following post-extrusion characterizations only showed minor signs of degradation, suggesting the successful design of these types of materials.

Ultimately, both fundamental and applied science has been produced in this work. The application of APNB membranes was expanded from CO_2/N_2 to CO_2/CH_4 separation; the processing method of a group of APNB was expanded to melt-processing; and microphase-separated block copolymers for gas separation were synthesized. Future work will be focused on

optimizing processing conditions and characterizing the block copolymer gas separation membranes.

Appendices

Appendix A Influence of Addition Polynorbornene Backbone Tacticity on Polymer Properties

Introduction

Polymer physical properties, such as solubility in common organic solvents, as well as thermal and mechanical properties, can be greatly influenced by the physical arrangement of the repeat units along the polymer chain backbone.[222] For a linear polymer chain, tacticity and connectivity are of critical importance. Tacticity refers to the arrangement of adjacent chiral centers within a macromolecule.[223] Depending on the arrangement of subsequent substituents, isotactic polymers are those in which the substituents at each chiral center have the same arrangement along the entire polymer chain. In contrast, syndiotactic polymers are those in which the substituents are placed in an alternating stereochemical configuration along the polymer chain. Lastly, atactic polymers are those in which the substituents are incorporated with random orientation along the polymer chain.[224] The simplest example of the influence that tacticity has on polymer properties is in the case of polypropylene (PP). Isotactic PP is a strong, crystalline polymer with a high melting temperature (T_m) of 165 °C, and is usually applied as a plastic and fiber. Whereas atactic PP is an amorphous polymer with an oily to waxy appearance, and is usually used in asphalt blends and adhesives formulations. Syndiotactic PP received less attention until recently, but it is also a crystalline polymer with a T_m about 20 °C lower than that of isotactic PP, and is more soluble in some organic solvents.[213]

Connectivity of subsequent repeating units within a chain-growth polymer is often described by their incorporation of “head-to-tail,” “head-to-head,” and “tail-to-tail” configurations. In a polymer chain formed via the polymerization of alkene or alkyne monomers, the double- or triple-

bonded carbon with a higher priority substituent is defined as the head, while the other carbon is defined as a tail.[224] Due to steric effects, repeat units generally tend to polymerize in a head-to-tail configuration; however, a head-to-head or a tail-to-tail configuration is also possible. Similar to tacticity, this head-tail configuration also influences the polymer's properties. For example, poly(3-(*n*-hexyl)thiophene) (P3HT) can be synthesized with all three configurations, but only the head-to-tail configuration shows high crystallinity due to the even placement of substituents along the polymer backbone.[224]

The aforementioned configurations are all strongly dependent on the monomers and catalysts used in a given polymerization. However, in reality, some small percentage of defects can often be found in a polymer chain, including some degree of mixing of different tacticities, and/or mixing of head-tail configurations, unless a polymerization catalyst is specially designed to prevent such errors. Thus, even in cases where the repeat units of two polymers are the same, the polymers obtained from the use of different catalysts may have diverse thermal and mechanical properties and may be useful for differing applications.

As discussed in Section 1.5.2, Addition polynorbornenes (APNBs) may possess different backbone configurations (2,3-threo disyndiotactic backbone configuration or 2,3-erythrodiisotactic backbone configuration).[105, 106] Though in previous literature reports have aimed to study the influence that vinyl addition polymerization catalyst choice has on polymer tacticity, those studies often employed monomers lacking substituents and whose solubility is dramatically limited,[107, 108] or they used monomers bearing substituents, but in which substituent tacticity and steric effects could not be completely ruled out.[109] Thus, the isolated catalyst effect on the backbone tacticity of APNBs, and their corresponding polymer properties, have not been fully explored.

To improve APNB solubility and eliminate the effects of substituent stereochemical configurations, herein, we have designed *exo*-disubstituted norbornene monomers. More specifically, we targeted monomers bearing identical substituents in both the 5- and 6-positions to eliminate any substituent steric effects. Additionally, we targeted *exo*-substituted monomers exclusively as *endo*-isomers are known to polymerize slower than their analogous *exo*-isomers due to the steric effects and potential chelation to the active metal center if a functional group is present.[16-20] The obtained monomers will then be polymerized using either a Ni- or Pd-based catalyst, and the resultant polymers will be characterized by ^{1}H NMR spectroscopy, rheology, and compared to results obtained via molecular dynamics simulations. To minimize the simulation complexity, functional groups such as carbonyl groups and phenyl groups were avoided intentionally.

Experimental Section

Synthesis of *cis*-5-norbornene-*exo*-2,3-dicarboxylic anhydride. The compound was obtained via a thermal isomerization of the *endo*-carbic anhydride (52 g, 316.8 mmol) at 180 ℃ for 4–5 h following a previous report.[16] The crude was recrystallized 5-6 times to isolate 10.4 g of the *exo*-isomer (≥98% purity, 20% yield). All characterizations matched prior literature reports.[16]

Synthesis of *exo*-5,6-bis(hydroxymethyl)-2-norbornene (HOMeNB). The compound was synthesized following a previous report with slight modifications.[16] $LiAlH_4$ (5.4 g, 141 mmol) was added slowly to dry THF at 0 ℃ under N_2. *cis*-5-Norbornene-*exo*-2,3-dicarboxylic anhydride (11.0 g, 67 mmol) solution in dry THF was added slowly to $LiAlH_4$ solution under N_2. After complete addition, the reaction mixture was gradually warmed to room temperature and stirred for an additional 16 h. The reaction mixture was cooled in an ice bath and cold distilled water was added

dropwise to quench the reaction until no bubble was observed and the mixture turned into an off-white color. The suspension was settled for an hour to allow easier filtration of the solids. After rinsing the solids with THF, the combined filtrates were roto-evaporated to remove THF, and the obtained compound was extracted with DCM/water, and dried over $MgSO_4$. The DCM was then removed under reduced pressure to yield 9.1 g of the title compound (89% yield). All characterizations matched prior literature reports.[16]

Synthesis of *exo*-5,6-bis(methoxymethyl)-2-norbornene (MeOMeNB). The compound was synthesized following a previous report[225] at a smaller scale (0.47 g NaH, 19.5 mmol), except that the reaction mixture was stirred for 2 h after the complete addition of the *exo*-5,6-bis(hydroxymethyl)-2-norbornene (1 g, 6.5 mmol), and was stirred for 16 h after complete addition of CH_3I (2.76 g, 19.5 mmol) in an ice bath. THF was removed after quenching the reaction dropwise with DI water in an ice bath, and the mixture was extracted with EtOAc/water, the organic phase was dried and columned with 2% EtOAc/hexane to isolate 0.5 g of the title compound (42% yield). All characterizations matched prior literature reports.[226]

Synthesis of *exo*-5,6-bismesylate-2-norbornene (MsOMeNB). The compound was synthesized following a previous report[227] (80% yield). ^{1}H NMR ($CDCl_3$): δ = 6.23 (s, 2H), 4.38 (m, 2H), 4.21 (m, 2H), 3.08 (s, 6H), 2.85 (s, 2H), 2.03 (s, 2H), 1.47 (m, 2H). ^{13}C NMR ($CDCl_3$): δ = 137.6, 70.6, 45.0, 43.1, 40.7, 37.7.

Synthesis of *exo*-5,6-bis(bromomethyl)-2-norbornene (BrMeNB). The compound was synthesized following a previous report[228] and purified by chromatography with 100% hexane (78% yield). ^{1}H NMR ($CDCl_3$): δ = 6.21 (s, 2H), 3.72 (m, 2H), 3.26 (m, 2H), 2.99 (s, 2H), 2.06 (m, 2H), 1.41 (m, 2H). ^{13}C NMR ($CDCl_3$): δ = 137.7, 47.5, 45.7, 42.5, 34.7.

Synthesis of *exo*-5,6-dimethyl-2-norbornene (MeNB). The compound was synthesized following a previous report with slightly modification.[229, 230] In a 1 L 3-neck flask with a condenser were placed LiH (5.1484 g, 647.6 mmol), LAH (24.5762 g, 647.6 mmol) and 400 mL dry THF. The mixture was heated to reflux under a N_2 balloon protection, and *exo*-5,6-bismesylate-2-norbornene (67.0 g, 215.9 mmol) slurry solution (300 mL THF) was slowly added via cannula transfer while stirring, note that lots of bubbles were formed during this time. After complete addition, the mixture was refluxed for an additional 30 h. After cooled to room temperature, the reaction mixture was placed in an ice bath and quenched with DI water and then a stochiometric balance of 12M HCl solution (270 mL, 3.2 mol). The slurry was distilled under N_2 at atmosphere pressure to remove most of the THF, filtered to remove residual salt, and then extracted with hexane/water for three times. The combined organic layer was collected, dried over $MgSO_4$, distilled to remove excess hexane, and the crude product was collected at 87–90 ℃ under 60 torr. The crude product was then purified by a pentane column, where excess pentane was then removed via atmosphere distillation under N_2, to yield 8.6 g of the product (32% yield). ^{1}H NMR ($CDCl_3$): δ = 6.11 (s, 2H), 2.38 (s, 2H), 1.54 (s, 2H), 1.52 (s, 1H), 1.26 (d, 1H), 0.98 (d, 6H). ^{13}C NMR ($CDCl_3$): δ = 137.3, 49.9, 42.1, 34.8, 16.9.

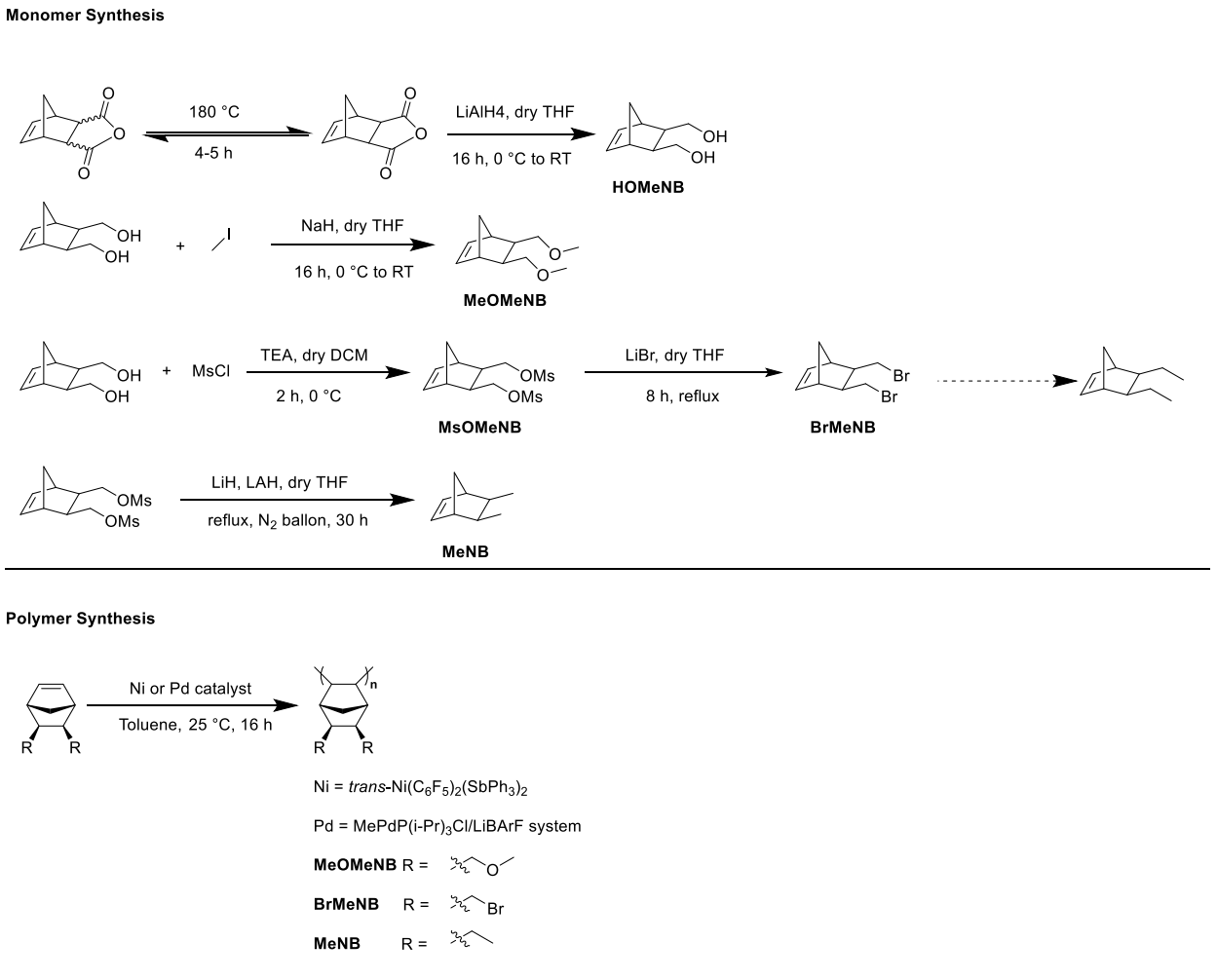
General polymerization of *exo*-disubstituted norbornene monomers. Vinyl-addition polymerizations with *exo*-disubstituted norbornene monomers were conducted with selected Ni- and Pd- catalyst, *trans*-$Ni(C_6F_5)_2(SbPh_3)_2$ and $MePdP(i\text{-}Pr)_3Cl$/LiBArF. All polymerization was conducted in a glove box. As an example, *exo*-5,6-dimethyl-2-norbornene (0.2 g, 1.63 mmol) was dissolved in 4.5 mL of toluene, which was then added with 1 mL of *trans*-$Ni(C_6F_5)_2(SbPh_3)_2$ catalyst solution (0.0017 g, 1.63×10^{-3} mmol, total monomer concentration of 4wt% in toluene). The polymerization was run for 16 h, concentrated, and stopped by precipitation in to MeOH. The

polymerization with MePdP(*i*-Pr)$_3$Cl/LiBArF was conducted following the similar procedures, except the catalyst MePdP(*i*-Pr)$_3$Cl was activated with LiBArF for 20 min before adding into the monomer solution.

Preliminary Results and Discussion

Monomer Synthesis. As shown in Scheme A.1, various *exo*-disubstituted norbornene monomer syntheses were attempted, with **MeOMeNB**, **BrMeNB** and **MeNB** being successfully synthesized and characterized. In general, **HOMeNB** was first synthesized by thermal isomerization *endo*-carbic anhydride to obtain the *cis*-5-norbornene-*exo*-2,3-dicarboxylic anhydride (20% yield), followed by $LiAlH_4$ reduction (89% yield). The **MeOMeNB** monomer was then synthesized by substituting the **HOMeNB** with methyl iodide (42% yield). Initial attempts to synthesize **BrMeNB** from a simple bromination step from **HOMeNB** with CBr_4/PPh_3 system[231] were unsuccessful with an isolated product yield inconsistently ranging from 10%–40%. Instead, the major product was a 5-membered cyclic ether, probably due to the faster kinetics of forming the stable 5-membered ring structure. Alternatively, **BrMeNB** was synthesized by a two-step route that first mesylated **HOMeNB** to obtain **MsOMeNB** (80% yield), followed by LiBr substitution (78% yield). It was worth noting that, following similar reaction conditions to generate bistosylate compound was unsuccessful, with an isolated product yield less than 10%. It was hypothesized that the tosylate groups introduce a stronger steric effect which restricted the reaction. Unfortunately, attempts to synthesize *exo*-5,6-dialkyl-2-norbornene with longer alkyl substituents (C_2+) from **BrMeNB** with either corresponding Grignard reaction (with alkyl-MgCl) or lithium-halogen exchange (with n-butyl lithium) followed by addition of a proton source were not successful, with either a low conversion (0–5%) or forming cyclic ether byproduct. Finally,

MeNB was synthesized by reducing **MsOMeNB** with LiH and LAH under N_2 ballon protection (32% yield). It was worth noting that a static, inert atmosphere was applied due to the low boiling point of the product, and starting material slurry needs to be added after refluxing the LiH/LAH THF slurry. In addition, the monomer should be stored in the glove box without molecular sieves, as unknown reactions (gel-forming) were observed while sitting over molecular sieves for two days.



Scheme A.1 Synthetic routes of various *exo*-disubstituted norbornene monomer and corresponding polymers.

Selected polymerization observations. Initial polymerizations were carried out with obtained norbornene monomers **BrMeNB**, **MeOMeNB**, or **MeNB**, as the conditions and observations were summarized in Table A.1. Overall, the **MeNB** polymerizations have the most promising results, while **MeOMeNB** and **BrMeNB** polymerizations were unsuccessful. In detail, **MeOMeNB** under general polymerization conditions with either catalyst did not yield any polymer (Table A.1, entry 1-2). Attempts with increasing monomer concentration were also not successful (data not shown). Similarly, **BrMeNB** polymerization with both catalysts yielded limited polymer. It was noted that the polymer obtained by *trans*-$Ni(C_6F_5)_2(SbPh_3)_2$ catalyst seemed to have limited solubility in toluene (Table A.1, entry 3), as the solution turned cloudy immediately after the addition of the catalyst solution. Thus, another attempt polymerization with THF was also conducted. Though the solution was clear throughout the reaction time, the overall yield was not improved. In contrast, polymerizations with **MeNB** yield nice polymer strips when precipitated into MeOH, suggesting that high molecular weight polymers were obtained (Table A.1, entry 6-7). However, with *trans*-$Ni(C_6F_5)_2(SbPh_3)_2$ catalyst, the solution turned into a "gel-like" form during the polymerization within 30 min of catalyst solution addition, and the obtained polymer has limited solubility in common organic solvents, including toluene, benzene, anisole, chlorobenzene, 1,2,4-tricholorobenzene, chloroform, dichloromethane, diethyl ether, tetrahydrofuran, hexane, *N*, *N*-dimethylformamide, and *N*, *N*-dimethylacetamide. On the other hand, the polymerization with MePdP(*i*-Pr)$_3$Cl/LiBArF system stay clear, and the obtained polymer has good solubility in solvents such as THF, $CHCl_3$, and toluene. This observation is also similar to that of the polymerization with **BrMeNB**. The solubility difference could be an indication of different polymer tacticity, suggesting that the polymer backbone obtained by *trans*-$Ni(C_6F_5)_2(SbPh_3)_2$ catalyst is more regular than that obtained by MePdP(*i*-Pr)$_3$Cl/LiBArF system.

Table A.1 Selected Polymerization Conditions and Observations[a]

Entry	Monomer	Catalyst	Work-up Observations
1	MeOMeNB	Ni	no polymer precipitate
2	MeOMeNB	Pd	no polymer precipitate
3[b]	BrMeNB	Ni	fine powder, not recoverable precipitate[e]
4[c]	BrMeNB	Ni	fine powder, not recoverable precipitate
5[b]	BrMeNB	Pd	fine powder, not recoverable precipitate
6	MeNB	Ni	polymer strips[f]
7	MeNB	Pd	polymer strips
8[d]	MeNB	Ni	polymer powder, 61% yield
9[d]	MeNB	Pd	polymer powder, 49% yield

[a]General polymerization conditions: [M] =4wt% in toluene, [M]:[C]=1000:1, T = 20 °C, and t = 16 h. Ni and Pd represents *trans*-Ni(C_6F_5)$_2$($SbPh_3$)$_2$ and MePdP(i-Pr)$_3$Cl/LiBArF system, respectively. Solution was clear during the polymerization unless otherwise noted, and the polymerizations were terminated by precipitated into MeOH. [b]Polymerization was run at a monomer concentration of 1M in toluene. [c]Polymerization was run at a monomer concentration of 1M in THF. [d]polymerization was run at 4wt% in chloroform and with a [M]:[C] = 100:1. [e]Polymerization turned cloudy immediately after catalyst solution addition. [f]After catalyst solution addition, the polymerization turned into "gel-like" form within 30 min.

This is similar to previous reports that Ni- and Pd-based catalysts could potentially introduce different backbone tacticity, which resulted in different solubility, though in their system, it was the Pd-based catalyst that resulted in a polymer with limited solubility.[107, 108] After optimizing the conditions, the **MeNB** was then polymerized with both catalysts at 4wt% in chloroform with a monomer:catalyst loading of 100:1 to lower their molecular weight and thus improve their solubility in organic solvents, and the purified polymers were dissolved in $CDCl_3$ for NMR studies.

HSQC NMR study. The aforementioned **MeNB** polymers were characterized by ^1H NMR and HSQC NMR. As shown in Figure A.1, the different signals in the highlighted area (especially ~1.3 ppm in ^1H spectra, which represent CH_2 signals of the bridge) suggested that the polymer obtained with *trans*-$Ni(C_6F_5)_2(SbPh_3)_2$ is more regular than that obtained with $MePdP(i\text{-}Pr)_3Cl$/LiBArF system, as the corresponding ^{13}C signals were more centralized. For polymer obtained with Ni catalyst, there was only one ^{13}C signal around 29 ppm. Whereas the two ^{13}C signals for polymer obtained with Pd catalyst were around 28 ppm and 32 ppm, suggesting that the bridge carbons could be in different stereo environments.

Simulation and rheology studies. These studies will be collaborated with Dr. Doxastakis and Dr. Stein group, to understand how theoretically different catalysts will interact with the monomer, as well as their impacts on the polymer backbone tacticity and the physical properties of corresponding polymers.

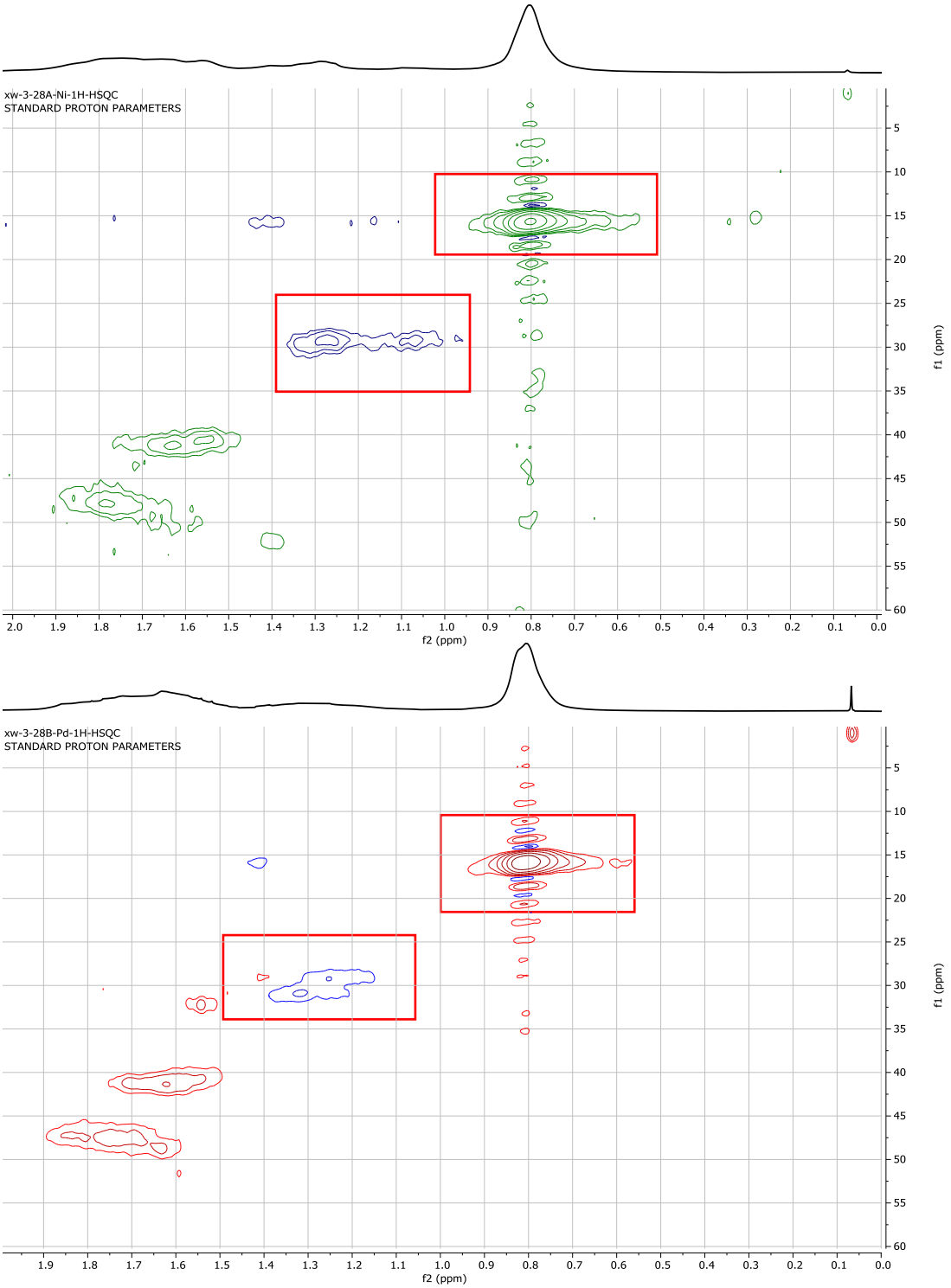


Figure A.1 HSQC NMR study of polymer obtained by *trans*-Ni(C_6F_5)$_2$($SbPh_3$)$_2$ catalyst (top) and MePdP(*i*-Pr)$_3$Cl/LiBArF catalyst system (bottom). The polymer obtained by Pd catalyst have more dispersed CH_2 signal than that obtained by Ni catalyst, suggesting that the former polymer may have more irregular back bone structure.

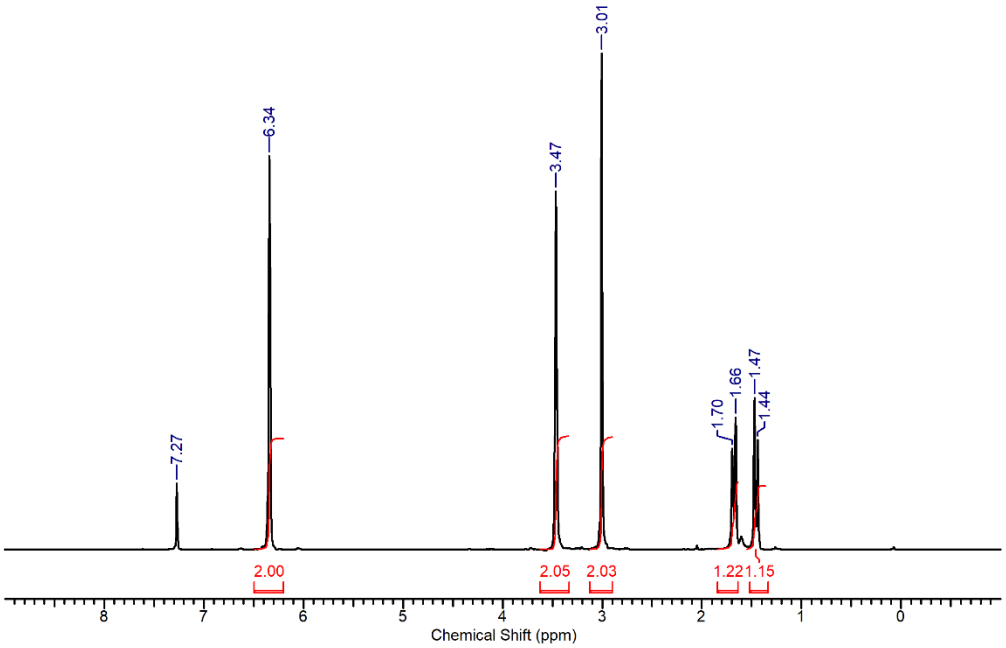


Figure A.2 ^{1}H NMR spectrum of *cis*-5-norbornene-*exo*-2,3-dicarboxylic anhydride

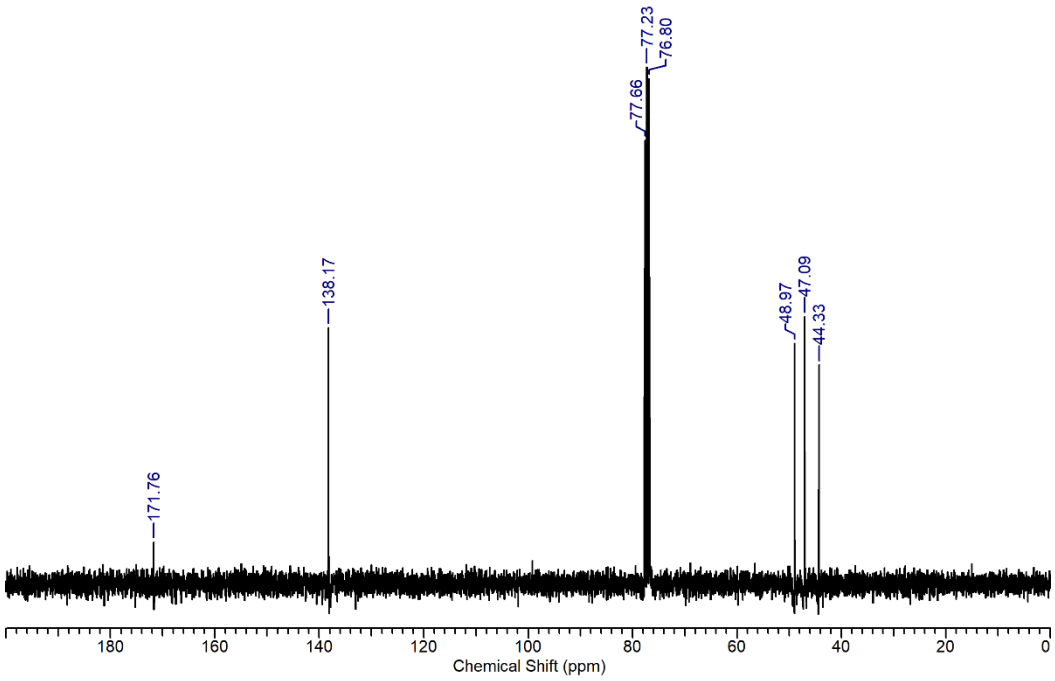


Figure A.3 ^{13}C NMR spectrum of *cis*-5-norbornene-*exo*-2,3-dicarboxylic anhydride

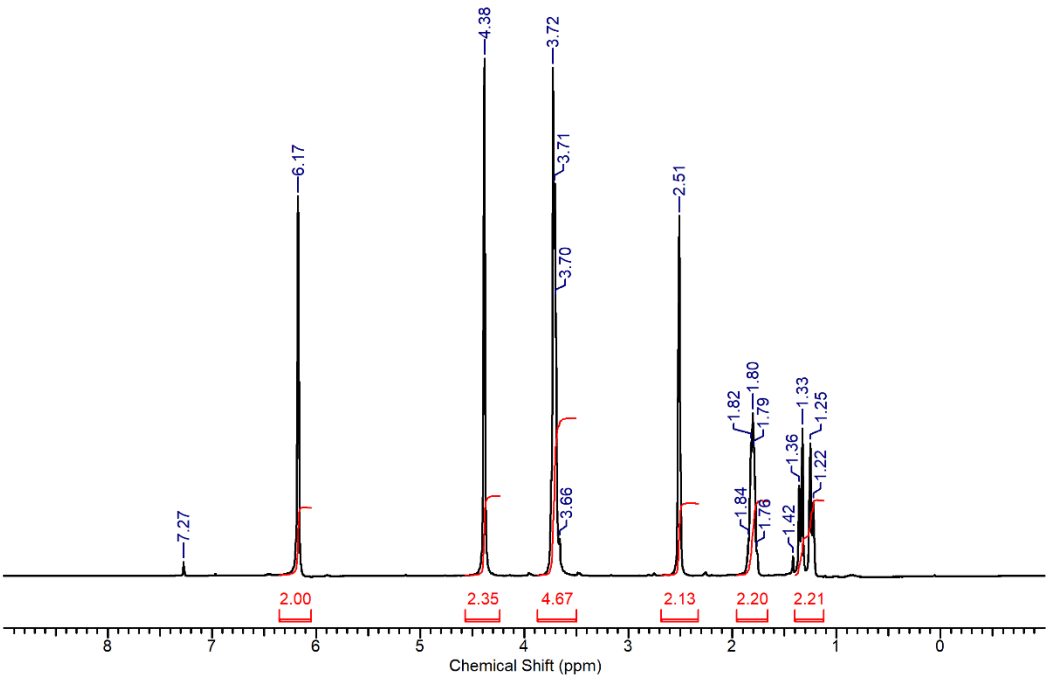


Figure A.4 ^{1}H NMR spectrum of *exo*-5,6-bis(hydroxymethyl)-2-norbornene

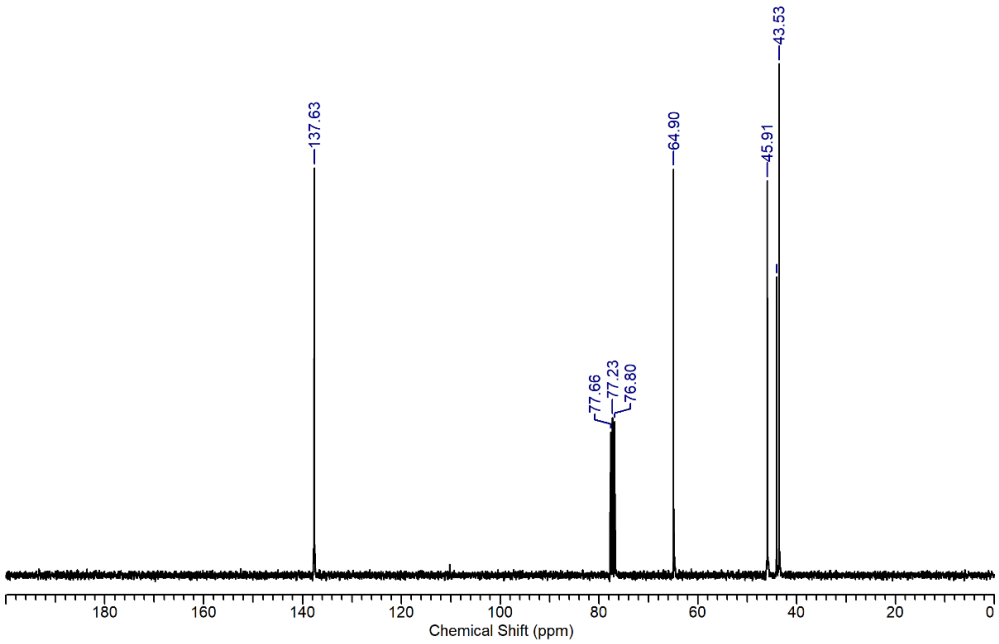


Figure A.5 ^{13}C NMR spectrum of *exo*-5,6-bis(hydroxymethyl)-2-norbornene

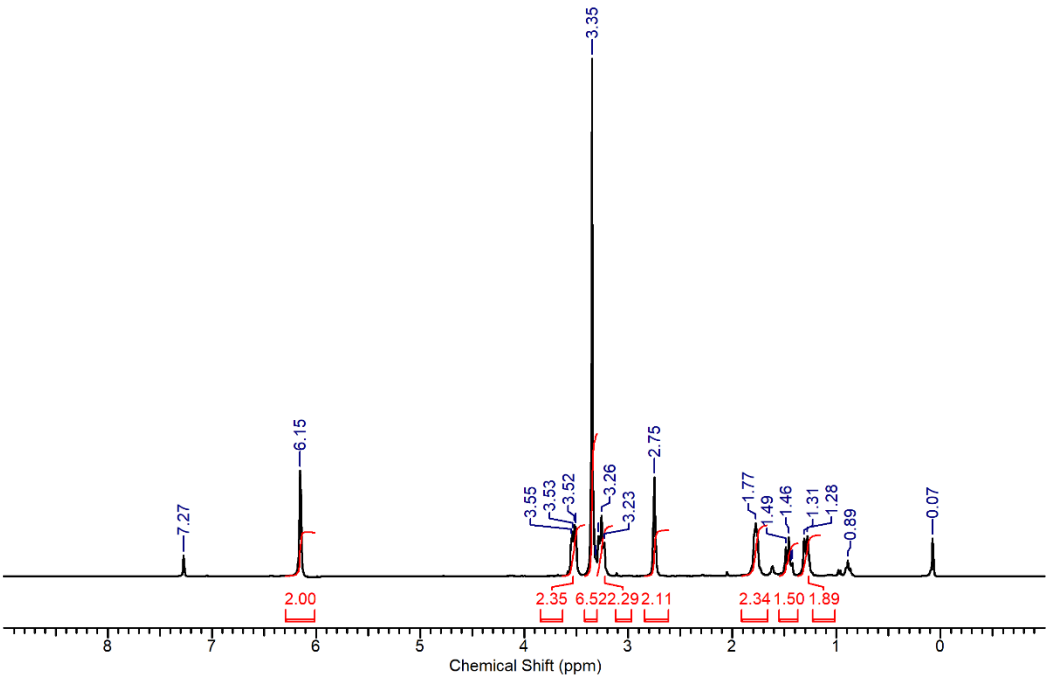


Figure A.6 ^{1}H NMR spectrum of *exo*-5,6-bis(methoxymethyl)-2-norbornene (MeOMeNB)

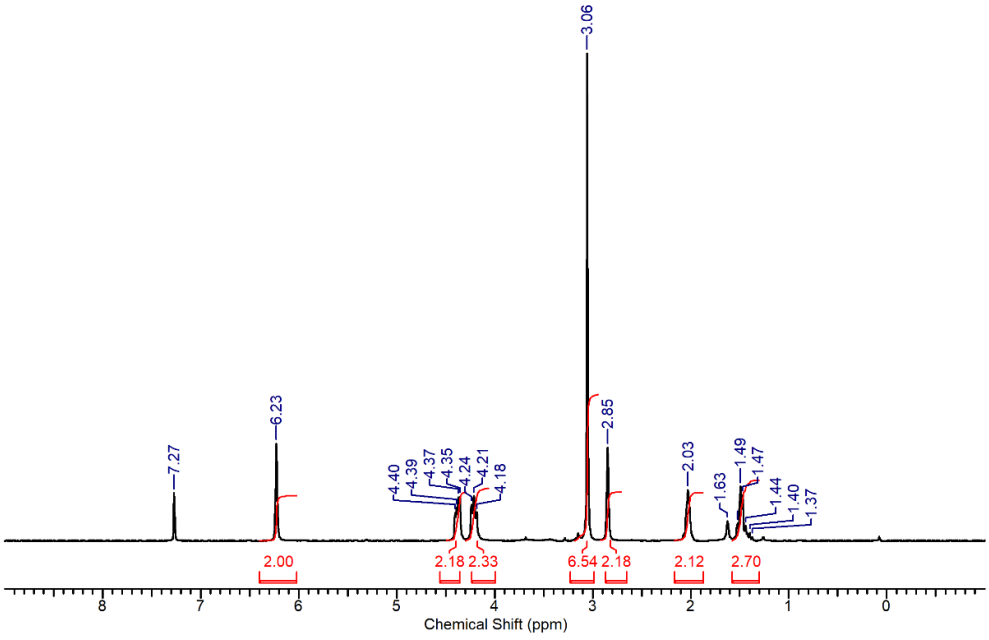


Figure A.7 ^{1}H NMR spectrum of *exo*-5,6-bismesylate-2-norbornene

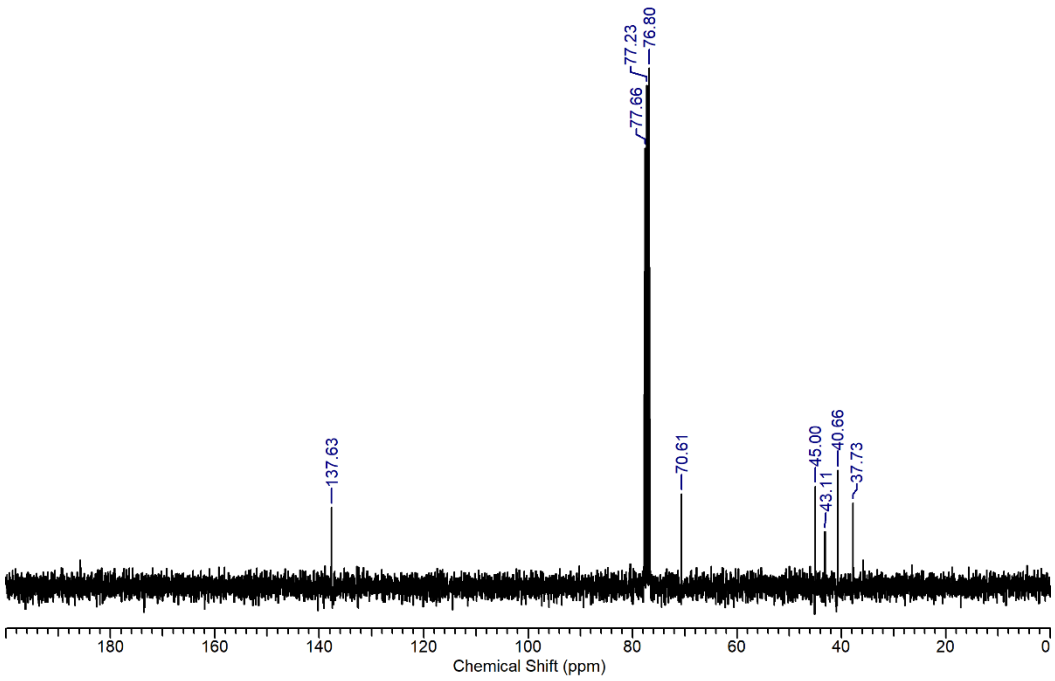


Figure A.8 ^{13}C NMR spectrum of *exo*-5,6-bismesylate-2-norbornene

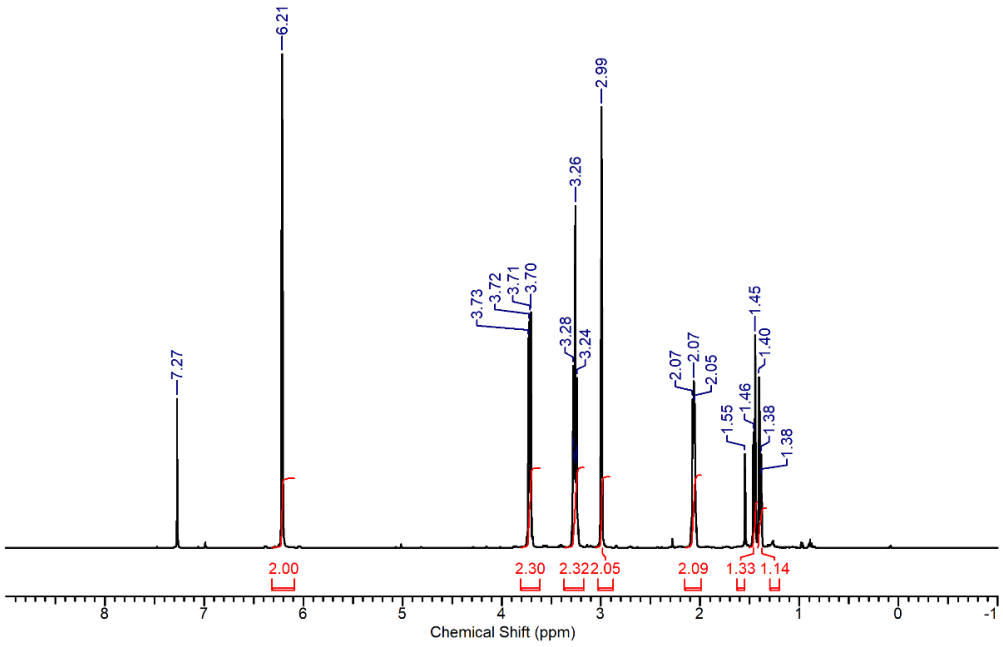


Figure A.9 ^{1}H NMR spectrum of *exo*-5,6-bis(bromomethyl)-2-norbornene (BrMeNB)

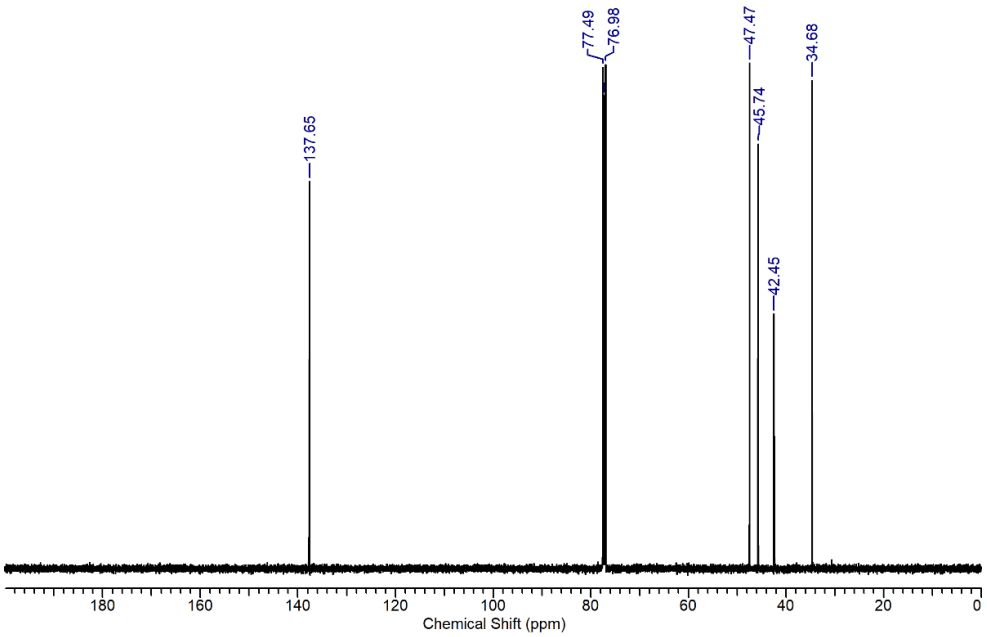


Figure A.10 ^{13}C NMR spectrum of *exo*-5,6-bis(bromomethyl)-2-norbornene (BrMeNB)

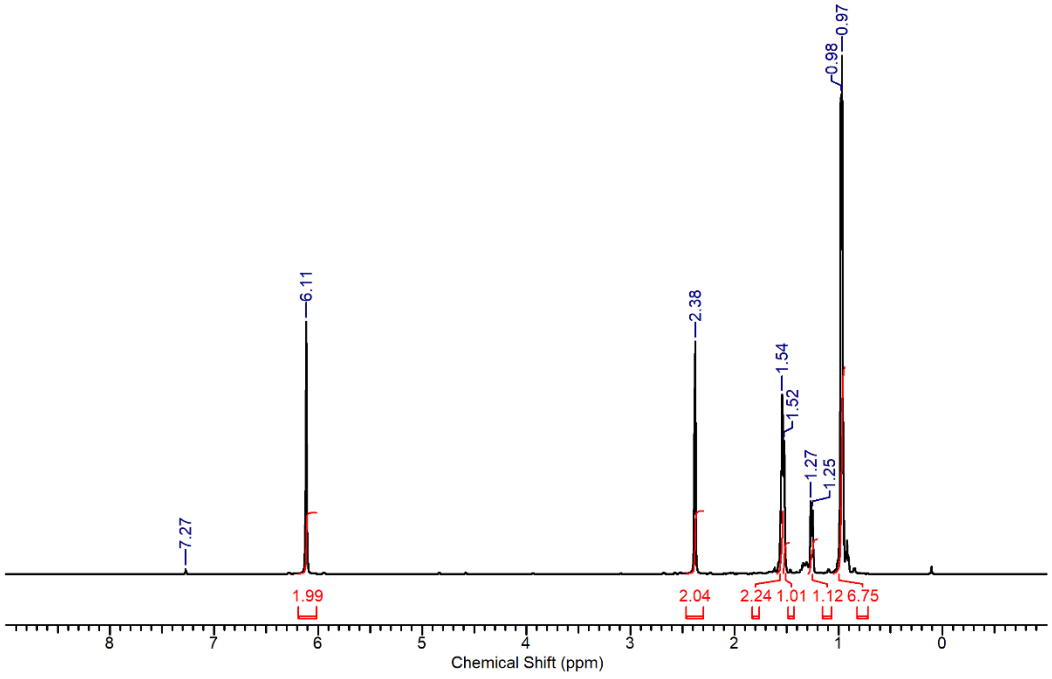


Figure A.11 ^{1}H NMR spectrum of *exo*-5,6-dimethyl-2-norbornene (MeNB)

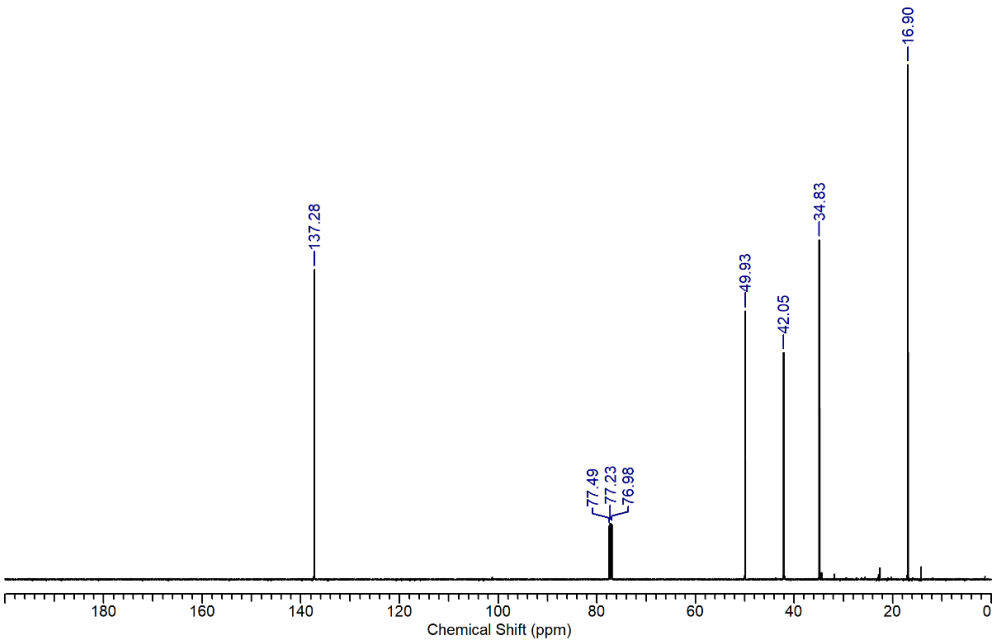


Figure A.12 ^{13}C NMR spectrum of *exo*-5,6-dimethyl-2-norbornene (MeNB)

References

16. Mulpuri, S. V.; Shin, J.; Shin, B.-G.; Greiner, A.; Yoon, D. Y., Synthesis and characterization of substituted polynorbornene derivatives. *Polymer* **2011,** *52* (19), 4377-4386.
17. Blank, F.; Janiak, C., Metal catalysts for the vinyl/addition polymerization of norbornene. *Coordination Chemistry Reviews* **2009,** *253* (7-8), 827-861.
18. Hennis, A. D.; Polley, J. D.; Long, G. S.; Sen, A.; Yandulov, D.; Lipian, J.; Benedikt, G. M.; Rhodes, L. F.; Huffman, J., Novel, efficient, palladium-based system for the polymerization of norbornene derivatives: scope and mechanism. *Organometallics* **2001,** *20* (13), 2802-2812.
19. Mathew, J. P.; Reinmuth, A.; Melia, J.; Swords, N.; Risse, W., (η3-Allyl) palladium (II) and palladium (II) nitrile catalysts for the addition polymerization of norbornene derivatives with functional groups. *Macromolecules* **1996,** *29* (8), 2755-2763.
20. Byun, G. S.; Kim, S. Y.; Cho, I., Pd (II)-catalyzed polymerization of optically active norbornene carboxylic acid esters. *Journal of Polymer Science Part A: Polymer Chemistry* **2006,** *44* (3), 1263-1270.
105. Ahmed, S.; Bidstrup, S. A.; Kohl, P.; Ludovice, P. In *Stereochemical structure-property relationships in polynorbornene from simulation*, Macromolecular Symposia, Wiley Online Library: 1998; pp 1-10.
106. Janiak, C.; Lassahn, P. G., The vinyl homopolymerization of norbornene. *Macromolecular rapid communications* **2001,** *22* (7), 479-493.
107. Barnes, D. A.; Benedikt, G. M.; Goodall, B. L.; Huang, S. S.; Kalamarides, H. A.; Lenhard, S.; McIntosh, L. H.; Selvy, K.; Shick, R. A.; Rhodes, L. F., Addition polymerization of norbornene-type monomers using neutral nickel complexes containing fluorinated aryl ligands. *Macromolecules* **2003,** *36* (8), 2623-2632.
108. Rieger, B.; Baugh, L. S.; Kacker, S.; Striegler, S., *Late transition metal polymerization catalysis*. Wiley Online Library: 2003.
109. Wilks, B. R.; Chung, W. J.; Ludovice, P. J.; Rezac, M. R.; Meakin, P.; Hill, A. J., Impact of average free-volume element size on transport in stereoisomers of polynorbornene. I. Properties at 35 C. *Journal of Polymer Science Part B: Polymer Physics* **2003,** *41* (18), 2185-2199.
213. Odian, G., *Principles of polymerization*. John Wiley & Sons: 2004.
222. Hadjichristidis, N.; Pispas, S.; Floudas, G., *Block copolymers: synthetic strategies, physical properties, and applications*. John Wiley & Sons: 2003.
223. Young, R. J.; Lovell, P. A., *Introduction to polymers*. CRC press: 2011.
224. Su, W.-F., *Principles of polymer design and synthesis*. Springer: 2013; Vol. 82.
225. Lynn, D. M.; Kanaoka, S.; Grubbs, R. H., Living ring-opening metathesis polymerization in aqueous media catalyzed by well-defined ruthenium carbene complexes. *Journal of the American Chemical Society* **1996,** *118* (4), 784-790.
226. Goll, J. M.; Fillion, E., Tuning the reactivity of palladium carbenes derived from diphenylketene. *Organometallics* **2008,** *27* (14), 3622-3625.
227. Zhang, M.; Flynn, D. L.; Hanson, P. R., Oligomeric benzylsulfonium salts: Facile benzylation via high-load ROMP reagents. *The Journal of Organic Chemistry* **2007,** *72* (9), 3194-3198.
228. Gunther, M. J.; Pavlovic, R. Z.; Fernandez, J. P.; Zhiquan, L.; Gallucci, J.; Hadad, C. M.; Badjic, J. D., Stereo-and regioselective synthesis of molecular baskets. *The Journal of organic chemistry* **2019,** *84* (7), 4392-4401.

229. Gajewski, J. J.; Salazar, J. D. C., Degenerate thermal rearrangement of 1, 3-dimethylenecyclopentane. Evidence for partially stereospecific biradical formation and closure in a 1, 3 shift. *Journal of the American Chemical Society* **1981,** *103* (14), 4145-4154.
230. Kramer, B. D.; Bartlett, P. D., Cycloaddition. XII. Photosensitized cycloaddition of the cis- and trans-2-butenes to cyclopentadiene. *Journal of the American Chemical Society* **1972,** *94* (11), 3934-3939.
231. Pavlović, R. Z.; Border, S. E.; Gallucci, J.; Badjić, J. D., Stereo-and regioselective halogenation of norbornenes directed by neighboring group participation. *Tetrahedron Letters* **2016,** *57* (50), 5584-5587.

Appendix B Supporting Information for Chapter 2

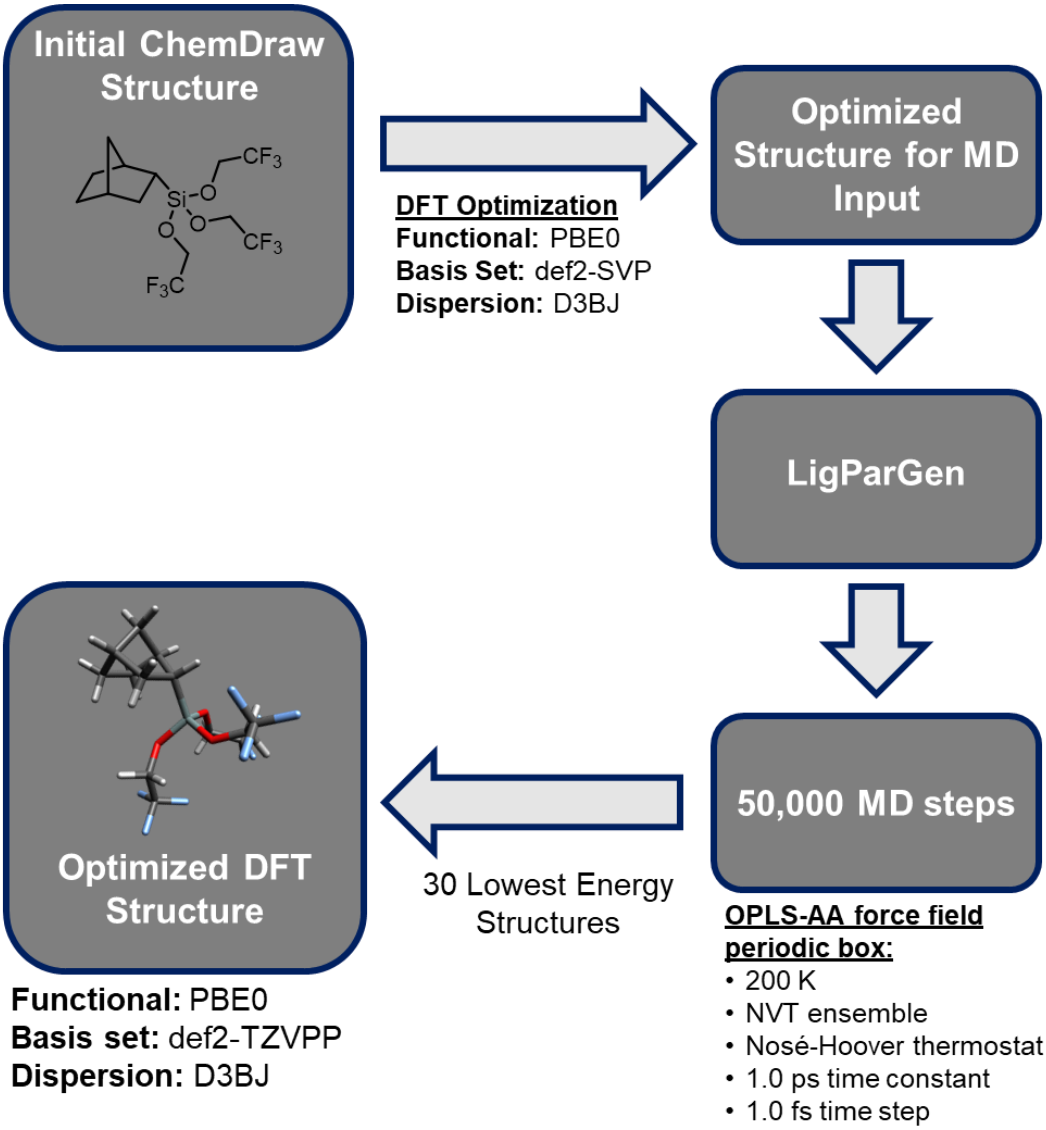


Figure B.1 Computational methodology used for this study.

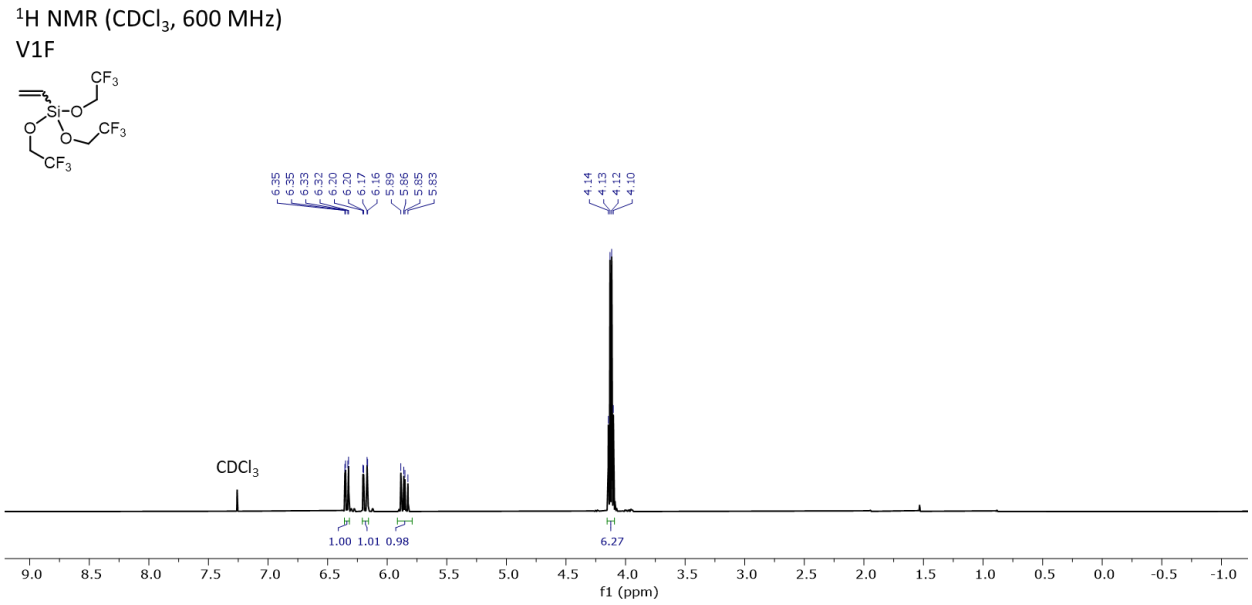


Figure B.2 ^{1}H NMR spectrum of **V1F.**

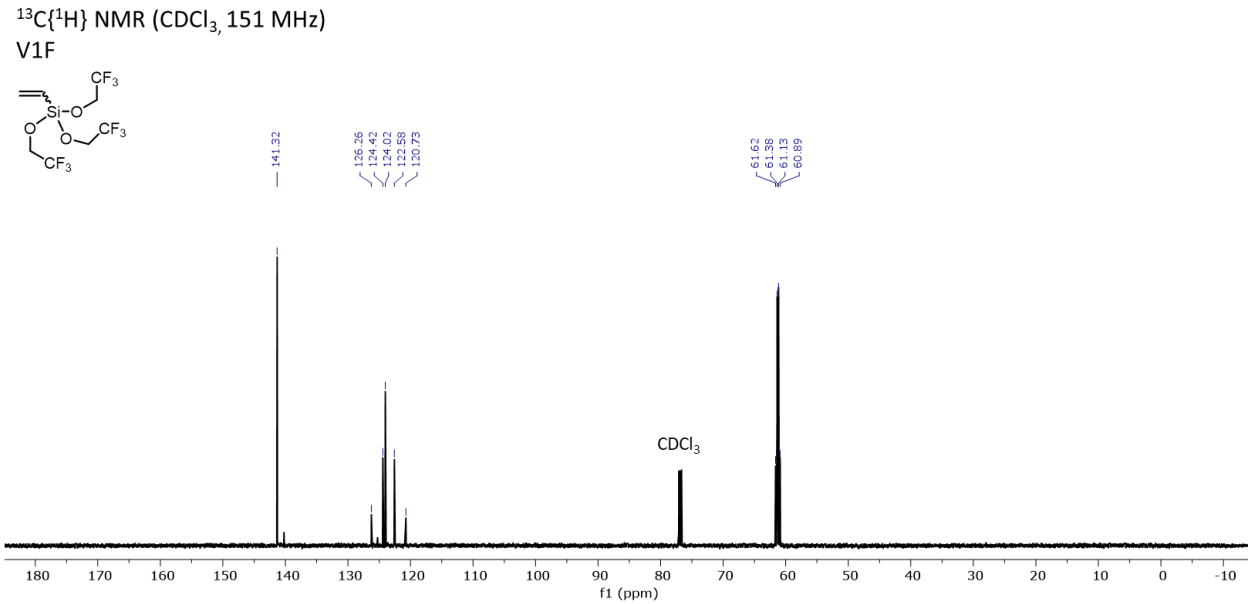


Figure B.3 ^{13}C {^{1}H} NMR spectrum of **V1F.**

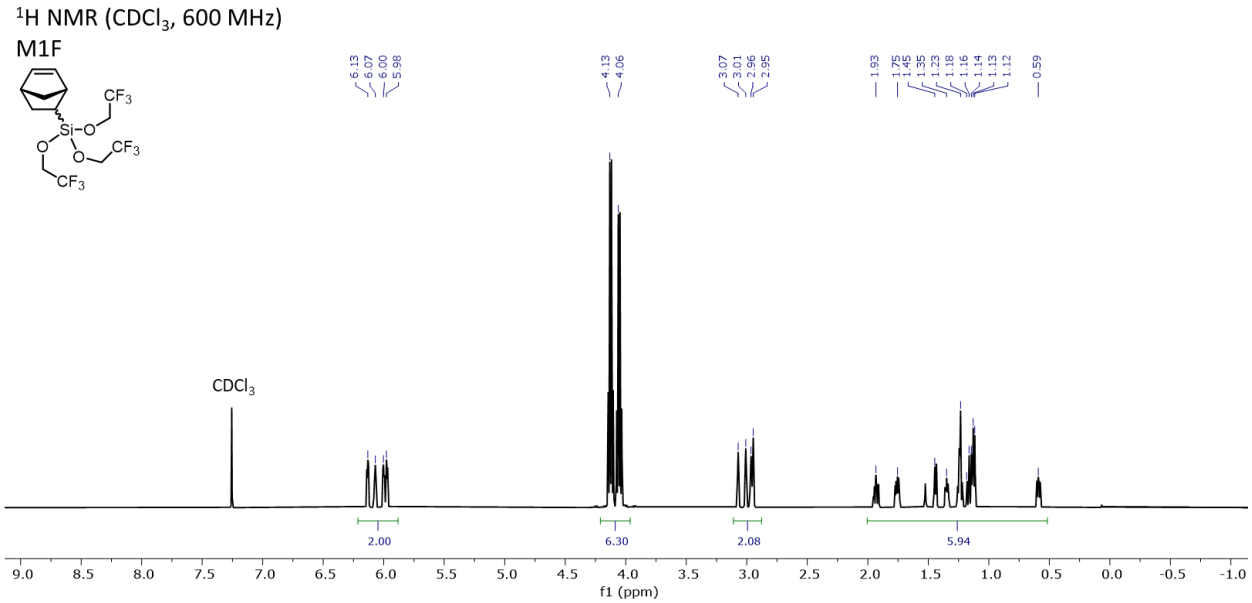


Figure B.4 ^{1}H NMR spectrum of **M1F**.

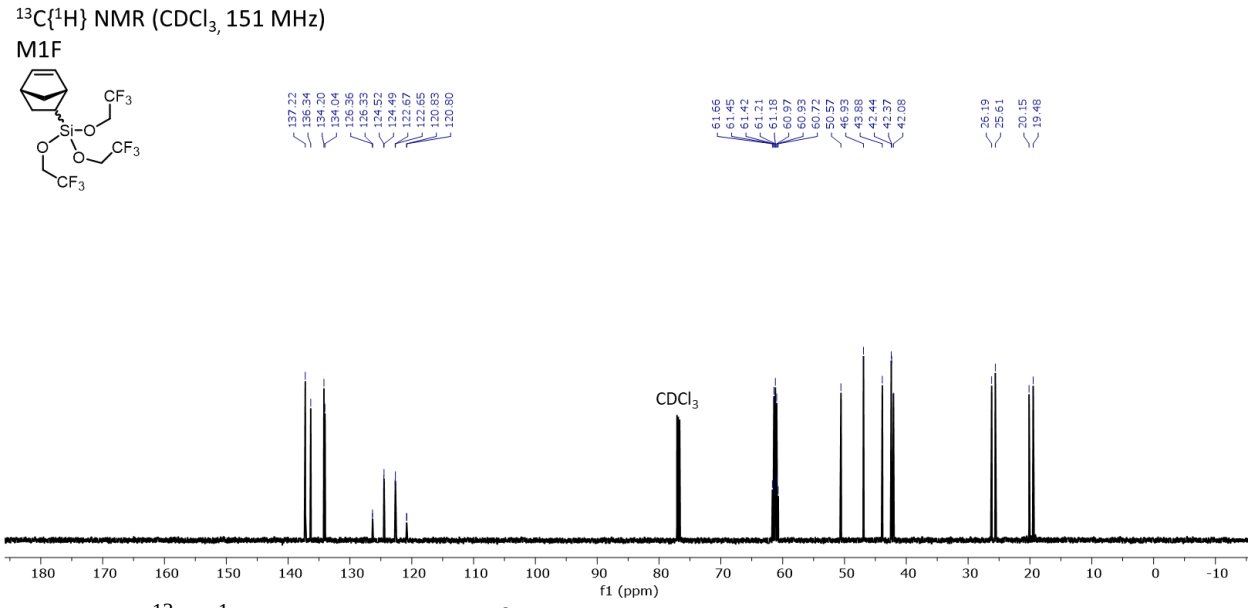


Figure B.5 ^{13}C {^{1}H} NMR spectrum of **M1F.**

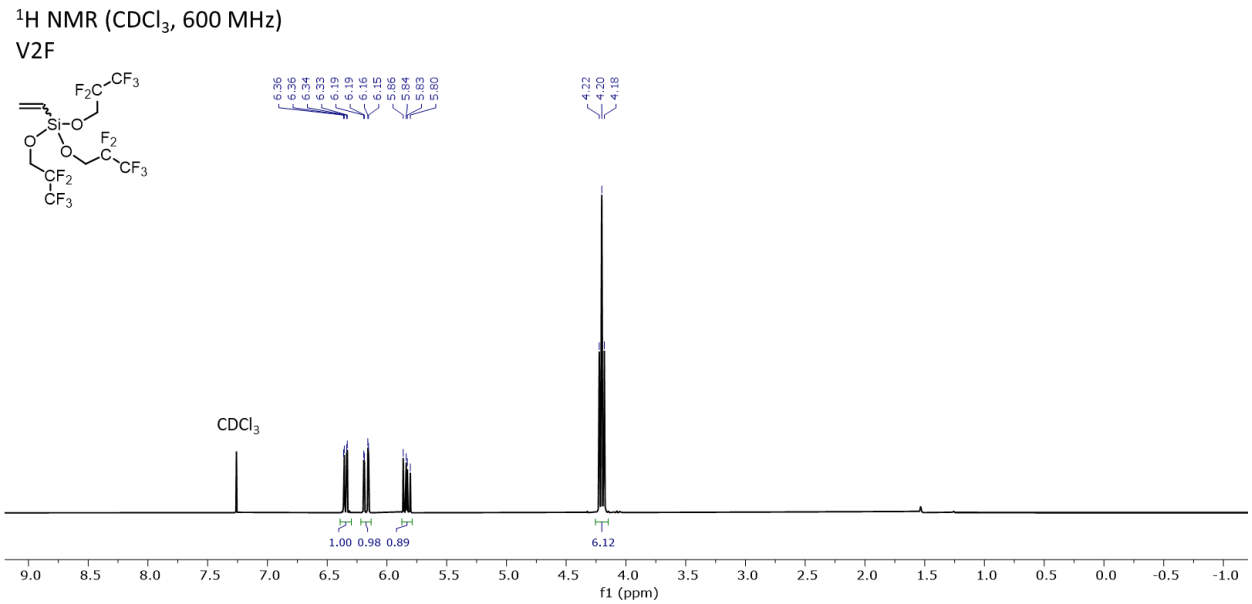


Figure B.6 ^{1}H NMR spectrum of **V2F.**

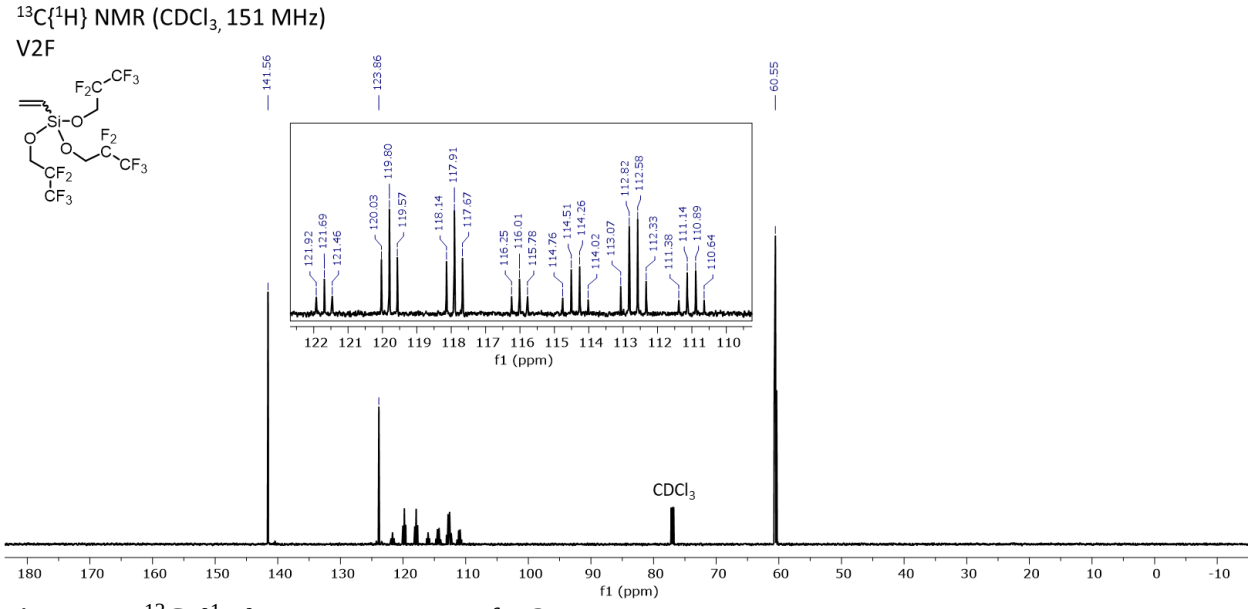


Figure B.7^{13}C {^{1}H} NMR spectrum of **V2F.**

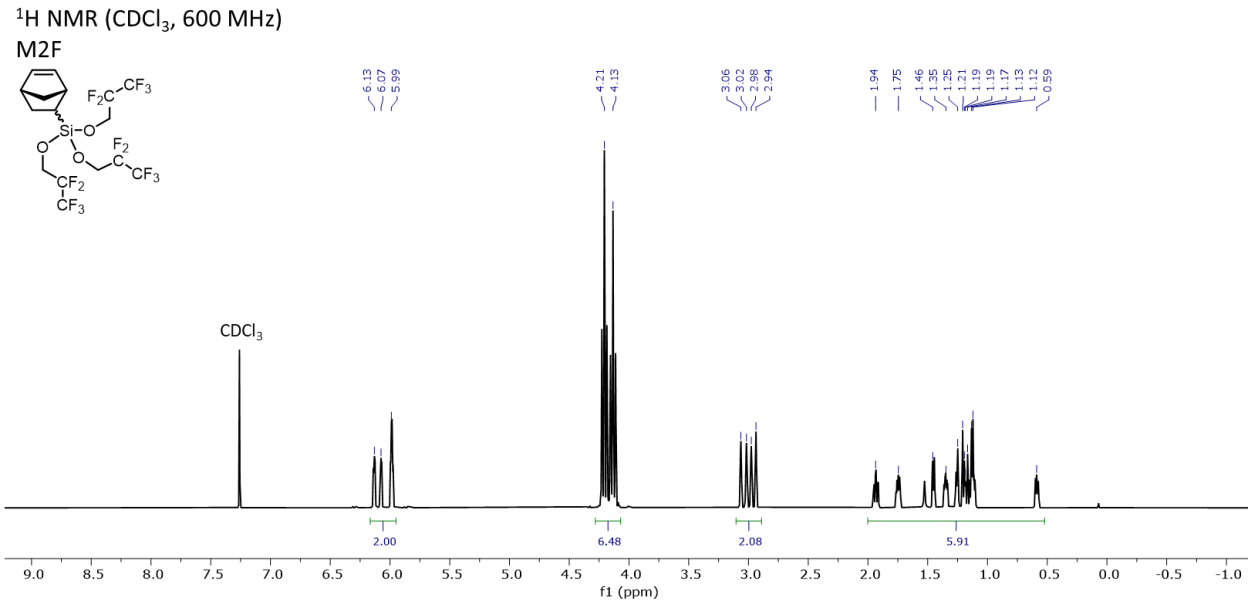


Figure B.8 ^{1}H NMR spectrum of **M2F.**

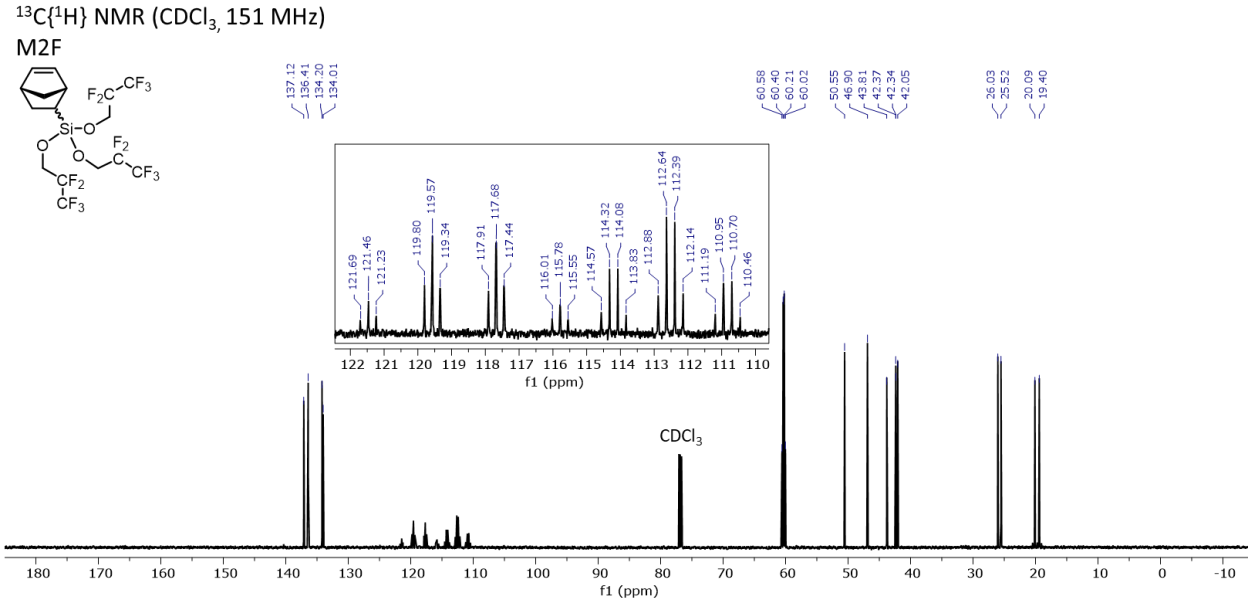


Figure B.9 ^{13}C {^{1}H} NMR spectrum of **M2F.**

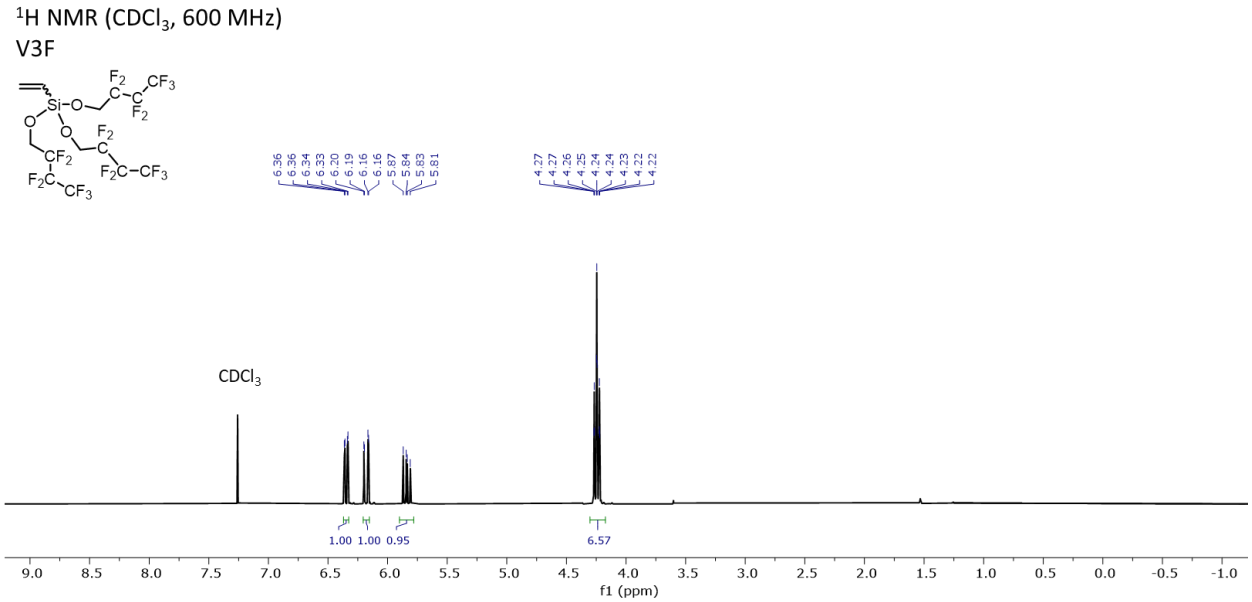


Figure B.10 ^{1}H NMR spectrum of **V3F.**

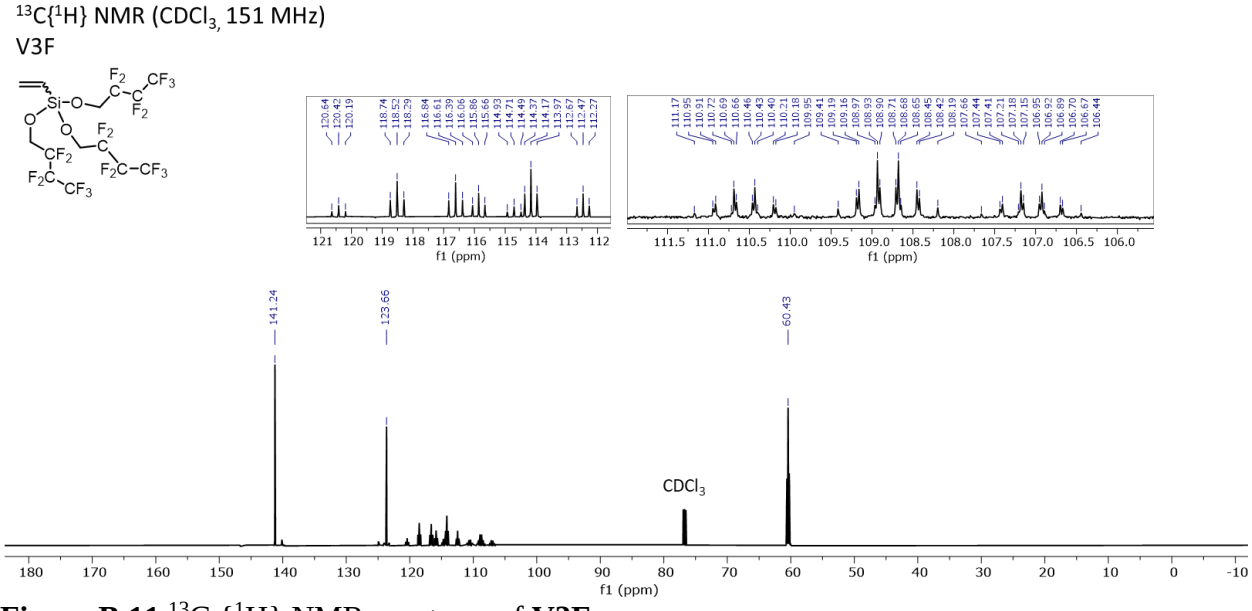


Figure B.11 ^{13}C {^{1}H} NMR spectrum of **V3F.**

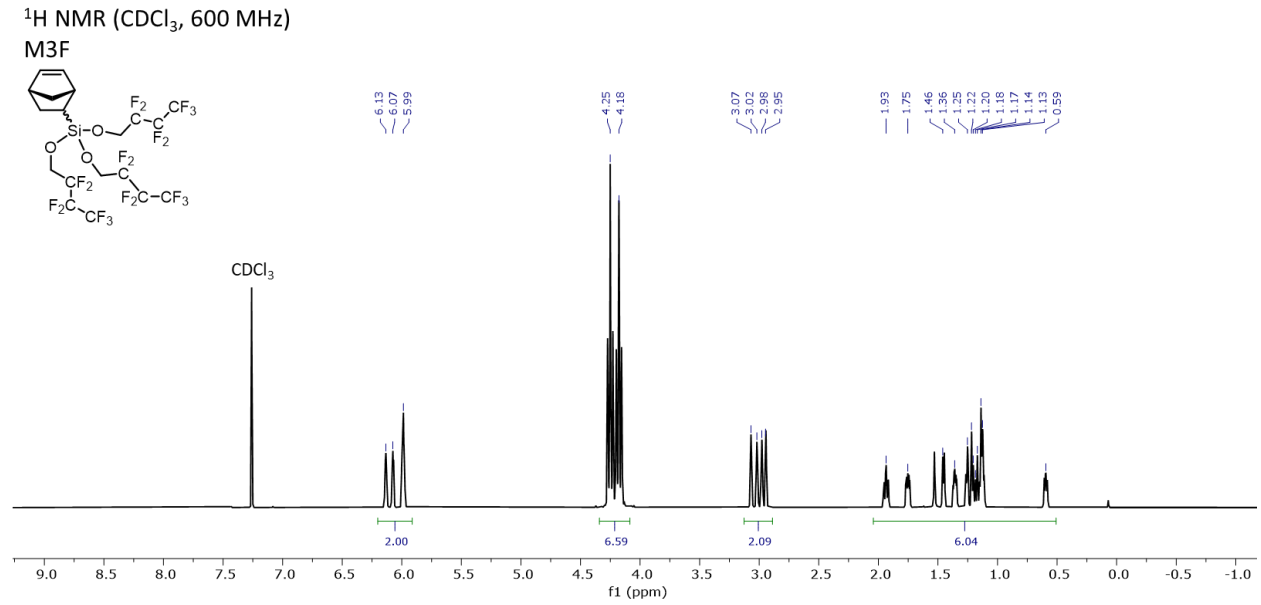


Figure B.12 ^{1}H NMR spectrum of **M3F.**

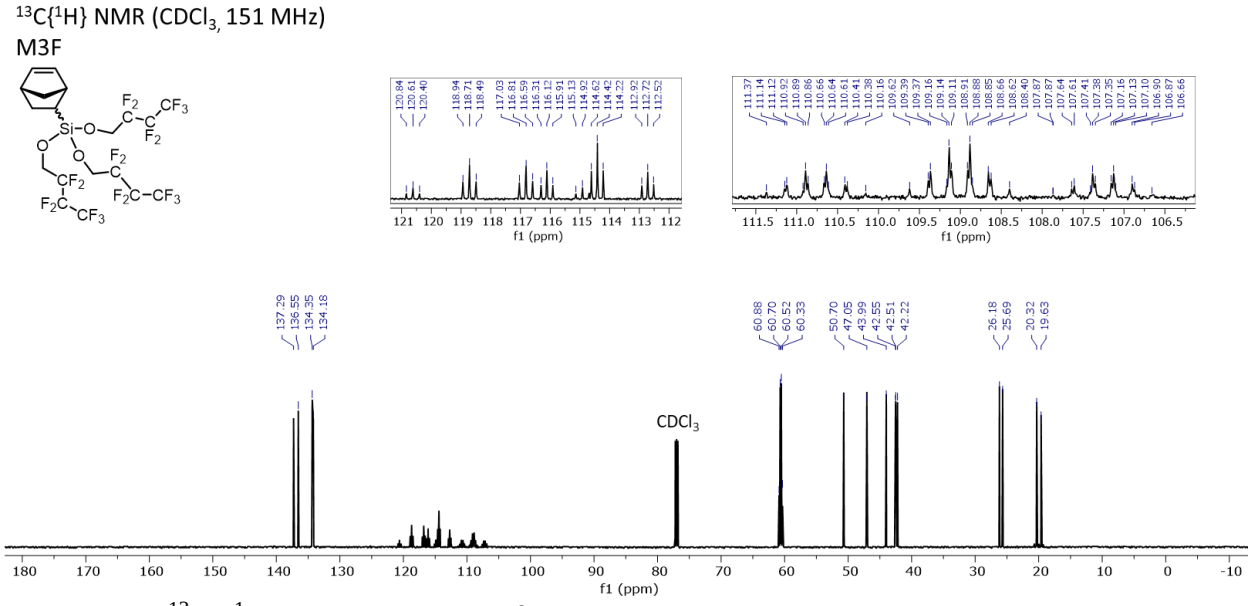


Figure B.13 ^{13}C {^{1}H} NMR spectrum of **M3F.**

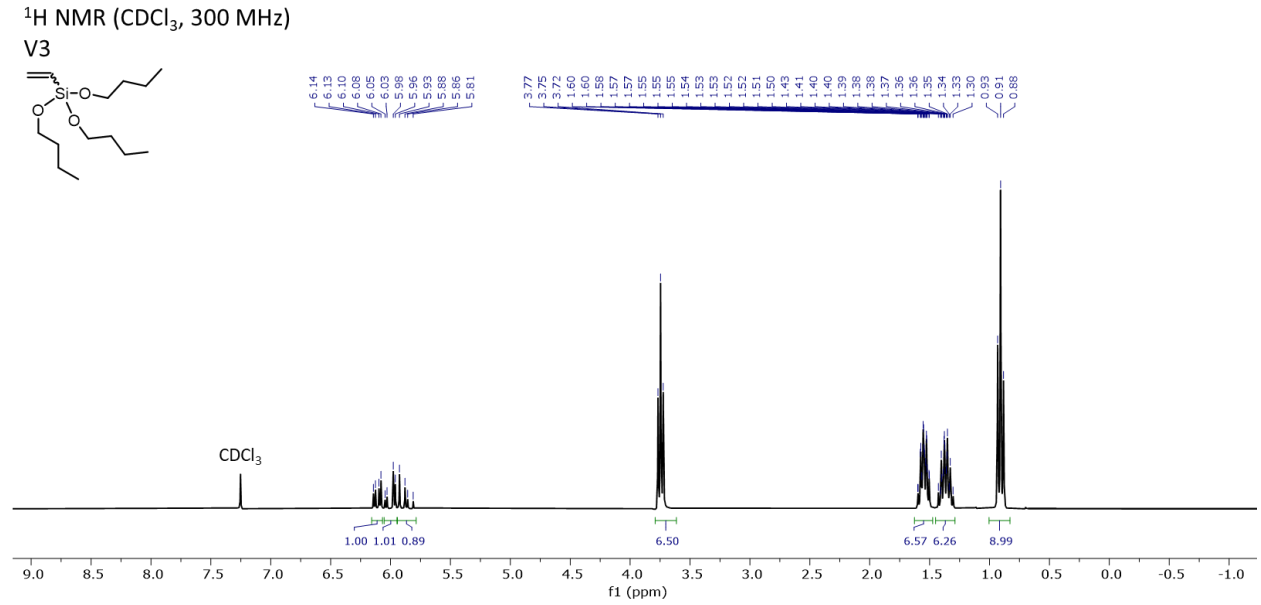


Figure B.14 ^{1}H NMR spectrum of **V3.**

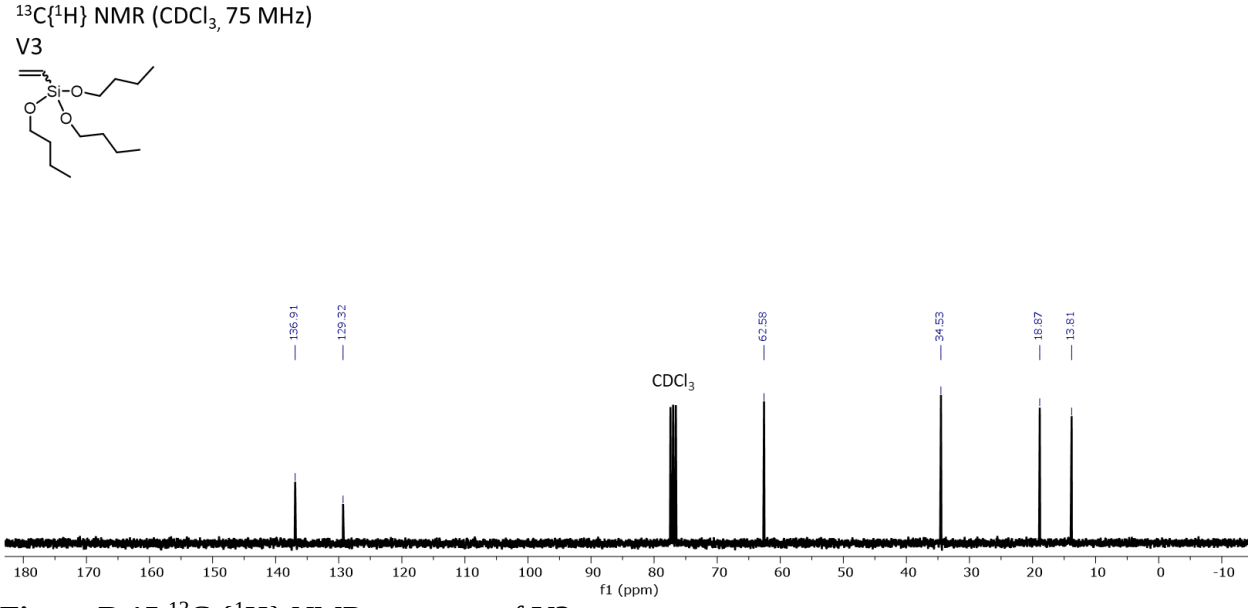


Figure B.15 ^{13}C {^{1}H} NMR spectrum of **V3.**

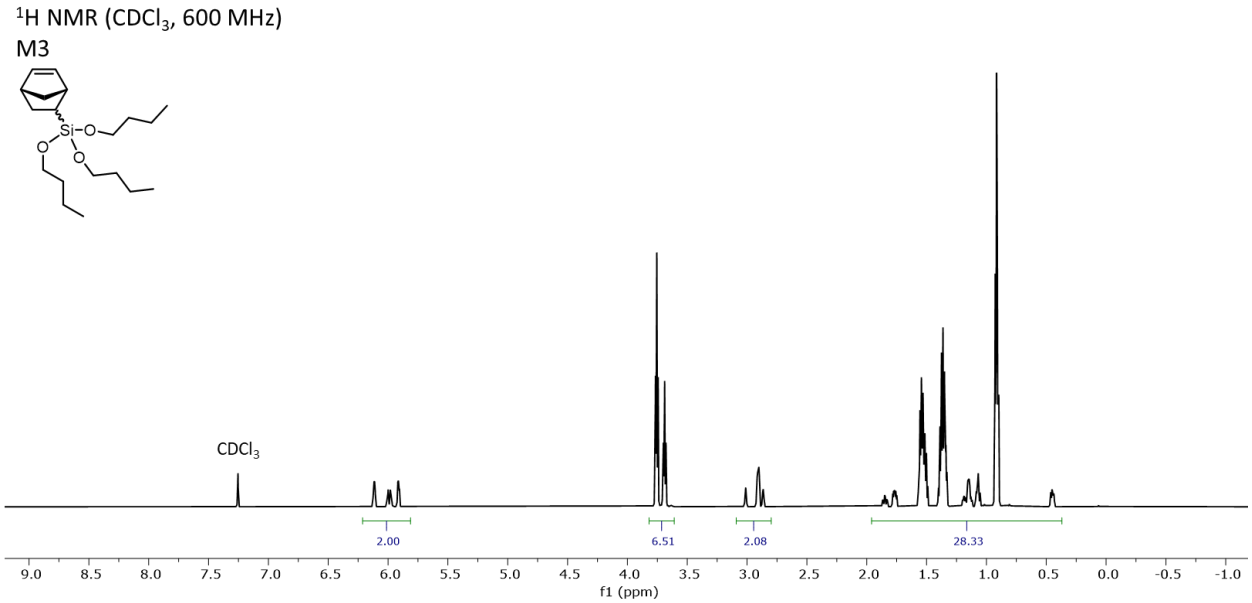


Figure B.16 ^{1}H NMR spectrum of **M3**.

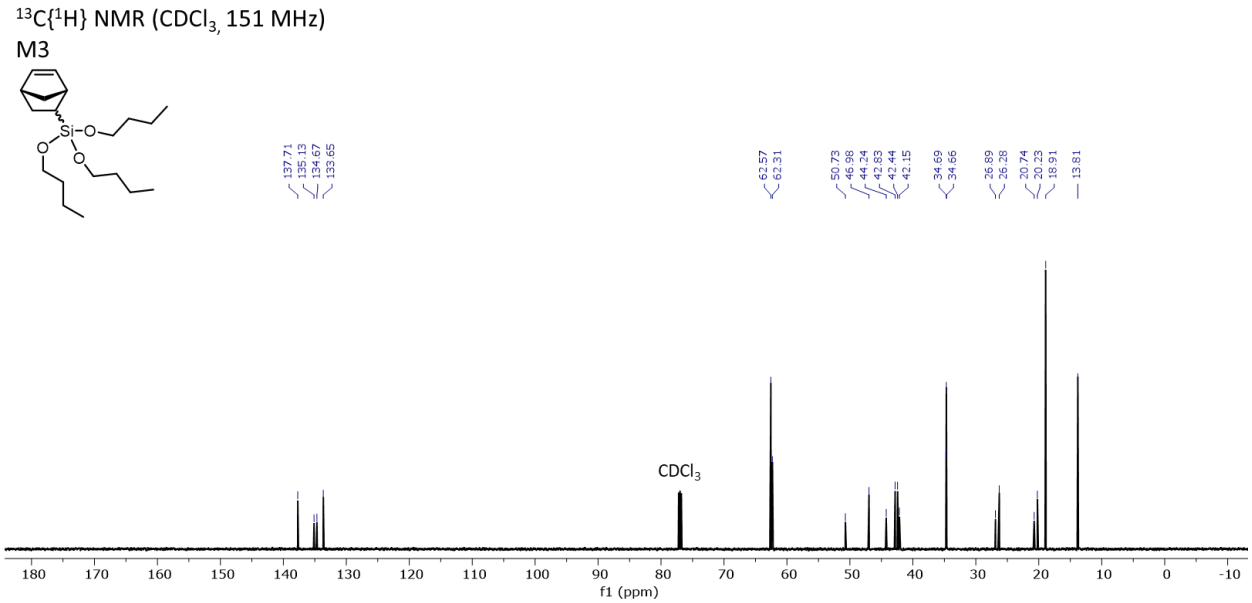


Figure B.17 ^{1}H NMR spectrum of **M3**.

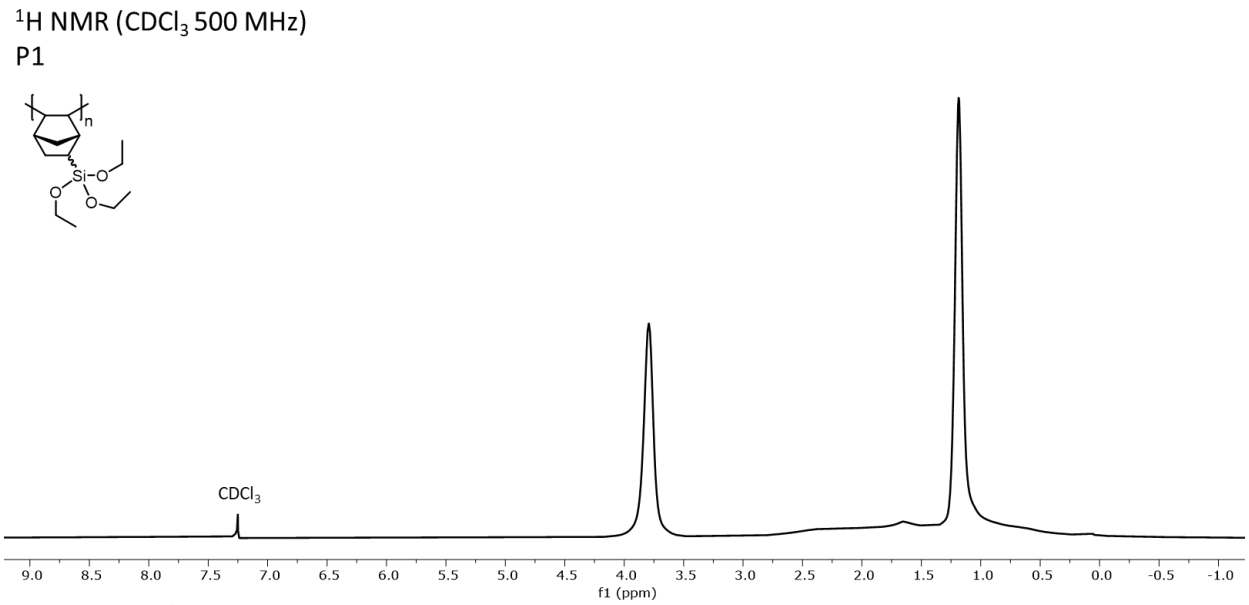


Figure B.18 ^{1}H NMR spectrum of **P1.**

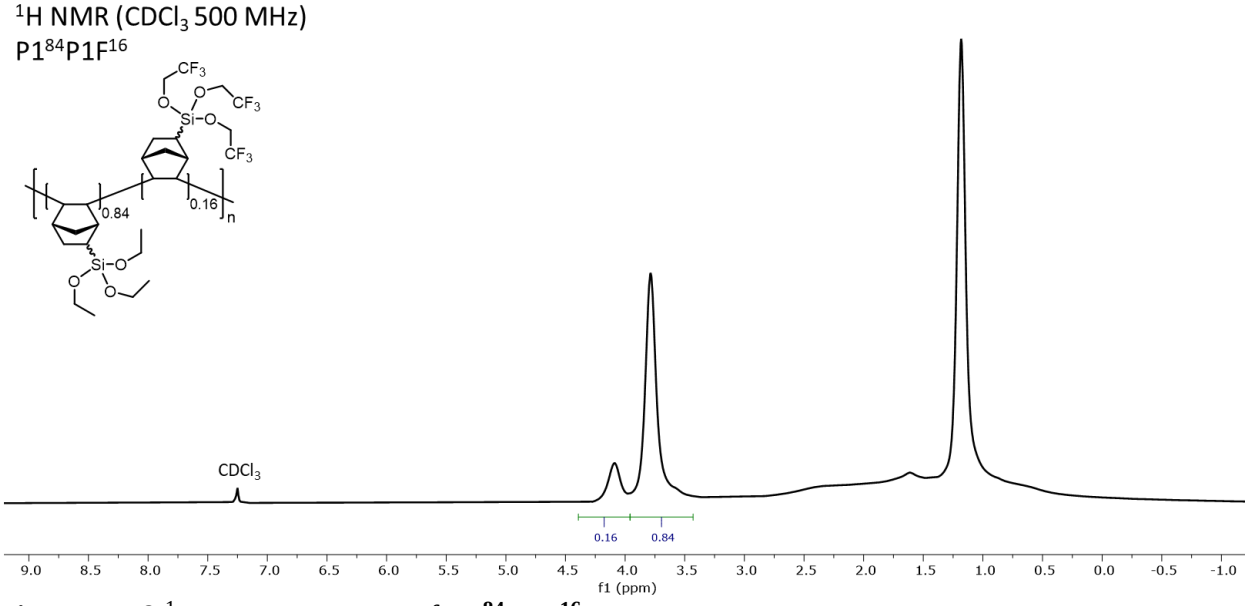


Figure B.19 ^{1}H NMR spectrum of **P1^{84}P1F^{16}.**

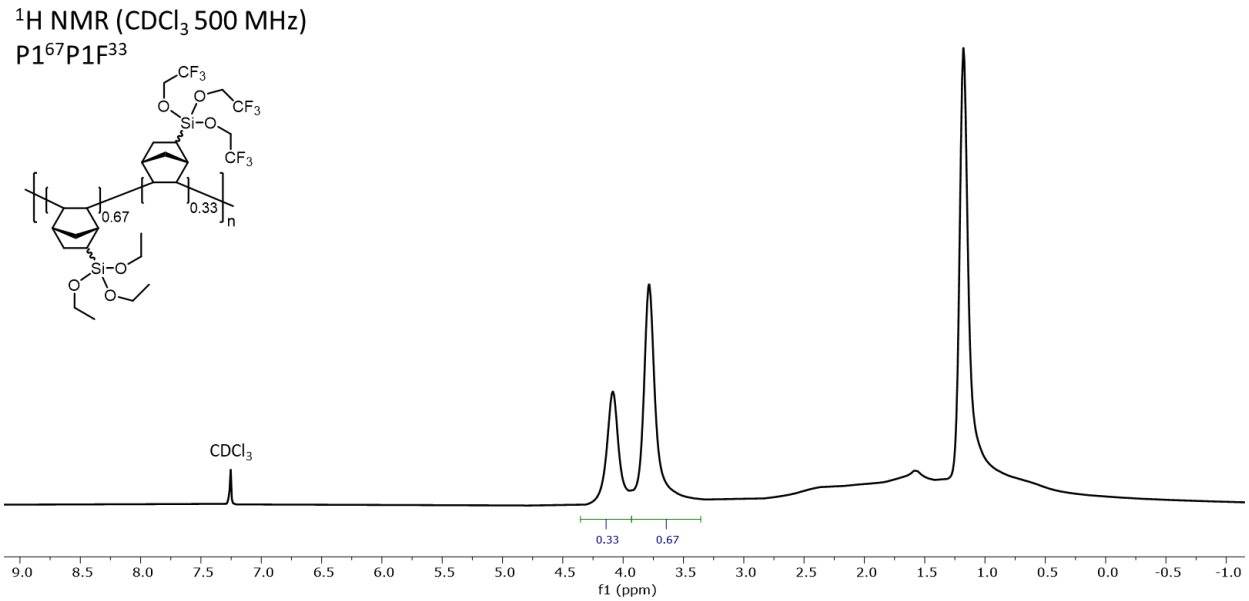


Figure B.20 ^{1}H NMR spectrum of **P1^{67}P1F^{33}.**

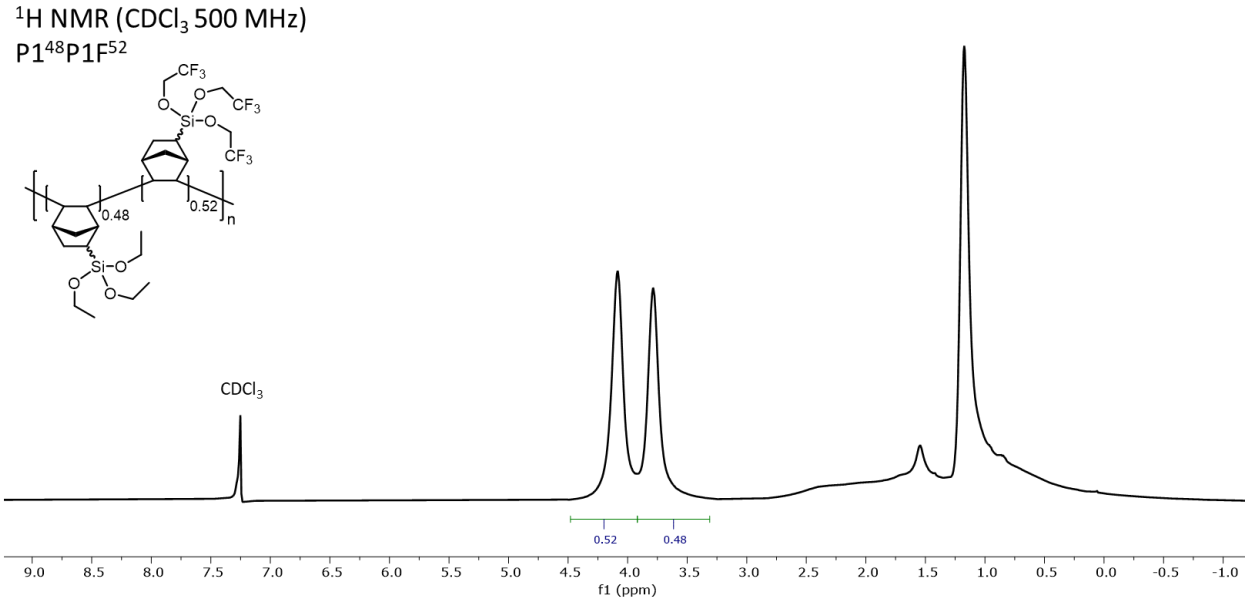


Figure B.21 ^{1}H NMR spectrum of **P1^{48}P1F^{52}.**

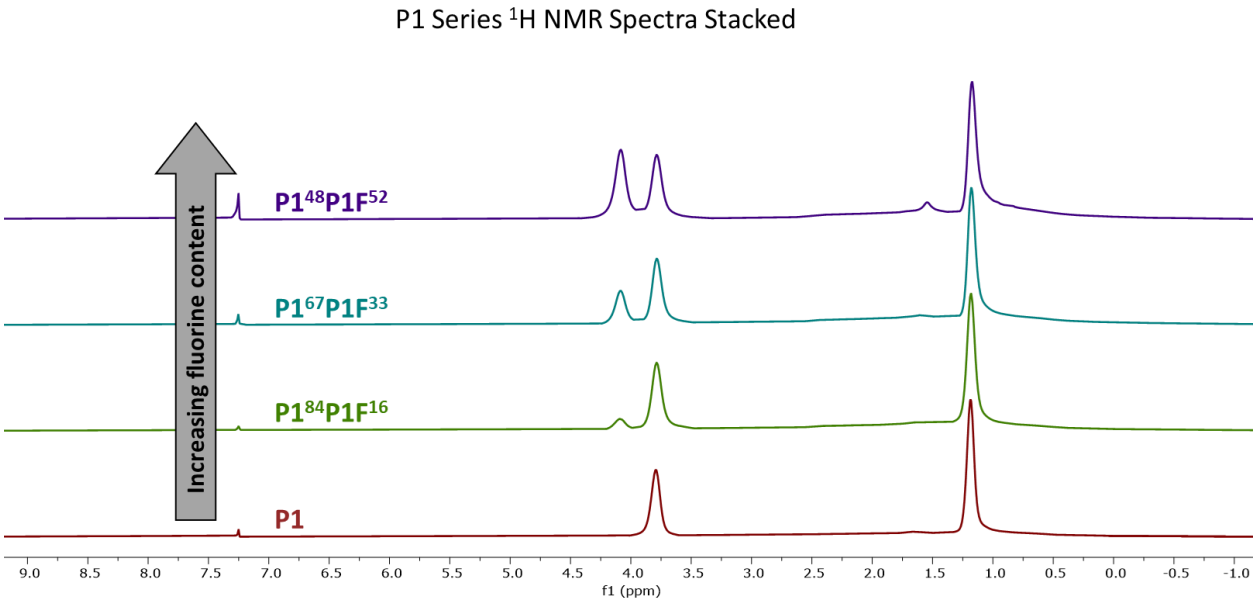


Figure B.22 Stacked ^{1}H NMR spectra of **P1** series copolymers**.** Homopolymer P1F was not shown due to limited solubility in $CDCl_3$ and thus unable to access ^{1}H NMR.

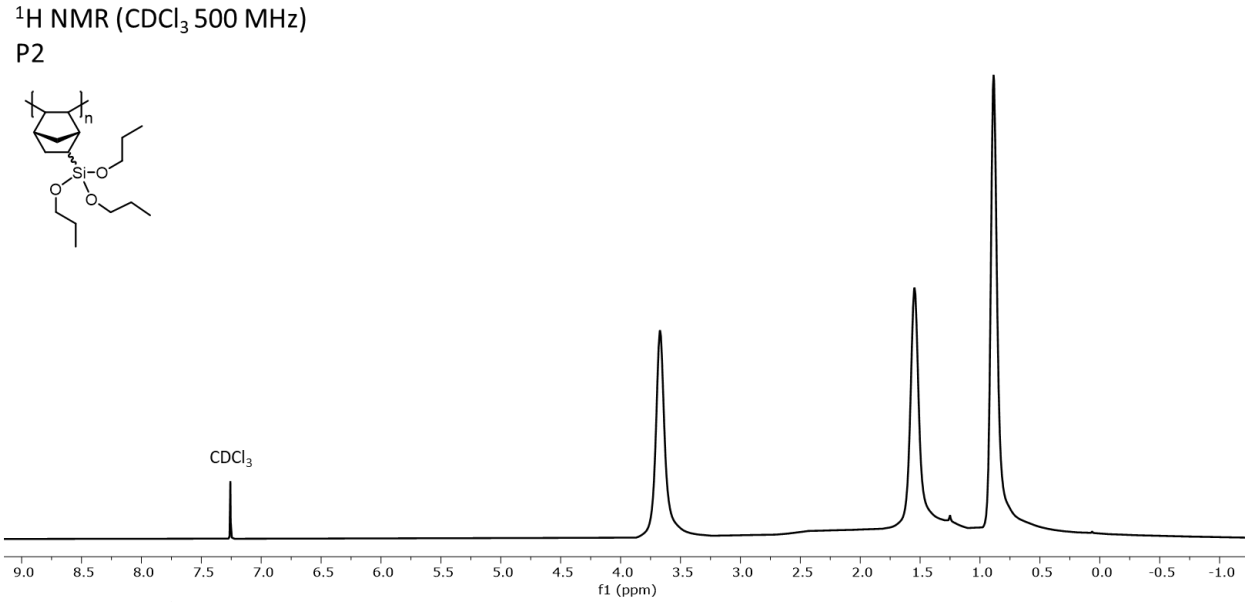


Figure B.23 ^{1}H NMR spectrum of **P2.**

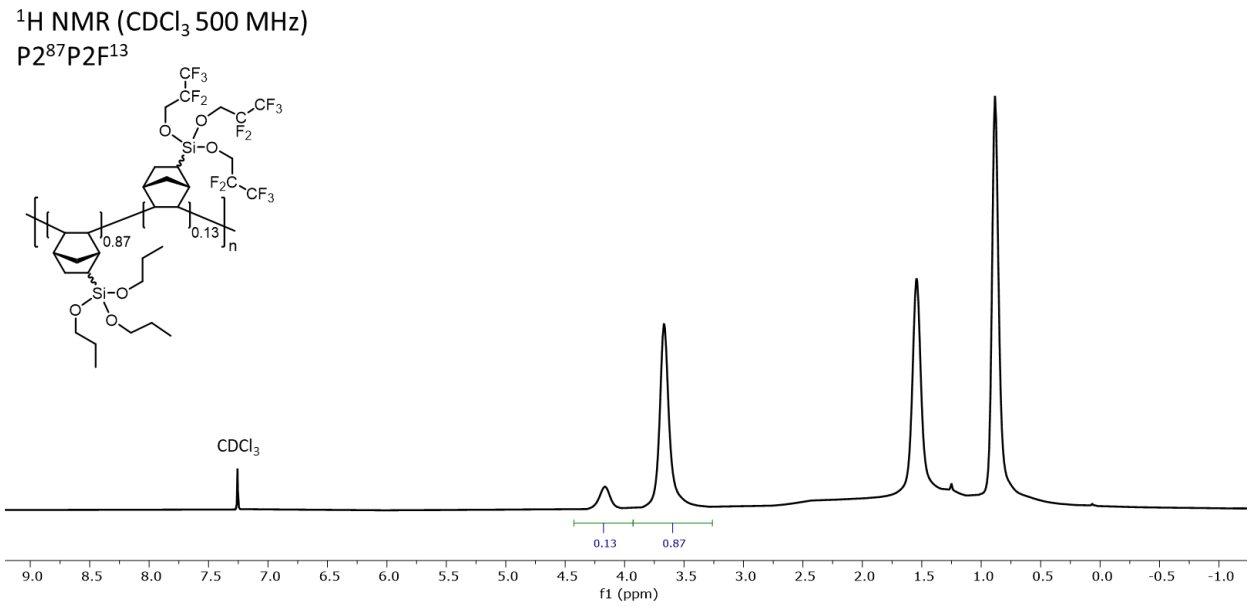


Figure B.24 ^{1}H NMR spectrum of **P2^{87}P2F^{13}.**

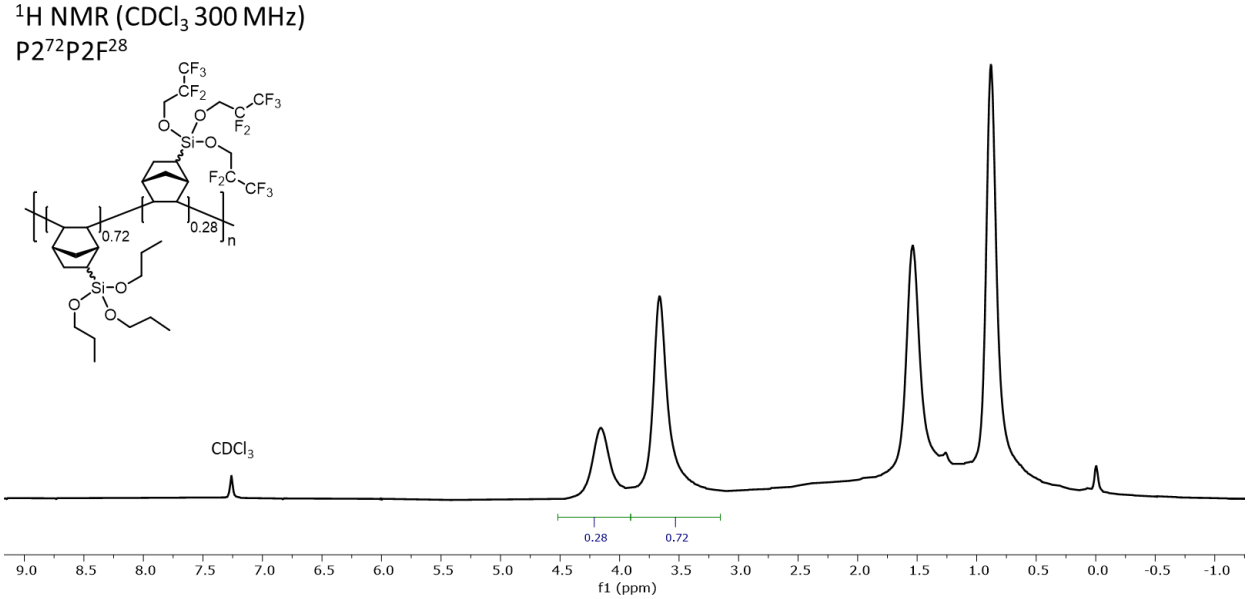


Figure B.25 ^{1}H NMR spectrum of **P2^{72}P2F^{28}.**

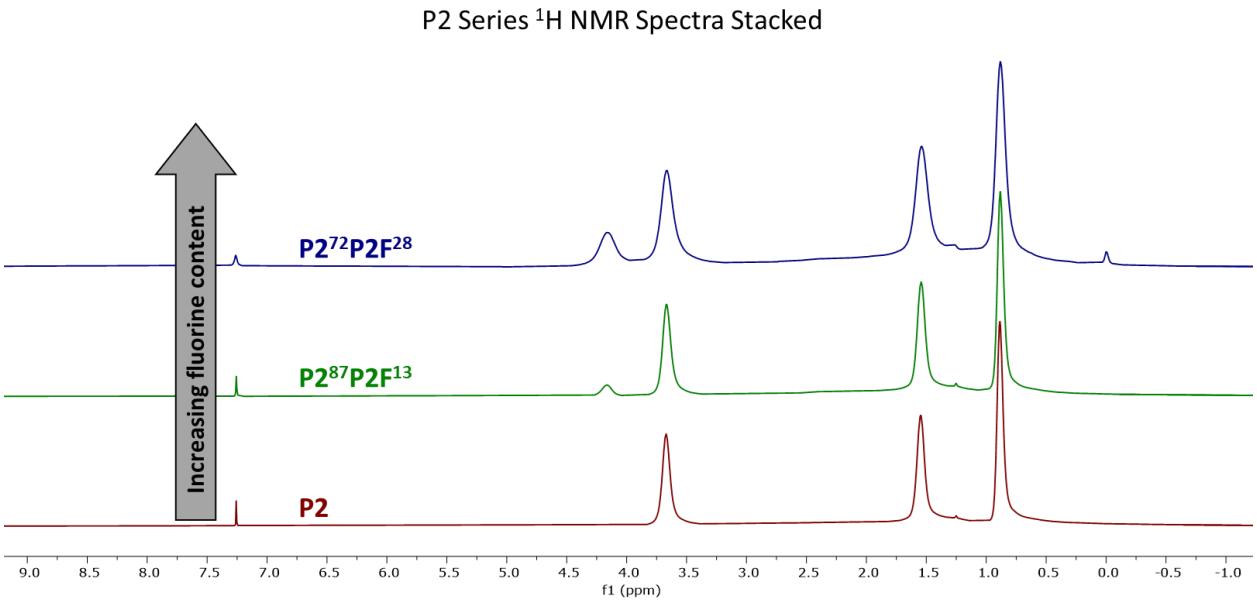


Figure B.26 Stacked ^{1}H NMR spectra of **P2** series copolymers**.**

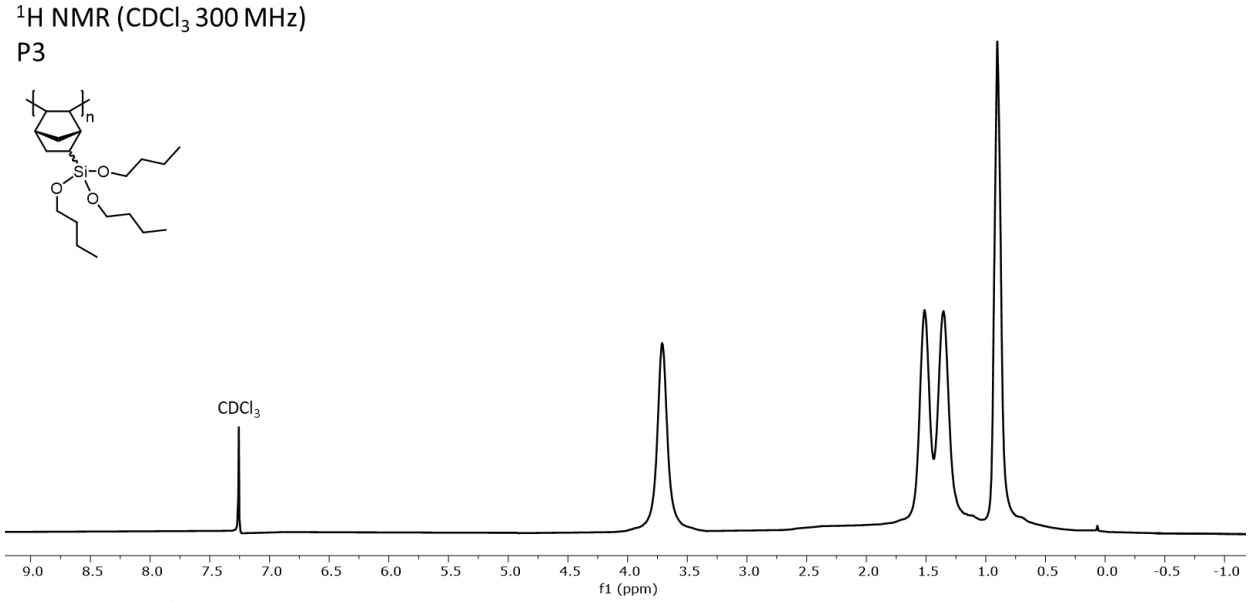


Figure B.27 ^{1}H NMR spectrum of **P3.**

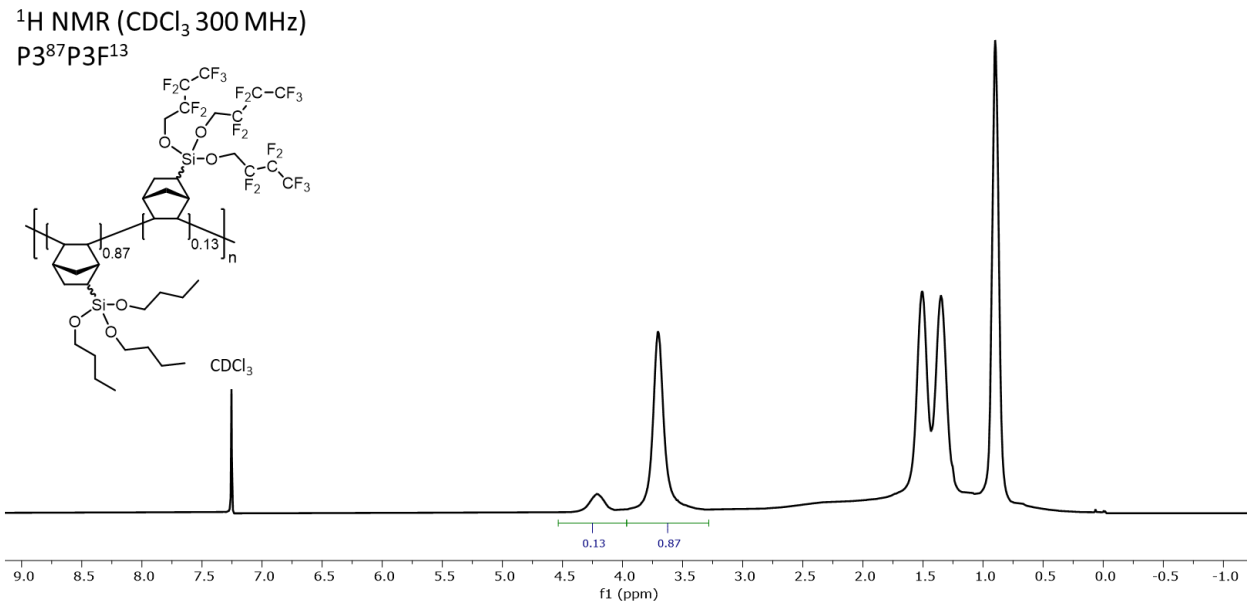


Figure B.28 [1]H NMR spectrum of **P3[87]P3F[13].**

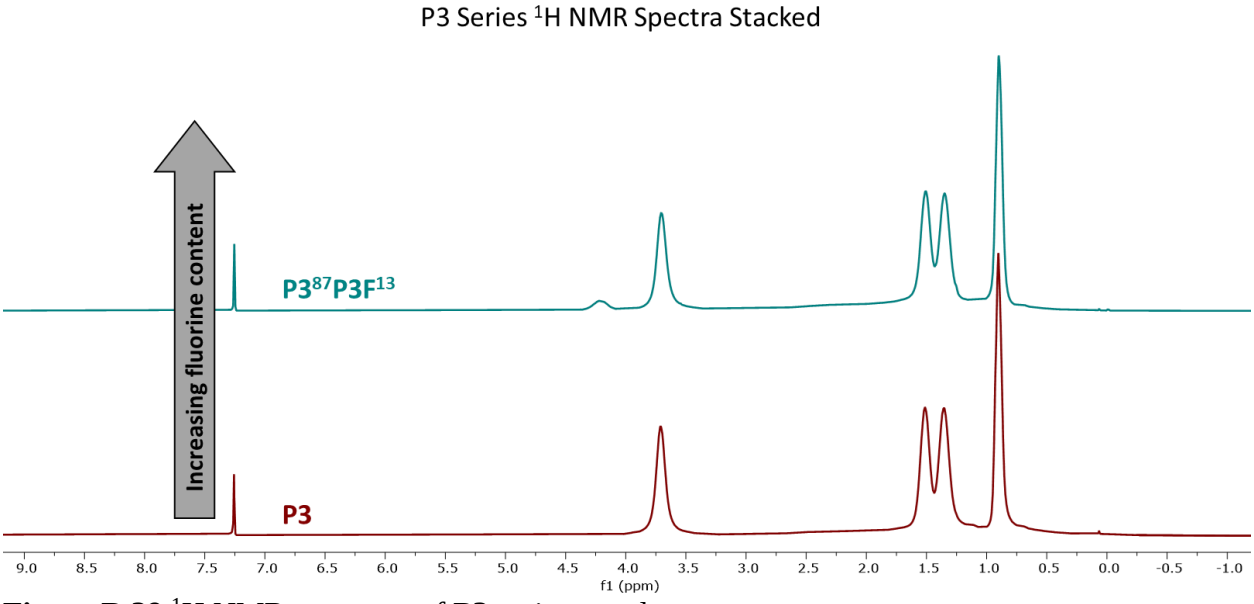


Figure B.29 [1]H NMR spectrum of **P3** series copolymers.

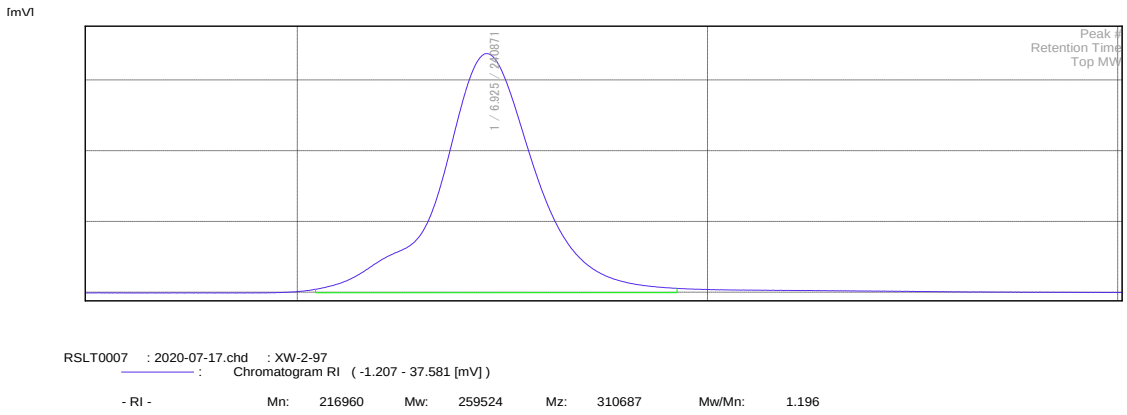


Figure B.30 GPC analysis of **P1**.

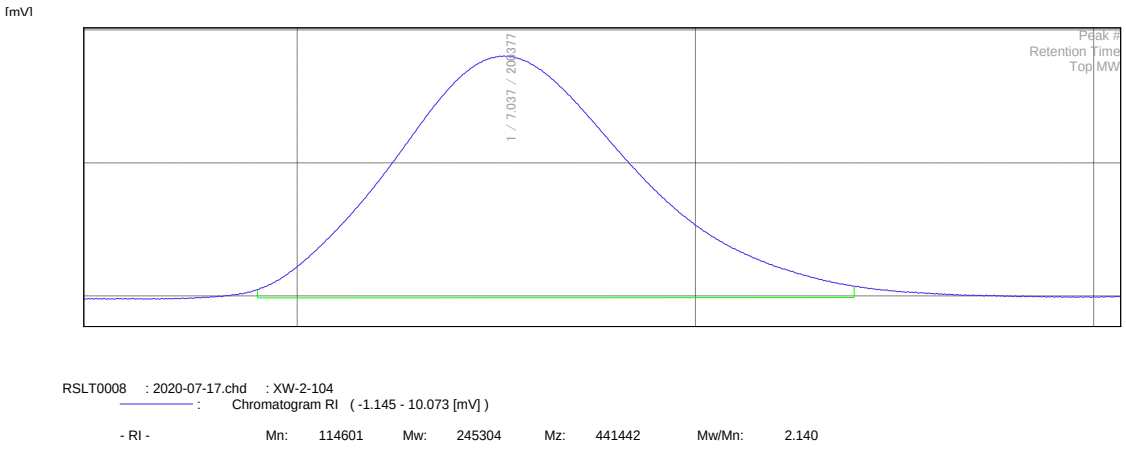


Figure B.31 GPC analysis of **P1^{84}P1F^{16}**.

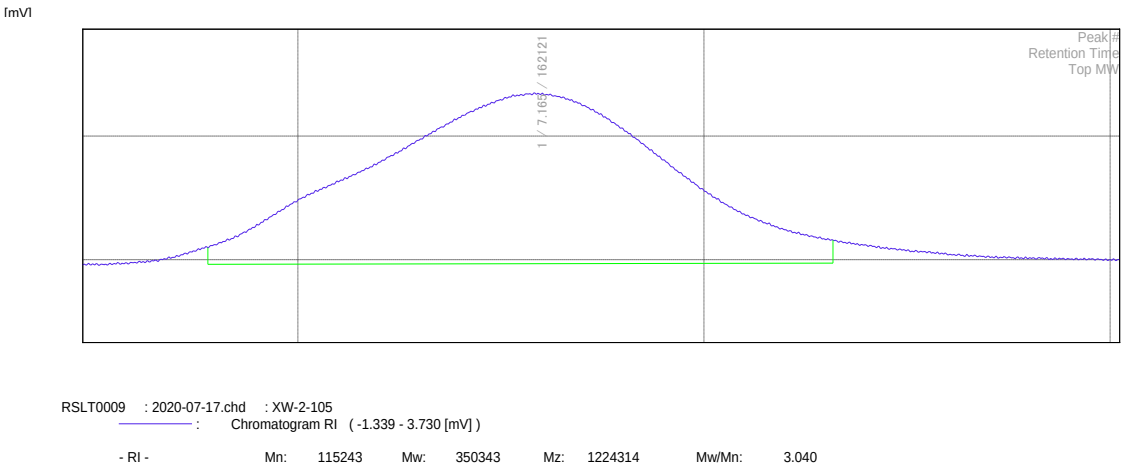


Figure B.32 GPC analysis of **P1^{67}P1F^{33}**.

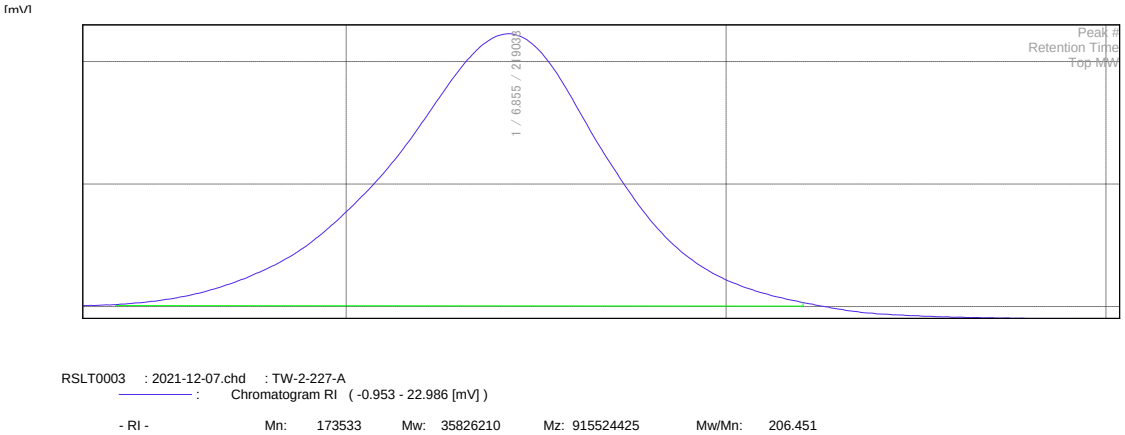


Figure B.33 GPC analysis of **P1^{48}P1F^{52}**. *NOTE: the high molar mass portion of this sample exceed the calibration standards used for this GPC and hence the molecular weight and dispersity values are likely inaccurate.*

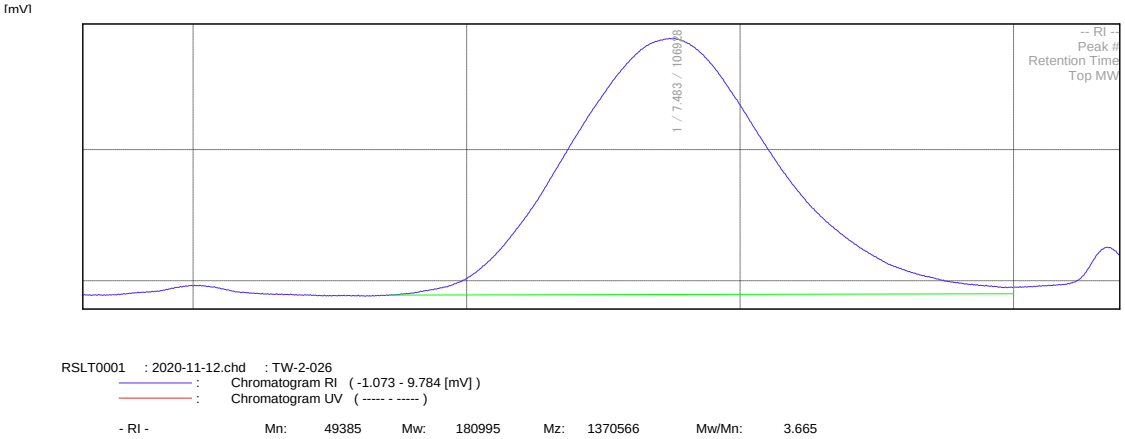


Figure B.34 GPC analysis of **P1F**.

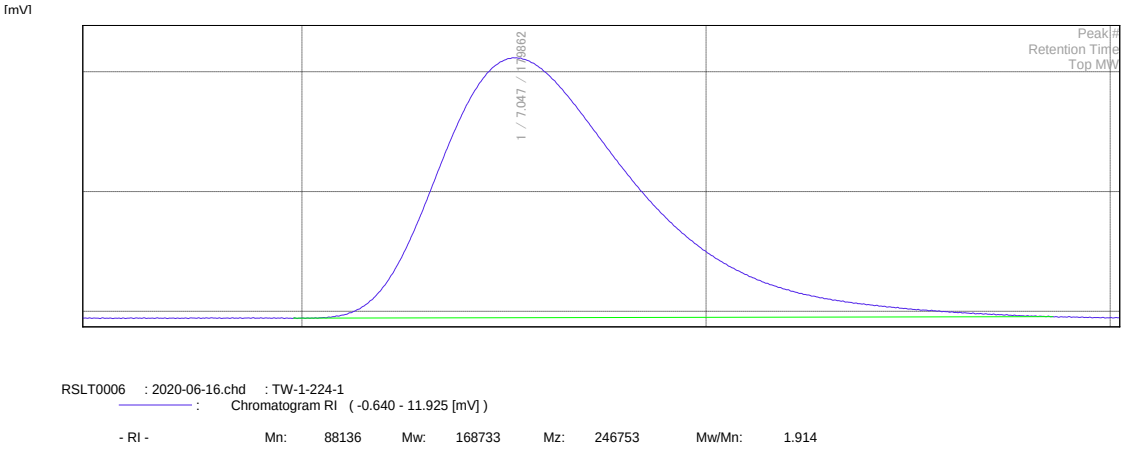


Figure B.35 GPC analysis of **P2**.

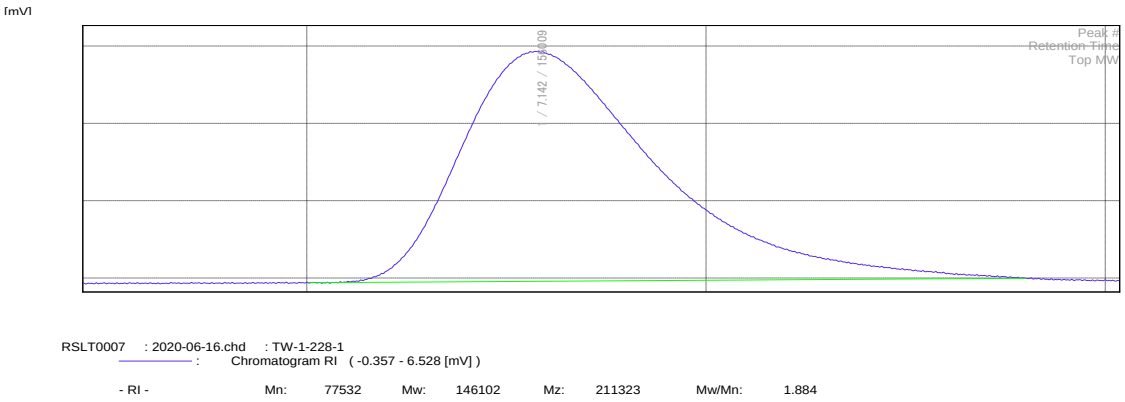


Figure B.36 GPC analysis of $\mathbf{P2^{87}P2F^{13}}$.

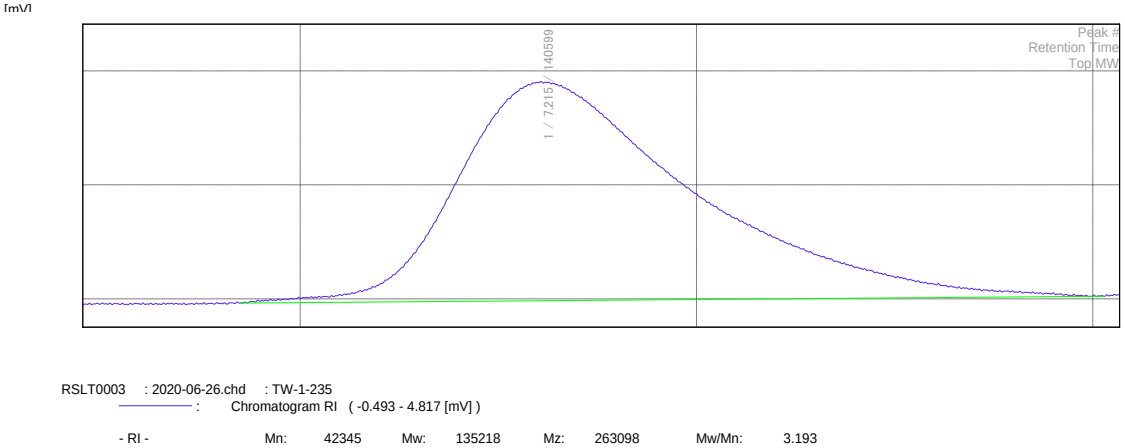


Figure B.37 GPC analysis of $\mathbf{P2^{72}P2F^{28}}$.

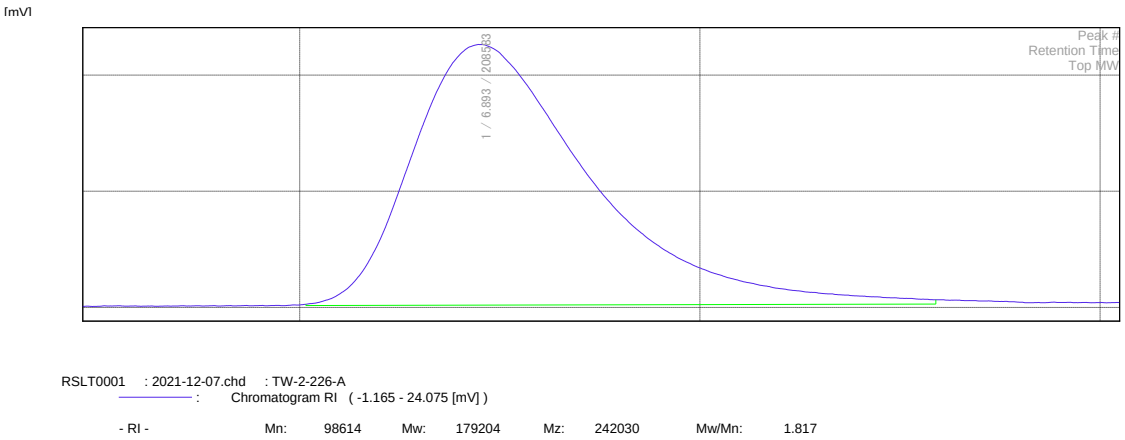


Figure B.38 GPC analysis of **P3**.

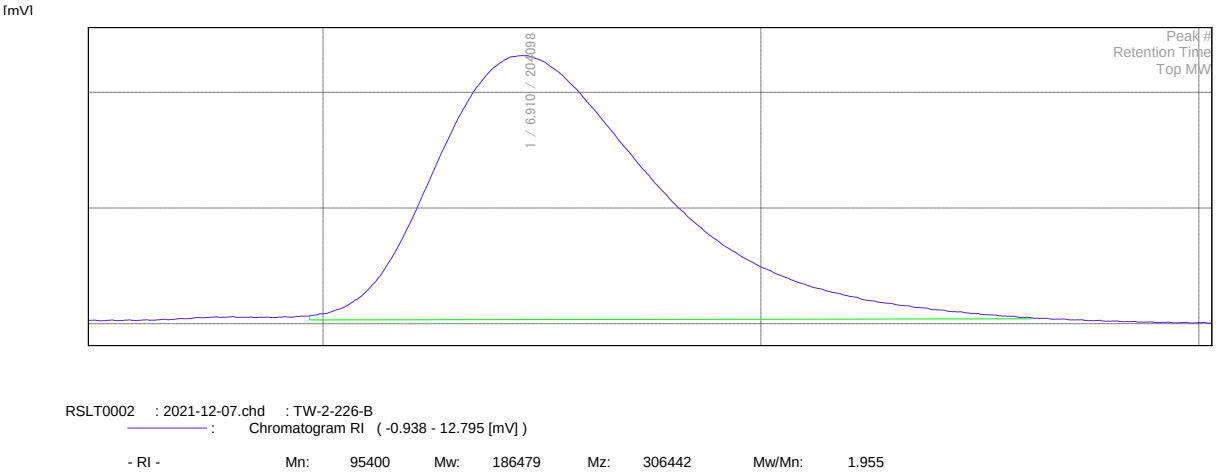


Figure B.39 GPC analysis of **P3^{87}P3F^{13}**.

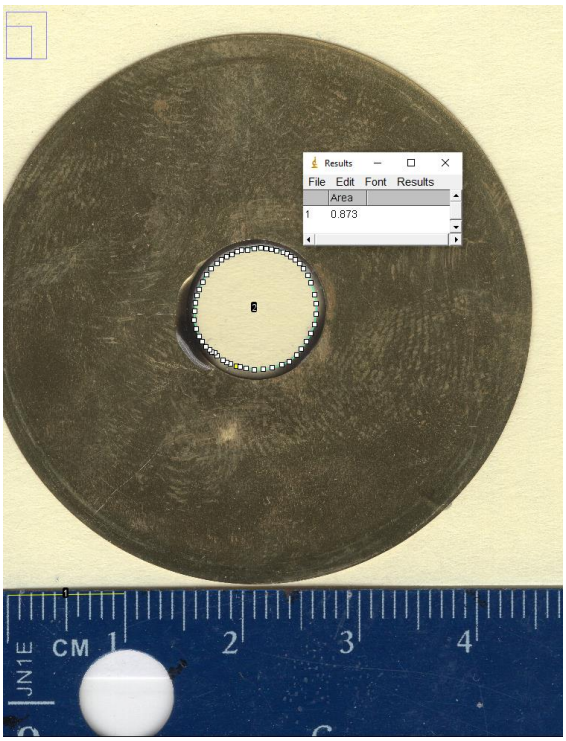


Figure B.40 Example surface area measurement of permeation sample using ImageJ.

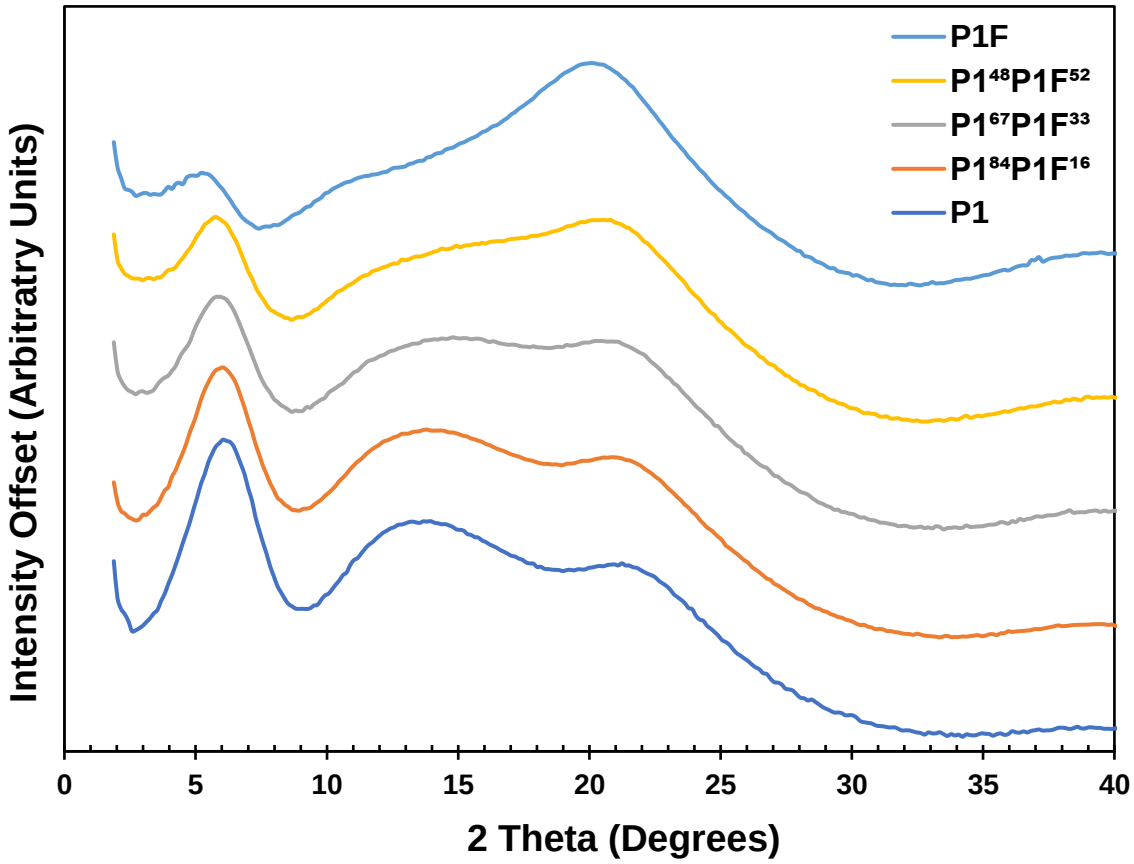


Figure B.41 WAXS spectra of the **P1/P1F** copolymer series.

Table B.1 Calculated *d*-spacing (d_B and d_{ic}) for **P1/P1F** copolymer series.

				d-spacing (Å)[a]		
Polymer	$(2\Theta_1)$(deg)	$(2\Theta_2)$(deg)	$(2\Theta_3)$(deg)	$(d_B/d_{ic})_1$	$(d_B/d_{ic})_2$	$(d_B/d_{ic})_3$
P1	6.13	13.78	21.23	14.4/17.6	6.4/7.8	4.2/5.1
P1^{84}P1F^{16}	6.05	13.78	20.92	14.6/17.8	6.4/7.8	4.2/5.1
P1^{67}P1F^{33}	5.85	13.81	20.53	15.1/18.4	6.4/7.8	4.3/5.2
P1^{48}P1F^{52}	5.76	-	20.37	15.3/18.7	-	4.3/5.3
PF1	5.29	-	20.06	16.7/20.4	-	4.4/5.4

[a]Measured using WAXS and d_B is calculated using Bragg's Law (Eq. 4) while d_{ic} is calculated using the correction factor expressed in Eq. 5

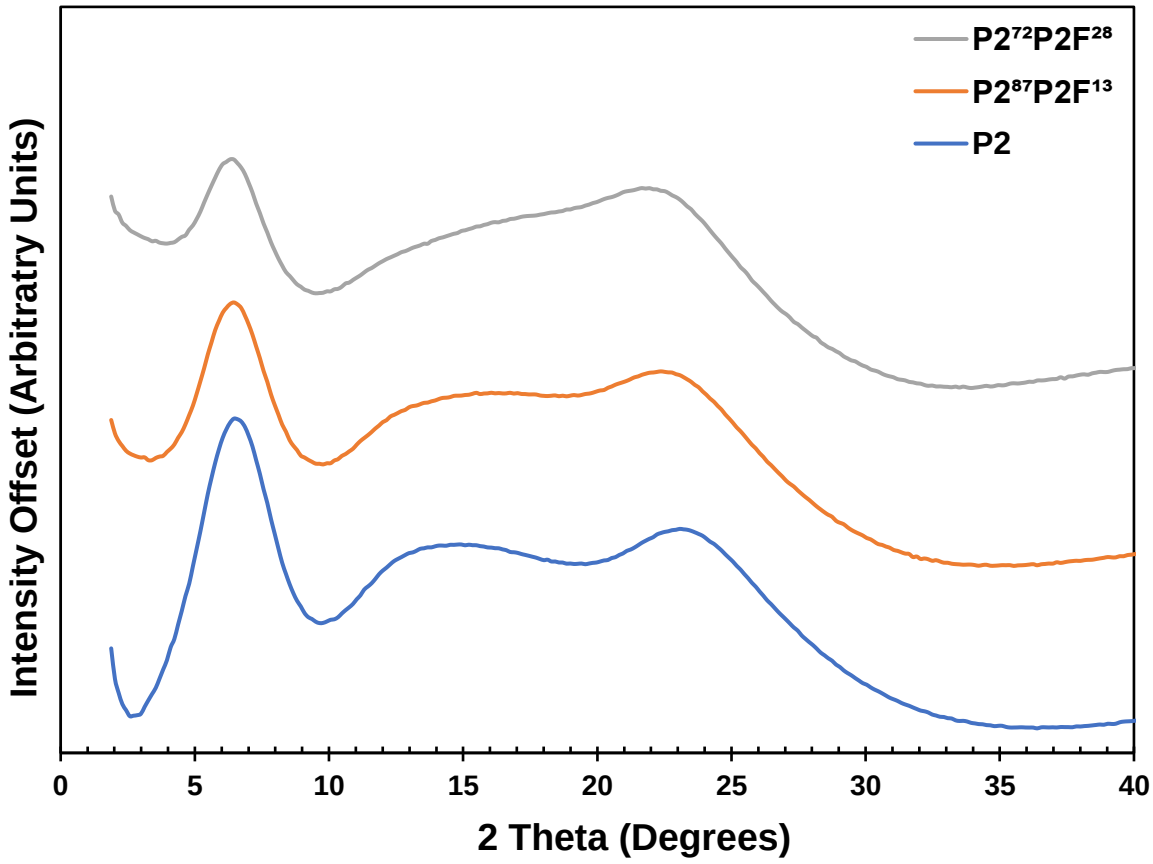


Figure B.42 WAXS spectra of the **P2/P2F** copolymer series.

Table B.2 Calculated *d*-spacing (d_B and d_{ic}) for **P2/P2F** copolymer series.

				d-spacing (Å)[a]		
Polymer	$(2\Theta_1)$(deg)	$(2\Theta_2)$(deg)	$(2\Theta_3)$(deg)	$(d_B/d_{ic})_1$	$(d_B/d_{ic})_2$	$(d_B/d_{ic})_3$
P2	6.54	14.87	32.09	13.5/16.5	5.9/7.2	3.8/4.7
P2^{87}P2F^{13}	6.42	-	22.41	13.7/16.8	-	3.9/4.8
P2^{72}P2F^{28}	6.38	-	21.81	13.8/16.9	-	4.1/4.9

[a]Measured using WAXS and d_B is calculated using Bragg's Law (Eq. 4) while d_{ic} is calculated using the correction factor expressed in Eq. 5

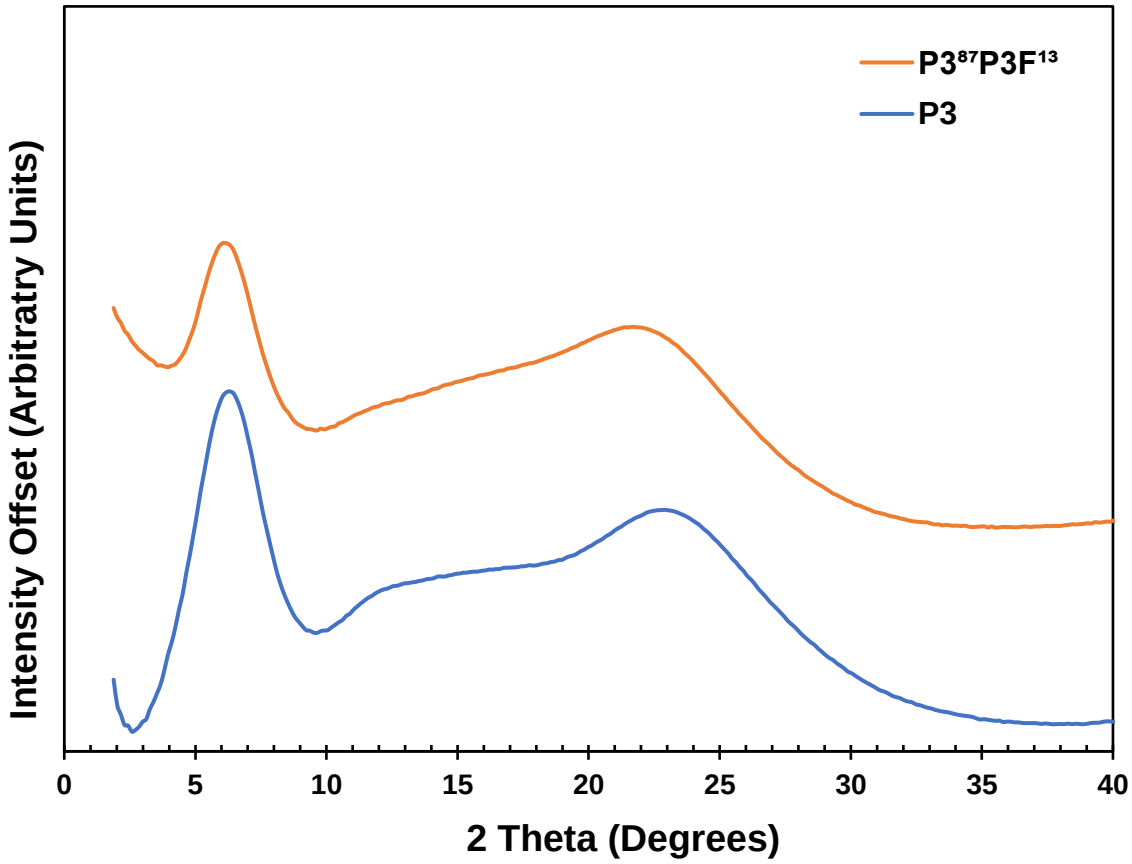


Figure B.43 WAXS spectra of the **P3/P3F** copolymer series.

Table B.3 Calculated *d*-spacing (d_B and d_{ic}) for the **P3/P3F** copolymer series.

				d-spacing (Å)[a]		
Polymer	$(2\Theta_1)$(deg)	$(2\Theta_2)$(deg)	$(2\Theta_3)$(deg)	$(d_B/d_{ic})_1$	$(d_B/d_{ic})_2$	$(d_B/d_{ic})_3$
P2	6.28	-	22.84	14.1/17.1	-	3.9/4.7
P3[87]P3F[13]	6.12	-	21.67	14.4/17.6	-	4.1/5.0

[a]Measured using WAXS and d_B is calculated using Bragg's Law (Eq. 4) while d_{ic} is calculated using the correction factor expressed in Eq. 5

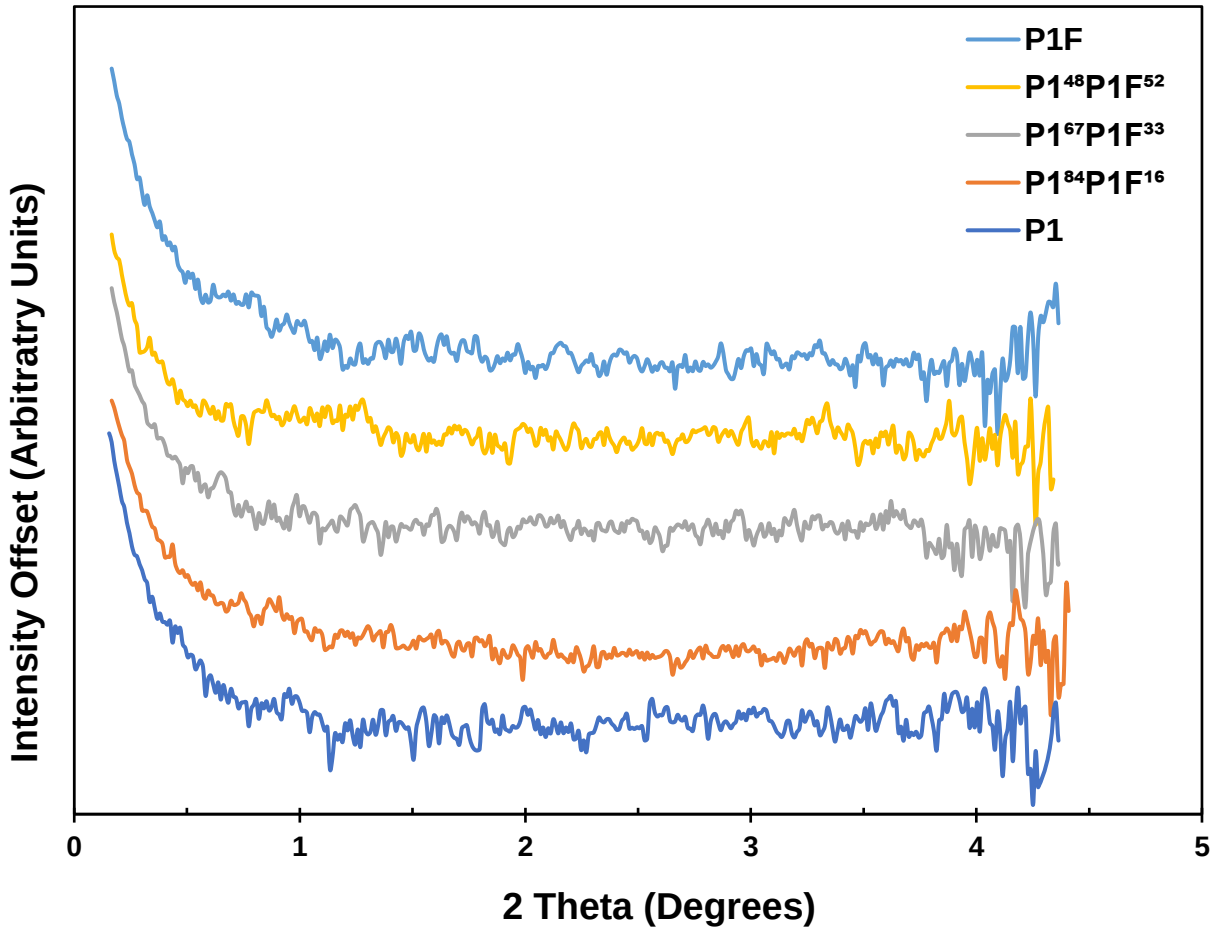


Figure B.44 SAXS spectra of the **P1/P1F** copolymer series.

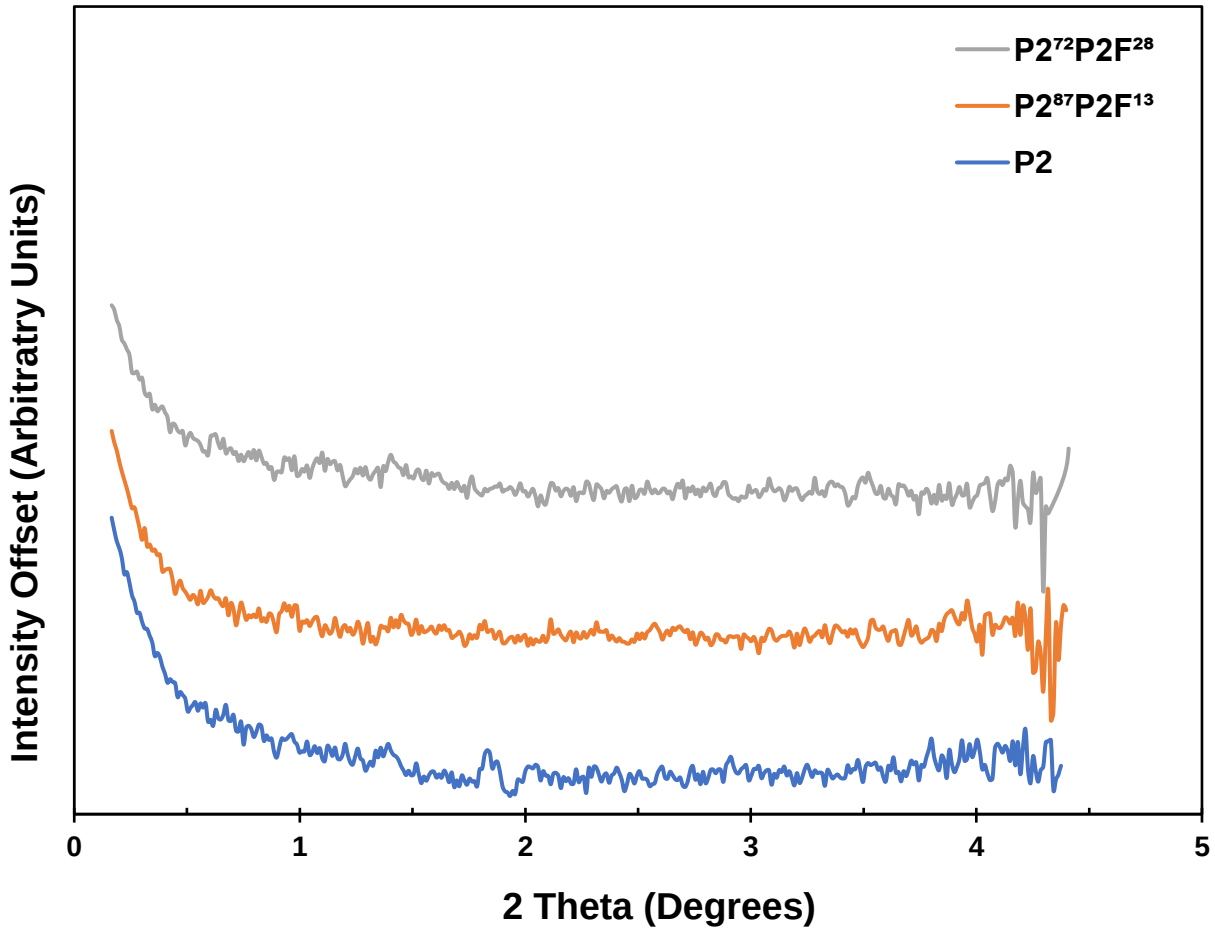


Figure B.45 SAXS spectra of the **P2/P2F** copolymer series.

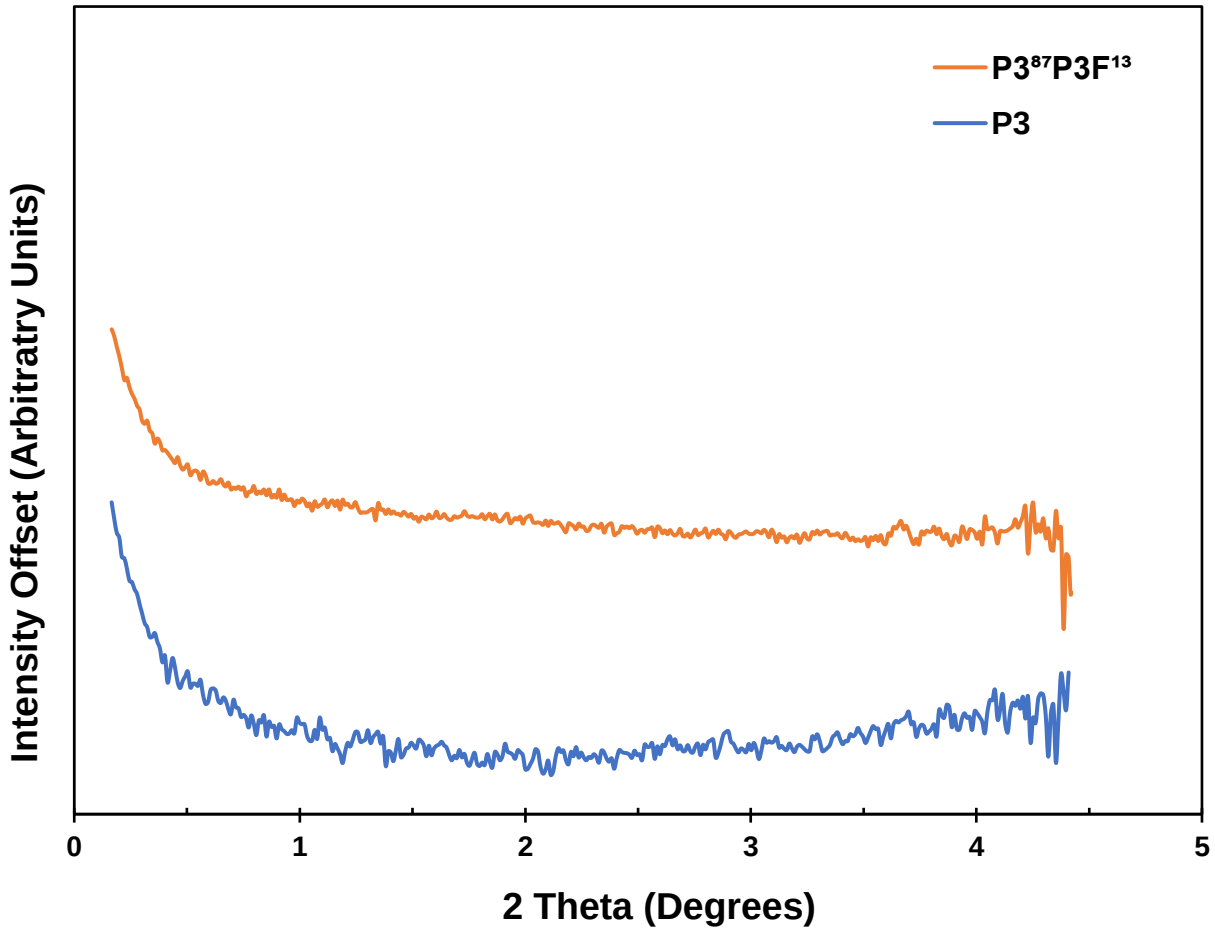


Figure B.46 SAXS spectra of the **P3/P3F** copolymer series.

Appendix C Supporting Information for Chapter 4

Table C.1 T_g, T_d, and service window of substituted APNB derivatives and unsubstituted PNB.

Entry	polymer	T_g (°C)[a]	T_d (°C)[b]	service window (T_d-T_g, °C)
1	**P1**	280	380	100
2	**P2**	209	377	168
3	**P3**	190	389	199
4	**P4**	119	381	262
5	**P5**	193	387	194
6	**P6**	184	316	132
7	**P2^{75}P4^{25}**	182	379	197
8	**P2^{50}P4^{50}**	150	378	228
9	**P2^{25}P4^{75}**	132	381	249
10	**P2^{68}P5^{32}**	206	382	176
11	**P2^{44}P5^{56}**	202	384	182
12	**P2^{15}P5^{85}**	197	386	189
13	**P2^{86}P6^{14}**	202	347	145
14	**P2^{65}P6^{35}**	191	327	136
15	**P2^{28}P6^{72}**	191	323	132
16	**PNB**[c]	380-390	415	~30

[a]T_g determined via DMA (tan δ). [b]T_d defined as the temperature at 5% mass loss. [c]Data was obtained from references 3 and 15.

Table C.2 T_g, T_d, and service window of substituted APNB derivatives and unsubstituted PNB.

Entry	polymer	M_n (KDa)[a]	T_g (°C)[b]
1	**P2**	64	208
2	**P2**	84	209
3	**P2**	170	211
4	**P2**	207	207
5	**P4**	92	114
6	**P4**	97	117
7	**P4**	129	119
8	**P5**	64	194
16	**P5**	89	193

[a]Molecular weights were measured using gel permeation chromatography at 40 °C in THF, and are reported relative to polystyrene standards. [b]T_g determined via DMA (tan δ).

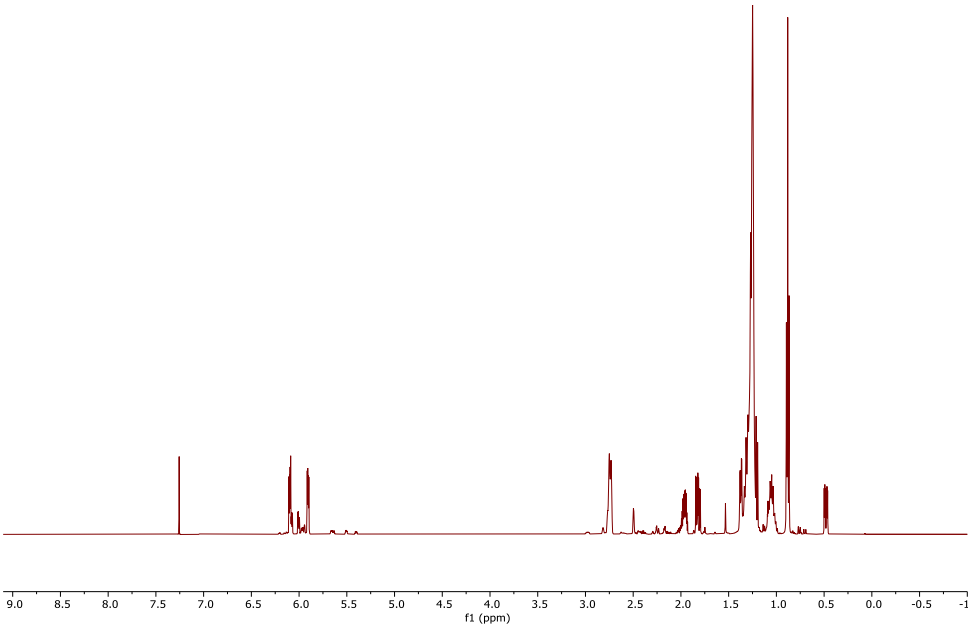


Figure C.1 ^{1}H NMR spectrum of monomer **M3**.

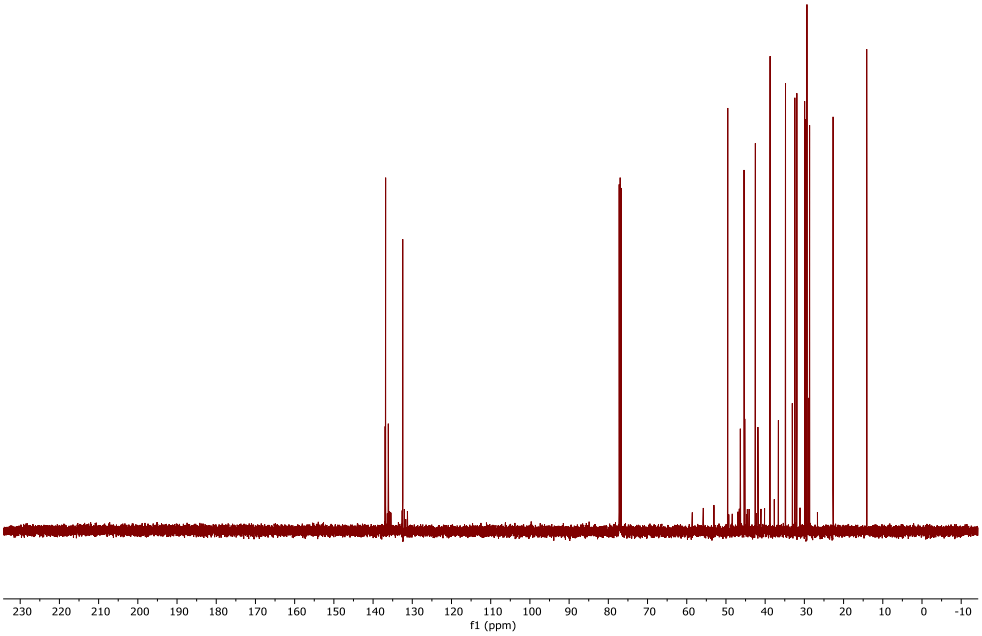


Figure C.2 ^{13}C NMR spectrum of monomer **M3**.

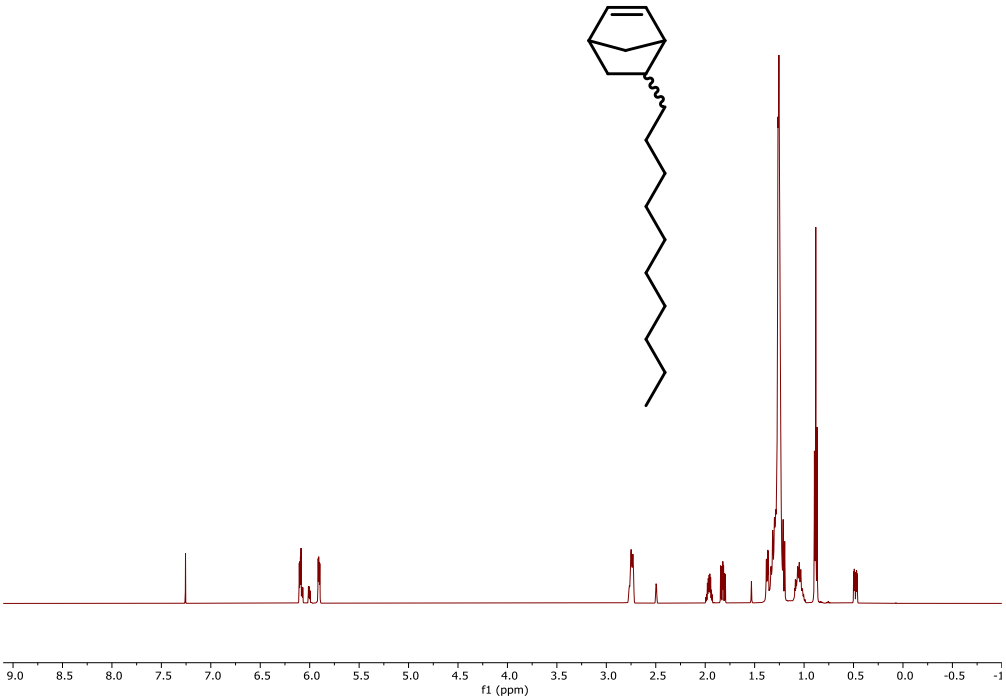


Figure C.3 ^{1}H NMR spectrum of monomer **M4**.

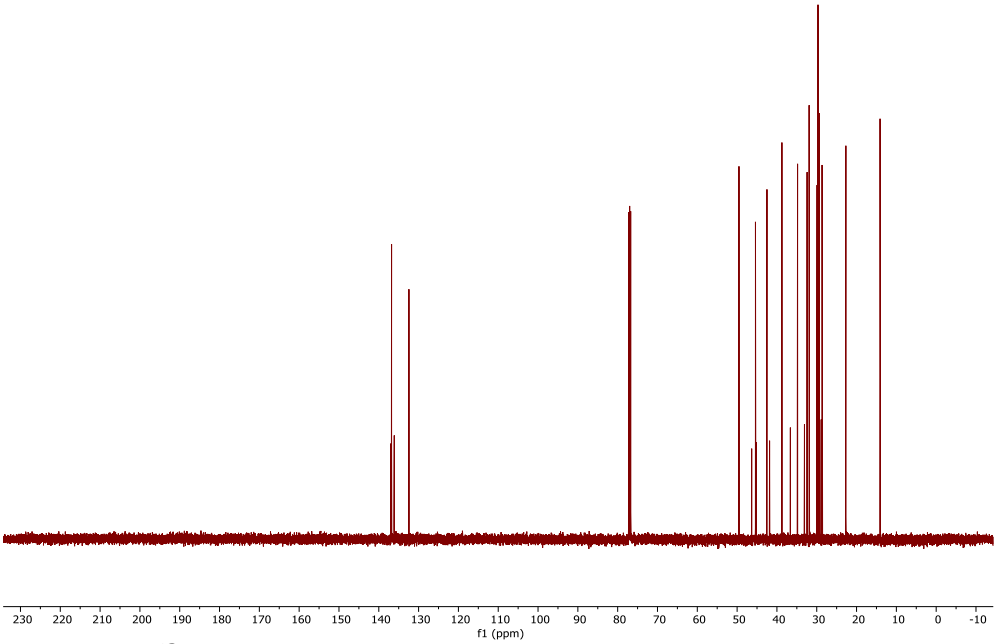


Figure C.4 ^{13}C NMR spectrum of monomer **M4**.

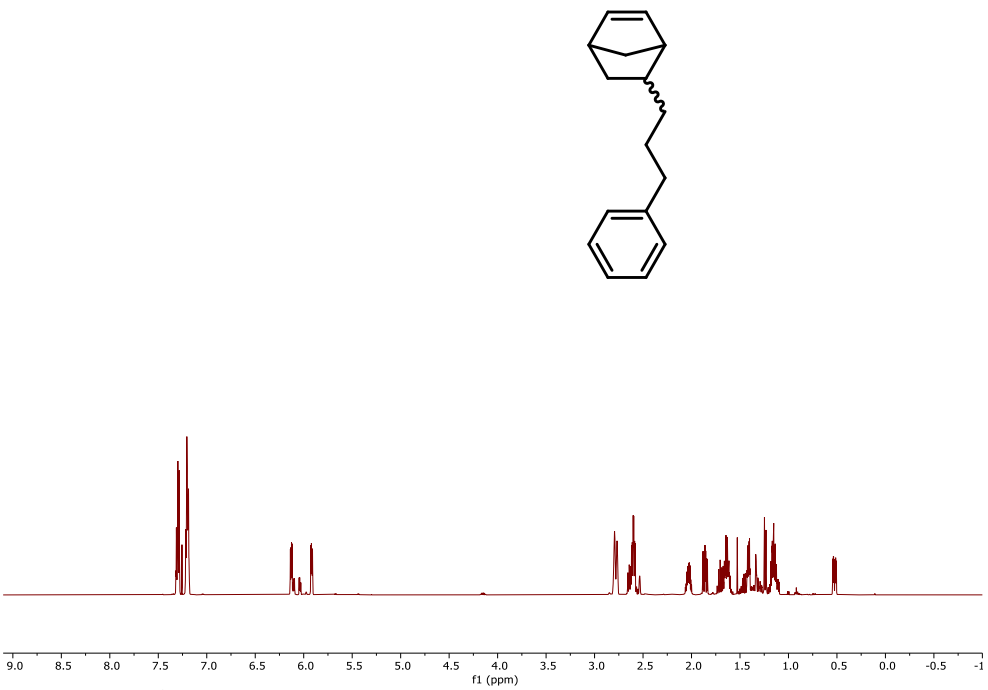


Figure C.5 ^{1}H NMR spectrum of monomer **M5**.

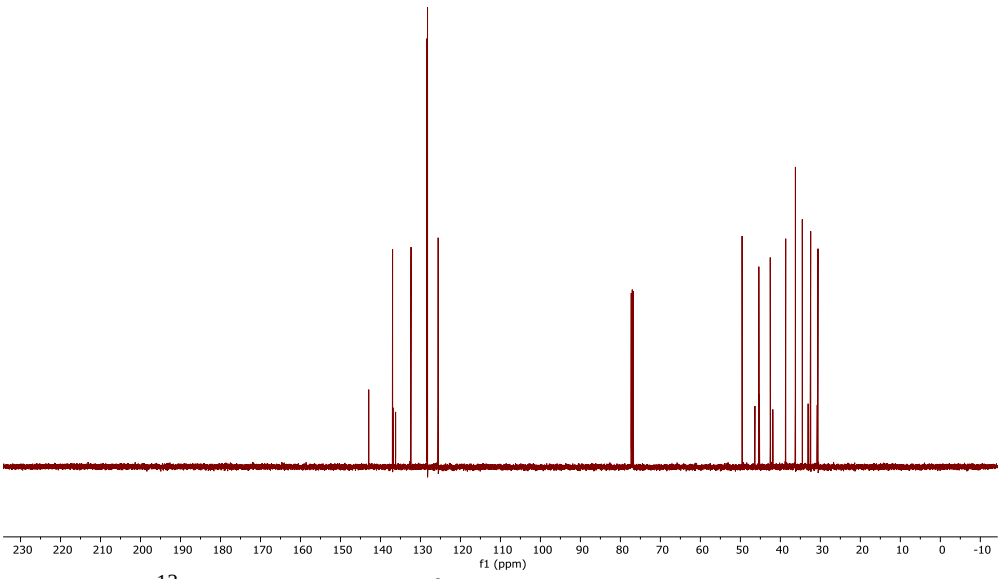


Figure C.6 ^{13}C NMR spectrum of monomer **M5**.

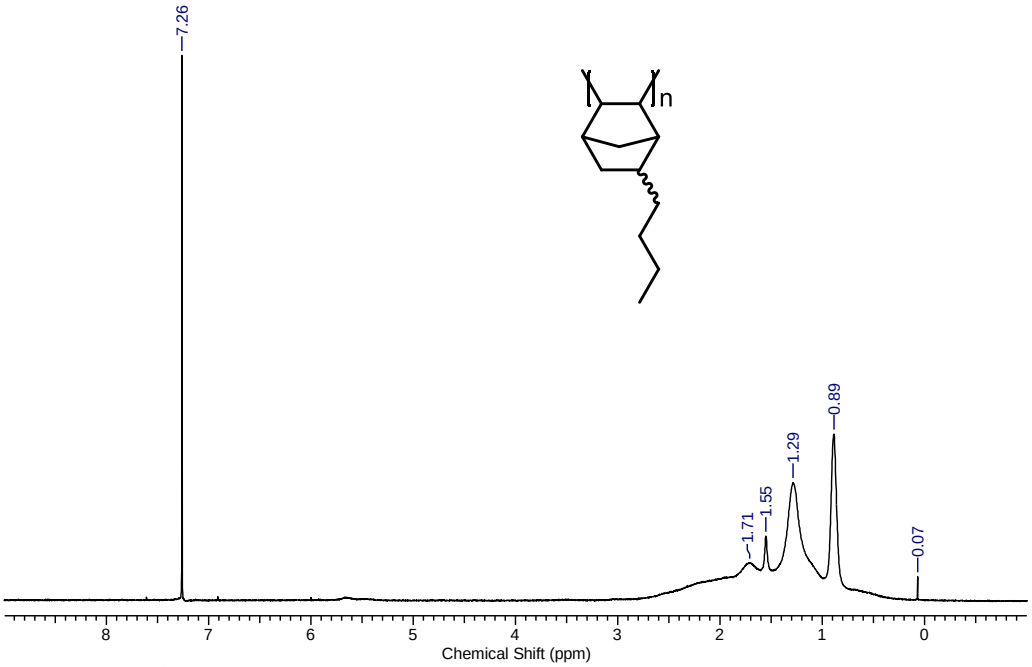


Figure C.7 ^{1}H NMR spectrum of polymer **P1**.

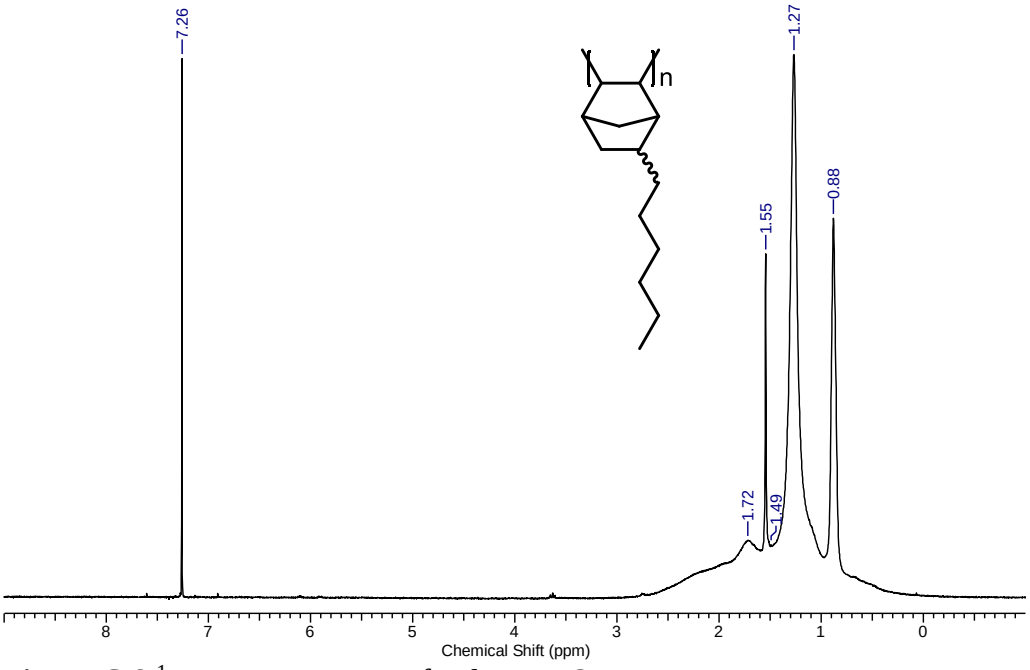


Figure C.8 ^{1}H NMR spectrum of polymer **P2**.

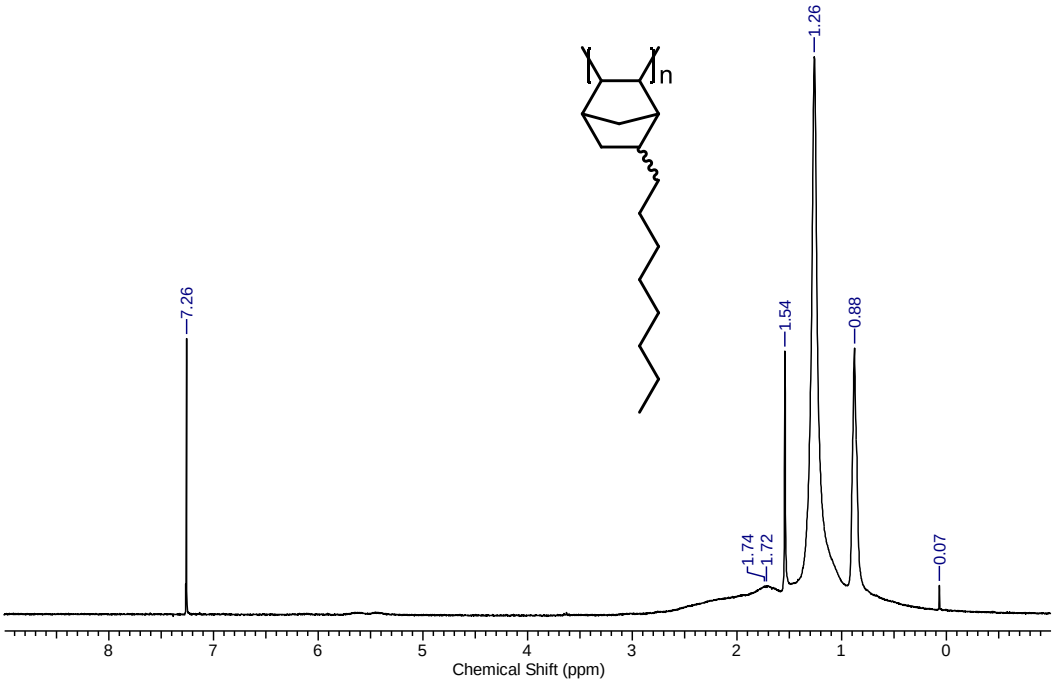


Figure C.9 ^{1}H NMR spectrum of polymer **P3**.

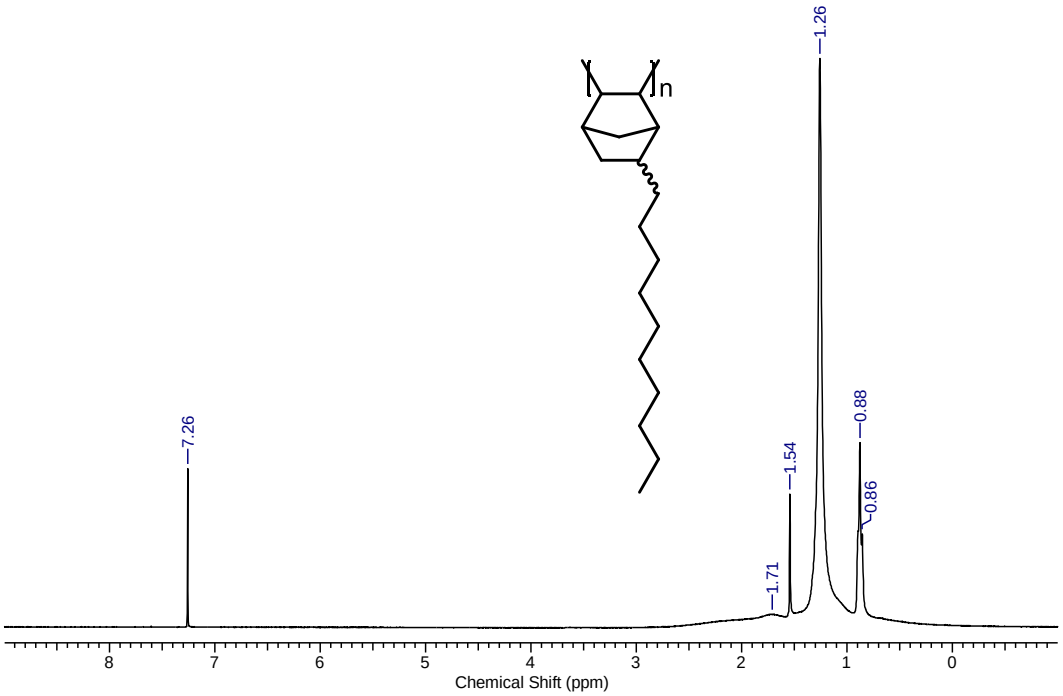


Figure C.10 ^{1}H NMR spectrum of polymer **P4**.

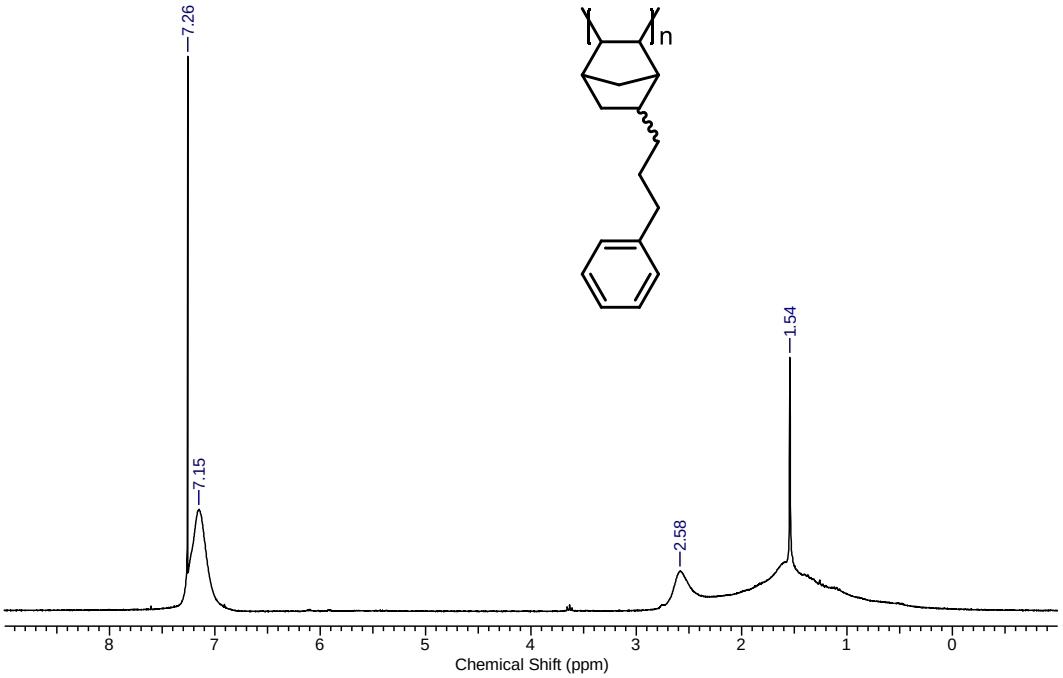


Figure C.11 ^{1}H NMR spectrum of polymer **P5**.

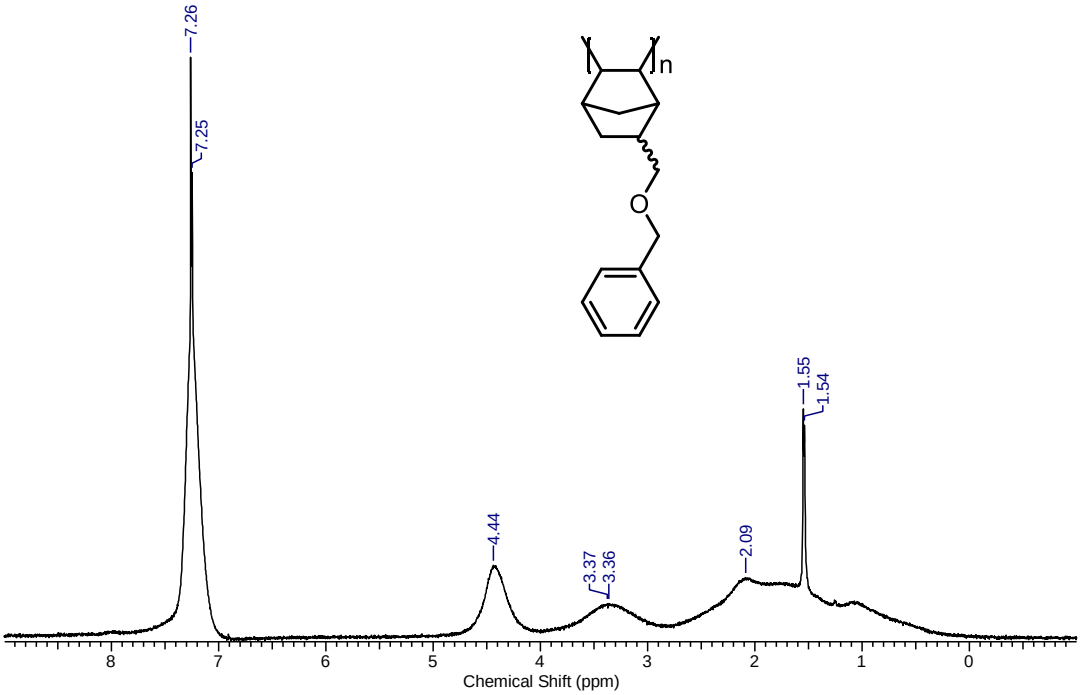


Figure C.12 ^{1}H NMR spectrum of polymer **P6**.

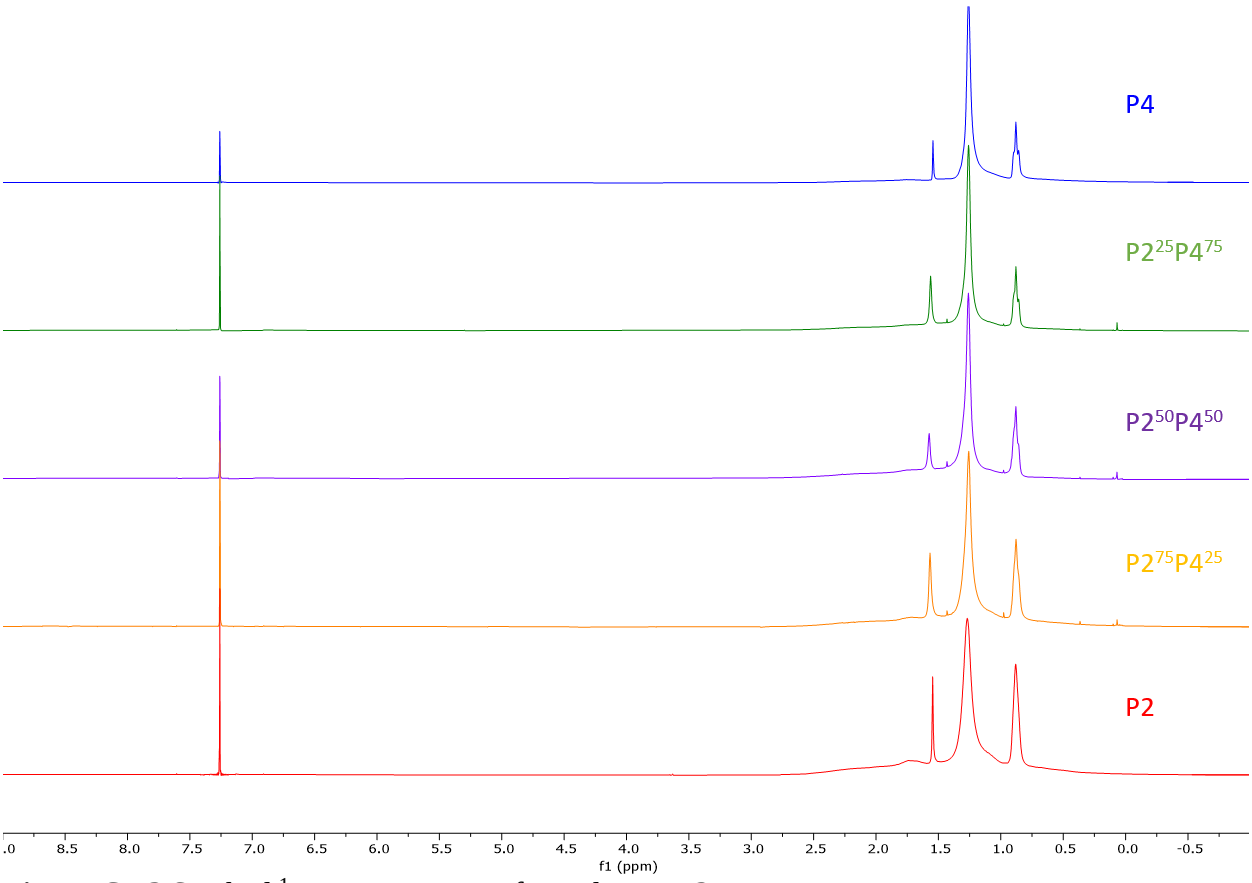


Figure C.13 Stacked ^{1}H NMR spectra of copolymer **P2P4** series. Monomer incorporation was not determine due to significant overlap of all peaks in the alkyl region. Thus, the superscript represents the theoretical monomer incorporation based upon feed ratios.

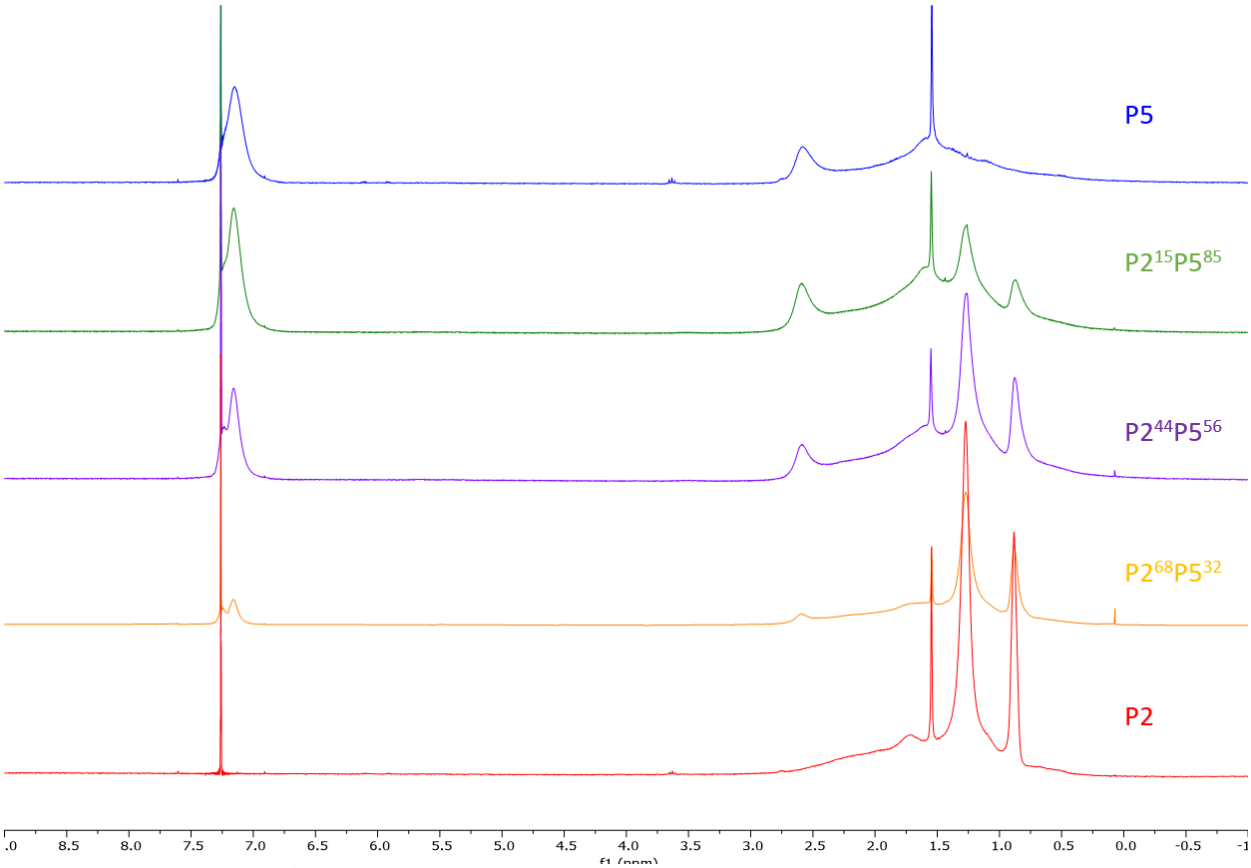


Figure C.14 Stacked ^{1}H NMR spectra of copolymer **P2P5** series. Resonances at 1.27 and 0.88 ppm correspond to the aliphatic protons in the alkyl pendant group of monomer **M2**, while the resonances at 7.23, 7.15 and 2.59 ppm correspond to the phenyl and benzylic protons of the phenylpropyl pendant group of monomer **M5**. Incorporation ratios were determined based upon integration the benzylic proton resonances (2.59 ppm) to all remaining protons in the alkyl region.

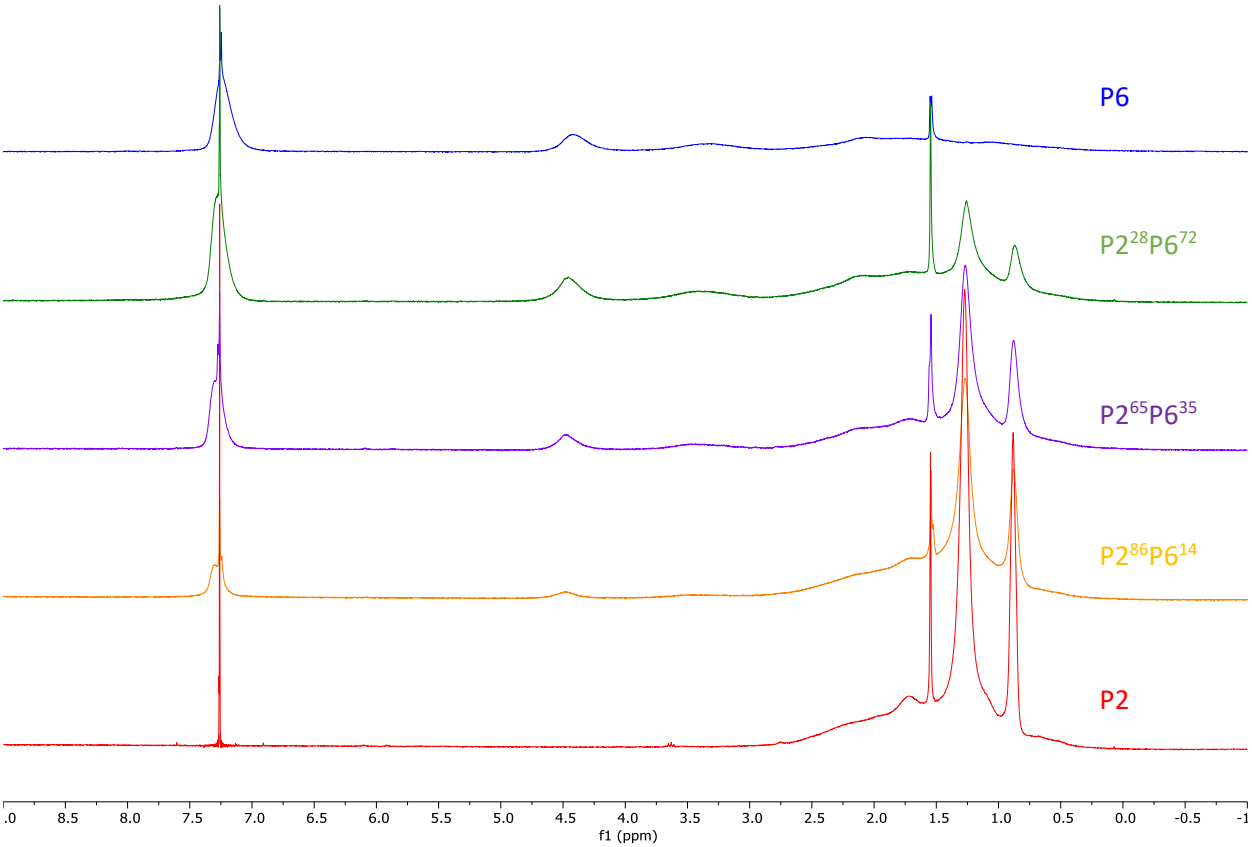


Figure C.15 Stacked ^{1}H NMR spectra of copolymer **P2P6** series. Resonances at 1.27 and 0.88 ppm correspond to the aliphatic protons on the alkyl pendant group of monomer **M2**, while the resonances at 7.25, 4.49 and 3.42 ppm correspond to the phenyl, benzylic, and ethereal protons of the benzyloxymethyl pendant group of monomer **M6**. Incorporation ratios were determined based upon the integration the benzylic proton resonance (4.49 ppm) to all remaining protons in the alkyl region.

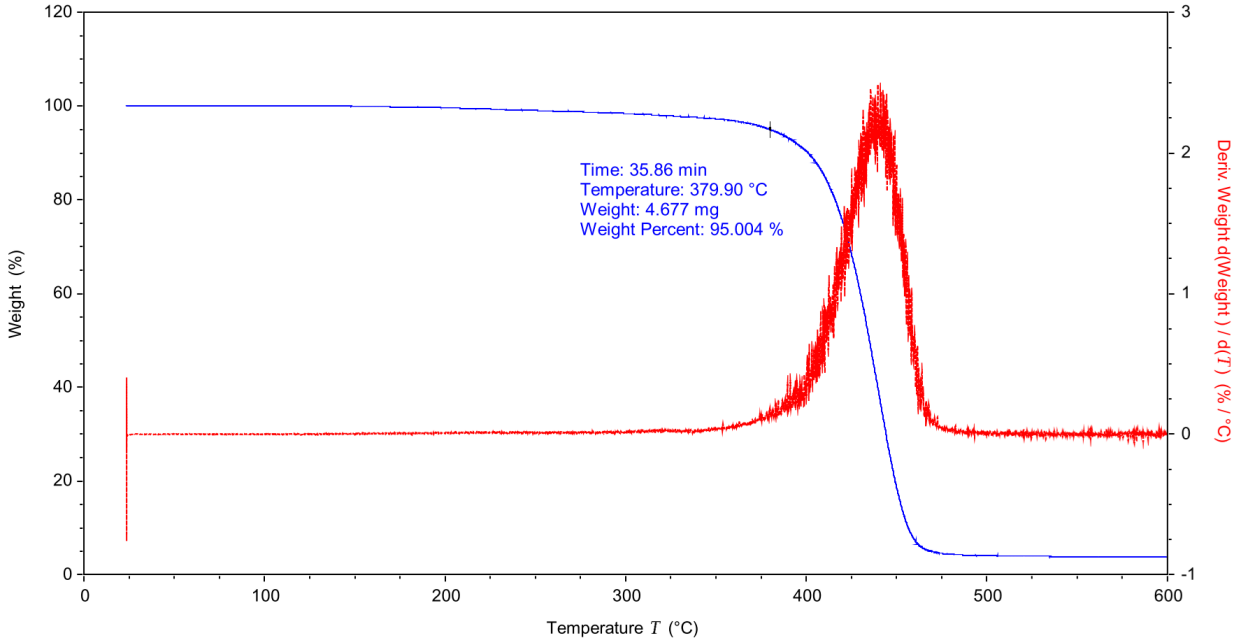


Figure C.16 TGA analysis of polymer **P1**.

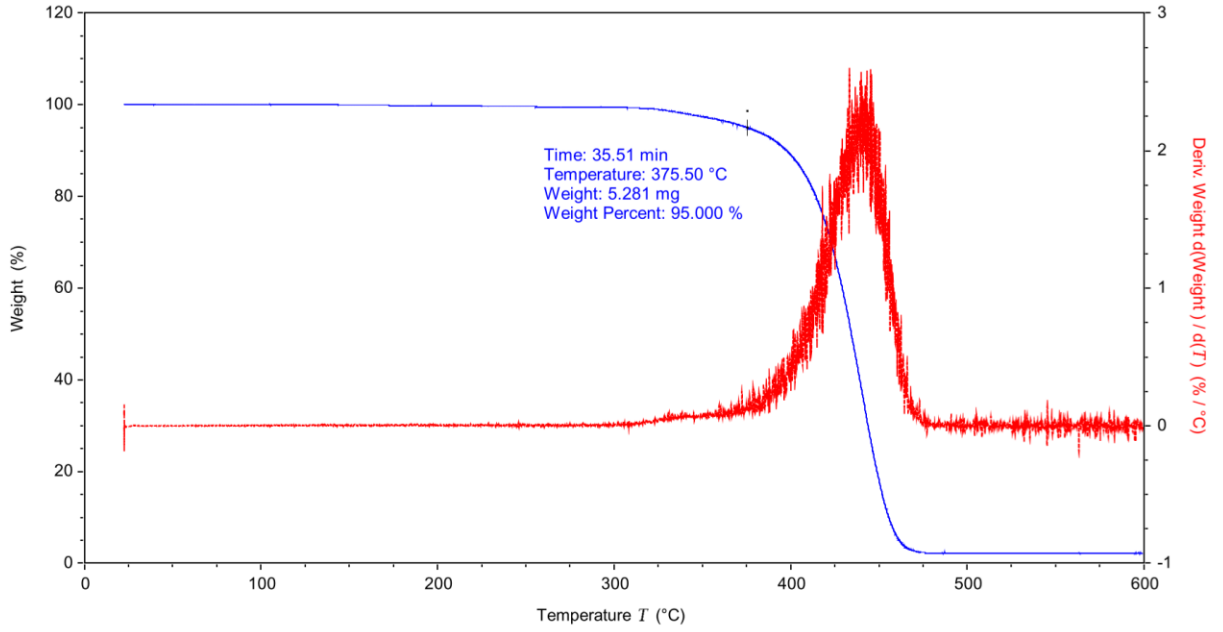


Figure C.17 TGA analysis of polymer **P2**.

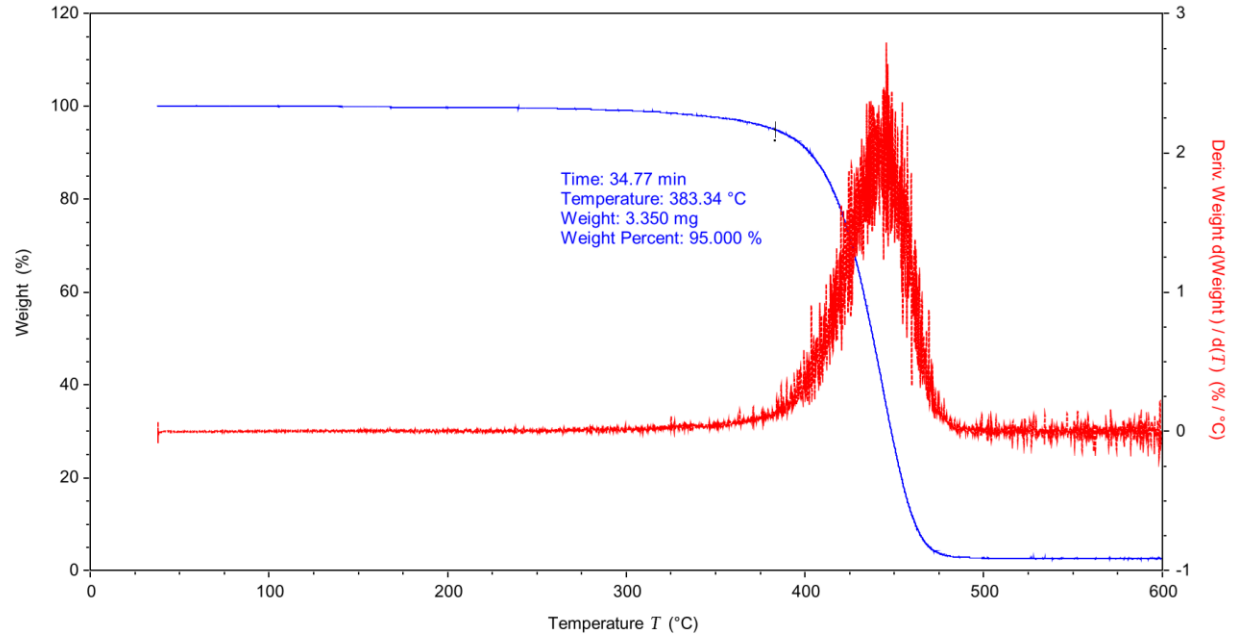


Figure C.18 TGA analysis of polymer **P3**.

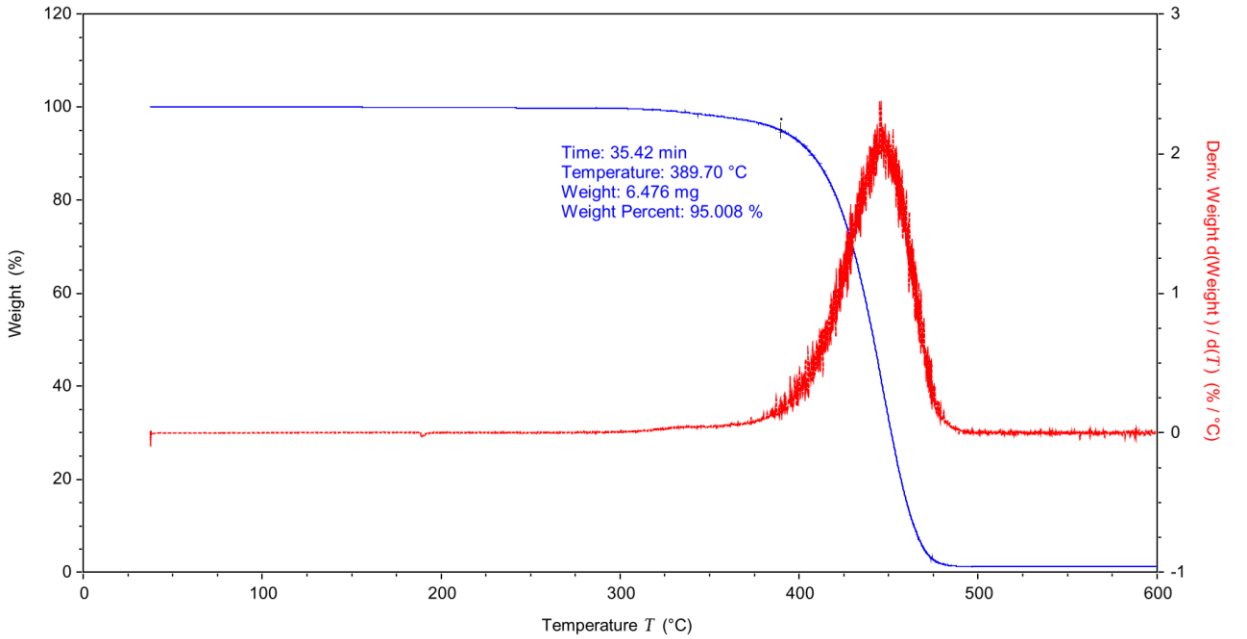


Figure C.19 TGA analysis of polymer **P4**.

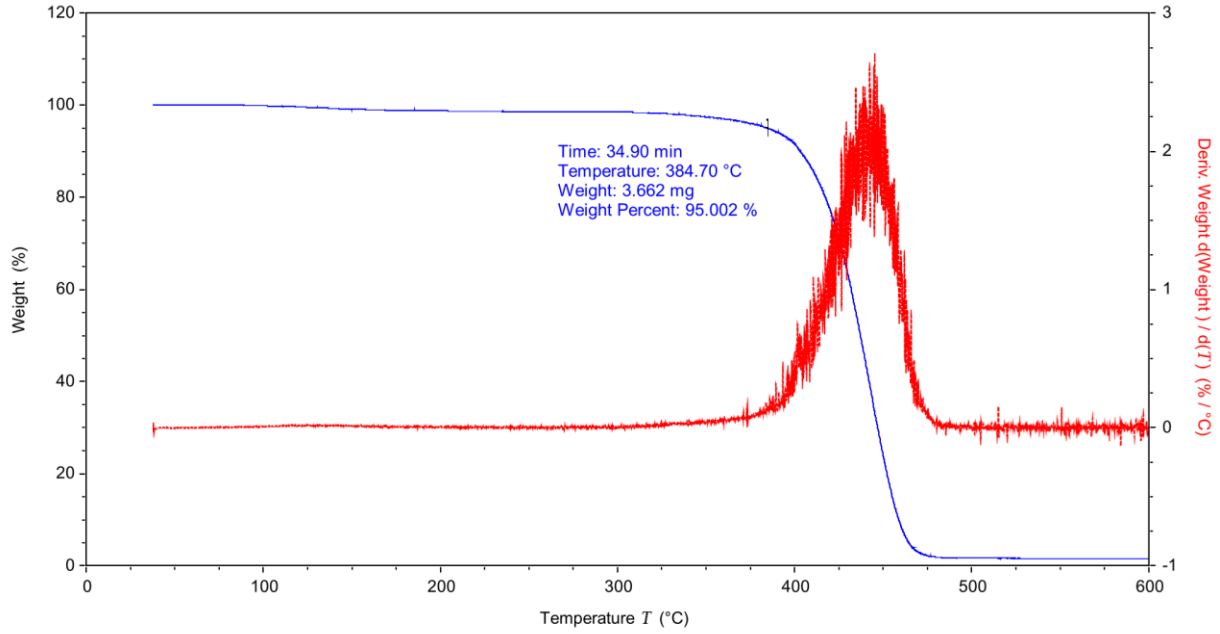


Figure C.20 TGA analysis of polymer **P5**.

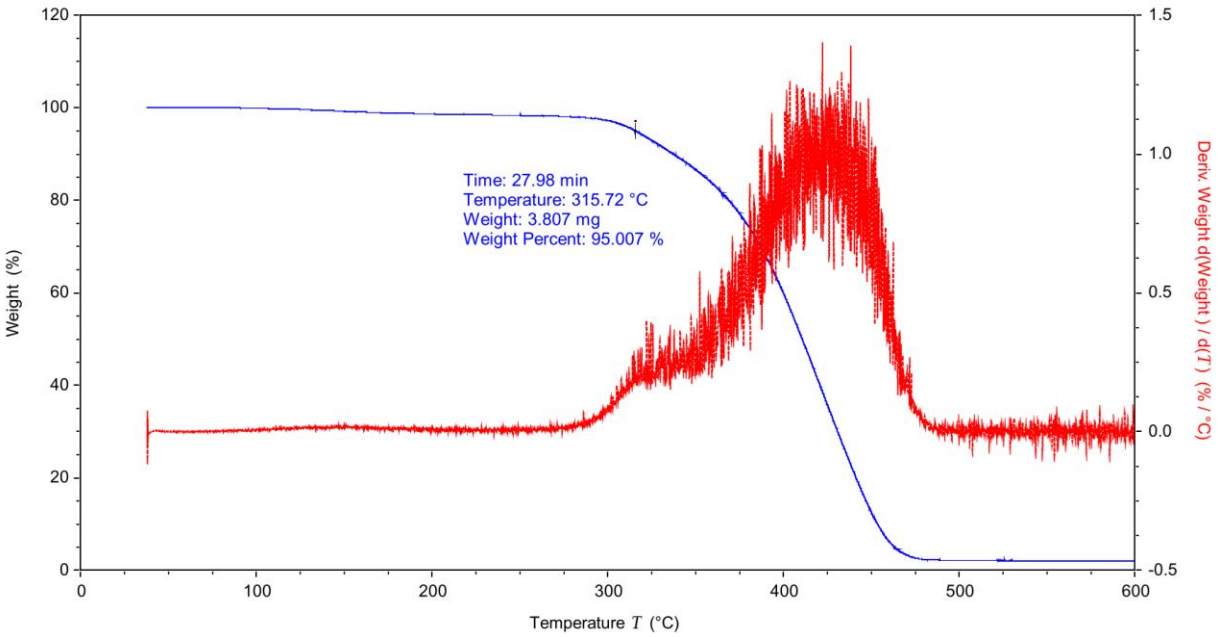


Figure C.21 TGA analysis of polymer **P6**. First derivative of weight loss versus temperature have two peaks, indicating the side group decompose before the decomposing of the polymer backbone, resulting in a depressed T_d.

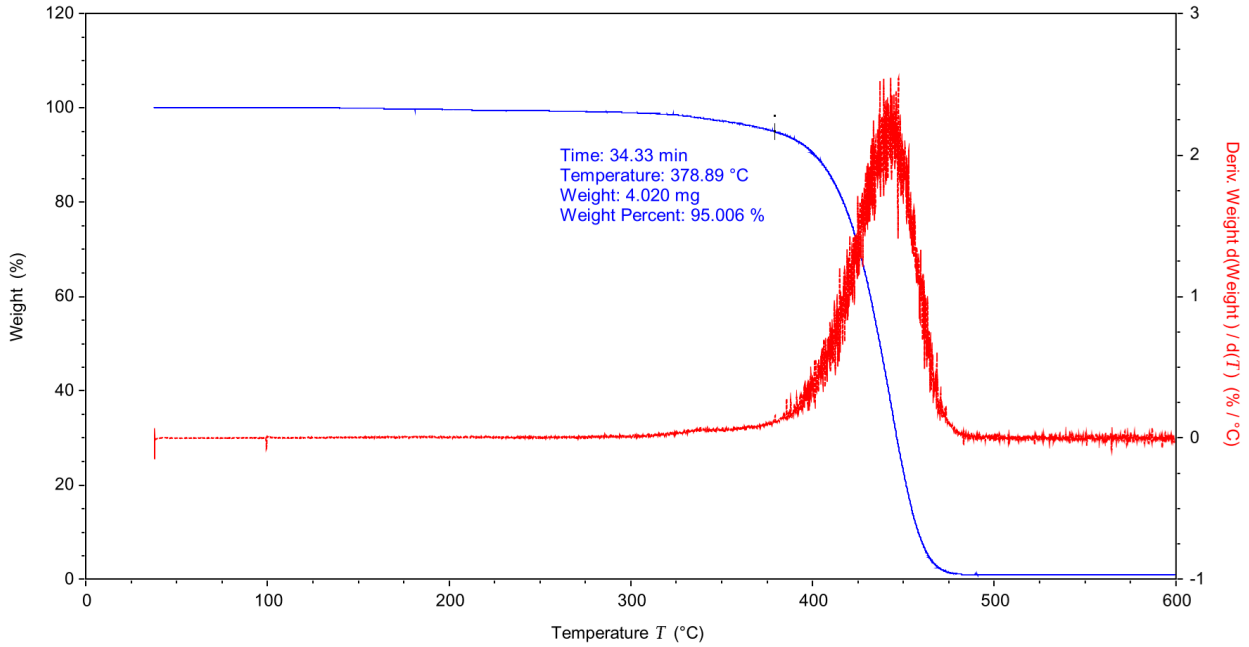


Figure C.22 TGA analysis of polymer $\mathbf{P2^{75}P4^{25}}$.

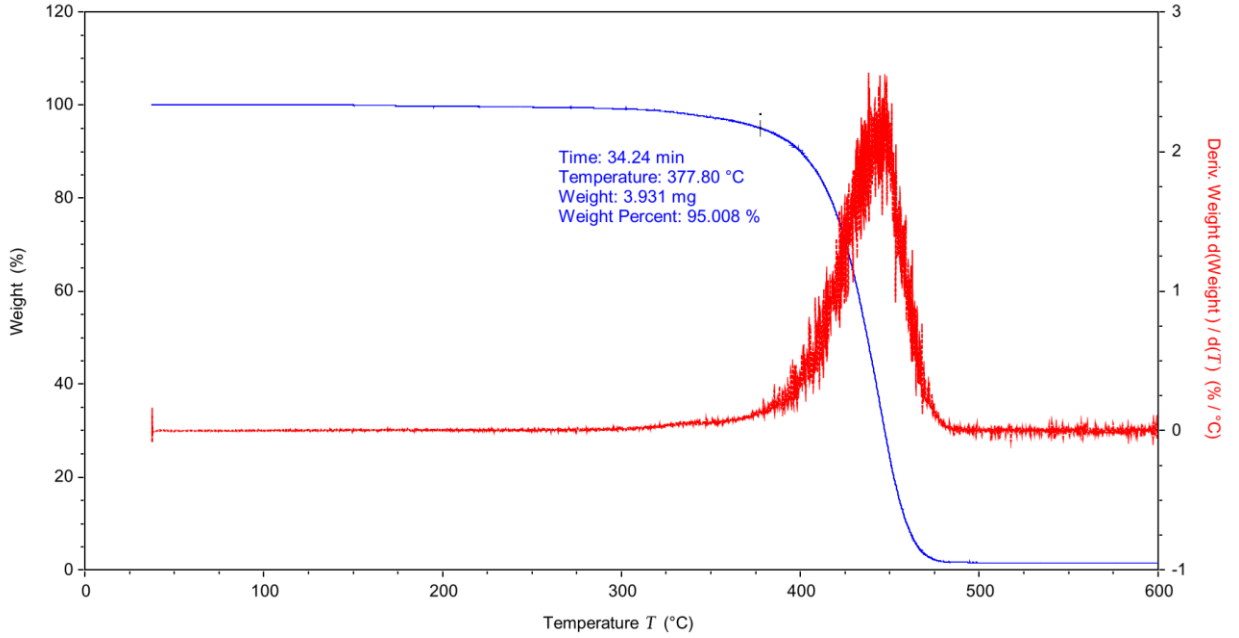


Figure C.23 TGA analysis of polymer $\mathbf{P2^{50}P4^{50}}$.

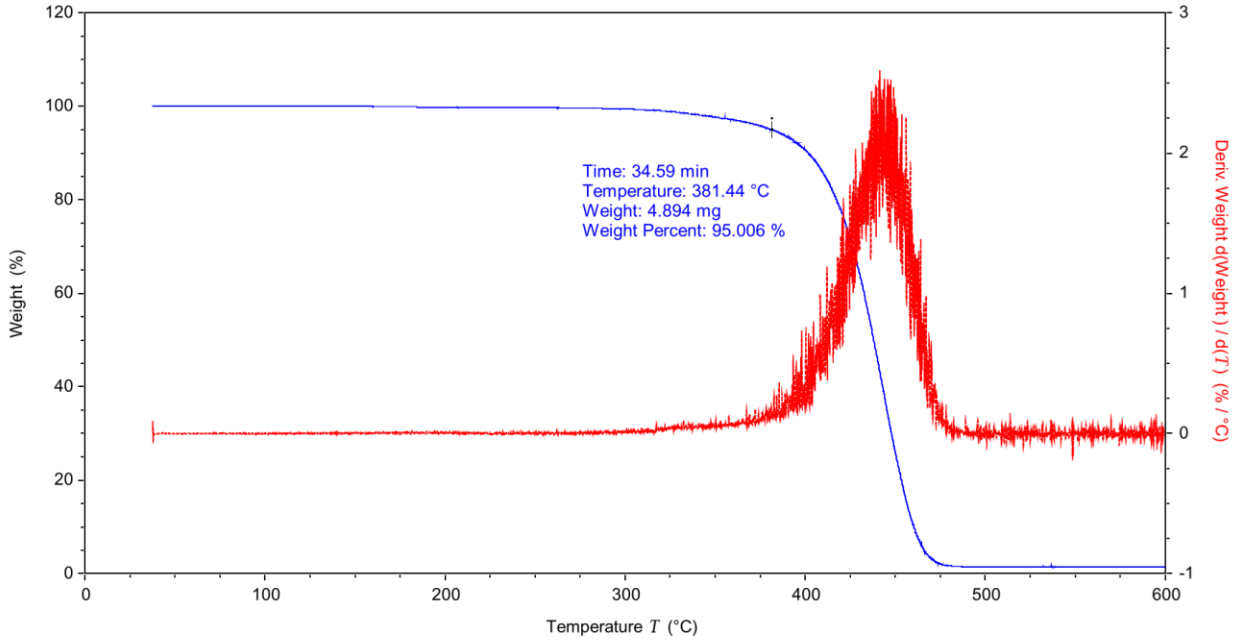


Figure C.24 TGA analysis of polymer $\mathbf{P2^{25}P4^{75}}$.

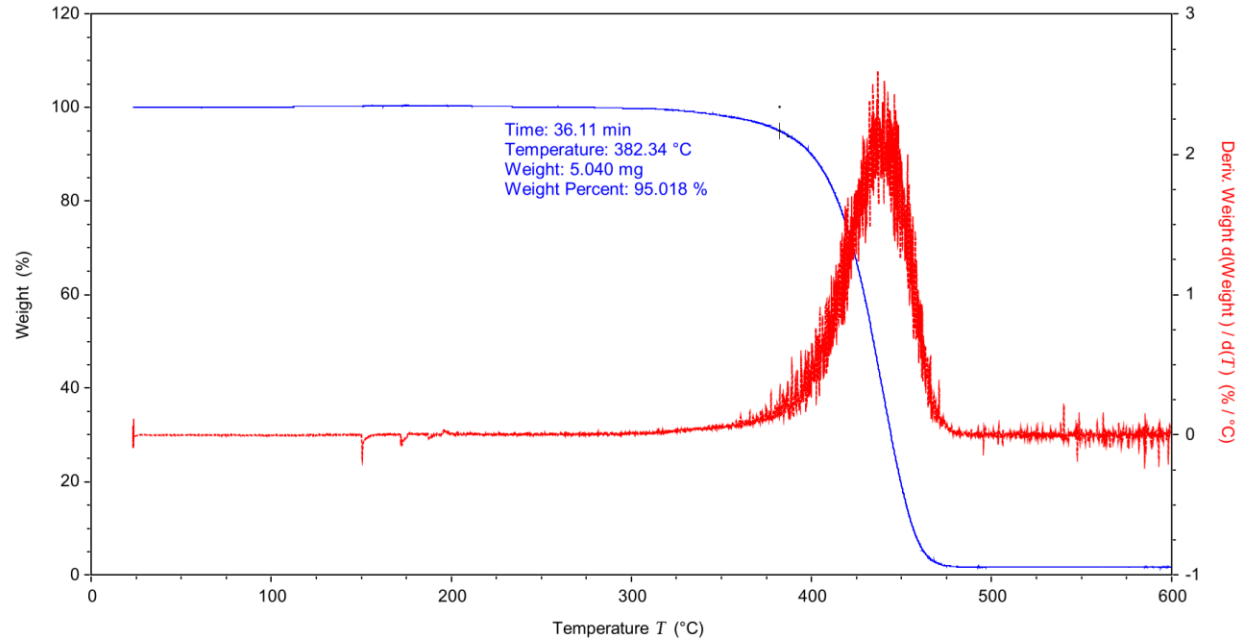


Figure C.25 TGA analysis of polymer $\mathbf{P2^{68}P5^{32}}$.

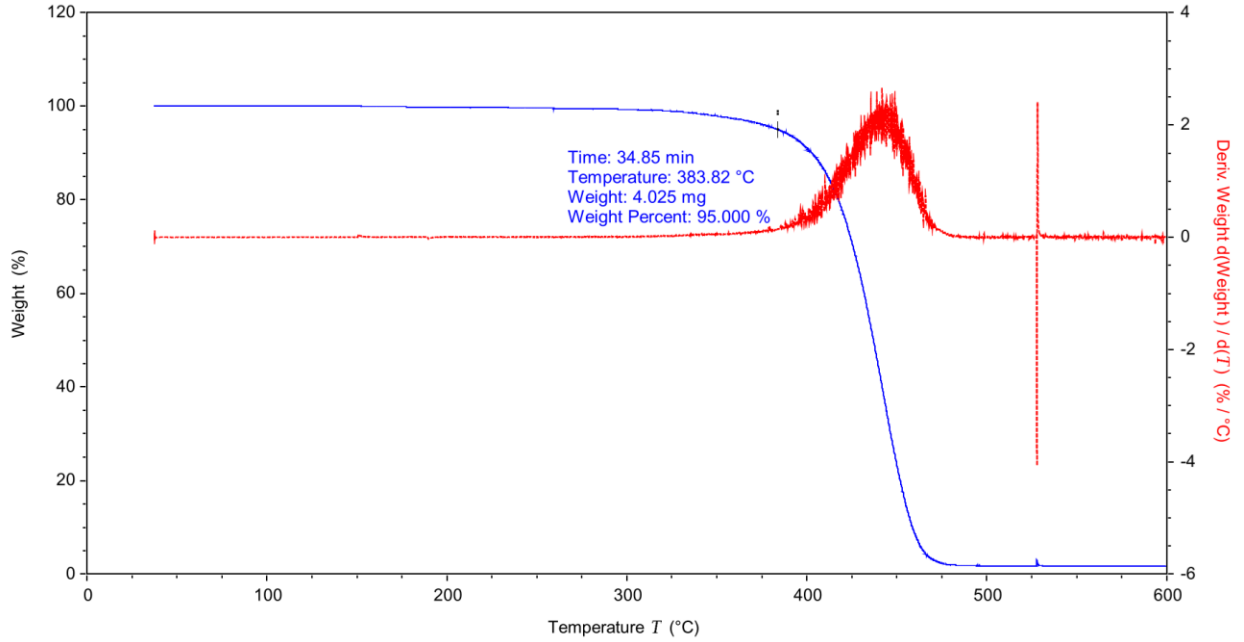


Figure C.26 TGA analysis of polymer $\mathbf{P2^{44}P5^{56}}$.

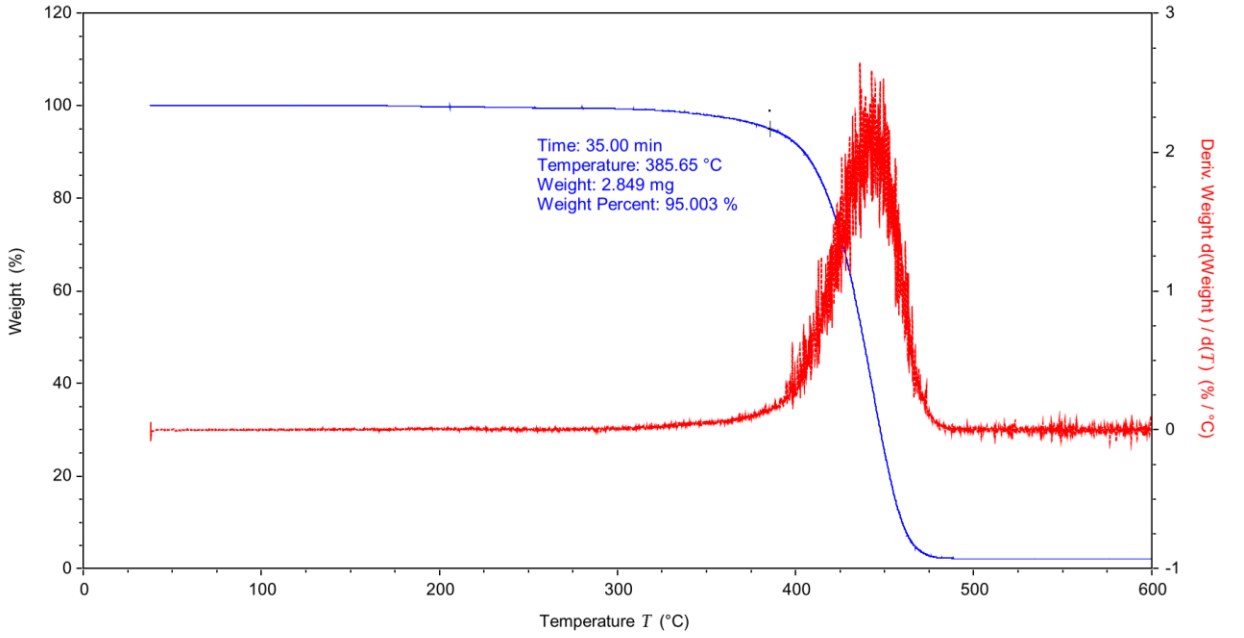


Figure C.27 TGA analysis of polymer $\mathbf{P2^{15}P5^{85}}$.

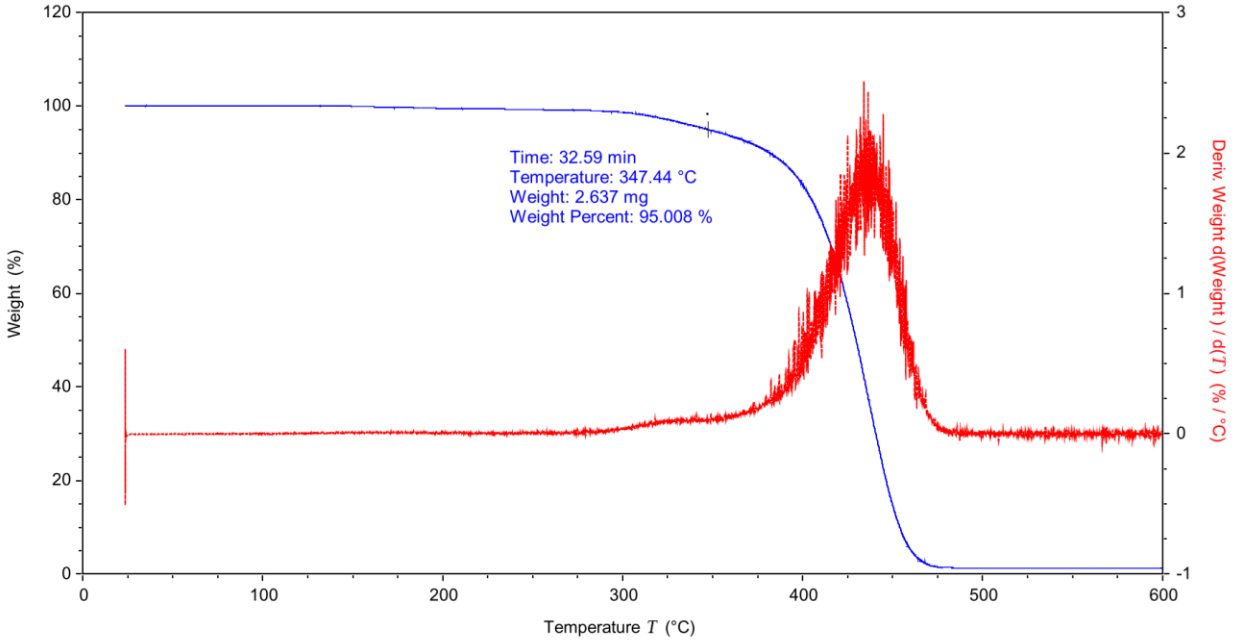


Figure C.28 TGA analysis of polymer $\mathbf{P2^{86}P6^{14}}$.

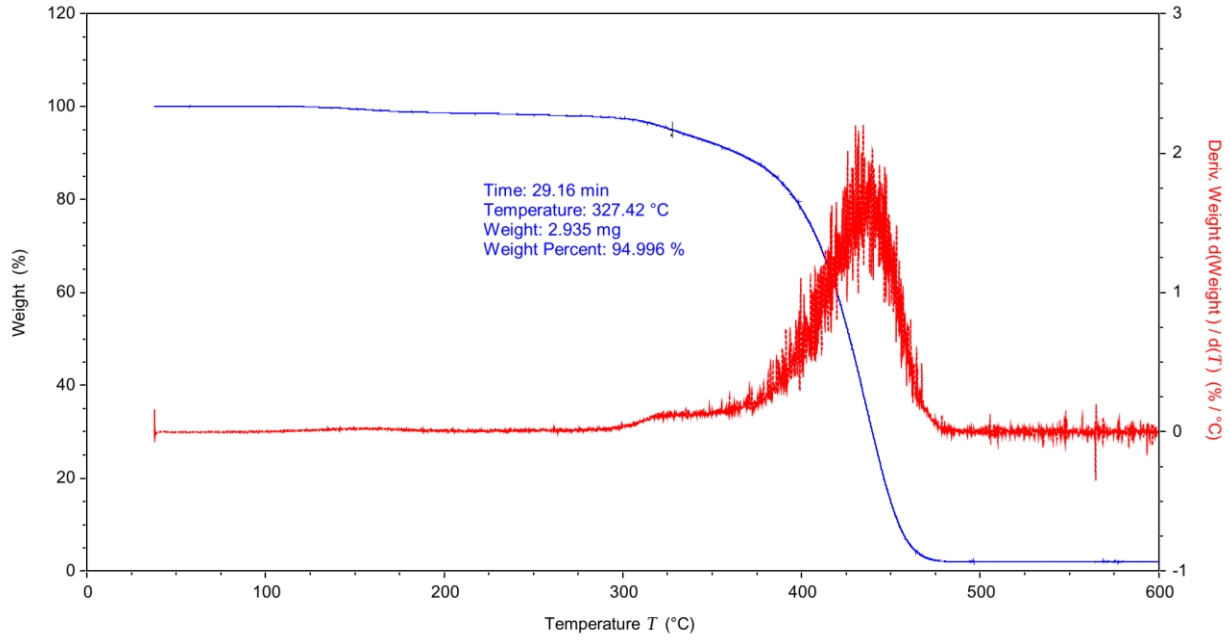


Figure C.29 TGA analysis of polymer $\mathbf{P2^{65}P6^{35}}$.

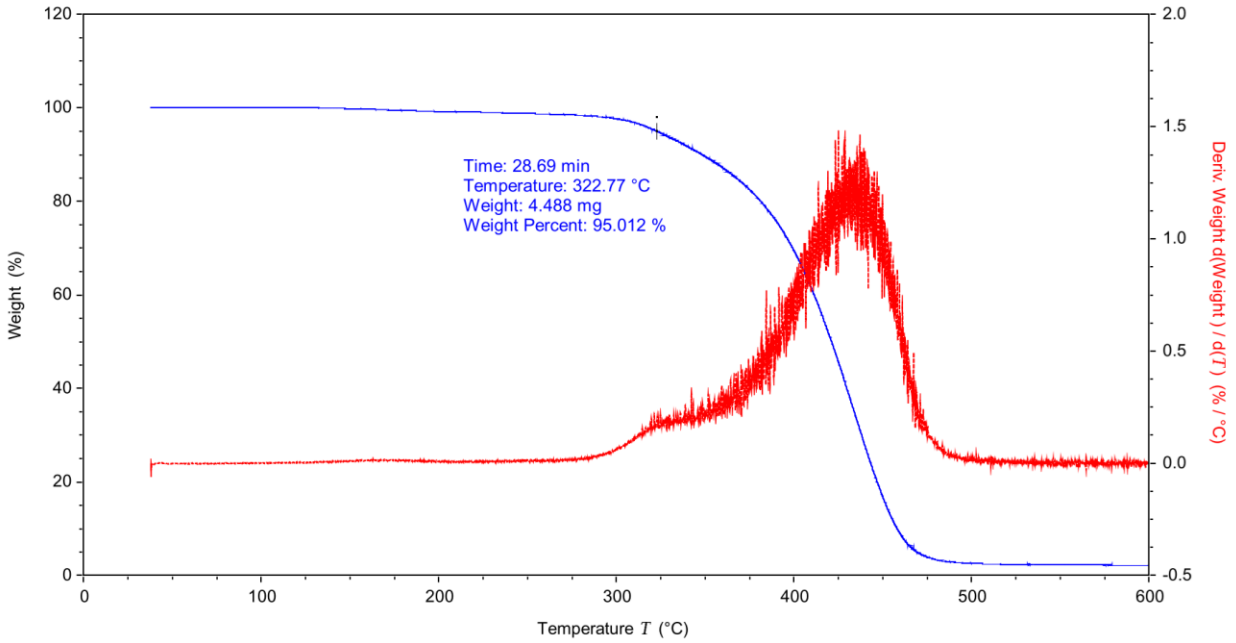


Figure C.30 TGA analysis of polymer **P2^{28}P6^{72}**.

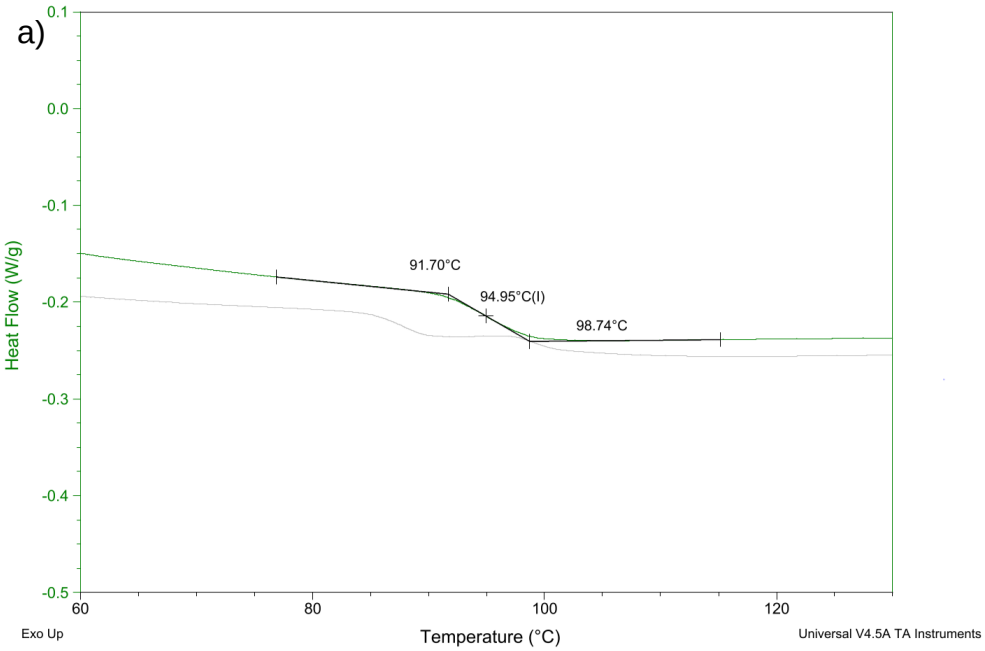


Figure C.31a DSC of **PS** control. Grey curve was the first heating cycle to erase sample thermal history.

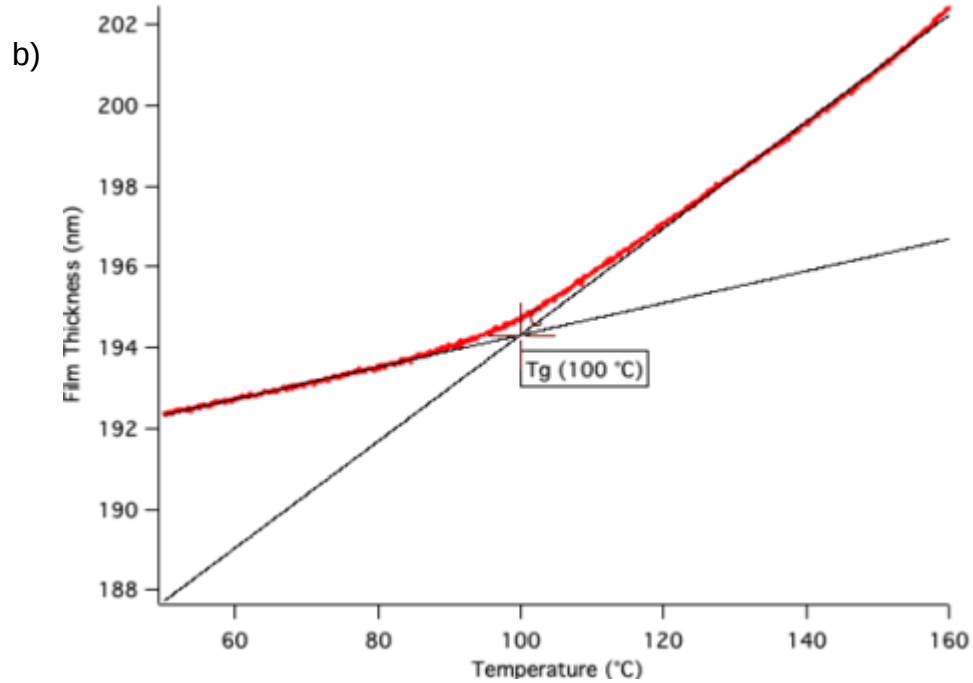


Figure C.31b T_g of **PS** control obtained by ellipsometry.

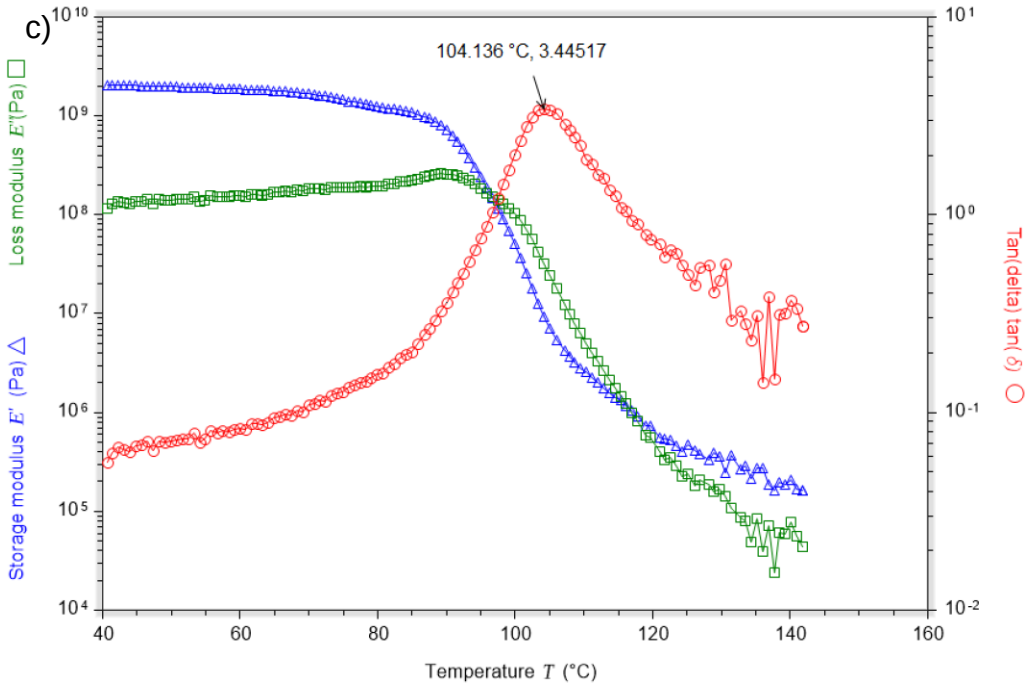


Figure C.31c T_g of **PS** control obtained by DMA.

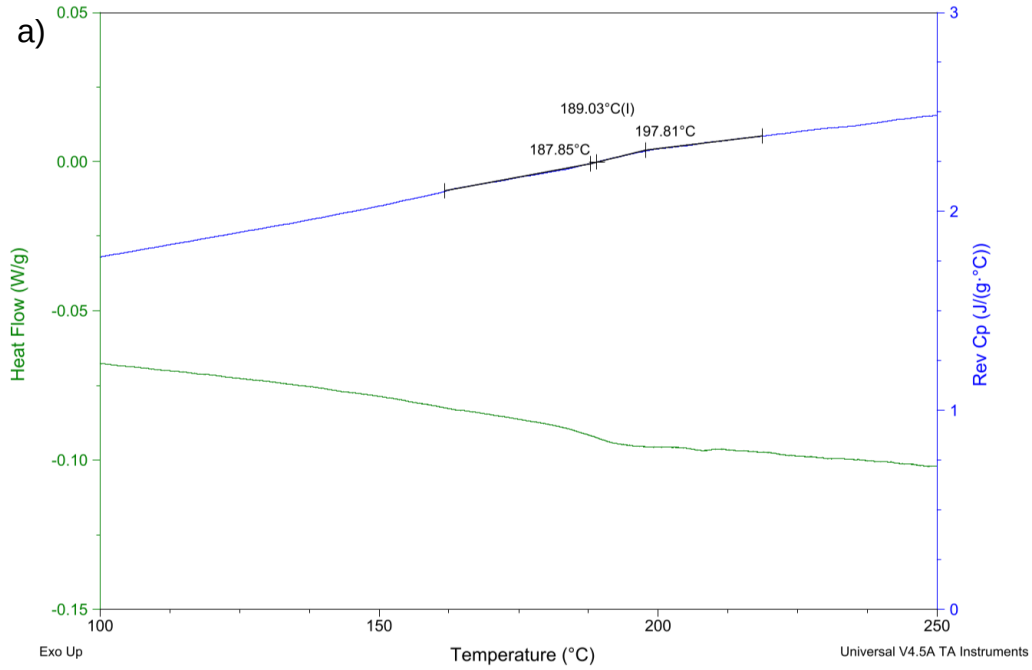


Figure C.32a T_g of polymer **P2** obtained by MDSC.

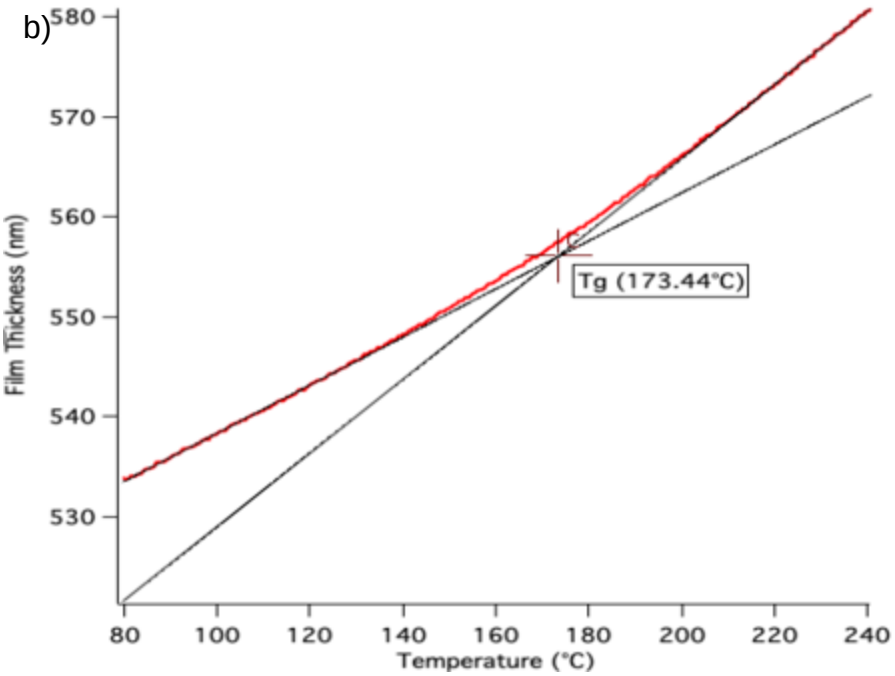


Figure C.32b T_g of polymer **P2** obtained by ellipsometry.

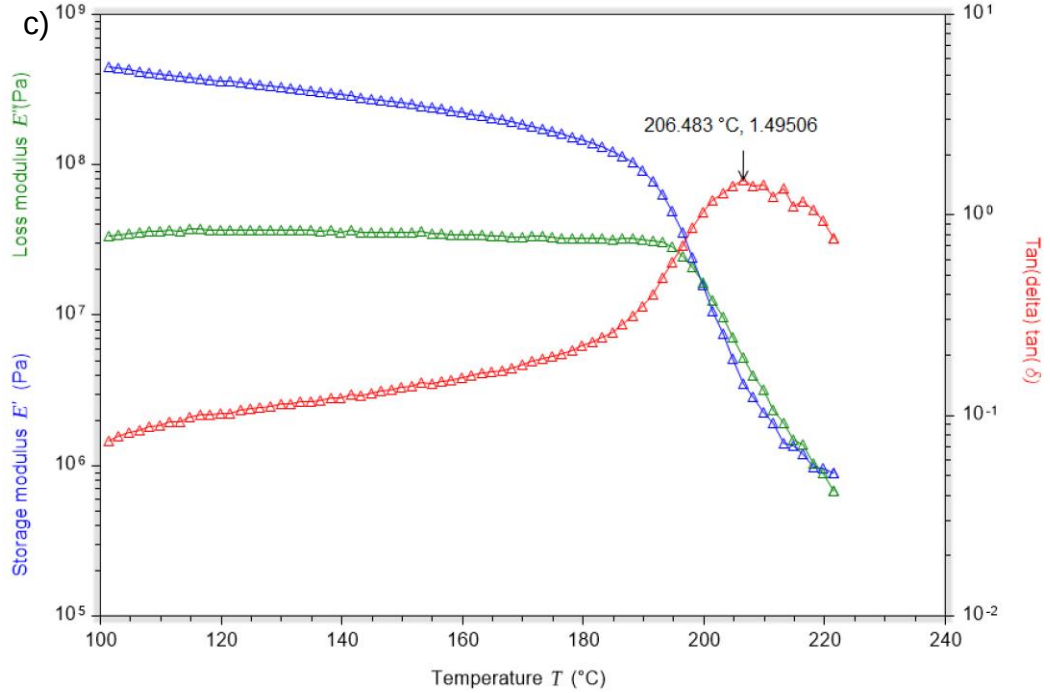


Figure C.32c T_g of polymer **P2** obtained by DMA.

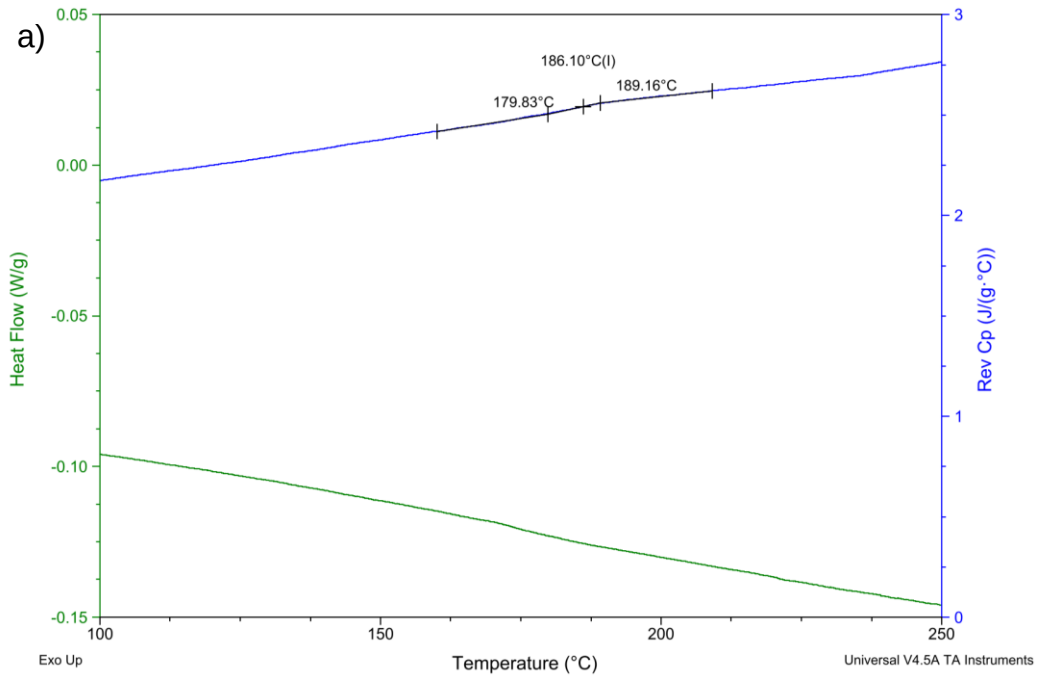


Figure C.33a T_g of polymer **P2^{86}P6^{14}** obtained by MDSC.

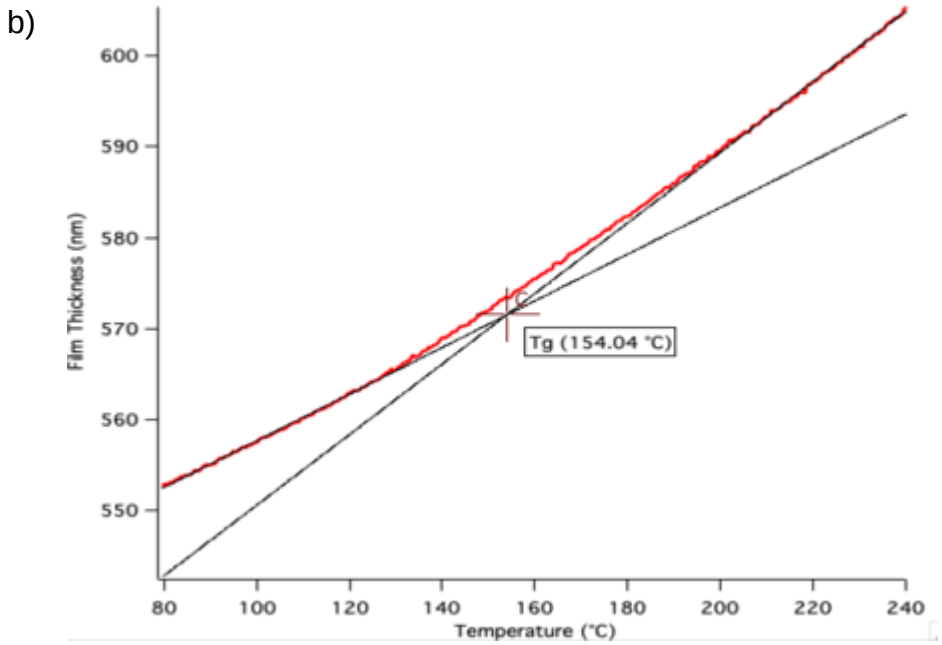


Figure C.33b T_g of polymer **P2^{86}P6^{14}** obtained by ellipsometry.

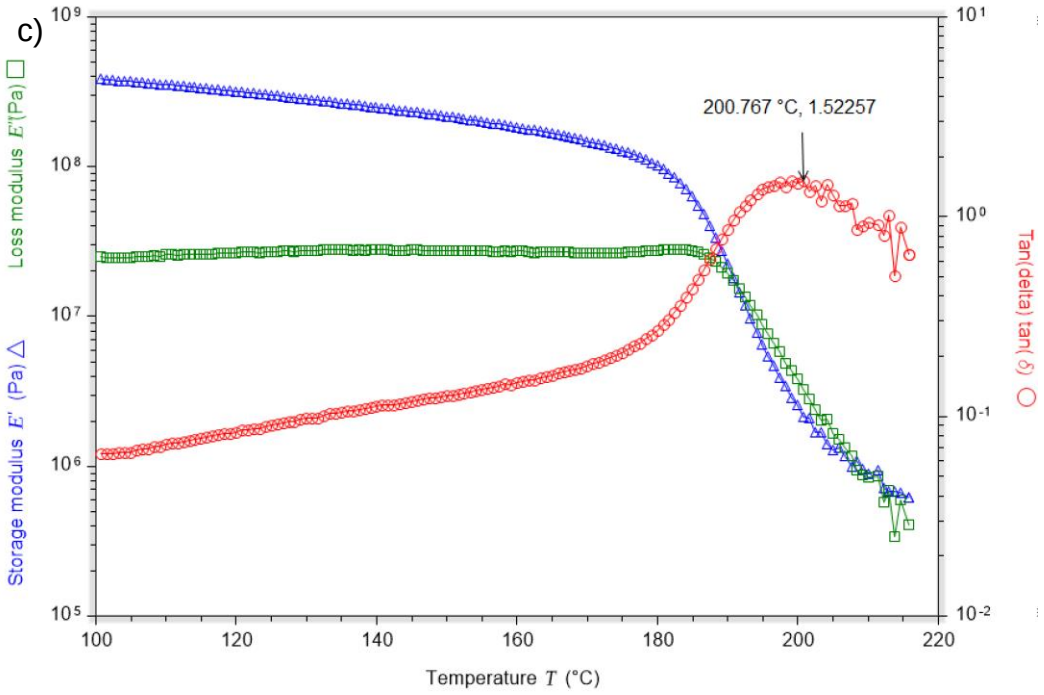


Figure C.33c T_g of polymer **P2^{86}P6^{14}** obtained by DMA.

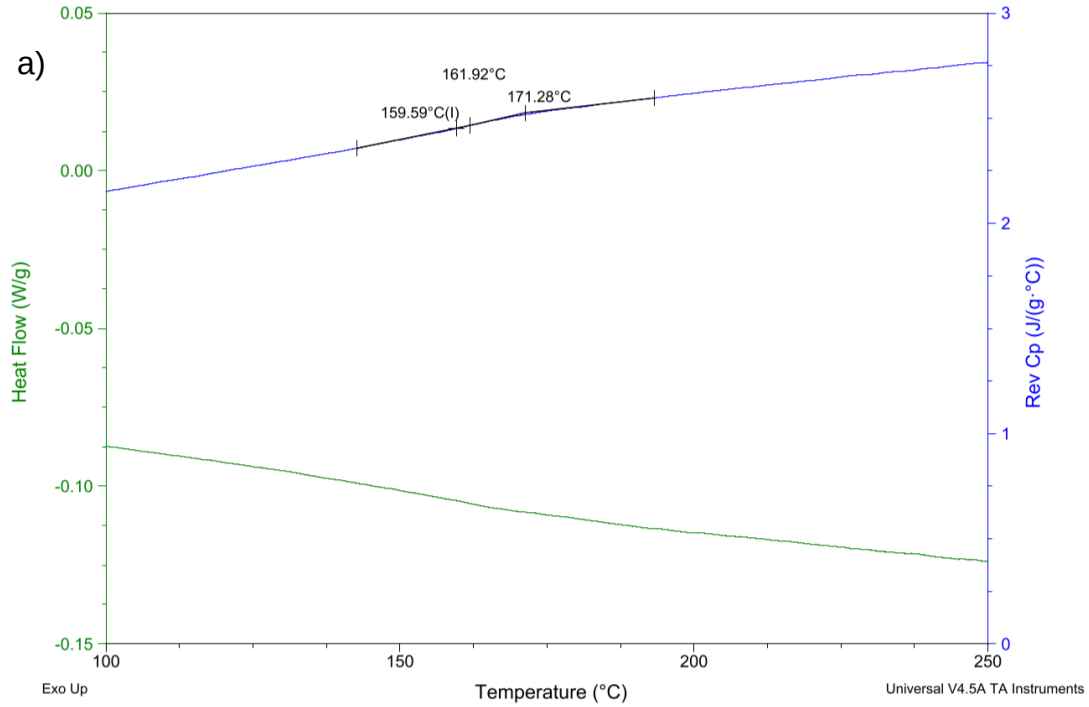


Figure C.34a T_g of polymer **P2^{65}P6^{35}** obtained by MDSC.

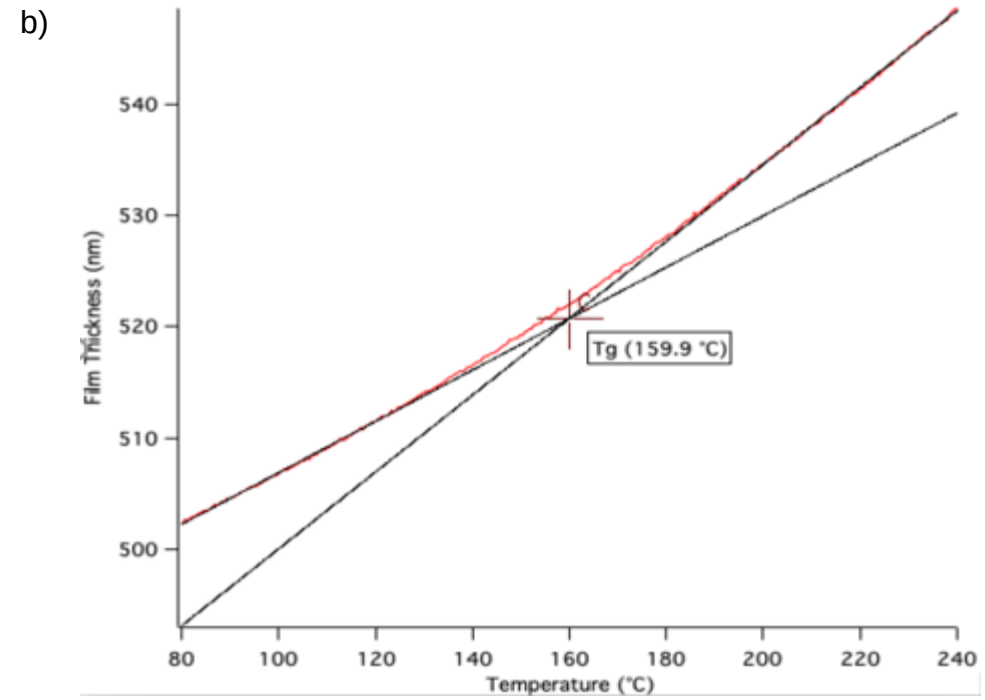


Figure C.34b T_g of polymer **P2^{65}P6^{35}** obtained by ellipsometry.

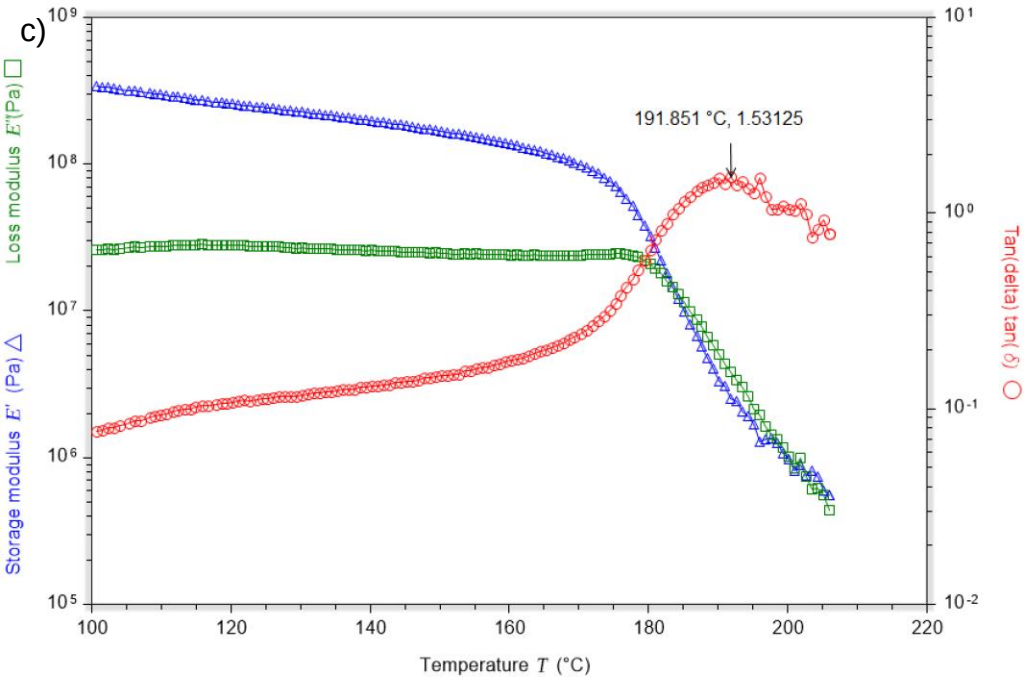


Figure C.34c T_g of polymer **P2^{65}P6^{35}** obtained by DMA.

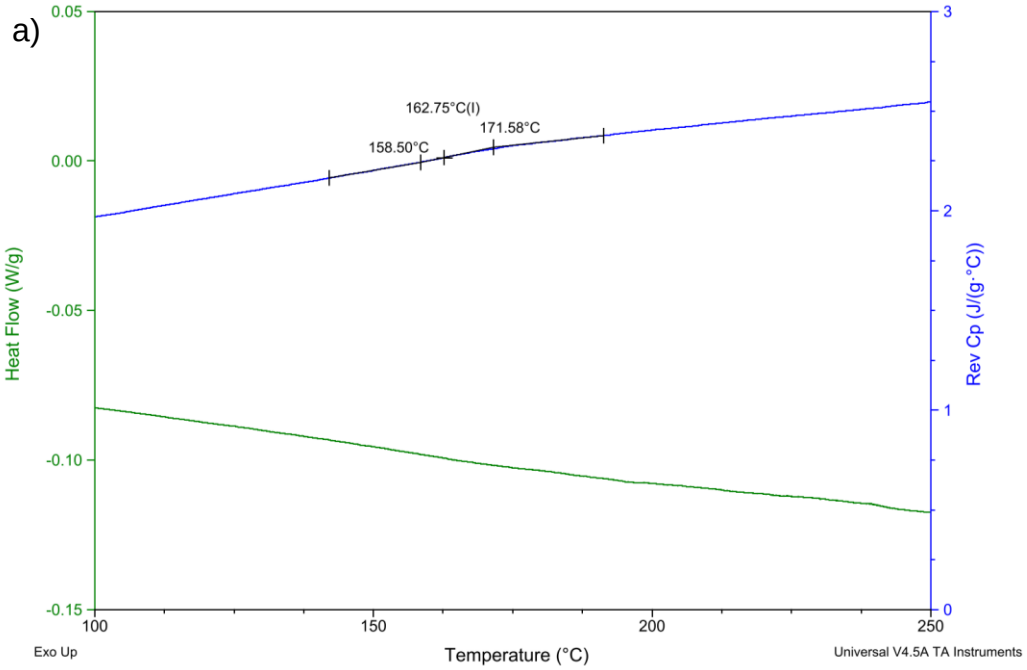


Figure C.35a T_g of polymer **P2^{28}P6^{72}** obtained by MDSC.

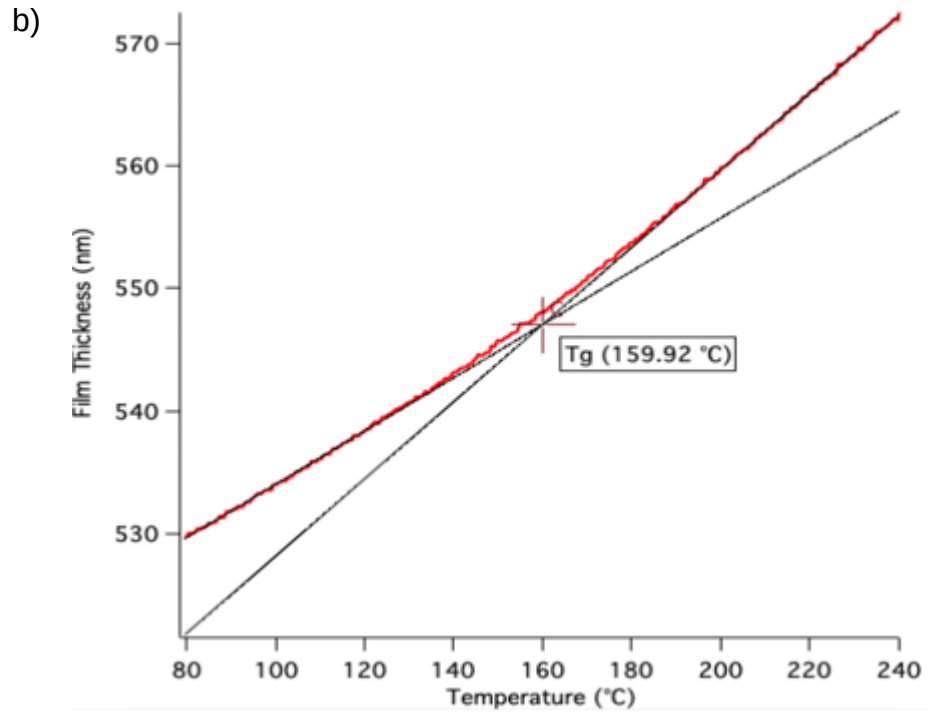


Figure C.35b T_g of polymer **P2^{28}P6^{72}** obtained by ellipsometry.

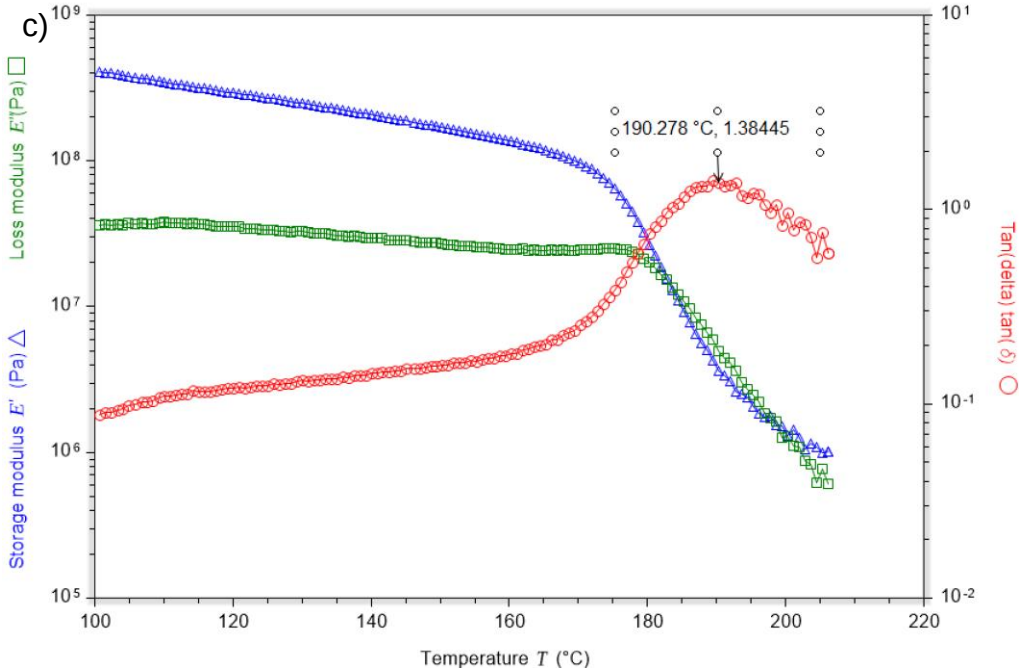


Figure C.35c T_g of polymer **P2^{28}P6^{72}** obtained by DMA.

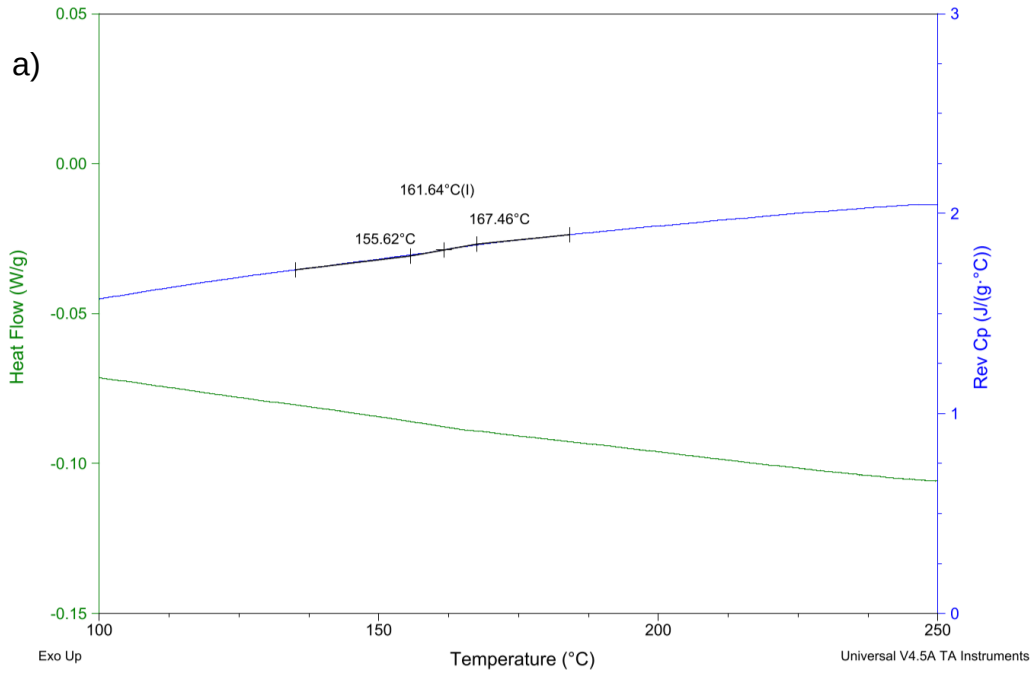


Figure C.36a T_g of polymer **P6** obtained by MDSC.

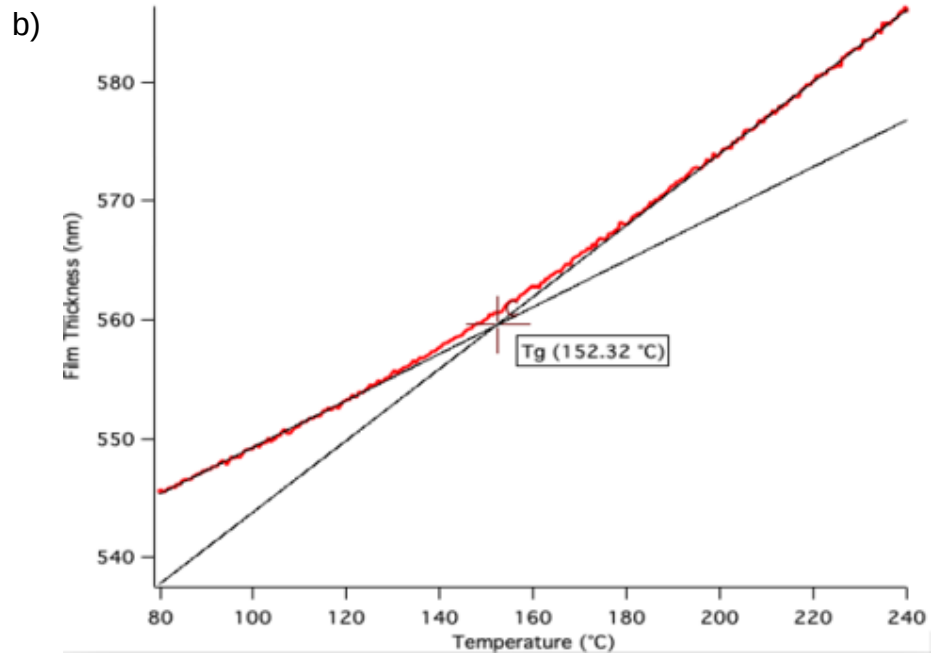


Figure C.36b T_g of polymer **P6** obtained by ellipsometry.

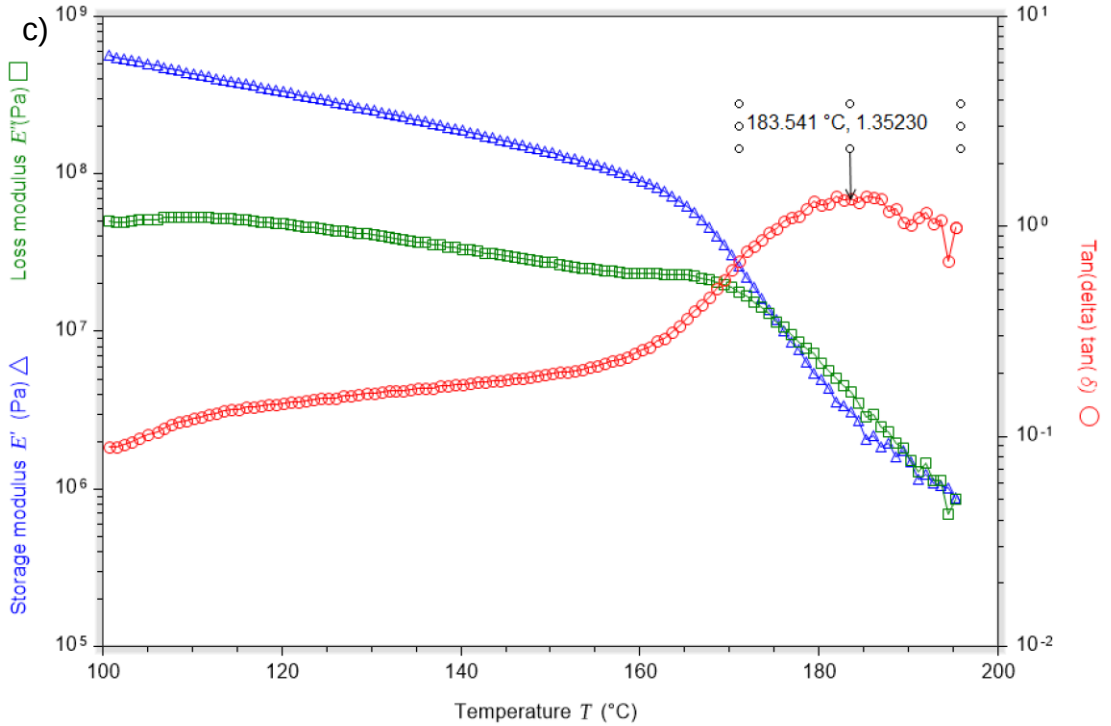


Figure C.36c T_g of polymer **P6** obtained by DMA.

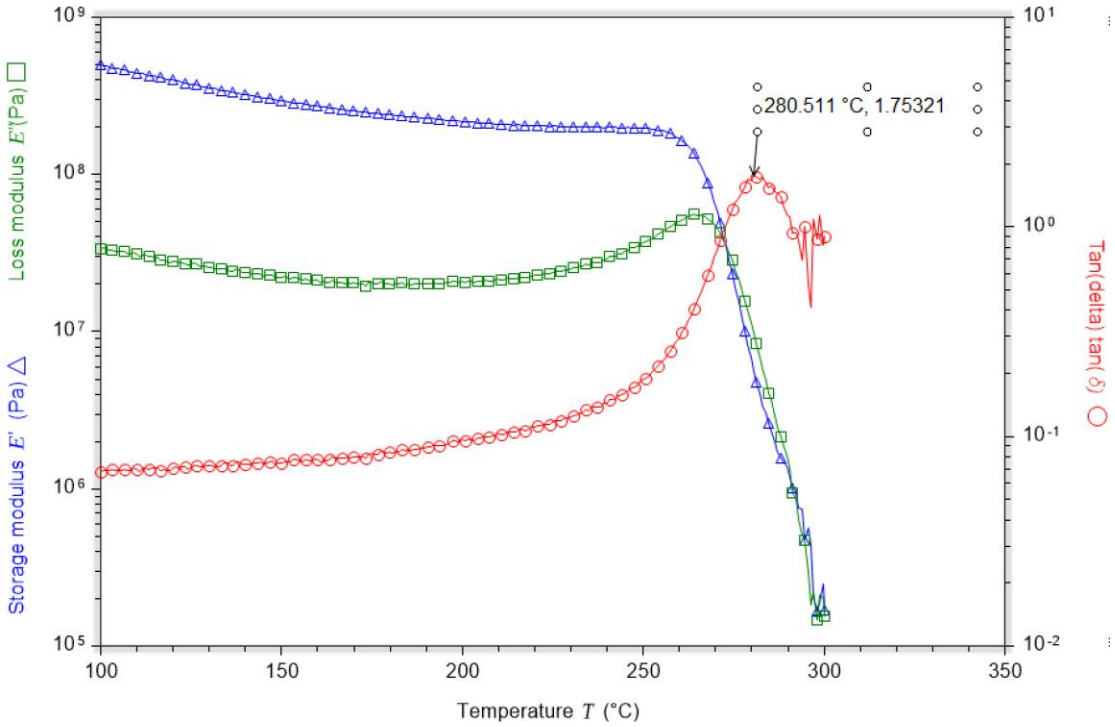


Figure C.37 DMA analysis of polymer **P1**.

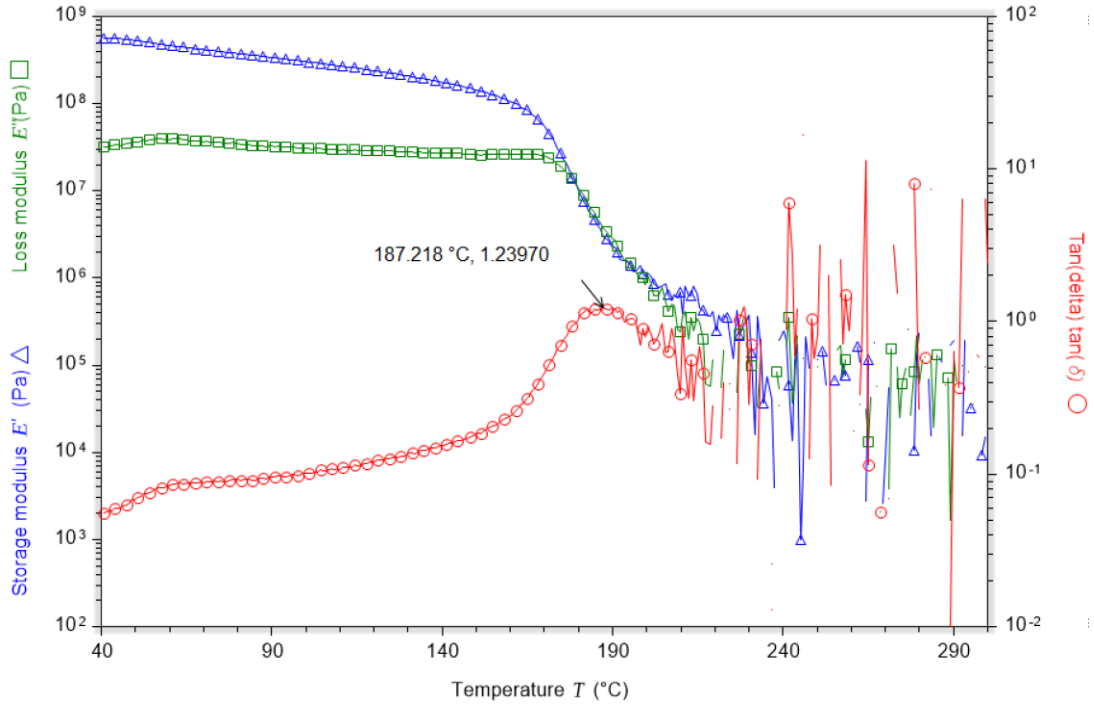


Figure C.38 DMA analysis of polymer **P3**.

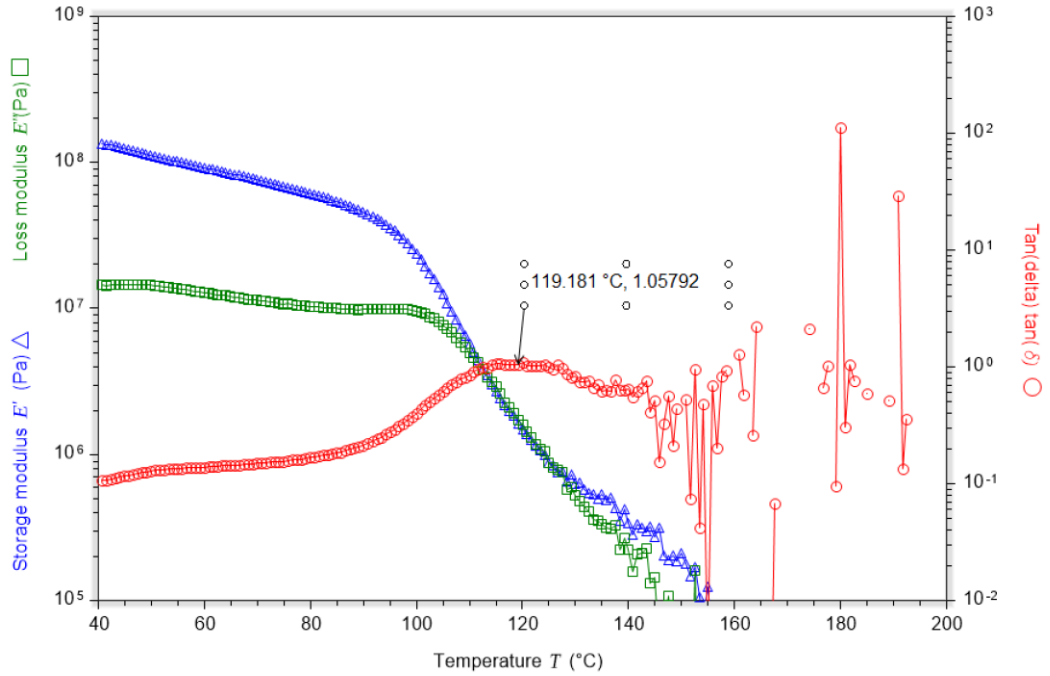


Figure C.39 DMA analysis of polymer **P4**.

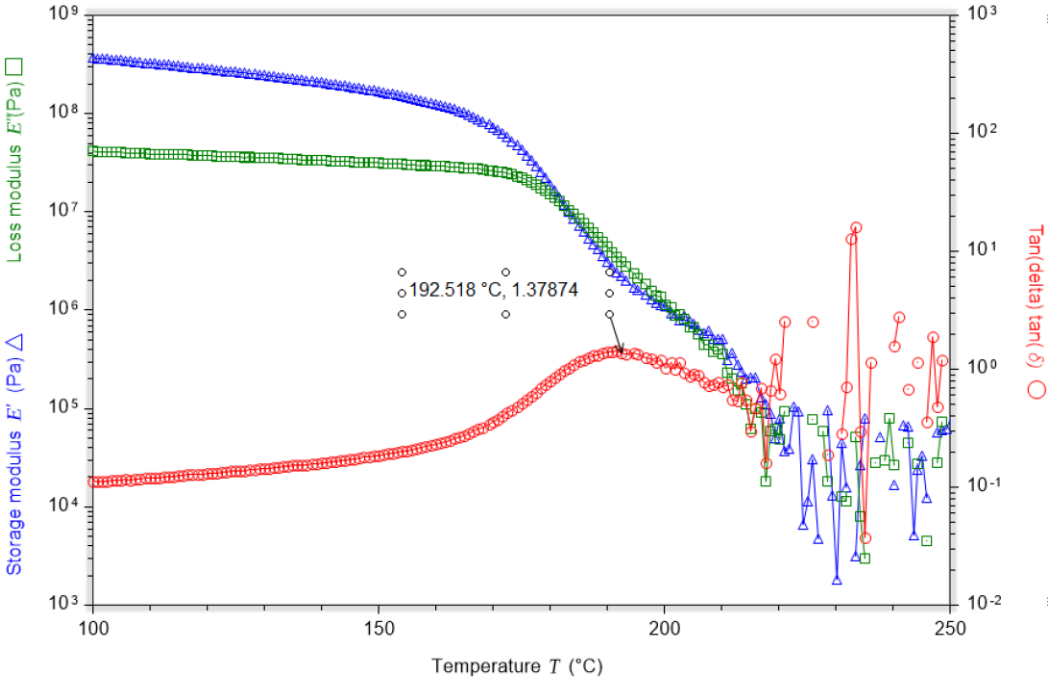


Figure C.40 DMA analysis of polymer **P5**.

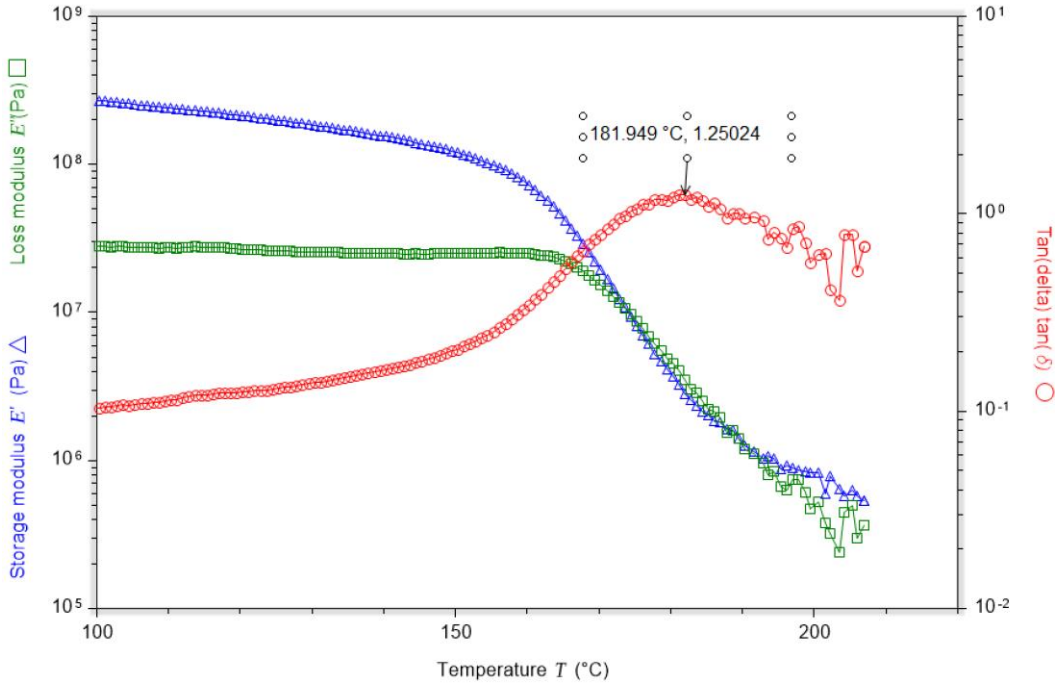


Figure C.41 DMA analysis of polymer **P2^{75}P4^{25}**.

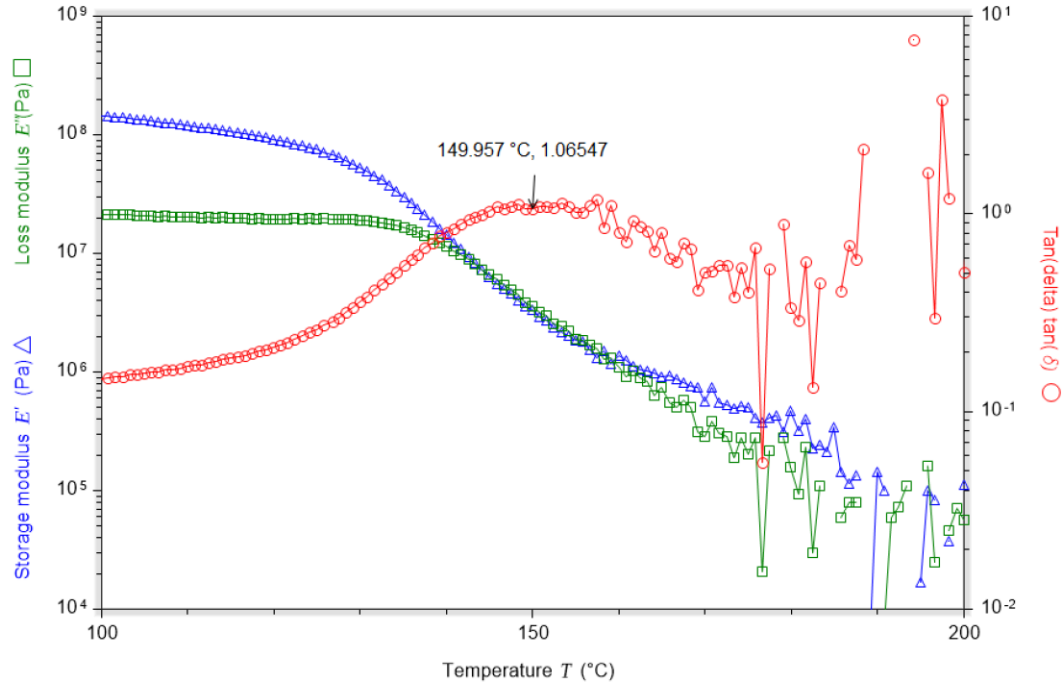


Figure C.42 DMA analysis of polymer **P2^{50}P4^{50}**.

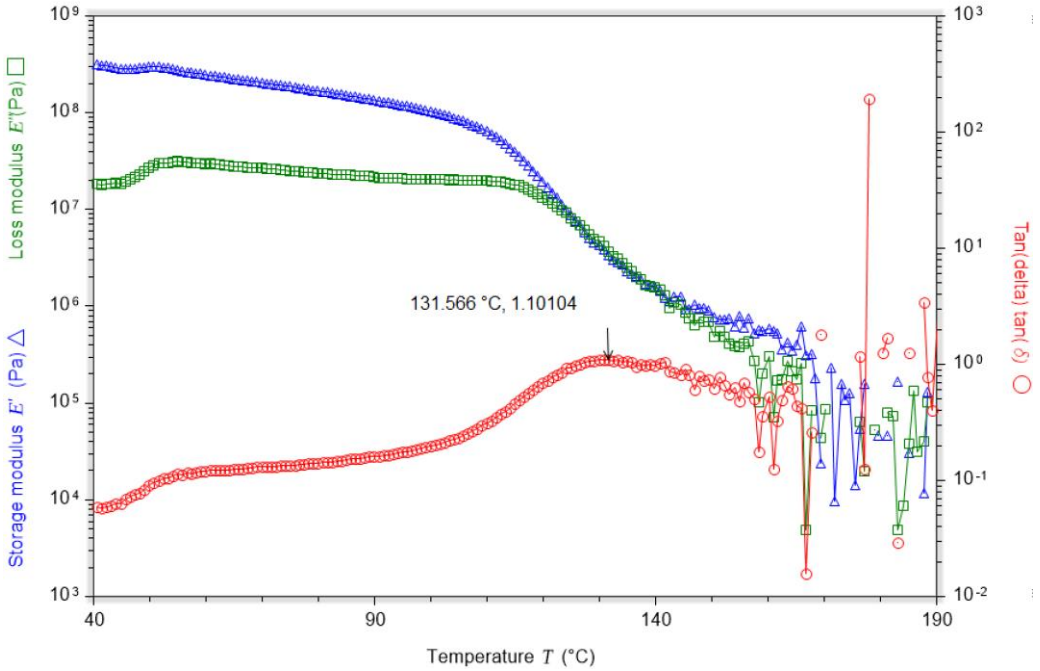


Figure C.43 DMA analysis of polymer **P2^{25}P4^{75}**.

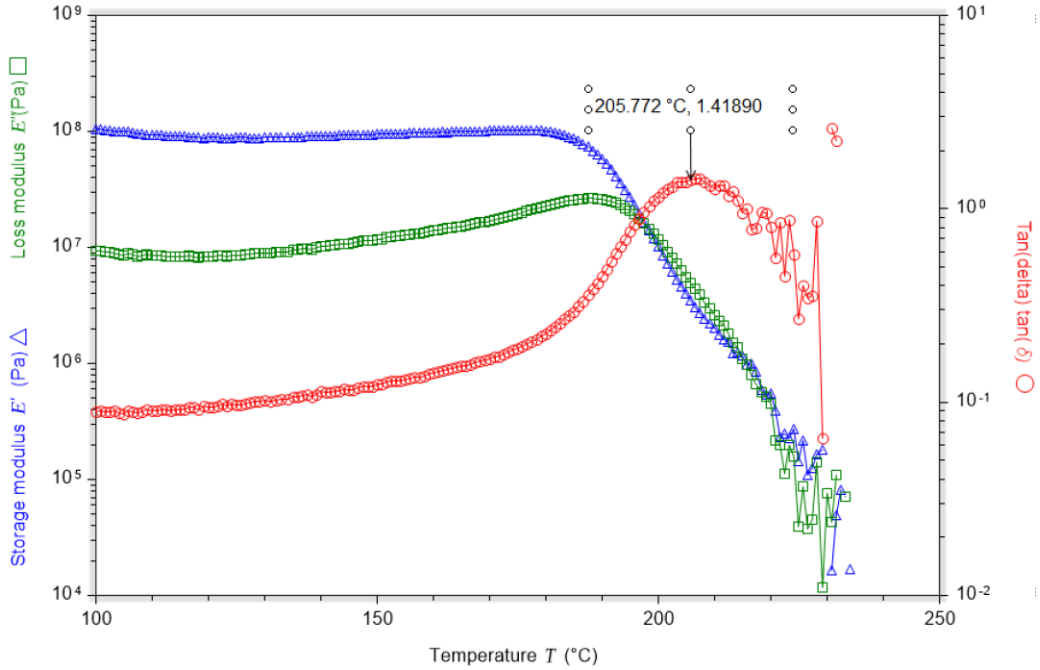


Figure C.44 DMA analysis of polymer **P2^{68}P5^{32}**.

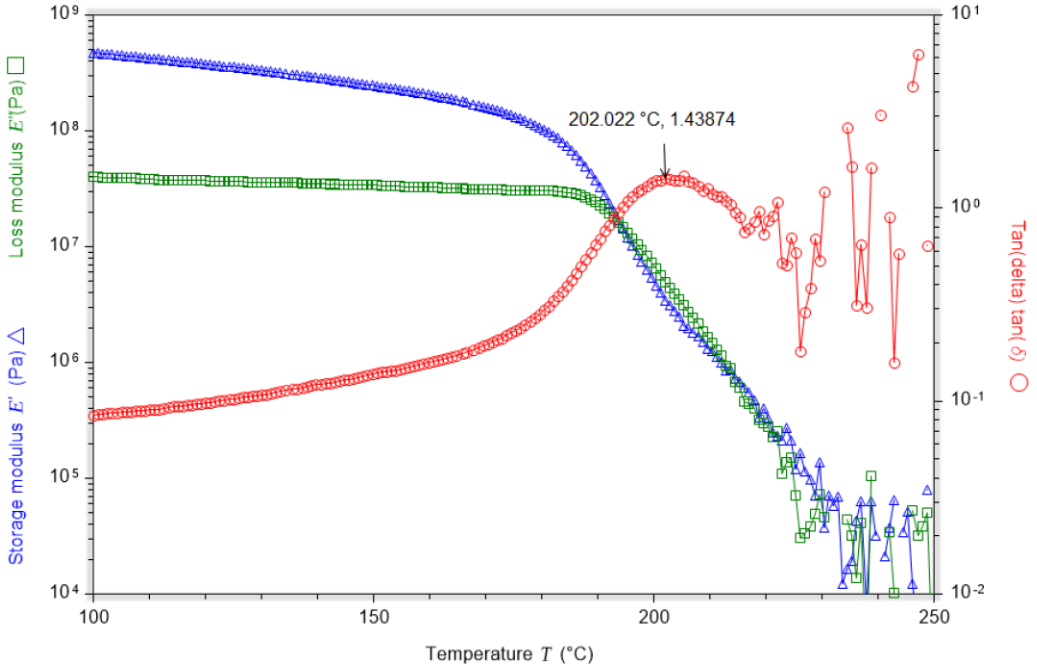


Figure C.45 DMA analysis of polymer **P2^{44}P5^{56}**.

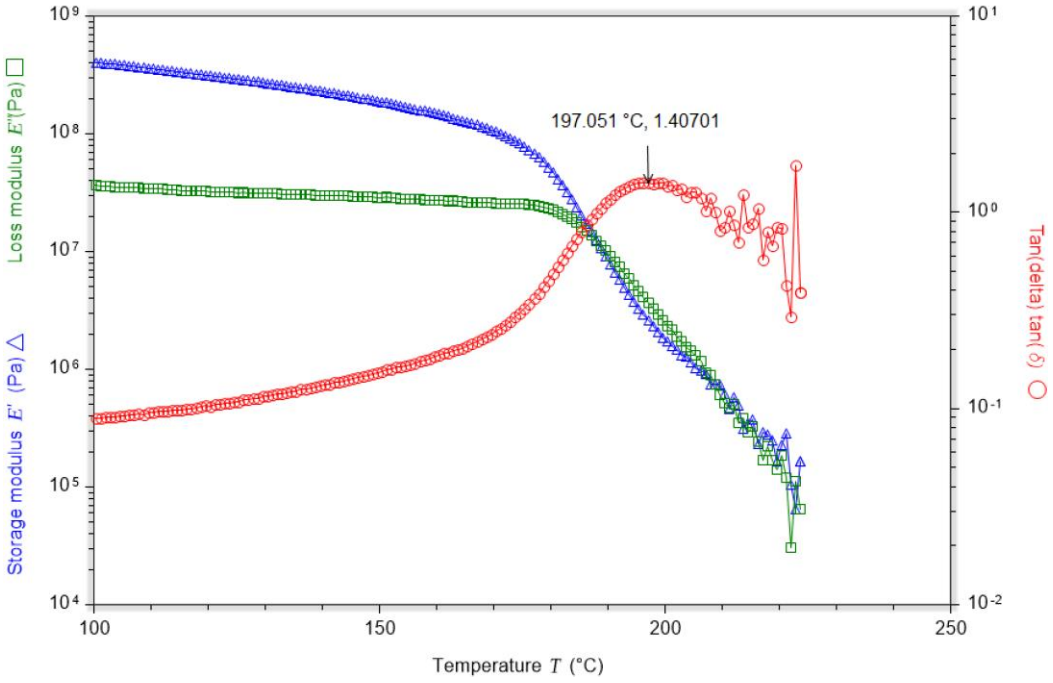


Figure C.46 DMA analysis of polymer **P2^{15}P5^{85}**.

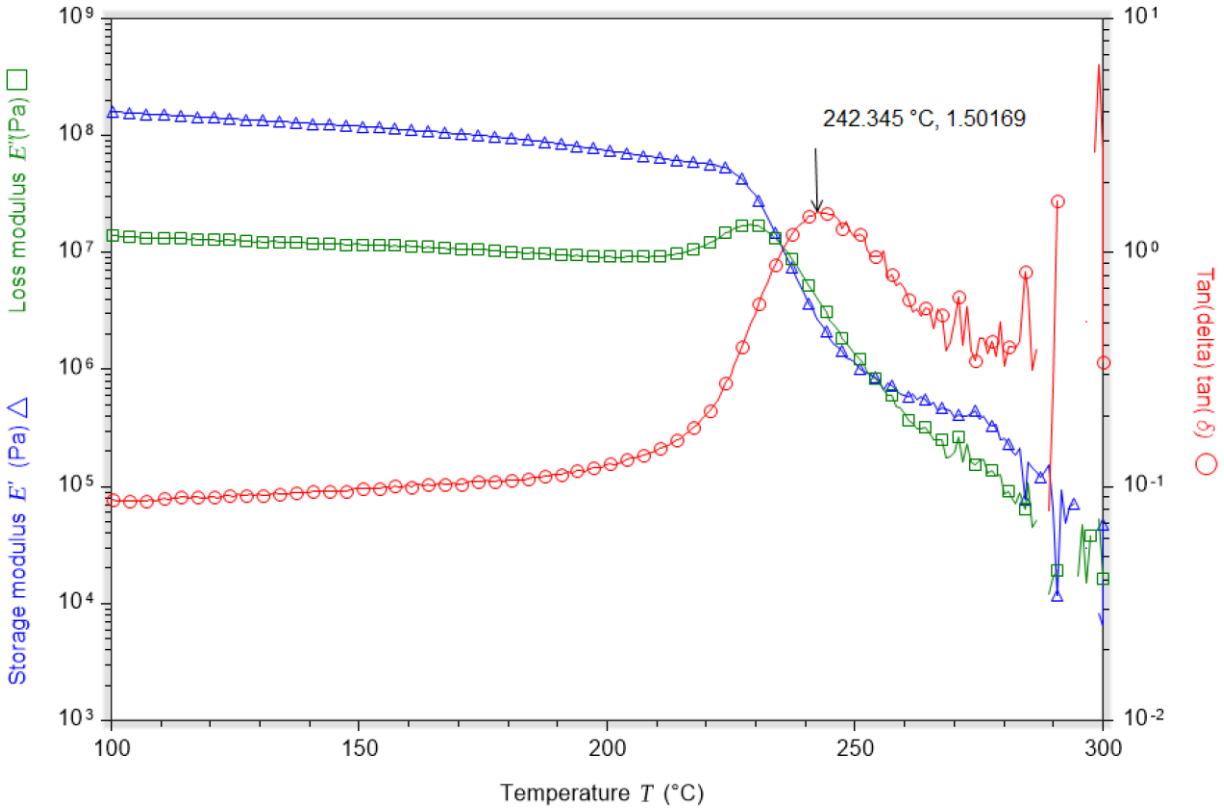


Figure C.47 DMA analysis of polymer **P2***, which has same repeat unit and similar M_n as **P2**, but synthesized using the Ni-based catalyst *trans*-[Ni(C_6F_5)$_2$($SbPh_3$)$_2$]. The T_g defined by tan δ is averaged as 241 °C by two individual tests, which is about 30 °C higher than that of **P2** (209 °C).

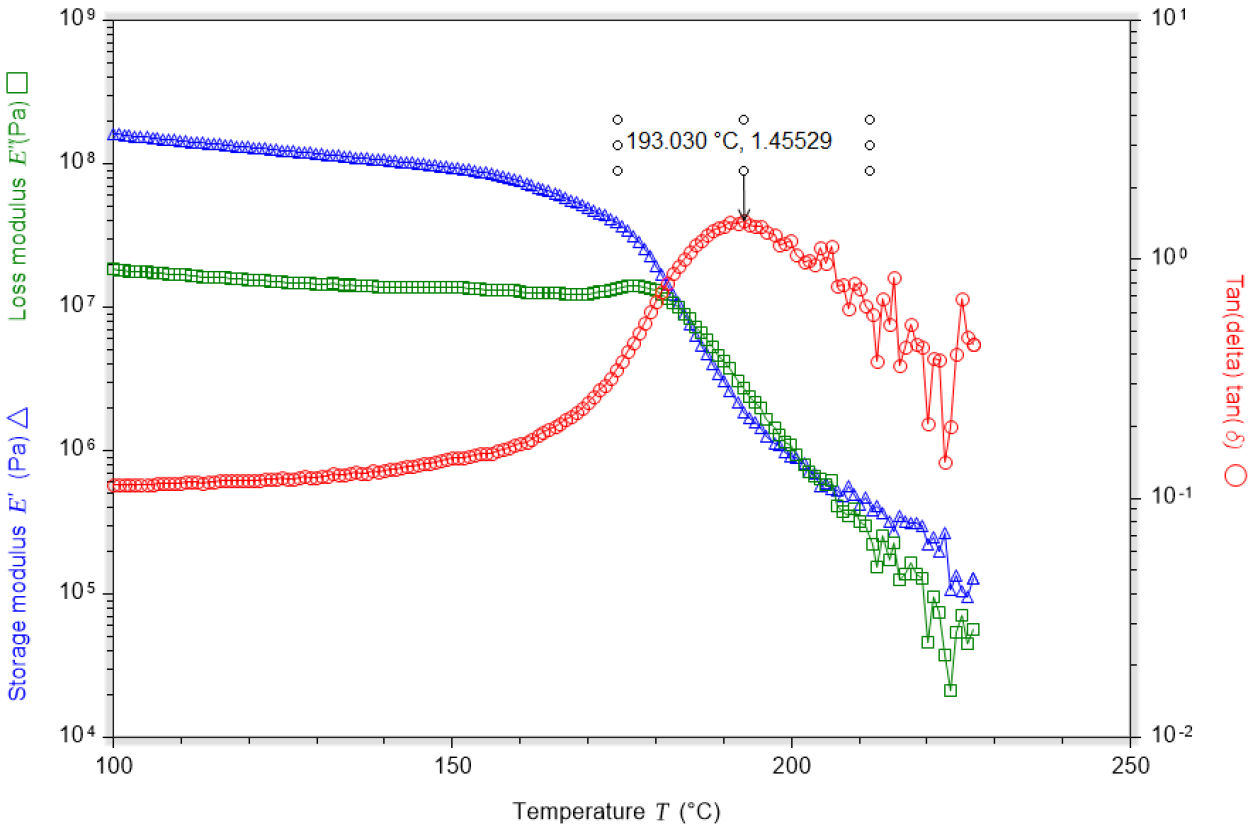


Figure C.48 DMA analysis of polymer **P3***, which has same repeat unit and similar M_n as **P3**, but synthesized using the Ni-based catalyst *trans*-[Ni(C_6F_5)$_2$($SbPh_3$)$_2$]. The T_g defined by tan δ is averaged as 194 °C by two individual tests, which is about 4 °C higher than that of **P3** (190 °C). Since **M3** contains tricyclopentadiene impurities, here the difference between T_g of **P3** and **P3*** was hypothesized to be diminished by some degree of crosslinking.

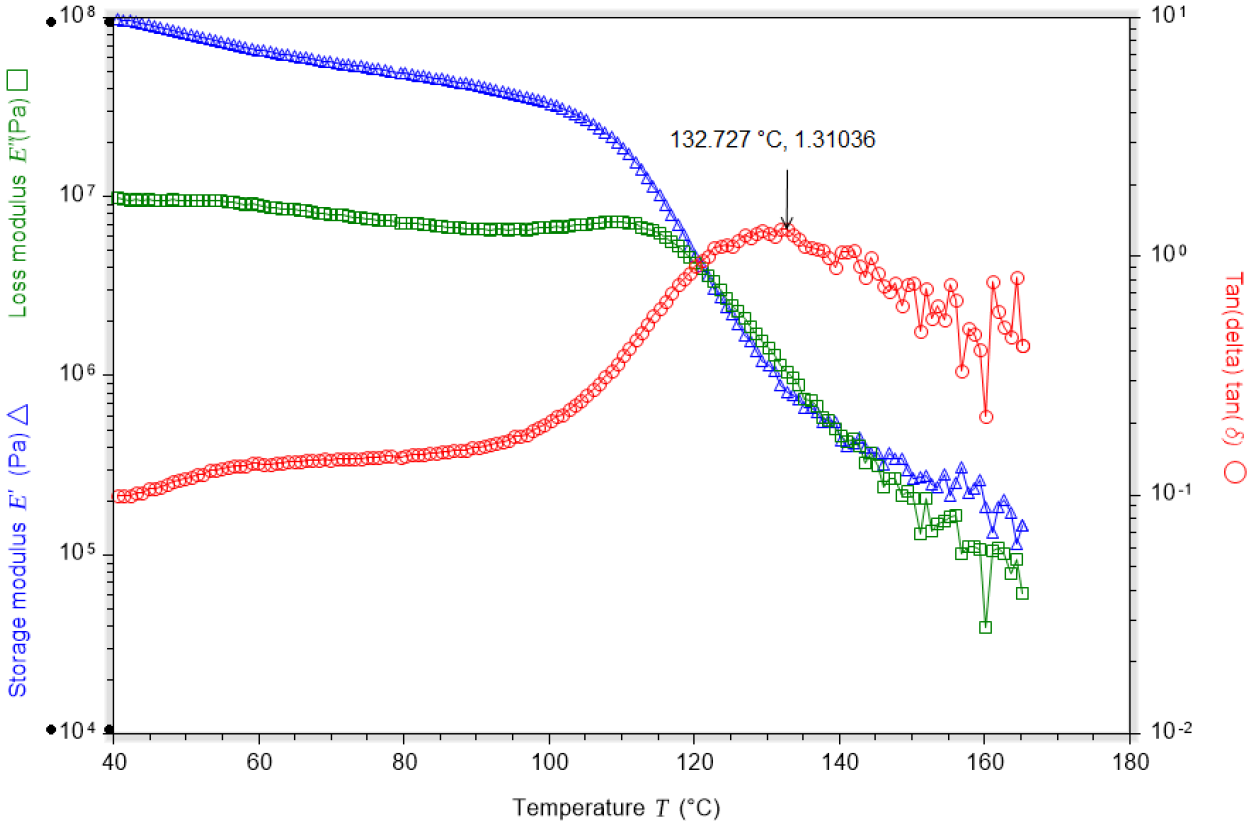


Figure C.49 DMA analysis of polymer **P4***, which has same repeat unit and similar M_n as **P4**, but synthesized using the Ni-based catalyst *trans*-[Ni(C_6F_5)$_2$(SbPh$_3$)$_2$]. The T_g defined by tan δ is averaged as 133 °C by two individual tests, which is about 14 °C higher than that of **P4** (119 °C).

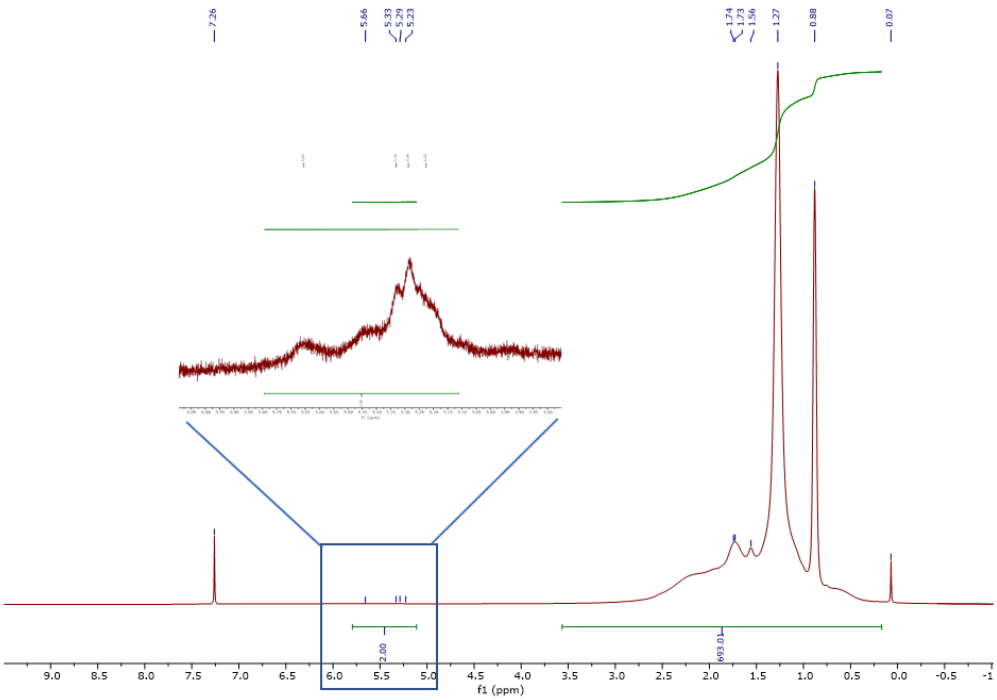


Figure C.50 [1]H NMR spectrum of **P2** after melt extrusion. A small set of new peak appear around 5.3 ppm (enlarged in blue square). These NMR signal correlate well with those found by Boydston and coworkers who showed that mechanical activation of APNB may lead to vinyl species following norbornyl ring-opening.

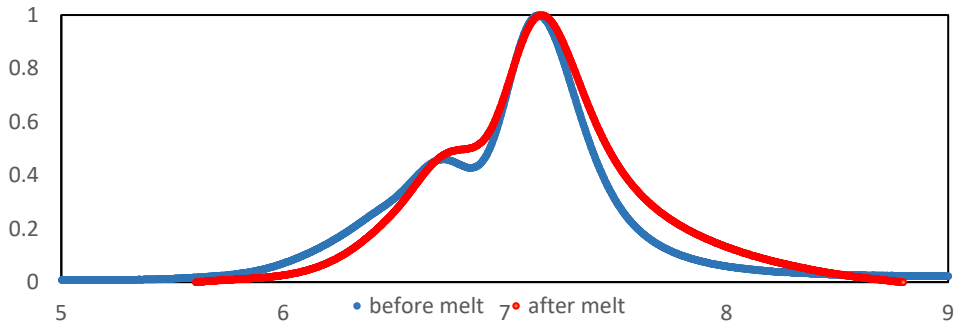


Figure C.51 GPC trace of **P2** before (blue curve) and after (red curve) melt extrusion.

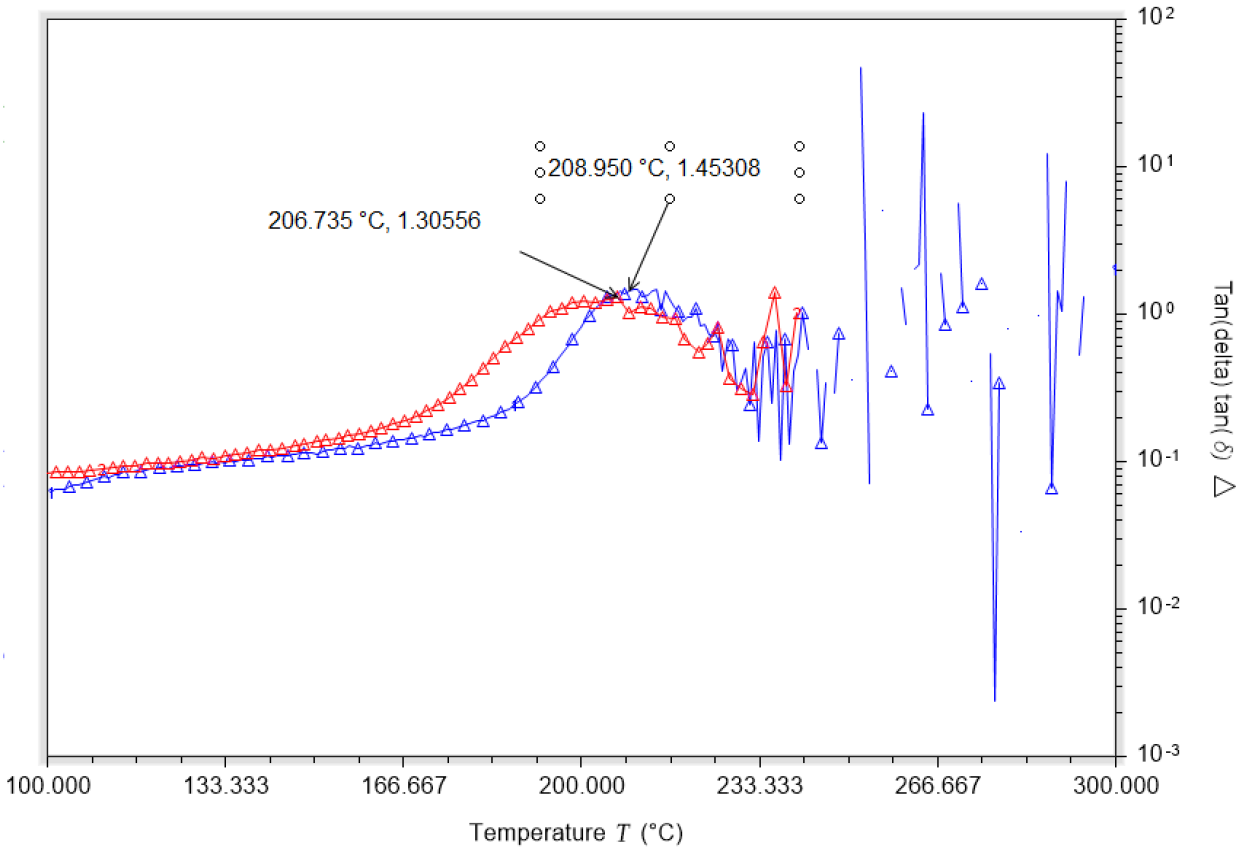


Figure C.52 DMA analysis of polymer **P2** before (blue curve) and after (red curve) melt extrusion. The averaged T_g over triplicate data points before and after are 209 °C and 205 °C, respectively. The deviation is ~2%.

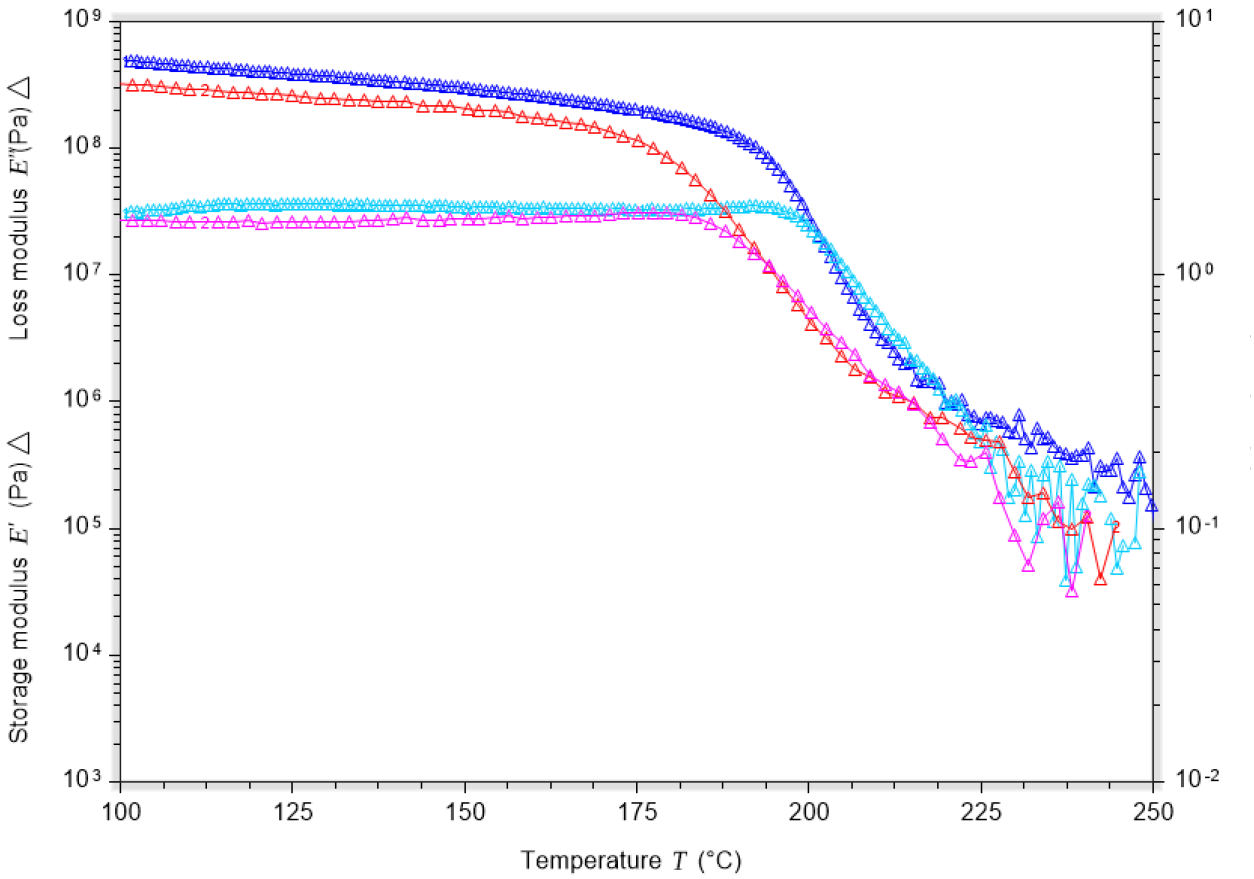


Figure C.53 DMA analysis of polymer **P2** before (dark blue curve of storage modulus E' and light blue curve of loss modulus E'') and after (red curve of storage modulus E' and pink curve of loss modulus E'') melt extrusion. Before melt extrusion: E'(100 °C) = 0.49 GPa, E'' (100 °C) = 0.031 GPa; after melt extrusion: E'(100 °C) = 0.32 GPa, E'' (100 °C) = 0.027 GPa.

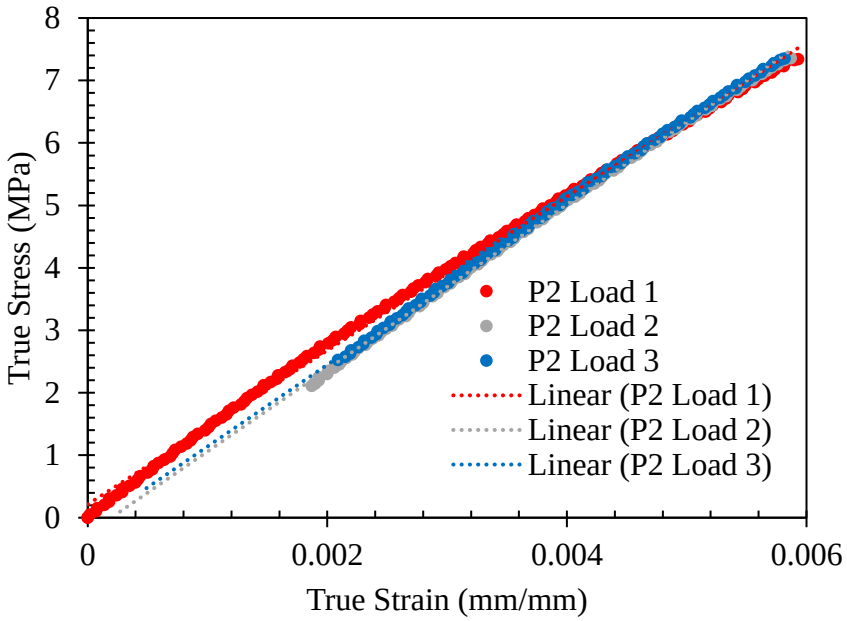


Figure C.54 Cyclic loading (three cycles) stress-strain curve of polymer **P2**.

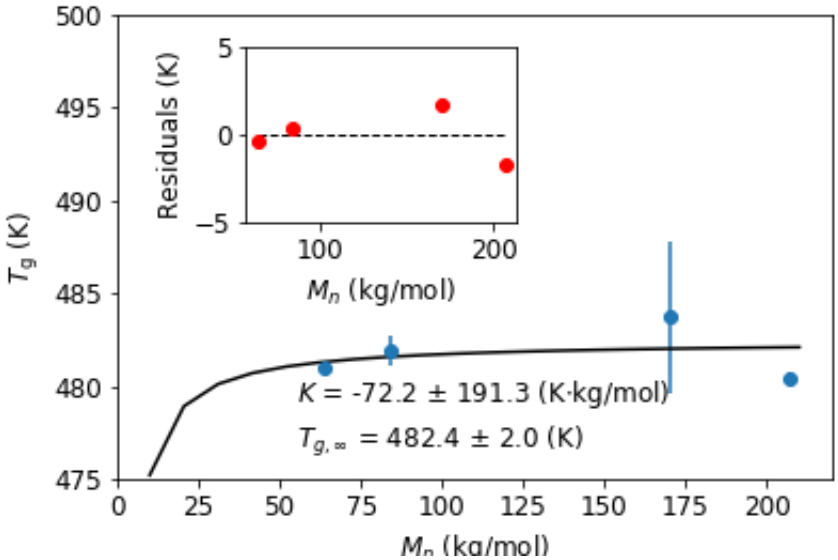


Figure C.55 The influence of M_n on the T_g of polymer **P2**. Blue symbols represent experimental data obtained for polymers with a M_n of 64, 84, 170, 207 kDa, respectively. The black curve represents the T_g predicted by the Flory-Fox equation. Red symbols in the box represent the deviation of experimental data from the predicted $T_{g,\infty}$.

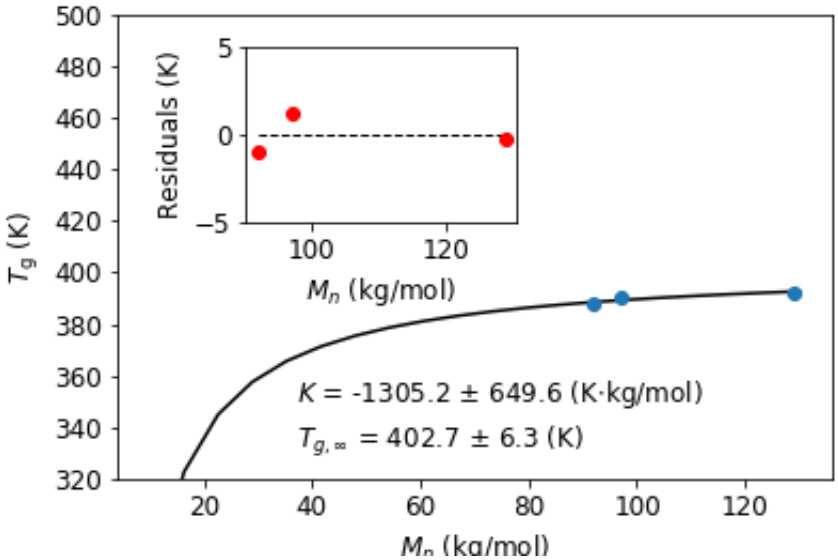


Figure C.56 The influence of M_n on the T_g of polymer **P4**. Blue symbols represent the experimental data obtained for polymers with a M_n of 92, 97, 129 kDa, respectively. The black curve represents the T_g predicted by the Flory-Fox equation. Red symbols in the box represent the deviation of experimental data from the predicted $T_{g,\infty}$. Both **Figures S73** and **S74** supported our hypothesis that in the molecular weight range studied, that the T_g of the polymer is asymptotic approaching to the $T_{g,\infty}$, and thus molecular weight effect is neglected in the rest comparison and analysis.

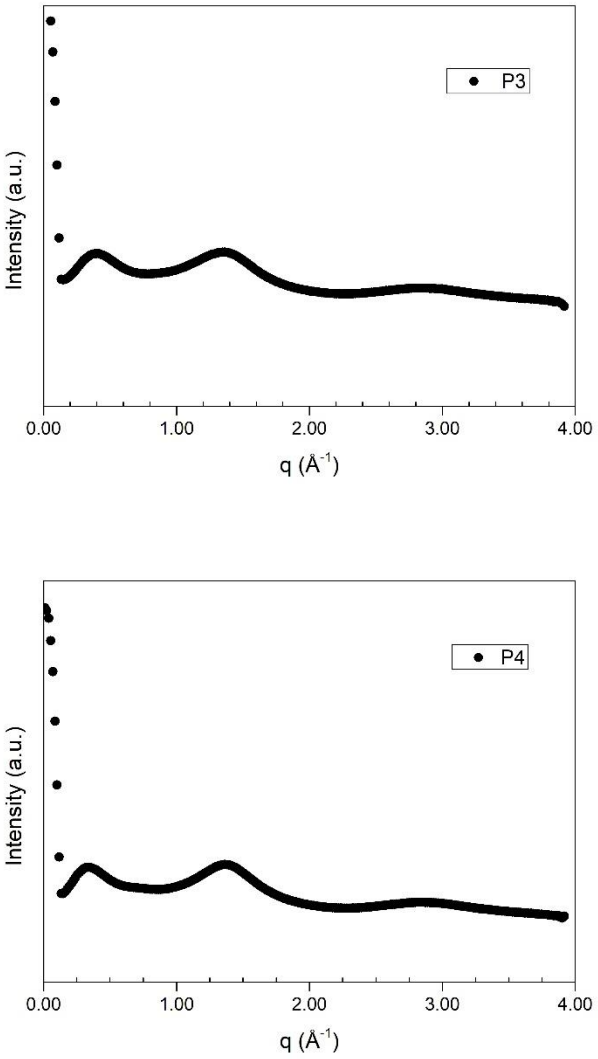


Figure C.57 WAXS data for polymer films of **P3** and **P4**, no crystalline peak was detected, indicating amorphous polymers.

Vita

Xinyi Wang was born in Shanghai, China. She obtained the Bachelor of Engineering Degree in Polymer Material Science and Engineering in June 2016 from East China University of Science and Technology. Following that, she then obtained the Master of Science Degree in Polymer Science in May 2017 from The University of Akron. She then joined Dr. Brian Long's lab at the University of Tennessee, Knoxville (UTK).

During her study and research at UTK, she worked on various research projects, including vinyl-addition fluoroalkoxysilyl-substituted polynorbornene membranes for CO_2/CH_4 separation, MPNB block copolymer gas separation membranes, catalyst effects on the APNB backbone tacticity, adamantane-based PIM gas separation membrane, and design and synthesis of melt-processible APNBs. These work leads to several publications in peer-reviewed journals, and presentations at national meetings.